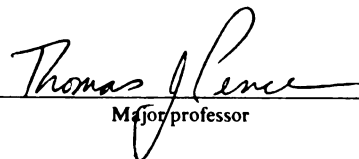This is to certify that the

dissertation entitled

ANALYTICAL AND NUMERICAL STUDY
OF PHASE TRANSFORMATION WITHIN A BAR
COMPOSED OF A STRAIN-SOFTENING NONLINEAR ELASTIC MATERIAL

presented by

Jiehliang Lin

has been accepted towards fulfillment
of the requirements for

Ph.D. _____ degree in __Mechanics__

Thomas J Pence
Major professor

Date 7/2/93

PLACE IN RETURN BOX to remove this checkout from your record.
TO AVOID FINES return on or before date due.

DATE DUE	DATE DUE	DATE DUE
_____	_____	_____
_____	_____	_____
_____	_____	_____
_____	_____	_____
_____	_____	_____
_____	_____	_____
_____	_____	_____

MSU Is An Affirmative Action/Equal Opportunity Institution

c:\circ\datedue.pm3-p.1

ANALYTICAL AND NUMERICAL STUDY
OF PHASE TRANSFORMATION WITHIN A BAR
COMPOSED OF A STRAIN-SOFTENING NONLINEAR ELASTIC MATERIAL

By

Jiehliang Lin

A DISSERTATION

Submitted to
Michigan State University
in partial fulfillment of the requirements
for the degree of

DOCTOR OF PHILOSOPHY

Department of Materials Science and Mechanics

1993

ABSTRACT

ANALYTICAL AND NUMERICAL STUDY
OF PHASE TRANSFORMATION WITHIN A BAR
COMPOSED OF A STRAIN-SOFTENING NONLINEAR ELASTIC MATERIAL

By

Jiehliang Lin

This study is concerned with a model describing phase transformations within a strain-softening bar induced by stress. In an analytical study we consider two materials with particular strain-softening constitutive laws. These materials have a non-convex strain energy density function and their equilibrium equations may be non-elliptic. The parts of the bar with strains corresponding to the strain-softening part of the constitutive law are regarded as being in a different phase from the rest of the bar. Two loading devices are the main concern: one is the hard device in which the bar is firmly fixed at one end while the other end is subjected to a given displacement; the other is the soft device in which the bar is also firmly fixed at one end while the other end is subjected to a given dead load. A detailed characterization is given for the associated nonunique solutions to this problem. Here these nonunique solutions represent different ways to distribute phase transformations within the system. Energy functions for the solutions are also given.

For both device loadings the problem is also studied within a quasi-static setting (which neglects inertial effects). Two separate criteria to resolve the nonuniqueness of the solutions to the problem are considered: a kinetic relation criterion and a minimum energy criterion.

In the numerical study we consider the finite element method. It is shown that the nonuniqueness of solutions to the problem in the continuous system is translated into nonuniqueness of solutions in the numerical system. The FEM is then successfully implemented for each of the two separate criteria mentioned above.

h

and

my

my

reco

prog

wher

agem

DAAL

State

ACKNOWLEDGEMENTS

It has been the author's privilege to have had the following gentlemen serve on his doctoral committee:

Professor	Nicholas J. Altiero
Professor	Phillip Duxbury
Professor	Dahsin Liu
Professor	Thomas J. Pence

From the beginning of my graduate education to the conclusion of my research and from conception to completion of the work for this dissertation has required not only my own devotion but also that of an experienced and patient advisor. I wish to express my sincere appreciation to Dr. Pence for his guidance and support during my research.

I wish to thank my parents for their constant support and encouragement. Special recognition is due to my daughter, Michelle, for her tolerance of the demands a doctoral program places on a father's time and disposition. And to my wife, Lingyuh Chern, where words are truly inadequate to express my appreciation for her continual encouragement and understanding.

Table of Contents

Part I: The continuum mechanical model for phase transformations in a strain-softening bar

Part II: Finite element approximation of the continuum mechanical model

List of Figures

Fig

Fig

Fig

Figu

Figu

Figu
Figu

Figu

Figu

Figur

Figur

Figure

1. Introduction

1.1 Statement of problem

Elasto-(quasi)-static fields associated with discontinuous strain in the fully nonlinear equilibrium theory of elasticity have been explored recently [1987A] in order to model phase transitions. Stress-induced phase transitions in solids can be modeled in a continuum elasticity setting by using non-convex strain energy density functions. For an elastic solid, if its strain energy density function is non-convex, then its displacement equation of equilibrium loses ellipticity and many new features of the theory emerge. For example, discontinuous strains can occur, solutions are less smooth than usual, and massive failure of uniqueness can occur in even the simplest boundary value problem. In addition, a breakdown of the familiar balance between the rate of work and the rate of increase of stored energy can occur [1979K]. In particular, the departure from the conventional elastic behavior arises in quasi-static motions of an elastic body in which, at each instant, the associated equilibrium field involves discontinuous strain.

The purpose of this study is to investigate the connection between analytical results and numerical results of phase transition behavior within a strain-softening bar subjected to either a given displacement or to a given load at ends. In particular, the bar may have a nonunique strain which is due to the strain-softening of the material. Moreover, we study loading behavior under two separate criteria for resolving the nonunique issue mentioned above, one is the minimum energy solution criterion, in which the bar always assumes configurations that have the minimum energy, the other is the kinetic criterion, in which the velocity of phase boundaries in the bar are determined by a kinetic relation. Finally we compare the analytical results and the numerical results that are obtained by using the finite element method.

1.2 Literature review

A material is said to be in a strain-softening state when the product of its strain rate and its stress rate is less than zero. Therefore the strain-softening takes place when the stiffness matrix is not positive definite. Strain-softening can be found in certain materials such as concrete, rocks, dense soils and some composites [1984R], [1985O]. Shan et al studied the fracture behavior of a "quasi-brittle" cement-based material by experimental methods [1993S]. The "quasi-brittle" material, which is different from a brittle material, responds nonlinearly prior to the peak stress and gradually decreases its stress after reaching the peak. One finds strain-softening in the constitutive equations for phenomena of damage models where the strain-softening is due to plastic fracturing [1979B]. Here the final collapse of compression test of concrete often happens after the maximum stress is reached. Both the size effect and the shape effect play important roles in the strain-softening of concrete. Belytschko et al studied transient solution for one-dimensional problems with two types of stress-strain relations: one where the stress remains constant after the strain-softening and the other where the stress increases again [1987B]. Bazant studied wave propagation within a strain-softening bar which is loaded by forcing both ends to move simultaneously outward, with constant opposite velocities. The analytical solutions and numerical solutions which are obtained by using the finite element method are given [1985B].

A simple model is useful since strain-softening involves issues related to material instability, nonuniqueness and existence. A one-dimensional bar is the simplest model studied for an elastic solid. Ericksen [1975E] considered a bar whose stress-strain relation is non-monotonic and explored it for material instability by using the equilibrium theory. This can be viewed as a simple model for phase transition in an elastic solid. Non-monotonicity of the stress response behavior in [1975E] may lead to three allowed values of strain which correspond to a single value of stress. These strains are in three different strain phases: low strain phase, intermediate strain phase and high strain phase. A prop-

agating strain discontinuity in these material may be either a shock wave or a phase boundary, according to whether the locations separated by the discontinuity are of the same phase or different phases. In [1975E] the intermediate strain phase is a phase in a behavior of strain-softening.

To formulate the problem, the formal presentation of basic laws is useful. Gurtin [1991G] proposed formal presentation of fundamental laws in a fully dynamical setting: balance laws for mass, forces and energy and a law of the entropy growth for a two-phase continuum with sharp phase-interface. In addition, he explained the ideas involved in the formulation of these basic laws and clarified the differences between various formulations.

The problem can be studied in either an equilibrium setting, a quasi-static setting or a dynamical setting. The quasi-static setting gives motion by advancing through a static case at each instant so that the difference between a quasi-static setting and a dynamical setting is the absence or presence of inertia. The dynamical setting usually involves wave propagation but there are no waves in the quasi-static setting. One might expect that the quasi-static setting would give the large time solution after waves have damped out.

If body forces are absent and the field is in equilibrium, then the equilibrium equation can be expressed in terms of stress σ as $\nabla \bullet \sigma = 0$, where $\nabla \bullet$ is divergence operator, and σ is the Piola stress which is the force per undeformed area [1977K]. Hence for an one-dimensional system the equilibrium equation can be expressed in terms of stress σ as $\sigma'(X) = 0$, here $'$ denotes differentiation. The equilibrium equation may be locally elliptic, parabolic or hyperbolic depending on the material and the deformation. Knowles and Sternberg (see [1978K]) showed that the equation type was established from the local slope of the stress-strain relation as follows

$$\bar{\sigma}'(\gamma) > 0 \Leftrightarrow elliptic,$$
$$\bar{\sigma}'(\gamma) = 0 \Leftrightarrow parabolic,$$
$$\bar{\sigma}'(\gamma) < 0 \Leftrightarrow hyperbolic,$$

where $\bar{\sigma}(\gamma)$ is stress and γ is strain. If the equilibrium field contains a curve along which the partial derivative of displacement fails to be continuous, the curve is known as an equilibrium shock or a stationary phase boundary. Equilibrium shocks affect the balance of the energy in the elastostatic field [1977K], [1978K] and [1979K]. Abeyaratne [1983A] has derived "equilibrium shocks" on which the deformation gradient and stress are discontinuous across certain internal material surfaces. Equilibrium equations, natural boundary conditions, traction continuity condition and a supplementary jump condition are also derived. Finally he concluded that this supplementary jump condition implied that a stable equilibrium shock must necessarily be dissipation-free. Kikuchi and Triantafyllidis [1982K] also explored the admissible equilibrium solutions to the Euler-Lagrange equation for a minimization problem of the energy.

Abeyaratne and Knowles [1987AA] have investigated a twist problem in the theory of finite deformations of elastic materials whose associated equation of equilibrium does not remain elliptic at all strains. Abeyaratne and Knowles [1989A] have concluded some elastic materials are capable of sustaining finite equilibrium deformations with discontinuous strains. Boundary value problems for such "unstable" elastic materials often pose an infinite number of solutions. Abeyaratne and Knowles [1987A] have considered maximally dissipative quasi-static motions and found the possibility of modeling dissipative mechanical response in solids, on the basis of the equilibrium theory of finite elasticity for materials that may lose ellipticity at large strains. The result permits the occurrence of discontinuous displacements gradients. For quasi-static motions, one can obtain an unique solution by requiring that all equilibrium states are minimizers of the potential energy functional. The present value of twist is then uniquely determined by the present value of torque and vice-versa, as in conventional elasticity. But in contrast, for maxi-

mally dissipative motions, twist depends on the past history of torque during the motion, as in plasticity.

Abeyaratne and Knowles [1987AA] have concluded that quasi-static motions, for which the equation of equilibrium does not remain elliptic at all strains, may be dissipative. In particular, they show that the macroscopic response in the problem treated may correspond to elastic-perfectly plastic behavior. It was shown that the quasi-static response of a bar to a prescribed force history is then fully determined if one considers additional information in the form of a kinetic relation [1989A]. In particular, they show how unstable elastic materials can be used to model macroscopic behavior as in viscoplasticity.

Neither the equilibrium setting nor the quasi-static setting treats truly dynamical problems involving wave propagation. Due to nonuniqueness of dynamical solutions, a number of authors have studied many criteria to single out an unique solution. An entropy is defined to be a ratio between the heat transfer to the system and the absolute temperature in a reversible process. Moreover a dissipation, or degradation, is defined to be the difference between the maximum possible work and the actual output. In an adiabatic system the dissipation is proportional to the increase of entropy. In this setting the principle of increase of the entropy is simply another statement of dissipation of energy. Both of which are also equivalent to the second law of thermodynamics. Dafermos [1973D] extended the entropy admissibility criterion of Lax [1973L] to entropy rate admissibility criterion for solutions of a hyperbolic system of conservation laws. The selected solutions are those in which the total entropy decreases with the highest possible rate.

Dynamical phase transitions are also a highly studied topic in gas dynamics [1983H], [1986H], [1991AAA]. The van der Waals fluid problem could be viewed as a counterpart of the phase transformation problem in finite elasticity. Moving phase boundaries are kinematically similar to other types of shock fronts in that velocity and

strain are discontinuous across them. Hagan and Slemrod [1983H] have investigated admissibility criteria for nonlinear conservation laws based on capillarity and viscosity, and found results consistent with experiment for materials which exhibit phase transitions by means of specific examples. Here an important concept is the *Maxwell stress* $\sigma = \sigma_{maxwell}$, which is uniquely defined by the requirement that the two loops enclosed by the stress-strain curve $\sigma = \bar{\sigma}(\gamma)$ and the horizontal line $\sigma = \sigma_{maxwell}$ are equal in area. Hattori [1986H] has treated special Riemann problems and shown that the well known Maxwell construction is admissible, according to the entropy rate criterion. Affouf and Caflisch [1991AAA] have presented a numerical study of isothermal fluid equations with a nonmonotone equation of state. It can serve as a model for describing dynamic phase transitions, and the model can explore an analytic argument for stability of phase transitions.

The analysis of the fully dynamical motion of a phase boundary for a specific class of elastic materials whose stress-strain relation in simple shear is nonmonotone can be found in Pence [1991P], [1991PP]. It was shown that the ringing of a shear pulse between the external boundaries and an internal phase boundary gives rise to periodic phase boundary motion for both the case of a completely reflecting phase boundary and the case of a completely transmitting phase boundary [1991P]. The possibly infinite solutions that are not completely reflecting or completely transmitting are examined from the perspective of energy and dissipation. It is shown that there also exist at most two solutions which involve no dissipation, and one solution that maximizes the mechanical energy dissipation rate [1991PP].

Similar topics in one-dimensional elasticity can be found in [1980J], [1986P], [1987P]. Pence investigated emergence and propagation of a phase boundary in an elastic bar, whose stress-strain relation is nonmonotonic [1986P]. An asymptotic description of the emergence of the phase boundary was provided for short times. The energetic behav-

ior of a phase boundary that is subjected to concurrent dynamic pulses under a maximally dissipative criterion and under a kinetic criterion is studied by Lin and Pence ([1992L], [1993L]).The results show that the total energy loss is different from that which would occur if the two pulses were not concurrent. The dissipation which is due to wave ringing in non-elliptic elastic materials for large time is explored by Lin and Pence ([1993LL]. They set up a framework for treating the resulting wave reverberations and computing the energy dissipation for large time. Their numerical results show that the large time energy dissipation matches that which is necessary to settle into a new energy minimal equilibrium state. They obtain the same results analytically for the special case of a small dynamical perturbation.

A very elegant mathematical investigation of a related problem can be found in Ball et al [1991B]. They explore mathematical models for the dynamical behavior of mechanical systems that dissipate energy as time increases, and establish global existence and uniqueness results for the long time behavior of the systems. This provides insight into the dynamical development of finer and finer microstructure by certain material phase transformations.

The lack of uniqueness of solutions to these problems can also be resolved by imposing two constitutive requirements, a nucleation criterion and a kinetic relation [1988AA], [1990A], [1991A], [1991AA]. A kinetic relation can be in a form $f = \varphi(\dot{s})$, where f is the driving traction acting at the phase boundary and $\dot{s}$ is the phase boundary velocity. The relation between the driving traction on the phase boundary and the phase boundary velocity is similar to the relation between maximum dissipation to the maximum plastic work [1992A]. If one adds the viscosity and second strain gradient to the elastic part of the stress, it is equivalent to the imposition of a particular kinetic relation at the phase boundaries that propagate subsonically [1988AA], [1991A]. In a general thermomechanical process, the kinetic relation could be function of the driving traction and tem-

io

di

[1

oc

in

Th

the

erg

equ

dyr

Bal

char

and

into

phas

posi

[198

wher

veloc

boun

plast

part (

phase

mech

ior of a phase boundary that is subjected to concurrent dynamic pulses under a maximally dissipative criterion and under a kinetic criterion is studied by Lin and Pence ([1992L], [1993L]).The results show that the total energy loss is different from that which would occur if the two pulses were not concurrent. The dissipation which is due to wave ringing in non-elliptic elastic materials for large time is explored by Lin and Pence ([1993LL]. They set up a framework for treating the resulting wave reverberations and computing the energy dissipation for large time. Their numerical results show that the large time energy dissipation matches that which is necessary to settle into a new energy minimal equilibrium state. They obtain the same results analytically for the special case of a small dynamical perturbation.

A very elegant mathematical investigation of a related problem can be found in Ball et al [1991B]. They explore mathematical models for the dynamical behavior of mechanical systems that dissipate energy as time increases, and establish global existence and uniqueness results for the long time behavior of the systems. This provides insight into the dynamical development of finer and finer microstructure by certain material phase transformations.

The lack of uniqueness of solutions to these problems can also be resolved by imposing two constitutive requirements, a nucleation criterion and a kinetic relation [1988AA], [1990A], [1991A], [1991AA]. A kinetic relation can be in a form $f = \varphi(\dot{s})$, where f is the driving traction acting at the phase boundary and $\dot{s}$ is the phase boundary velocity. The relation between the driving traction on the phase boundary and the phase boundary velocity is similar to the relation between maximum dissipation to the maximum plastic work [1992A]. If one adds the viscosity and second strain gradient to the elastic part of the stress, it is equivalent to the imposition of a particular kinetic relation at the phase boundaries that propagate subsonically [1988AA], [1991A]. In a general thermomechanical process, the kinetic relation could be function of the driving traction and tem-

perature [1990A]. It is also possible that a modified version of the entropy rate admissibility criterion can act as a particular kind of kinetic relation.

For complicated boundary value problems, it is very difficult to find analytical solutions. Therefore we need numerical analysis to obtain approximate solutions. Numerical analysis using these types of phase transition models can be found in [1988SS]. Silling applied numerical analysis to plane strain equilibrium problems in finite elasticity using a finite-difference dynamic relaxation method. He has claimed this method is useful for the study of localization and phase changes in elastic solids.

Silling [1988S] has also applied numerical analysis to the equilibrium anti-plane shear deformations for materials in which the governing equation varies in type locally from elliptic to hyperbolic. This extends Ericksen's analysis for bars to the two-dimensional case by numerical analysis. He has shown the emergence of surfaces of discontinuity in the displacement field in a weakening material and in a trilinear material, and has also found the solution to equilibrium problems by using the dynamic relaxation method.

1.3 Section overview

It is obvious from the literature review that nonuniqueness of the strain-softening material is an important issue which is not yet fully resolved. In order to better understand the nonuniqueness of the strain-softening material, we choose a simple system, a bar, to model the behavior. We study the phase transition behavior of the bar both analytically and numerically. Unfortunately, there are few numerical analysis results obtained by using finite element method (FEM) for this kind of problem. One of the purposes of this thesis is to study the connections between the analytical results and numerical results which are obtained by using FEM.

We are concerned with the phase transformation induced by stress within a strain-softening bar. The main goal is comparing the solutions of the analytical study with those

of the numerical study. That is why we devote nine sections, from Section 1 to Section 9, to the analytical study.

This dissertation is divided into sixteen sections. The first section is an introduction. The next fourteen sections, from Section 2 to Section 15, are grouped into two parts. In Part I, from Section 2 to Section 9, there is an analytical study of a continuous system. In Part II, from Section 10 to Section 15, there is a numerical study (FEM) of the associated discrete system. Two example materials: material A and material B, meaning two specific nonlinear elastic response functions, are considered in detail. The material properties which give strain-softening behavior are described in Section 2 (see Figure 1). Phase-I is defined to be the phase of strain between 0 and 1, while phase-II is defined to be the phase with strains greater than 1. Section 2 derives the elastic stress response density function, the corresponding strain energy function, and an elastic secant modulus function.

In Section 3, two loading devices, the soft device and the hard device, are introduced. For the soft device the bar is firmly fixed at one end while the other end is subjected to a given dead load. Correspondingly, for the hard device the bar is also firmly fixed at one end while the other end is subjected to a given displacement.

If we consider the material described in Section 2, then at each point in the bar there are two possible phases, either the lower strain phase (phase-I) or the high strain phase (phase-II), to choose from. For a bar having, at most, two regions in different phases, there exist four possible ways to arrange these phases: (1,1), (1,2), (2,1) and (2,2). For example the (1,2)-case is a state with the lower strain phase on the left and the high strain phase on the right. Section 4 is devoted to the study of two phase equilibrium configurations with a single phase boundary. The energy functions for the soft device and hard device are also derived.

In Section 5 we introduce and discuss the *solution region* for problems with a single phase boundary. This is done for both devices. By solution region we mean, in brief, a parameter plane region of stress σ vs. average strain γ_o for possible solutions. We study the solution region in the (1,2)-case. In particular we first explore the lines of constant stress σ where σ is defined in (3). Secondly we explore the lines of constant strain γ_o where γ_o is defined in (18). Finally we explore the lines of constant s where s is a non-dimensional location parameter for the phase boundary and is defined in (22).

The corresponding hard device energy functions on the boundary, lines of constant σ, lines of constant γ, and lines of constant s within the solution region in the (1,2)-case are discussed in Section 6. The minimum energy criterion is introduced at the end of the section. Similarly, Section 7 is devoted to the soft device.

Quasi-static motion is defined and introduced in Section 8. The dissipation and the driving traction at the phase boundary of a bar are discussed. We study the admissible direction of movement of the phase boundary by the second law of thermodynamics under isothermal conditions. Finally we study the admissible paths which have a non-negative product of the phase boundary velocity and the driving traction at the phase boundary.

Recall from literature review that if the local slope of stress-strain relation is negative then the equilibrium equation is non-elliptic. For a non-elliptic equilibrium equation the solutions are not always unique. Since the massive failure of uniqueness is related to the stress-strain relation which is the constitutive relation of material, this kind of non-uniqueness has been viewed by some as a constitutive deficiency. To resolve a constitutive deficiency, one may supplement the theory with a kinetic criterion which applies to phase boundaries only [1989A]. The kinematics of the phase boundary and the admissible paths with such a kinetic criterion are discussed in Section 9.

To analyze this boundary value problem (sketched in Figure 3) numerically we choose the finite element method. At first the basic finite element formulation of a bar element is derived in Section 10. Second, we select two-node elements to compute the interpolation functions (160) and the element equation (163). Third we assemble the element equations of each element into a resulting system equation (175). After this we consider boundary conditions for both the hard and soft devices to find a reduced system equation ((184) or (188)) for a general N-element model. Finally we discuss an iterative scheme to find the solution from an initial guess.

In Section 11 we first find the solutions of the system equation for a two-element model. We study the relations between the solutions and the possible nodal displacements to explore the nonuniqueness. This simplest of all possible cases allows us to observe how the nonuniqueness in analytical solutions translates into nonuniqueness in numerical FEM solutions. Then we investigate the corresponding energy as a function of the possible nodal displacements and relate this to the convergence and divergence of the iteration scheme.

Similarly in Section 12 the available solutions for a three-element model are discussed as in Section 11. In Section 13 the available solutions for $N>3$ are discussed.

For resolving the nonuniqueness issues mentioned above we explore the numerical results using the finite element method under either a minimum energy solution criterion or else a kinetic criterion. Several algorithms are chosen to implement the kinetic criterion. Then the results obtained by using these algorithms are compared. This is done for material A in Section 14 and for material B in Section 15. In particular, for the kinetic criterion we compare the exact solutions and the solutions which are obtained by using the finite element method. Finally we determine the FEM solutions obtained using the kinetic criterion for three ramp loadings with different loading rates.

In Section 16 we have the conclusions from this study and recommendations for future work.

2. The material model

In this thesis we consider a compressible homogeneous isotropic hyperelastic bar with unit cross section area. The bar in the reference configuration is described by the region $R = \{0 \le X \le L\}$. In the deformed configuration the particle at X in the undeformed state is moved to $X + u(X)$, where $u(X)$ is the displacement of the particle originally at X. The strain $\hat{\gamma} = du(X)/dX$ of the particle at X is restricted to the range $\hat{\gamma} \ge -1$ in order to assure that the mapping $X \to X + u(X)$ is invertible; in fact, we shall limit attention to $\hat{\gamma} \ge 0$. The elastic stress response function of the bar is taken to be in the following:

$$\hat{\sigma}(\hat{\gamma}) = \begin{cases} \hat{\sigma}_I(\hat{\gamma}) = \hat{E}\hat{\gamma}, & \hat{\gamma} \le \hat{\gamma}_M, \\ \hat{\sigma}_{II}(\hat{\gamma}), & \hat{\gamma} > \hat{\gamma}_M, \end{cases} \tag{1}$$

where $\hat{\sigma}_{II}(\hat{\gamma})$ will be given in what follows. Note that $\hat{\sigma}_I(\hat{\gamma})$ is a linear function of $\hat{\gamma}$ and $\hat{E}$ is a positive constant, but $\hat{\sigma}_{II}(\hat{\gamma})$ may not be. In particular, the behavior of a strain-softening $\hat{\sigma}_{II}(\hat{\gamma})$, *a behavior in which the stress declines for increasing strain*, is investigated. Note from Figure 1 that $\hat{\sigma}_{II}(\hat{\gamma})$ is strictly decreasing (and hence invertible) and has the fol-
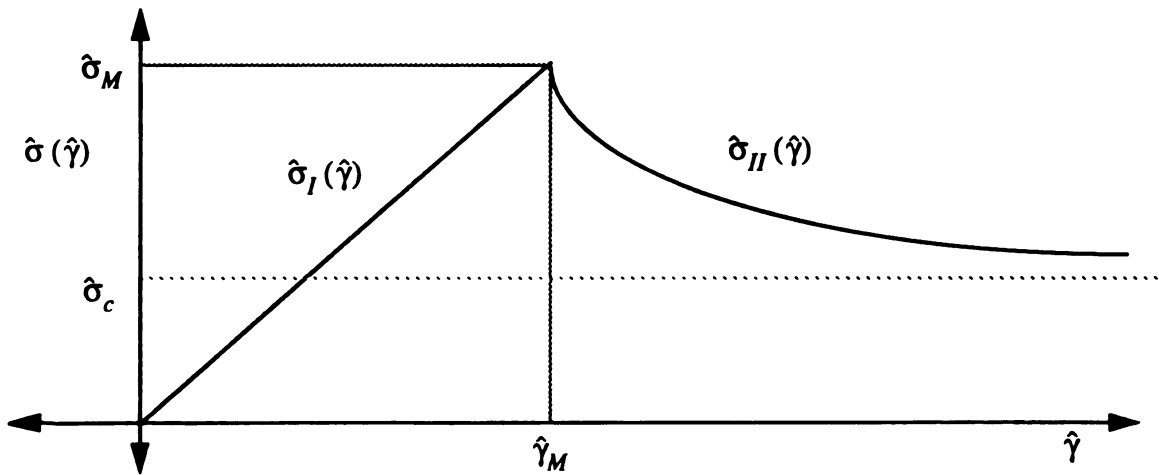
Figure 1. The stress response function of the bar with positive strain.

lowing properties:

$$\hat{\sigma}_c < \hat{\sigma}_{II}(\hat{\gamma}) \le \hat{\sigma}_M,$$

$$\hat{\sigma}_{II}'(\hat{\gamma}) < 0,$$

$$\hat{\sigma}_{II}''(\hat{\gamma}) > 0, \qquad (2)$$

$$\hat{\sigma}_{II}(\hat{\gamma}) \to \hat{\sigma}_c \ge 0, \qquad \text{when} \qquad \hat{\gamma} \to \infty.$$

Here ' denotes differentiation. The stress response function of the bar is described by two

strain phases: the phase of strain from 0 to $\hat{\gamma}_M$ is called the lower strain phase (phase-I) and

the phase of strain greater than $\hat{\gamma}_M$ is called the high strain phase (phase-II).

If two non-dimensional parameters are introduced

$$\gamma = \frac{\hat{\gamma}}{\hat{\gamma}_M}, \qquad \bar{\sigma} = \frac{\hat{\sigma}}{\hat{\sigma}_M}, \qquad (3)$$

then the non-dimensionalized stress response function (see Figure 2) of the bar may be re-

written as

$$\bar{\sigma}(\gamma) = \begin{cases} \bar{\sigma}_I(\gamma) = \gamma, & \gamma \le 1, \\ \bar{\sigma}_{II}(\gamma), & \gamma > 1. \end{cases} \qquad (4)$$
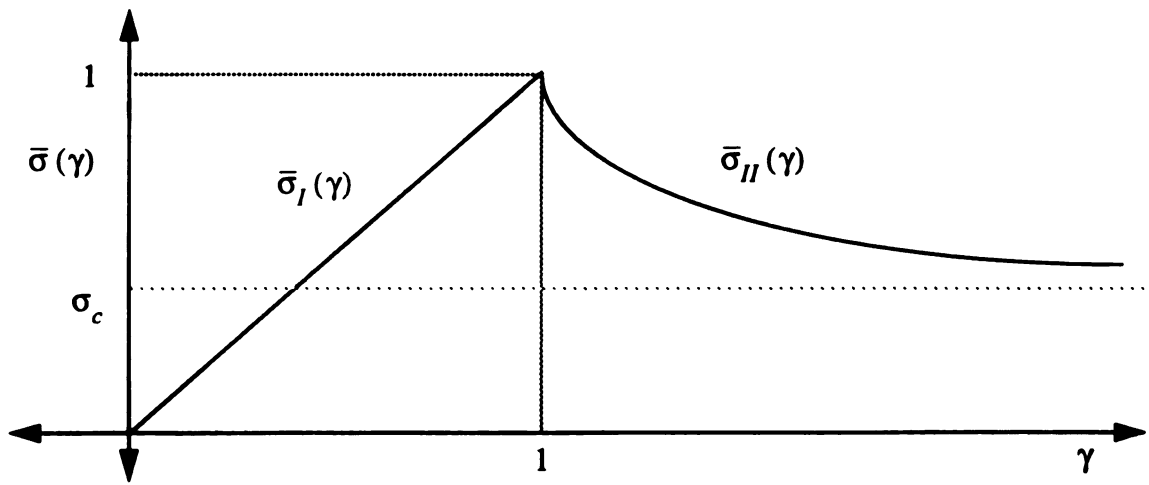
Figure 2. The non-dimensionalized stress response function of the bar which is used in
this thesis.

Note that $\bar{\sigma}_I(\gamma)$ is also a linear function of γ and $\bar{\sigma}_{II}(\gamma)$ has the following properties:

$$\sigma_c < \bar{\sigma}_{II}(\gamma) \leq 1,$$
$$\bar{\sigma}_{II}'(\gamma) < 0,$$
$$\bar{\sigma}_{II}''(\gamma) > 0,$$
$$\bar{\sigma}_{II}(\gamma) \to \sigma_c \geq 0 \quad \text{when} \quad \gamma \to \infty, \tag{5}$$

where $\sigma_c = \hat{\sigma}_c/\hat{\sigma}_M$. Now phase-I is the phase of strain from 0 to 1 and phase-II is the phase of strain greater than 1.

Since both $\bar{\sigma}_I(\gamma)$ and $\bar{\sigma}_{II}(\gamma)$ are invertible, the associated inverse functions can be rewritten in terms of σ. This gives the corresponding inverse functions

$$\gamma = \Gamma_i(\sigma), \qquad i = I \text{ or } II. \tag{6}$$

Note from (4)$_1$ that $\Gamma_I(\sigma) = \sigma$. The corresponding normalized strain energy density function $W(\gamma)$ is given by

$$W(\gamma) = \begin{cases} \dfrac{\gamma^2}{2}, & \gamma \leq 1, \\ \dfrac{1}{2} + \int_1^\gamma \bar{\sigma}_{II}(\gamma)\,d\gamma, & \gamma > 1, \end{cases} \tag{7}$$

so that the stress is equal to the first derivative of the strain energy density function,

$$\bar{\sigma}(\gamma) = W'(\gamma). \tag{8}$$

Note since $\bar{\sigma}_{II}(\gamma) \to \sigma_c \geq 0$ as $\gamma \to \infty$ that

$$\lim_{\gamma \to \infty} W(\gamma) > 0, \tag{9}$$

however the limit

$$\lim_{\gamma \to \infty} (W(\gamma) - \gamma\sigma_c) \equiv W_c > 0 \tag{10}$$

may or may not be finite depending on the rate at which $\bar{\sigma}_{II}(\gamma) \to \sigma_c$. Here W_c is the area under the stress-strain curve which is also above the horizontal line $\sigma = \sigma_c$.

Two particular functions for $\bar{\sigma}_{II}(\gamma)$ are given in Appendix-A and Appendix-B.

These functions are used from time to time in examples in this thesis. Thus we say that these functions define two example materials: material A and material B. Both of these materials have $\sigma_c = 1/2$, however material A has $W_c = \infty$ while material B has a finite value of W_c.

Let $\sigma(X)$ be the stress field in the bar, then the equilibrium equation, with no body force, is given by

$$\frac{d}{dX}\sigma(X) = 0. \tag{11}$$

Therefore, the stresses along the bar are spatially constant,

$$\sigma(X) = \text{constant}, \qquad 0 \le X \le L. \tag{12}$$

In what follows it will be convenient to define an elastic secant modulus function by

$$E(\gamma) = \bar{\sigma}(\gamma)/\gamma, \tag{13}$$

giving

$$E(\gamma) = \begin{cases} E_I(\gamma) = 1, & \gamma \le 1, \\ E_{II}(\gamma) = \dfrac{\bar{\sigma}_{II}(\gamma)}{\gamma}, & \gamma > 1. \end{cases} \tag{14}$$

3. Two loading devices

In this study two standard types of loading procedures, the soft device and the hard device as depicted pictorially in Figure 3, are considered.

3.1 Soft device (Figure 3)

Here the bar is firmly fixed at one end while the other end is subjected to a given dead constant load $F = F_o = A\sigma_o = \sigma_o$. Since the cross sectional area $A = 1$, the boundary conditions are $u(0) = 0$ and $\sigma|_{X=L} = \sigma_o$. This is the so-called *force problem* that consists of finding an unknown displacement field u satisfying the boundary conditions. The solution is not unique in this problem. For example:

$$\sigma_o < \sigma_c \Rightarrow 1 \text{ solution,}$$
$$\sigma_c < \sigma_o < 1 \Rightarrow \infty \text{ solutions,} \qquad (15)$$
$$\sigma_o > 1 \Rightarrow \text{no solution.}$$
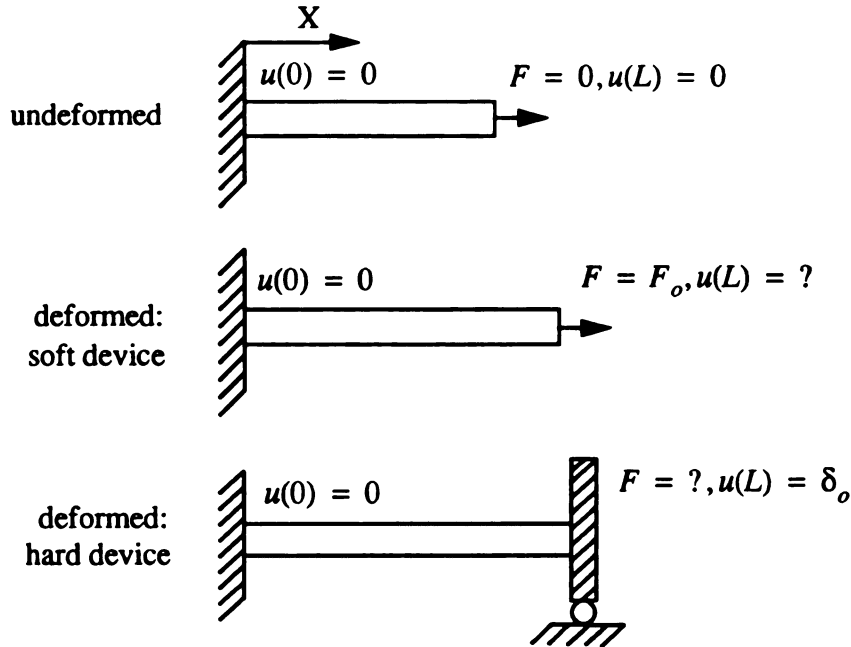
Figure 3. Undeformed and deformed configurations of soft device and hard device.

From (4), (5) and Figure 2 the only admissible value of strain whenever $\sigma_o < \sigma_c$ is $\gamma = \sigma_o$, so that the bar has one solution which is phase-I everywhere. Hence σ_c has the interpretation of being the low limit on the stress that can support phase-II. It is impossible to have solutions for $\sigma > 1$ because the bar cannot resist the stress greater than 1. The case $\sigma_c < \sigma < 1$ is more complicated and interesting. The bar could be in a mixed state of phase-I and phase-II, since then two values of strain are compatible with the one value of stress. The final elongation will then depend on the fraction of the bar which is in phase-I versus the fraction of the bar which is in phase-II. In particular, if the bar is partitioned into n sections, then each section could be in either phase-I or phase-II. In fact, there would be 2^n choices. Therefore, if the number of sections is increased, then the number of choices is increased too. In this way an infinite number of solutions could be constructed. For the force problem, classical absolutely stable equilibrium configurations must minimize the following soft device energy function

$$\Xi = \int_0^1 W(\gamma) d(\frac{X}{L}) - \frac{\sigma_o u(L)}{L}. \tag{16}$$

3.2 Hard device (Figure 3)

On the other hand, if the bar is firmly fixed at one end while the other end is subjected to a given constant displacement $\delta_o > 0$, then the boundary conditions are $u(0) = 0$ and $u(L) = \delta_o$. Let $\gamma_o \equiv \delta_o/L$ be the average strain in the bar. This is the so-called *elongation problem* that consists of finding of an unknown constant force $F = \sigma_o$ and a displacement field $u(X)$ satisfying the boundary conditions. Again the solution is not unique in this problem and it will be described in more detail in Section 5. For this problem, classical absolutely stable equilibrium configurations must minimize the following hard device energy function

$$\Lambda = \int_0^1 W(\gamma) d\left(\frac{X}{L}\right). \tag{17}$$

In what follows the applied load σ_o will be replaced by σ for simplicity. In this study, the hard device problem is our main focus, and unless it is to remark otherwise, the reader should assume that the hard device case is under consideration.

4. Two phase equilibrium configurations with a single phase boundary

The nonmonotone stress response function permits two values of strain to give the same value of stress. Thus solutions (12) to (11) may involve alternating regions along the bar of these two strain values. Imagine that there are two different strain regions in the bar, each with constant strain γ_L and γ_R separated at $X = h$ with $0 < h < L$. If γ_L and γ_R are the strains of the left hand side and the right hand side respectively, then

$$\gamma = \begin{cases} \gamma_L, & 0 \leq X \leq h, \\ \gamma_R, & h \leq X \leq L. \end{cases} \tag{18}$$

Note from (12) that the stresses are equal on the both sides of the phase boundary location,

$$\sigma = \bar{\sigma}_i(\gamma_L) = \bar{\sigma}_j(\gamma_R), \qquad i, j = I \text{ or } II. \tag{19}$$

Therefore the inverse functions in (6) can be written as

$$\begin{aligned} \gamma_L &= \Gamma_i(\sigma), & i = I \text{ or } II, \\ \gamma_R &= \Gamma_i(\sigma), & i = I \text{ or } II. \end{aligned} \tag{20}$$

Accordingly, there are four cases which will be denoted by

$$\begin{aligned} &(1,1)\text{-case} & when & \quad 0 \leq \gamma_L \leq 1 & and & \quad 0 \leq \gamma_R \leq 1 \Rightarrow i = I,\ j = I, \\ &(1,2)\text{-case} & when & \quad 0 \leq \gamma_L \leq 1 & and & \quad \gamma_R \geq 1 \Rightarrow i = I,\ j = II, \\ &(2,1)\text{-case} & when & \quad \gamma_L \geq 1 & and & \quad 0 \leq \gamma_R \leq 1 \Rightarrow i = II,\ j = I, \\ &(2,2)\text{-case} & when & \quad \gamma_L \geq 1 & and & \quad \gamma_R \geq 1 \Rightarrow i = II,\ j = II. \end{aligned} \tag{21}$$

For the (1,1)-case and the (2,2)-case, the strains γ_L and γ_R are equal and so the location h is not of significance. However it will be important to consider these two "trivial" cases in what follows as naturally limiting states when either $h \to 0$ or $h \to L$. The location $X = h$ in the (1,2)-case and the (2,1)-case have the interpretation of being a phase boundary.

It is useful to introduce a non-dimensional phase boundary location parameter

$$s = \frac{h}{L}, \tag{22}$$

then by virtue of the boundary conditions $u(0) = 0$ and $u(L) = \delta_o$, it can be obtained that

20

$$\gamma_L s + \gamma_R (1 - s) = \frac{\delta_o}{L} \equiv \gamma_o. \tag{23}$$

Now, by using (17), the hard device energy function of the bar is given by

$$\Lambda_{ij} = \int_0^s W_i(\gamma_L) d\left(\frac{X}{L}\right) + \int_s^1 W_j(\gamma_R) d\left(\frac{X}{L}\right) \left.\vphantom{\int}\right\} \begin{array}{l} i = 1(\mathrm{I}) \text{ or } 2(\mathrm{II}), \\ j = 1(\mathrm{I}) \text{ or } 2(\mathrm{II}). \end{array} \tag{24}$$
$$= W_i(\gamma_L) s + W_j(\gamma_R)(1 - s) = \hat{\Lambda}_{ij}(\sigma, \gamma_o) \left.\vphantom{\int}\right\}$$

In this thesis, a superposed $\wedge$ will indicate that the quantity is regarded as a function of σ

and γ_o. For $\hat{\Lambda}_{ij}(\sigma, \gamma_o)$ this requires the use of (6) for γ_L and γ_R; also the elimination of s

uses (23) to define the function $\hat{s}_{ij}(\sigma, \gamma_o)$, where

$$s = \frac{\gamma_R - \gamma_o}{\gamma_R - \gamma_L} = \frac{\Gamma_j(\sigma) - \gamma_o}{\Gamma_j(\sigma) - \Gamma_i(\sigma)} \equiv \hat{s}_{ij}(\sigma, \gamma_o). \tag{25}$$

Similarly, from (16), the soft device energy function of the bar is provided by

$$\Xi_{ij} = \int_0^s W_i(\gamma_L) d\left(\frac{X}{L}\right) + \int_s^1 W_j(\gamma_R) d\left(\frac{X}{L}\right) - \sigma\gamma_o \left.\vphantom{\int}\right\} \begin{array}{l} i = 1(\mathrm{I}) \text{ or } 2(\mathrm{II}), \\ j = 1(\mathrm{I}) \text{ or } 2(\mathrm{II}). \end{array} \tag{26}$$
$$= W_i(\gamma_L) s + W_j(\gamma_R)(1 - s) - \sigma\gamma_o = \hat{\Xi}_{ij}(\sigma, \gamma_o) \left.\vphantom{\int}\right\}$$

Note that $\hat{\Xi}_{ij}(\sigma, \gamma_o)$ is also a function of σ and γ_o.

5. The solution region with a single phase boundary

The two-phase hard device problem involves finding σ satisfying (23), (6) and the condition $\bar{\sigma}(\gamma_L) = \bar{\sigma}(\gamma_R)$. Here the freedom to let s take on any value in $0 < s < 1$ gives rise to similar nonuniqueness phenomena as discussed for the soft device problem in Section 3.1. In particular, given γ_o, there is often a range of σ that satisfy the above conditions. This range shall be denoted by $\Pi(\gamma_o)$. As γ_o increases from 0, it can be imagined that this set $\Pi(\gamma_o)$ sweeps out a solution region $\Omega = \{ (\gamma_o, \Pi(\gamma_o)) | \gamma_o > 0 \}$ in a (γ_o, σ)-plane. This "solution region" representation will be extremely useful in this thesis and so will be described now in some detail for each of the four cases given in (21). The solution regions will be denoted by Ω_{ij} for each separate case.

Solutions only exist for the (1,1)-case if $0 < \gamma_o < 1$. Then the range $\Pi(\gamma_o)$ collapses to a point and the associated solution region is the straight line (see Figure 4)

$$\Omega_{11} = \{ (\gamma_o, \sigma) | \sigma = \bar{\sigma}_I(\gamma_o), 0 < \gamma_o < 1 \}. \tag{27}$$

Solution only exist for the (2,2)-case if $\gamma_o > 1$. Then again the range $\Pi(\gamma_o)$ collapses to a point and the associated solution region is the curve (see Figure 5)

$$\Omega_{22} = \{ (\gamma_o, \sigma) | \sigma = \bar{\sigma}_{II}(\gamma_o), \gamma_o > 1 \}. \tag{28}$$

On the other hand for the (1,2)-case, solutions exist if $\gamma_o > \sigma_c$ and are given by (see Figure 6):
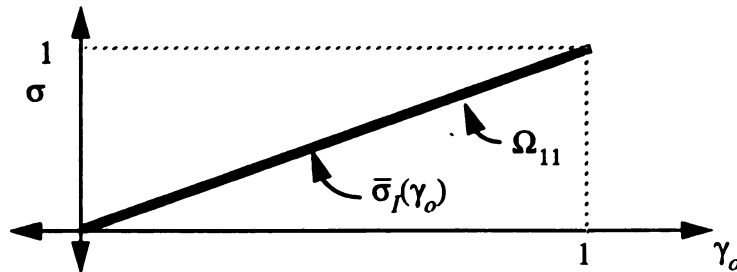
Figure 4. The solution region Ω_{11}.
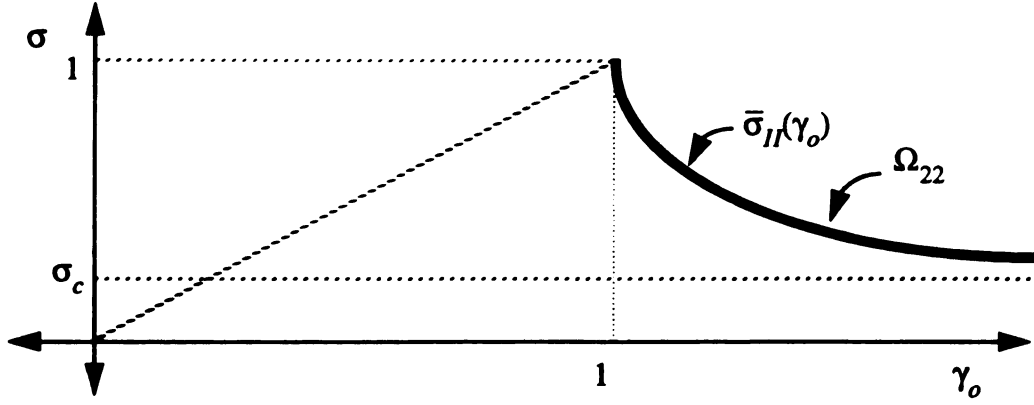
Figure 5. The solution region Ω_{22}.

$$\Omega_{12} = \{ (\gamma_o, \sigma) \mid \sigma_c < \sigma < \bar{\sigma}_I(\gamma_o), \text{ if } \sigma_c < \gamma_o < 1; \sigma_c < \sigma < \bar{\sigma}_{II}(\gamma_o), \text{ if } \gamma_o \geq 1 \}. \qquad (29)$$

Here $\Pi(\gamma_o)$ is the stress interval $\sigma_c < \sigma < \bar{\sigma}_I(\gamma_o)$ if $\sigma_c < \gamma_o < 1$, while $\Pi(\gamma_o)$ is the stress interval $\sigma_c < \sigma < \bar{\sigma}_{II}(\gamma_o)$ if $\gamma_o > 1$. For a given $(\gamma_o, \sigma) \in \Omega_{12}$, the associated phase boundary location s is given by (25), and values of s on the boundary of Ω_{12} are shown in Figure 6. Similarly, it is found that

$$\Omega_{21} = \Omega_{12}. \qquad (30)$$

However these solutions involve $s_{21} \to 1 - s_{12}$ so that the values of s on the boundary of Ω_{21} are shown in Figure 7. Finally the solution regions for the all four cases are shown in
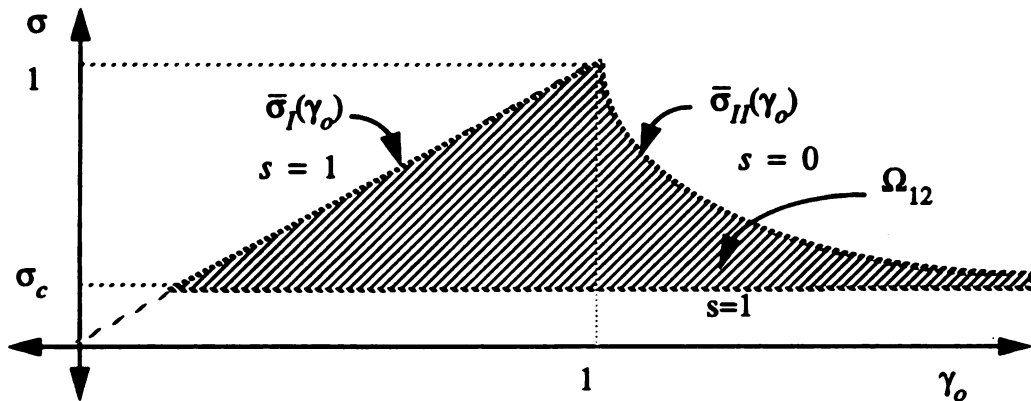
Figure 6. The solution region Ω_{12}.
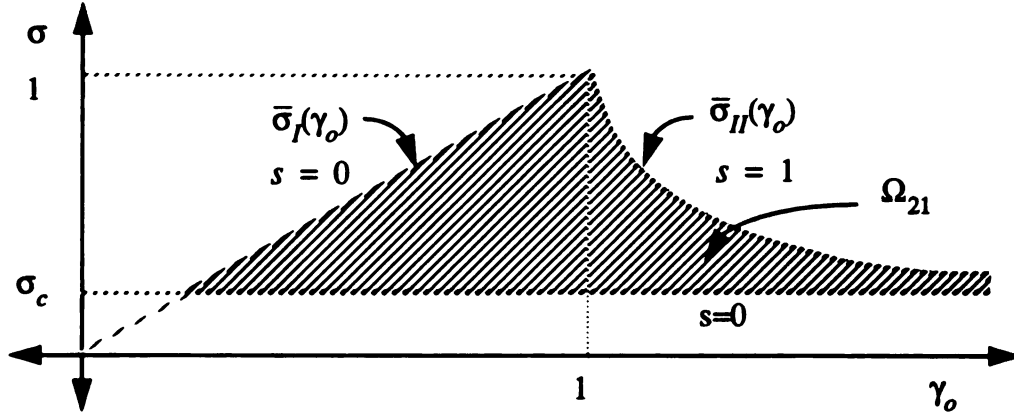
Figure 7. The solution region Ω_{21}.
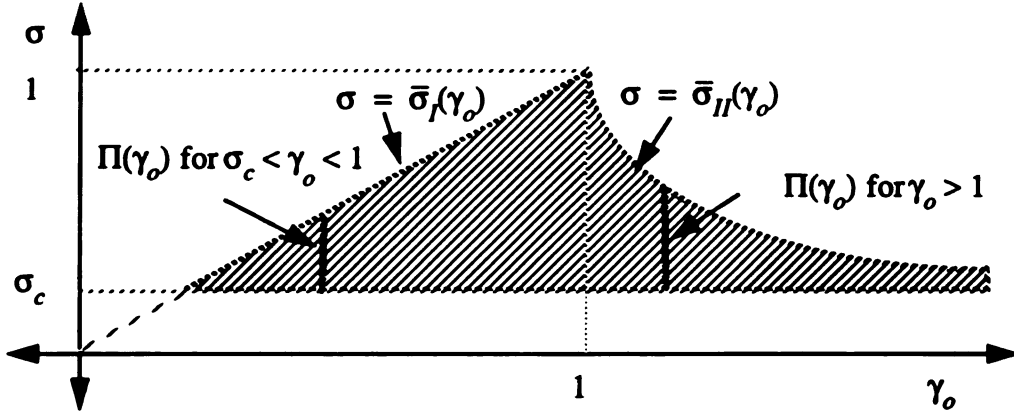
Figure 8. The solution regions Ω_{11}, Ω_{12}, Ω_{21} and Ω_{22}.

Figure 8.

The above discussions of Ω_{11}, Ω_{12}, Ω_{21} and Ω_{22} are based on the hard device problem, however, they also can apply to the soft device problem. That is, given σ, there is also a range of γ_o that satisfy (23). And according to $0 < s < 1$ the value of γ_o is always between $\Gamma_I(\sigma)$ and $\Gamma_{II}(\sigma)$. As σ increases from 0 to σ_c there is an unique solution $\sigma = \gamma_o$. While as σ increases from σ_c, it is easy to imagine the range of γ_o which satisfies (23) sweeping out the same solution region.

In what follows, the (1,2)-case is studied. The following discussion will further

make clear why Ω_{12} has the form given in Figure 6.

5.1 The boundary of Ω_{12}

From (29) and Figure 6 the boundary of Ω_{12} consists of three curves: $\sigma = \bar{\sigma}_I(\gamma_o)$, $\sigma = \bar{\sigma}_{II}(\gamma_o)$ and $\sigma = \sigma_c$. These three separate curves can be considered as limiting cases and are described in the following:

The curve $\sigma = \bar{\sigma}_I(\gamma_o)$ coincides with Ω_{11}. Therefore, it corresponds to a case in which the phase-II region has vanished. Since this phase-II region is to the right of the phase boundary for the (1,2)-case, the phase boundary has squeezed the phase-II region all the way to the end $X = L$, thus $s = 1$. The solutions along the curve $\sigma = \bar{\sigma}_I(\gamma_o)$ are therefore pure phase-I. Let's define $\varnothing_1$ to be this set of ordered pairs (γ_o, σ) which are pure phase-I solutions on the interval $\sigma_c < \sigma \leq 1$:

$$\varnothing_1 = \{ (\gamma_o, \sigma) | (\gamma_o = \sigma, \sigma_c < \sigma \leq 1) \}. \tag{31}$$

Similarly, the curve $\sigma = \bar{\sigma}_{II}(\gamma_o)$ coincides with Ω_{22}. So it corresponds to a case in which the phase-I region has disappeared. Since this phase-I region is to the left of the phase boundary for the (1,2)-case, the phase boundary has squeezed phase-I region all the way to the end $X = 0$, thus $s = 0$. The solutions along the curve $\sigma = \bar{\sigma}_{II}(\gamma_o)$ are pure phase-II solutions.

On the other hand, the curve $\sigma = \sigma_c$ has the interpretation of being an unattainable limit corresponding to an infinitely strained phase-II region of vanishing length. Like Ω_{11} it also corresponds to a case in which the phase-II region has vanished, but it doesn't coincide with the pure phase-I solutions of Ω_{11}. To understand this, recall that the total elongation is given by (23). Since phase-II is to the right of the phase boundary, the phase boundary squeezes the phase-II region all the way to the end $X = L$ when $s \to 1$. But the main

difference from Ω_{11} is that the phase-I region on the left $(0 \leq X \leq h)$ has the elongation

$\delta_o^l = \Gamma_I(\sigma_c) \lim_{h \to L} h = \sigma_c L$ while the phase-II region on the right $(h \leq X \leq L)$ has the elon-

gation $\delta_o^r = \lim_{\sigma \to \sigma_c} \Gamma_{II}(\sigma) \lim_{h \to L} (L - h)$. Here $\lim_{\sigma \to \sigma_c} \Gamma_{II}(\sigma) = \infty$ and $\lim_{h \to L} (L - h) = 0$ so

that the product which defines δ_o^r corresponds to $\infty \cdot 0$ where the rate of the one limit with

respect to the other is chosen so that the product δ_o^r remains fixed. Moreover the total elon-

gation at L is matched to $\delta_o^l + \delta_o^r = \delta_o = \gamma_o L$. For different points (γ_o, σ) along the

curve $\sigma = \sigma_c$ the elongations δ_o^l are always fixed at $\delta_o^l = \sigma_c L$ while the elongations δ_o^r

take on different values to match their corresponding γ_o, that is $\delta_o^r = \gamma_o L - \delta_o^l = $

$(\gamma_o - \sigma_c) L$ which is greater than zero since these solutions only exist for $\gamma_o > \sigma_c$.

5.2 Lines of constant γ_o in Ω_{12}

The lines of constant γ_o in Ω_{12} imply that the elongation is prescribed while there is a range

of nonunique σ which satisfy (25). Prescribing γ_o is the definition of the hard device.

Therefore, the lines of constant γ_o in Ω_{12} represent solutions to the hard device problem

for given average strain $\gamma_o = \delta_o / L$ associated with elongation δ_o. If the bar is elongated

with $\delta_o < \sigma_c L$, then the only possible solution corresponds to Ω_{11}. This means the elonga-

tion is not enough to reach phase-II. As a result, the bar is in pure phase-I and there is no

phase transition at this stage. If the bar is elongated with $\sigma_c L < \delta_o < L$, then the bar could

still be in pure phase-I. However it could also be in a mixed state of phase-I and phase-II,

but it cannot be in pure phase-II. On the other hand, if the bar is elongated with $\delta_o > L$, then

the bar could be in a pure phase-II solution; it could also be in a mixed state of phase-I and

phase-II but it cannot be in pure phase-I.

5.3 Lines of constant σ in Ω_{12}

The lines of constant stress σ with $\sigma > \sigma_c$ in Ω_{12} represent possible solutions to the soft device problem for given $F = \sigma > \sigma_c$. If the force $F = \sigma$ is prescribed with $\sigma < \sigma_c$, then the only possible solution corresponds to Ω_{11}. This also means that the prescribed force is not strong enough to reach the phase-II. As a result, the bar is in pure phase-I and there is also no phase transition at this stage. But if the bar is prescribed by the force $F = \sigma$ with $\sigma_c < \sigma < 1$, then there are an infinite number of possibilities corresponding to points in the lines of constant σ in Ω_{12}. The bar could then be in pure phase-I, pure phase-II or a mixed state of phase-I and phase-II.

5.4 Curves of constant s in Ω_{12}

It is to be noted from (25) that

$$s = \hat{s}_{12}(\sigma, \gamma_o) = \frac{\Gamma_{II}(\sigma) - \gamma_o}{\Gamma_{II}(\sigma) - \Gamma_{I}(\sigma)} \tag{32}$$

is a function of γ_o and σ in the (γ_o, σ)-plane and it is easy to imagine the level curves of fixed s in Ω_{12}. In this section the form of these curves in Ω_{12} is investigated. An example of the level curves is given in Figure 9 for a particular material (this particular choice of the function $\bar{\sigma}_{II}(\gamma)$ is given by (a.1) of Appendix-A). It will be convenient for our subsequent discussion to reorient to solution region Ω_{12} so that stress σ is the horizontal axis and average strain γ_o is the vertical axis. The reorientation that this gives for the constant s curves of Figure 9 are shown in Figure 10. For each fixed value of $s \in (0, 1)$, let $\gamma_o = \hat{\gamma}_o(\sigma)$ give the solutions to (32) so that the function $\hat{\gamma}_o(\sigma)$ defines a smooth curve on the (σ, γ_o)-plane. There is a family of such curves on the (σ, γ_o)-plane. Each curve corresponds to a different value of $s \in (0, 1)$ and it can be shown to be a single semi-infinite curve. The endpoint
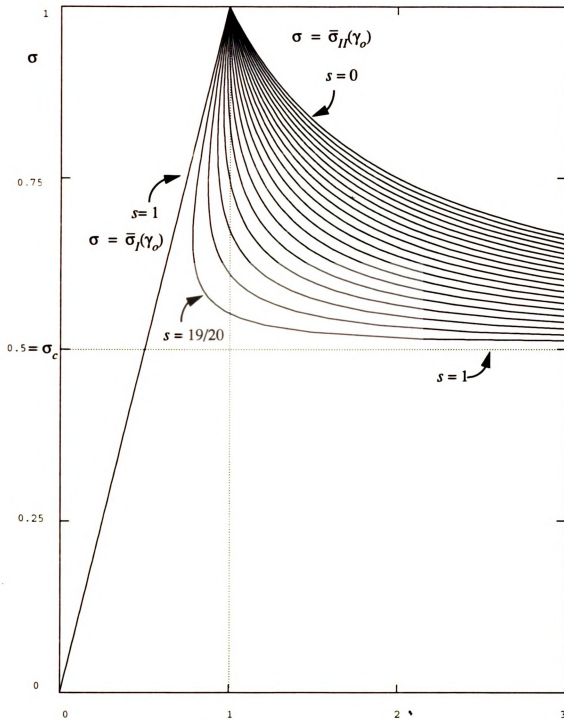
Figure 9. The curves of constant $s=(0.05, 0.1, 0.15,..., 0.95)$ in the solution region Ω_{12} with the choice of the function $\bar{\sigma}_{II}(\gamma)$ given by (a.1) of Appendix-A. The limiting case of $s=0$ corresponds to $\sigma=\bar{\sigma}_{II}(\gamma_o)$ and the limiting case of $s=1$ corresponds to both $\sigma=\gamma_o$ with $\sigma>\sigma_c$ and $\sigma=\sigma_c$.
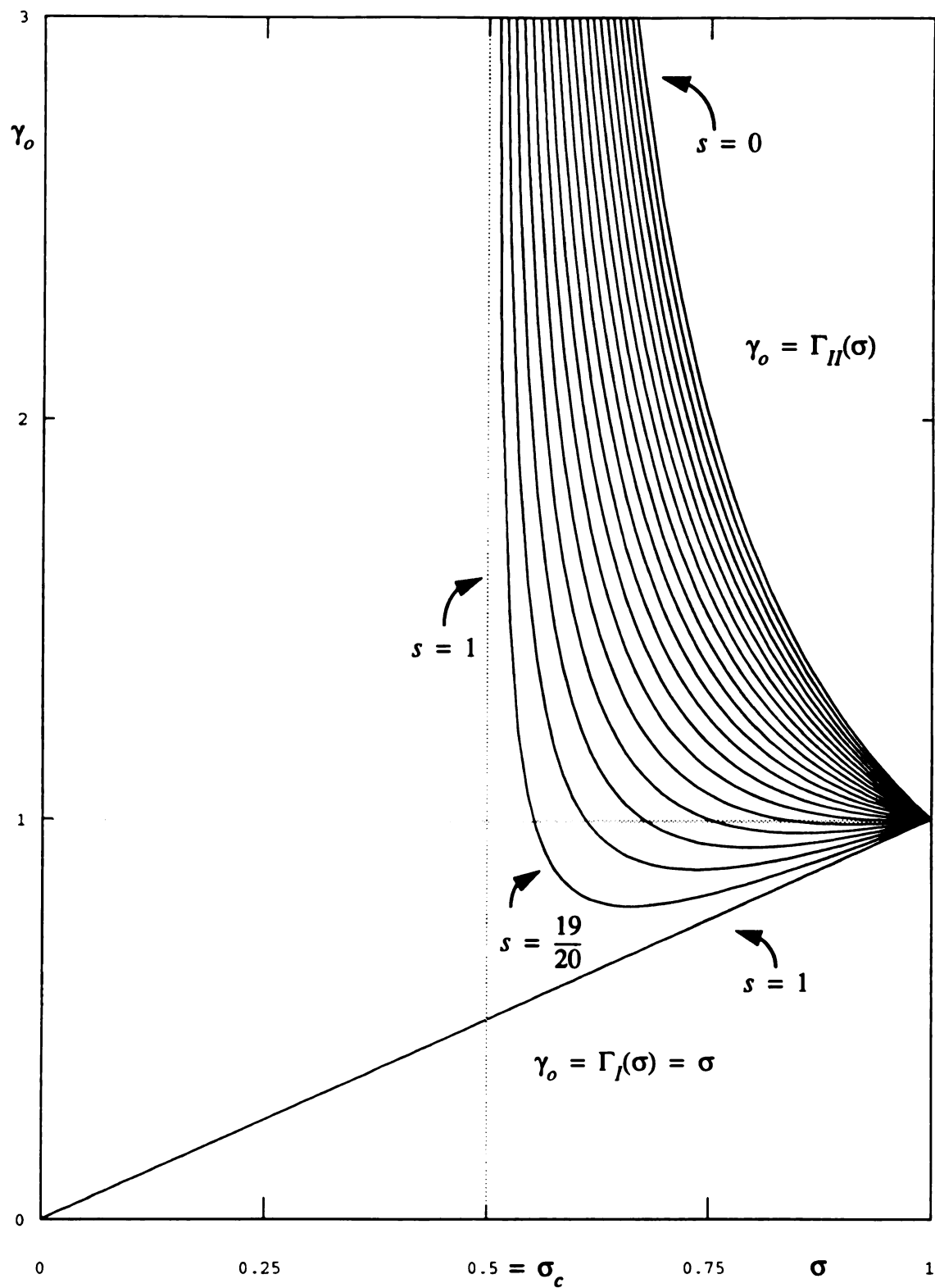
Figure 10. It is convenient to reorient the solution region of Figure 4-Figure 9 so that the constant s curves display a minima. We shall use this orientation for the solution region Ω_{12} in the rest of this thesis.

of each curve is the point at $(\sigma, \gamma_o) = (1, 1)$, this curve is unbounded for large γ and in the limit as $\gamma \to \infty$ it tends to the asymptote $\sigma = \sigma_c$. Equation (23) gives that

$$\left. \frac{\partial \gamma_o}{\partial s} \right|_\sigma = \gamma_L - \gamma_R, \qquad \text{on } s \in (0, 1). \tag{33}$$

Since $\gamma_L \le 1 \le \gamma_R$ it follows that the different members of this family of curves do not intersect each other except possibly if $\gamma_L = \gamma_R \Rightarrow \gamma_L = \gamma_R = 1$. Furthermore, a curve corresponding to a larger value of s lies under that of the smaller value of s. Although the example in Figure 9 is for a particular $\bar{\sigma}_{II}(\gamma)$ with $\sigma_c = 1/2$, similar properties of these constant s curves are found for other functions $\bar{\sigma}_{II}(\gamma)$ of the type obeying (5).

It is to be noted from Figure 10 that if s is sufficiently small, then the constant s curves are monotonically decreasing from $(\sigma, \gamma_o) = (\sigma_c, \infty)$ to $(\sigma, \gamma_o) = (1, 1)$. However if s is sufficiently large, then these curves first decrease and then increase. There is a transition value of s, say s_{trans}, separating these two groups of s curves (for the example material in Figure 10 it is found that $s_{trans} = 2/3$). For $s > s_{trans}$, the constant s curves have an internal minimum point while for $s \le s_{trans}$ they don't. It will be useful to know the location of these minimum points to the curves of constant s. Taking partial derivative with respect to σ with fixed s in (23) gives

$$\left. \frac{\partial \gamma_o}{\partial \sigma} \right|_s = \hat{\gamma}_o'(\sigma) = \Gamma_I'(\sigma)s + \Gamma_{II}'(\sigma)(1-s), \tag{34}$$

and setting this equal to zero gives

$$\Gamma_I'(\sigma)s + \Gamma_{II}'(\sigma)(1-s) = 0, \tag{35}$$

or

$$s = \frac{\Gamma_{II}'(\sigma)}{\Gamma_{II}'(\sigma) - \Gamma_I'(\sigma)} \equiv s^{**}(\sigma), \tag{36}$$

as a condition for $\left.\dfrac{\partial \gamma_o}{\partial \sigma}\right|_s = 0$. It is to be noted that the transition value of s is given by

$$s_{trans} = s^{**}(1). \tag{37}$$

To verify that it is minimum at (σ, γ_o) satisfying (35) we take partial derivative with respect to σ in (34) again. As a result, it is found that

$$\left.\dfrac{\partial^2}{\partial \sigma^2} \gamma_o\right|_s = \hat{\gamma}_o''(\sigma) = \Gamma_I''(\sigma)s + \Gamma_{II}''(\sigma)(1-s). \tag{38}$$

Since $\bar{\sigma}_I(\gamma)$ is a linear function and $\Gamma_I(\sigma)$ is the inverse function of $\bar{\sigma}_I(\gamma)$, $\Gamma_I(\sigma)$ is a linear function too and

$$\bar{\sigma}_I'(\gamma) = 1, \qquad \Gamma_I'(\sigma) = 1, \qquad \bar{\sigma}_I''(\gamma) = \Gamma_I''(\sigma) = 0. \tag{39}$$

Thus the combination of (39) and (38) gives

$$\left.\dfrac{\partial^2}{\partial \sigma^2} \gamma_o\right|_s = \Gamma_{II}''(\sigma)(1-s). \tag{40}$$

Since $1 - s > 0$ it follows that $\left.\dfrac{\partial^2}{\partial \sigma^2} \gamma_o\right|_s$ and $\Gamma_{II}''(\sigma)$ have the same sign provided that $s \neq 1$.

Note that $\Gamma_{II}(\sigma)$ is the inverse function of $\bar{\sigma}_{II}(\gamma)$ so that

$$\sigma = \bar{\sigma}_{II}(\gamma) = \bar{\sigma}_{II}(\Gamma_{II}(\sigma)). \tag{41}$$

Taking first derivative with respect to σ from (41) gives

$$1 = \bar{\sigma}_{II}'(\gamma)\Gamma_{II}'(\sigma). \tag{42}$$

The combination of $(5)_2$ and (42) now gives

$$\bar{\sigma}_{II}'(\gamma) < 0, \qquad \Gamma_{II}'(\sigma) < 0. \tag{43}$$

Taking second derivative with respect to σ from (41) gives

$$0 = \bar{\sigma}_{II}''(\gamma)(\Gamma_{II}'(\sigma))^2 + \bar{\sigma}_{II}'(\gamma)\Gamma_{II}''(\sigma). \tag{44}$$

Since, by (5), $\bar{\sigma}_{II}'(\gamma) < 0$ and $\bar{\sigma}_{II}''(\gamma) > 0$, it is found that

$$\Gamma_{II}{}''(\sigma) > 0 \tag{45}$$

and so (40) yields

$$\left.\frac{\partial^2}{\partial\sigma^2}\gamma_o\right|_s > 0. \tag{46}$$

Thus (40) shows that the curvature restriction $\bar{\sigma}_{II}{}''(\gamma) > 0$ given in (5) ensure that there are no maximum points to the constant s curves. These curves monotonically decay to the minimum point from $(\sigma, \gamma_o) = (\sigma_c, \infty)$ after which they monotonically increase to the point $(\sigma, \gamma_o) = (1, 1)$. Note that if the curvature restriction $\bar{\sigma}_{II}{}''(\gamma) > 0$ in (5) is dropped then other interesting possibilities of solutions for the constant s curves will occur, but these will not be discussed here.

The minimum points along the curves of constant s could be obtained by (23) and (36), namely

$$\gamma_o\big|_s = \frac{\Gamma_I(\sigma)\Gamma_{II}{}'(\sigma) - \Gamma_{II}(\sigma)\Gamma_I{}'(\sigma)}{\Gamma_{II}{}'(\sigma) - \Gamma_I{}'(\sigma)}. \tag{47}$$

Let's define $\varnothing_2$ to be set of ordered pairs (σ, γ_o) which are minimum points for the various curves of constant s (see Figure 11). Then $\varnothing_2$ is also a curve on the interval $\sigma_c < \sigma \le 1$. From (47) it is found that

$$\varnothing_2 = \left\{ (\sigma, \gamma_o) \,\middle|\, \gamma_o = \frac{\Gamma_I(\sigma)\Gamma_{II}{}'(\sigma) - \Gamma_{II}(\sigma)\Gamma_I{}'(\sigma)}{\Gamma_{II}{}'(\sigma) - \Gamma_I{}'(\sigma)}, \sigma_c < \sigma \le 1 \right\}. \tag{48}$$

Since the $\varnothing_2$ curve is very interesting and important in this study, we briefly look into its form. Note that the first derivative of γ_o in (47) is given by

$$\left.\frac{d\gamma_o}{d\sigma}\right|_{\varnothing_2} = \frac{(\Gamma_{II}(\sigma) - \Gamma_I(\sigma))\,\Gamma_I{}'(\sigma)\Gamma_{II}{}''(\sigma)}{(\Gamma_{II}{}'(\sigma) - \Gamma_I{}'(\sigma))^2}. \tag{49}$$

Since, by (45), $\Gamma_{II}{}''(\sigma) > 0$ and if $\sigma_c < \sigma < 1$ then $\Gamma_{II}(\sigma) - \Gamma_I(\sigma) > 0$ and $\Gamma_I{}'(\sigma) = 1$, this gives
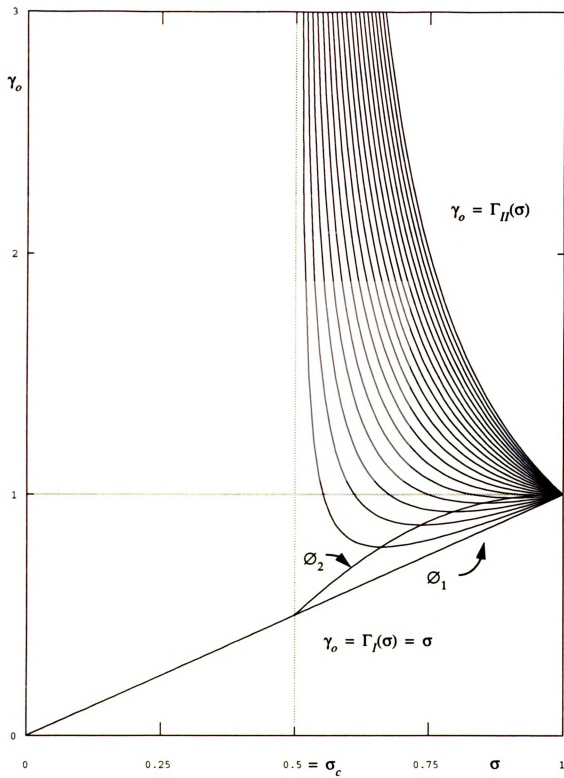
Figure 11. The $\emptyset_2$ curve in the solution region Ω_{12} (again the choice of the function $\overline{\sigma}_{II}(\gamma)$ is given by (a.1) of Appendix-A).

$$\frac{d\gamma_o}{d\sigma}\bigg|_{\varnothing_2} > 0. \tag{50}$$

This shows that γ_o is increasing along $\varnothing_2$ with increasing stress. It is to be noted that the point $(\sigma, \gamma_o) = (1, 1)$ is the right end point of $\varnothing_2$ and thus gives the largest stress σ on $\varnothing_2$. Therefore, it is found that $\gamma_o \leq 1$ along the curve $\varnothing_2$. Since $\varnothing_2$ is monotonically increasing we can invert (50) and so can parametrize this curve by γ_o, that is $\sigma = \bar{\sigma}_{\varnothing_2}(\gamma_o)$.

In addition (36) is invertible and the inverse function shall be denoted $\sigma = \sigma_{\Phi_2}(s)$.

6. The hard device energy function on Ω_{12}

The distribution of the hard device energy function in Ω_{12} can be described by (24),

$$\Lambda_{12} = \hat{\Lambda}_{12}(\sigma, \gamma_o) = W_I(\Gamma_I(\sigma))\hat{s}_{12}(\sigma, \gamma_o) + W_{II}(\Gamma_{II}(\sigma))(1 - \hat{s}_{12}(\sigma, \gamma_o)).$$ Level curves of

fixed Λ_{12} in the region Ω_{12} are functions of γ_o and σ. An example of these level curves is

given in Figure 12 for a particular material, that is a particular choice of the function $\bar{\sigma}_{II}(\gamma)$

(in fact it is the same material used for the constant s curves in Figure 9). For this material

and each fixed value of $\Lambda_{12} \in (0.125, \infty)$, the equation $\hat{\Lambda}_{12}(\sigma, \gamma_o) = \Lambda_{12}$ defines a

smooth curve on the (σ, γ_o)-plane again. There is a family of such curves on the (σ, γ_o)-

plane. Each curve corresponds to a different value of $\Lambda_{12} \in (0.125, \infty)$. In what follows

the hard device energy functions $\hat{\Lambda}_{12}(\sigma, \gamma_o)$ on the boundary of Ω_{12}, on the lines of con-

stant σ, on the lines of constant γ_o and on the lines of constant s are examined. Note that

the general discussion applies to materials for which the function $\bar{\sigma}_{II}(\gamma)$ has the properties

as given by (5).

6.1 The hard device energy function on the boundary of Ω_{12}

First of all, the boundary $\gamma_o = \Gamma_I(\sigma)$ of the solution region Ω_{12} is in phase-I. As a result,

the hard device energy function will be $\Lambda_{12} = W_I(\Gamma_I(\sigma))$. Secondly, the boundary

$\gamma_o = \Gamma_{II}(\sigma)$ of the solution region Ω_{12} is in phase-II. As a consequence, the hard device

energy function will be $\Lambda_{12} = W_{II}(\Gamma_{II}(\sigma))$. Finally, recall that the boundary $\sigma = \sigma_c$ of the

solution region Ω_{12} is the non-attainable limit corresponding to an infinitely strained

phase-II region of vanishing length. It is to be noted that $\gamma_1 = \sigma_c$ and $\gamma_2 \to \infty$ on the

boundary $\sigma = \sigma_c$ in the (1,2)-case, and also from (25) it is verified that $s = \dfrac{\gamma_R - \gamma_0}{\gamma_R - \gamma_L} = 1$.
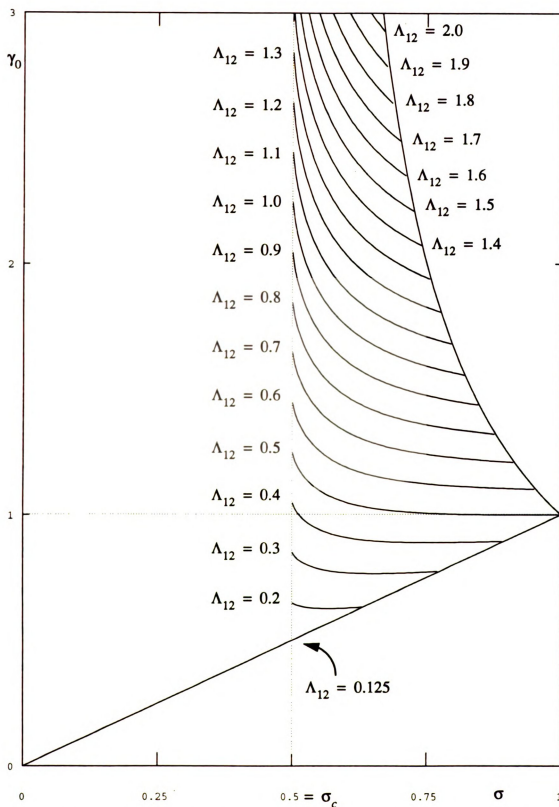
Figure 12. The level curves of constant hard device energy function Λ_{12} in the solution region Ω_{12} with the choice of the function $\overline{\sigma}_{II}(\gamma)$ given by (a.1) of Appendix-A.

We now show that the hard device energy function Λ_{12} on $\sigma = \sigma_c$ is given by

$\Lambda_{12} = \sigma_c(\gamma_0 - \sigma_c/2)$: from (24), (25) and (7) the hard device energy function is given by

$$\Lambda_{12} = \left(W_I(\Gamma_I(\sigma_c))\frac{\gamma_R - \gamma_0}{\gamma_R - \gamma_L} + W_{II}(\Gamma_{II}(\sigma_c))\frac{\gamma_0 - \gamma_L}{\gamma_R - \gamma_L} \right)\Bigg|_{\substack{\gamma_L = \sigma_c \\ \gamma_R \to \infty}}$$

$$= \frac{\sigma_c^2}{2} + \left[\int_0^{\gamma_R} \bar{\sigma}_{II}(\gamma)d\gamma \right]\frac{\gamma_0 - \gamma_L}{\gamma_R - \gamma_L}\Bigg|_{\substack{\gamma_L = \sigma_c \\ \gamma_R \to \infty}}, \qquad \text{on } \sigma = \sigma_c.$$

(51)

Now by the L'Hospital's rule, the hard device energy function can be rewritten as

$$\Lambda_{12} = \frac{\sigma_c^2}{2} + (\gamma_0 - \sigma_c)\lim_{\gamma_2 \to \infty}\frac{\int_0^{\gamma_2}\bar{\sigma}_{II}(\gamma)d\gamma}{\gamma_2 - \sigma_c} = \frac{\sigma_c^2}{2} + (\gamma_0 - \sigma_c)\lim_{\gamma_2 \to \infty}\bar{\sigma}_{II}(\gamma_2)$$

$$= \frac{\sigma_c^2}{2} + \sigma_c(\gamma_0 - \sigma_c) = \sigma_c(\gamma_0 - \frac{\sigma_c}{2}).$$

(52)

It is to be noted that if $\gamma_o = \sigma_c$, then $\Lambda_{12} = \sigma_c^2/2$ which indeed matches the hard device energy for pure phase-I solutions at $(\sigma, \gamma_o) = (\sigma_c, \sigma_c)$. It is also to be noted that

$\Lambda_{12} = \sigma_c^2/2$ gives the smallest energy in the solution region Ω_{12} and that is why we had

0.125 for the example material. It is easy to show, at a given constant γ_o, that the hard de-

vice energy on $\sigma = \sigma_c$ is less than the hard device energy on $\gamma_o = \Gamma_I(\sigma)$. For example for

a given constant γ_o obeying $\sigma_c < \gamma_o \leq 1$ the difference between the hard device energy on

$\sigma = \sigma_c$ and the hard device energy on $\gamma_o = \Gamma_I(\sigma)$ is given by

$$\Lambda_{12}\big|_{\text{on } \sigma = \sigma_c} - \Lambda_{12}\big|_{\text{on } \gamma_o = \Gamma_I(\sigma)} = \sigma_c(\gamma_0 - \frac{\sigma_c}{2}) - \frac{\gamma_0^2}{2} = -\frac{(\gamma_0 - \sigma_c)^2}{2} < 0.$$

(53)

In summary the hard device energy functions on the boundary of Ω_{12} are given by

$$\Lambda_{12} = \begin{cases} W_I(\Gamma_I(\sigma)) = \dfrac{\sigma^2}{2} = \dfrac{\gamma_o^2}{2}, & \text{on } \gamma_o = \Gamma_I(\sigma), \\[3mm] W_{II}(\Gamma_{II}(\sigma)), & \text{on } \gamma_o = \Gamma_{II}(\sigma), \\[3mm] W_I(\Gamma_I(\sigma_c)) + W_{II}(\Gamma_{II}(\sigma_c))\dfrac{\gamma_0 - \sigma_c}{\Gamma_{II}(\sigma_c) - \sigma_c} = \sigma_c(\gamma_0 - \dfrac{\sigma_c}{2}), & \text{on } \sigma = \sigma_c. \end{cases} \qquad (54)$$

6.2 The hard device energy function for Ω_{12} on the lines of constant σ

Now that the hard device energy function Λ_{12} on the boundary of the solution region Ω_{12} has been studied we would like to study Λ_{12} on the lines of constant σ. Consider two different states with the same stress but different strains: state A corresponds to $(\sigma, \gamma_o) = (\sigma_A, \gamma_A)$; state B corresponds to $(\sigma, \gamma_o) = (\sigma_B, \gamma_B) = (\sigma_A, \gamma_B)$ with $\gamma_B > \gamma_A$. Which state has more energy? It is reasonable to guess that state B needs more energy. To prove this and study the distribution of the hard device energy function along the lines of constant σ, we take partial derivative with respect to γ_o in (24) for constant σ. If σ is a constant, then $\gamma_L = \Gamma_I(\sigma)$ and $\gamma_R = \Gamma_{II}(\sigma)$ are constants too. Therefore, $\Lambda_{12} = \Lambda_{12}^*(\gamma_o)$ and $s = s^*(\gamma_o)$ are also functions of γ_o only, and it is found that

$$\left.\frac{\partial \Lambda_{12}}{\partial \gamma_o}\right|_\sigma = \Lambda_{12}^{*\prime}(\gamma_o) = (W_I(\Gamma_I(\sigma)) - W_{II}(\Gamma_{II}(\sigma)))\, s^{*\prime}(\gamma_o). \qquad (55)$$

From (25), a similar process gives

$$\left.\frac{\partial s}{\partial \gamma_o}\right|_\sigma = s^{*\prime}(\gamma_o) = \frac{1}{\Gamma_I(\sigma) - \Gamma_{II}(\sigma)}. \qquad (56)$$

Finally, substitution from (56) into (55) yields

$$\left.\frac{\partial \Lambda_{12}}{\partial \gamma_o}\right|_\sigma = \Lambda_{12}^{*\prime}(\gamma_o) = \frac{W_{II}(\Gamma_{II}(\sigma)) - W_I(\Gamma_I(\sigma))}{\Gamma_{II}(\sigma) - \Gamma_I(\sigma)} > 0. \qquad (57)$$

This means that the hard device energy function Λ_{12} monotonically increases along each

line of constant σ as γ_o increases. This also implies that $(\sigma, \gamma_o) = (\sigma, \Gamma_I(\sigma))$ gives the minimum value of Λ_{12} for a given constant σ whenever $\sigma_c < \sigma < 1$. In conclusion, state B indeed has more energy than state A.

It will be useful in what follows to define the ratio appearing in (57) as *a pseudo stress function*

$$\sigma_{ps} = \frac{W_{II}(\Gamma_{II}(\sigma)) - W_I(\Gamma_I(\sigma))}{\Gamma_{II}(\sigma) - \Gamma_I(\sigma)} \equiv \sigma_{ps}(\sigma), \qquad \sigma_c < \sigma \le 1. \tag{58}$$

Equation (58) means that σ_{ps} is the average height of the stress-strain curve in the interval

$\gamma_1 = \Gamma_I(\sigma) < \gamma_0 < \gamma_2 = \Gamma_{II}(\sigma)$. Note that $\left.\frac{\partial \Lambda_{12}}{\partial \gamma_o}\right|_\sigma = \sigma_{ps}(\sigma)$. The expression (58) is inde-

terminate at both $\sigma \to \sigma_c$ and $\sigma = 1$, however the limiting values of $\sigma_{ps}(\sigma)$ can be obtained by the following:

Taking the limit $\sigma \to 1$ from (58) gives

$$\lim_{\sigma \to 1} \sigma_{ps}(\sigma) = \lim_{\sigma \to 1} \frac{W_{II}(\Gamma_{II}(\sigma)) - W_I(\Gamma_I(\sigma))}{\Gamma_{II}(\sigma) - \Gamma_I(\sigma)}. \tag{59}$$

It is to be noted that

$$W_I'(\Gamma_I(\sigma)) = \sigma\Gamma_I'(\sigma), \qquad W_{II}'(\Gamma_{II}(\sigma)) = \sigma\Gamma_{II}'(\sigma). \tag{60}$$

Using the L'Hospital's rule (since now (58) is of the form $\frac{0}{0}$) and substitution from (60) into (59) gives

$$\lim_{\sigma \to 1} \sigma_{ps}(\sigma) = \lim_{\sigma \to 1} \frac{\sigma\Gamma_{II}'(\sigma) - \sigma\Gamma_I'(\sigma)}{\Gamma_{II}'(\sigma) - \Gamma_I'(\sigma)} = \lim_{\sigma \to 1} \sigma = 1. \tag{61}$$

Similarly taking the limit $\sigma \to \sigma_c$ from (58) and using the L'Hospital's rule (since now (58) is of the form $\frac{\infty}{\infty}$) gives

$$\lim_{\sigma \to \sigma_c} \sigma_{ps}(\sigma) = \lim_{\sigma \to \sigma_c} \frac{W_{II}(\Gamma_{II}(\sigma)) - W_I(\Gamma_I(\sigma))}{\Gamma_{II}(\sigma) - \Gamma_I(\sigma)}$$

$$= \lim_{\sigma \to \sigma_c} \frac{\sigma \Gamma_{II}'(\sigma) - \sigma \Gamma_I'(\sigma)}{\Gamma_{II}'(\sigma) - \Gamma_I'(\sigma)} = \lim_{\sigma \to \sigma_c} \sigma = \sigma_c. \tag{62}$$

Since the stress in this interval $\gamma_L < \gamma_0 < \gamma_R$ is greater than the stress $\sigma = \bar{\sigma}_I(\gamma_L) = \bar{\sigma}_{II}(\gamma_R)$ at the interval endpoints, it can be concluded that

$$\left(\begin{array}{ll} \sigma_{ps}(\sigma) > \sigma, & \text{if } \sigma_c < \sigma < 1, \\ \sigma_{ps}(\sigma) = \sigma, & \text{if } \sigma = 1 \text{ or if } \sigma = \sigma_c. \end{array} \right. \tag{63}$$

An example of the function $\sigma_{ps}(\sigma)$ is shown in Figure 13.

Moreover the first derivative of $\sigma_{ps}(\sigma)$ is given by

$$\sigma_{ps}'(\sigma) = \frac{(W_{II}(\Gamma_{II}(\sigma)) - W_I(\Gamma_I(\sigma)) - \sigma(\Gamma_{II}(\sigma) - \Gamma_I(\sigma)))(\Gamma_I'(\sigma) - \Gamma_{II}'(\sigma))}{(\Gamma_{II}(\sigma) - \Gamma_I(\sigma))^2}$$

$$= \frac{(\sigma_{ps}(\sigma) - \sigma)(\Gamma_I'(\sigma) - \Gamma_{II}'(\sigma))}{\Gamma_{II}(\sigma) - \Gamma_I(\sigma)}. \tag{64}$$

Note from (63)$_1$, (39)$_2$, and (43)$_2$ that $\sigma_{ps}(\sigma) > \sigma$, $\Gamma_I'(\sigma) = 1$ and $\Gamma_{II}'(\sigma) < 0$ in the inter-
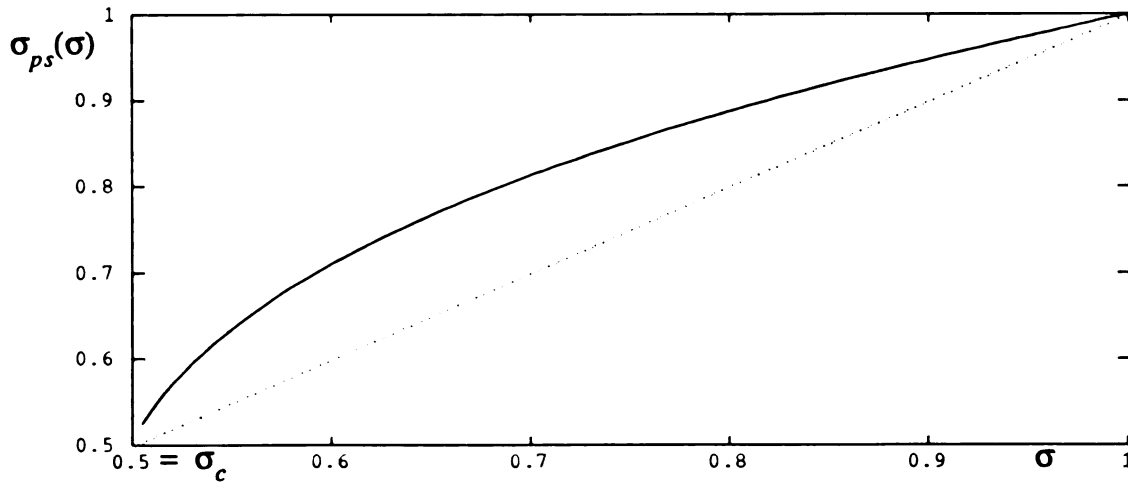
Figure 13. The function $\sigma_{ps}(\sigma)$ with the choice of the function $\bar{\sigma}_{II}(\gamma)$ given by (a.1) of Appendix-A. Note that (63)$_1$ ensures that this curve is above the dotted line.

val $\sigma_c < \sigma < 1$. It is also to be noted that $\Gamma_{II}(\sigma) > \Gamma_I(\sigma)$ in this interval. Therefore

$\sigma_{ps}'(\sigma) > 0$ in the interval $\sigma_c < \sigma < 1$. To complete this subsection we now look at the two

limiting cases: $\sigma_{ps}'(\sigma_c)$ and $\sigma_{ps}'(1)$. Taking the limit $\sigma \to 1$ from (64) and using the

L'Hospital's rule (since now (64) is of the form $\frac{0}{0}$) gives

$$
\begin{aligned}
\lim_{\sigma \to 1} \sigma_{ps}'(\sigma) &= \lim_{\sigma \to 1} \frac{(\sigma_{ps}(\sigma) - \sigma)\,(\Gamma_I'(\sigma) - \Gamma_{II}'(\sigma))}{\Gamma_{II}(\sigma) - \Gamma_I(\sigma)} \\
&= \lim_{\sigma \to 1} (\Gamma_I'(\sigma) - \Gamma_{II}'(\sigma))\, \lim_{\sigma \to 1} \frac{(\sigma_{ps}(\sigma) - \sigma)}{\Gamma_{II}(\sigma) - \Gamma_I(\sigma)}.
\end{aligned}
\tag{65}
$$

Note that there is a finite value in the first term of (65), while the second term of (65) is of

the form $\frac{0}{0}$. Therefore, using the L'Hospital's rule gives

$$
\begin{aligned}
\lim_{\sigma \to 1} \sigma_{ps}'(\sigma) &= \lim_{\sigma \to 1} (\Gamma_I'(\sigma) - \Gamma_{II}'(\sigma))\, \lim_{\sigma \to 1} \frac{(\sigma_{ps}'(\sigma) - 1)}{\Gamma_{II}'(\sigma) - \Gamma_I'(\sigma)} \\
&= 1 - \lim_{\sigma \to 1} \sigma_{ps}'(\sigma).
\end{aligned}
\tag{66}
$$

Therefore

$$
\lim_{\sigma \to 1} \sigma_{ps}'(\sigma) = \frac{1}{2}.
\tag{67}
$$

Similarly from (64) the other limiting case of $\sigma \to \sigma_c$ can be shown to be given by

$$
\begin{aligned}
\lim_{\sigma \to \sigma_c} \sigma_{ps}'(\sigma) &= \lim_{\sigma \to \sigma_c} \frac{(\sigma_{ps}(\sigma) - \sigma)\,(\Gamma_I'(\sigma) - \Gamma_{II}'(\sigma))}{\Gamma_{II}(\sigma) - \Gamma_I(\sigma)} \\
&= \lim_{\sigma \to \sigma_c} \frac{\Gamma_I'(\sigma) - \Gamma_{II}'(\sigma)}{\Gamma_{II}(\sigma) - \Gamma_I(\sigma)}\, \lim_{\sigma \to \sigma_c} (\sigma_{ps}(\sigma) - \sigma).
\end{aligned}
\tag{68}
$$

Note that $\Gamma_{II}(\sigma) - \Gamma_I(\sigma)$ is divergent as $\sigma \to \sigma_c$. Hence let's assume $\Gamma_{II}(\sigma) - \Gamma_I(\sigma)$ has an

n-th order pole as $\sigma \to \sigma_c$. This implies that

$$
\lim_{\sigma \to \sigma_c} (\Gamma_{II}(\sigma) - \Gamma_I(\sigma))\,(\sigma - \sigma_c)^n = \text{constant}
\tag{69}
$$

and $\Gamma_{II}'(\sigma) - \Gamma_I'(\sigma)$ has an (n+1)-th order pole:

$$\lim_{\sigma \to \sigma_c} (\Gamma_{II}{}'(\sigma) - \Gamma_I{}'(\sigma)) \ (\sigma - \sigma_c)^{n+1} = (-n) \text{ constant.} \tag{70}$$

Therefore

$$\lim_{\sigma \to \sigma_c} \frac{\Gamma_I{}'(\sigma) - \Gamma_{II}{}'(\sigma)}{\Gamma_{II}(\sigma) - \Gamma_I(\sigma)} = \lim_{\sigma \to \sigma_c} \frac{n}{\sigma - \sigma_c}. \tag{71}$$

Substitution from (71) into (68) gives

$$\lim_{\sigma \to \sigma_c} \sigma_{ps}{}'(\sigma) = \lim_{\sigma \to \sigma_c} \frac{(\sigma_{ps}(\sigma) - \sigma) \, n}{\sigma - \sigma_c}. \tag{72}$$

Note that (72) has the form $\dfrac{0}{0}$ and using the L'Hospital's rule gives that

$$\lim_{\sigma \to \sigma_c} \sigma_{ps}{}'(\sigma) = \lim_{\sigma \to \sigma_c} (\sigma_{ps}{}'(\sigma) - 1) \, n. \tag{73}$$

From (73) and $\sigma_{ps}{}'(\sigma) > 0$ whenever $\sigma_c < \sigma < 1$ it is found that

$$\lim_{\sigma \to \sigma_c} \sigma_{ps}{}'(\sigma) = \begin{cases} \dfrac{n}{n-1} & \text{if} \quad n > 1, \\ \infty & \text{if} \quad n \leq 1, \end{cases} \tag{74}$$

where n implies the rate of $\bar{\sigma}_{II}(\gamma) \to \sigma_c$ as $\sigma \to \sigma_c$ by virtue of (69).

If the function $\bar{\sigma}_{II}(\gamma)$ given by (a.1) of Appendix-A is considered, then it is found that $n = 1$ and $\lim_{\sigma \to \sigma_c} \sigma_{ps}{}'(\sigma) = \infty$. Similarly, if the function $\bar{\sigma}_{II}(\gamma)$ given by (b.1) of Section Appendix-B is considered, then it is found that $n = 1/2$ and $\lim_{\sigma \to \sigma_c} \sigma_{ps}{}'(\sigma) = \infty$. In summary

$$\begin{cases} \sigma_{ps}{}'(\sigma) > 0, & \text{if } \sigma_c < \sigma < 1, \\ \sigma_{ps}{}'(\sigma) = 0.5, & \text{if } \sigma = 1, \\ \sigma_{ps}{}'(\sigma) = \begin{cases} \dfrac{n}{n-1} & \text{if } \sigma = \sigma_c \text{ and } n > 1, \\ \infty & \text{if } \sigma = \sigma_c \text{ and } 0 < n \leq 1. \end{cases} \end{cases} \tag{75}$$

The first derivative of the function $\sigma_{ps}(\sigma)$ with the choice of the function $\bar{\sigma}_{II}(\gamma)$ given by (a.1) of Appendix-A is shown in Figure 14.

6.3 The hard device energy function for Ω_{12} on the lines of constant γ_o

From Section 6.2 we found that the hard device energy function Λ_{12} monotonically increases along each line of constant σ as γ_o increases. Now we study whether the hard device energy function Λ_{12} along the lines of constant γ_o is increasing or decreasing with σ.

Consider two different states with the same strain but different stresses on any line of constant γ_o: state A corresponds to $(\sigma, \gamma_o) = (\sigma_A, \gamma_A)$; state B corresponds to $(\sigma, \gamma_o) = (\sigma_B, \gamma_B) = (\sigma_B, \gamma_A)$ where $\sigma_B > \sigma_A$. Is it true that state B has a larger energy value? To answer this question and study the distribution of the hard device energy function along the lines of constant γ_o again, we take partial derivative with respect to σ in (24) with fixed γ_o. If γ_o is a constant, then $\Lambda_{12} = \Lambda_{12}^{**}(\sigma)$ and $s = s^{**}(\sigma)$ are functions of σ only. From (24) and (60) it is found that

$$\left. \frac{\partial \Lambda_{12}}{\partial \sigma} \right|_{\gamma_o} = \Lambda_{12}^{**\prime}(\sigma) = (W_I(\Gamma_I(\sigma)) - W_{II}(\Gamma_{II}(\sigma))) \, s^{**\prime}(\sigma) +$$
$$\sigma \Gamma_I{}'(\sigma)s + \sigma \Gamma_{II}{}'(\sigma)(1-s). \tag{76}$$

Similarly, by the same mathematical process in (25), it is found that
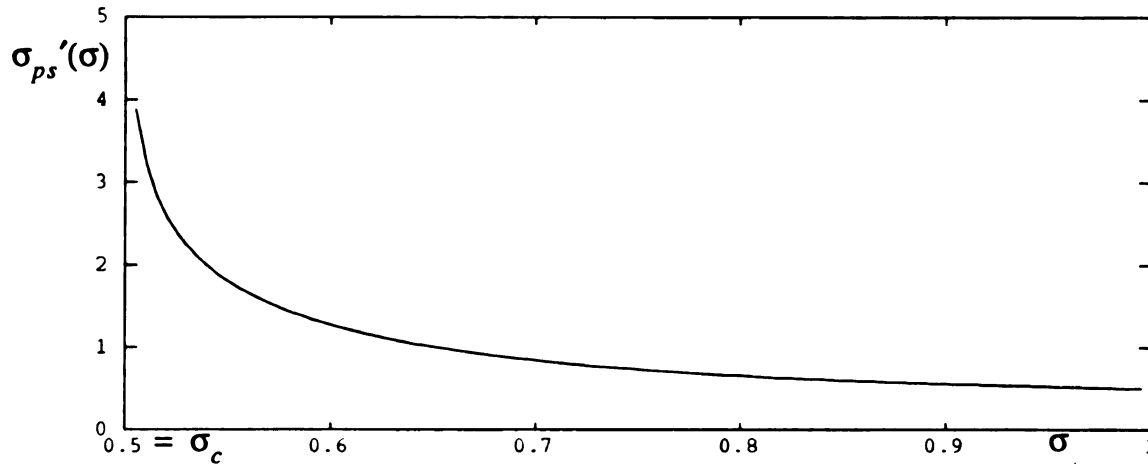
Figure 14. The first derivative of function $\sigma_{ps}(\sigma)$ with the choice of the function $\bar{\sigma}_{II}(\gamma)$ given by (a.1) of Appendix-A.

$$\frac{\partial s}{\partial \sigma}\Big|_{\gamma_o} = s^{**\prime}(\sigma) = \frac{\Gamma_I{}'(\sigma)s + \Gamma_{II}{}'(\sigma)(1-s)}{(\Gamma_{II}(\sigma) - \Gamma_I(\sigma))}. \tag{77}$$

Substitution of (58) and (77) into (76) shows that

$$\frac{\partial \Lambda_{12}}{\partial \sigma}\Big|_{\gamma_o} = \Lambda_{12}^{**\prime}(\sigma) = (\Gamma_I{}'(\sigma)s + \Gamma_{II}{}'(\sigma)(1-s))(\sigma - \sigma_{ps}(\sigma)). \tag{78}$$

According to (34), equation (78) is equivalent to

$$\frac{\partial \Lambda_{12}}{\partial \sigma}\Big|_{\gamma_o} = \frac{\partial \gamma_o}{\partial \sigma}\Big|_s (\sigma - \sigma_{ps}(\sigma)). \tag{79}$$

Since $(63)_1$ gives that $\sigma - \sigma_{ps}(\sigma) < 0$ whenever $\sigma \neq \sigma_c$ or $\sigma \neq 1$ it follows that $\dfrac{\partial \Lambda_{12}}{\partial \sigma}\Big|_{\gamma_o}$ and

$\dfrac{\partial \gamma_o}{\partial \sigma}\Big|_s$ have opposite signs for $\sigma_c < \sigma < 1$. This also implies that any extremum solutions of

the hard device energy Λ_{12} along the lines of constant γ_o occurs where γ_o is stationary

(stops increasing or decreasing) on the curves of constant s as a function of σ. Recall from

Section 5 that (σ, γ_o) on $\varnothing_2$ *is a minimum point in the* (σ, γ_o) *-plane for the correspond-*

ing curve of constant s. Therefore it can be concluded that points on $\varnothing_2$ are also the ex-

tremum points of the hard device energy function Λ_{12} along the lines of constant γ_o.

The hard device energy function Λ_{12} at (σ, γ_o) on $\varnothing_2$ could be a maximum or a

minimum along the lines of constant γ_o. This implies that

$$\Gamma_I{}'(\sigma)s + \Gamma_{II}(\sigma)'(1-s) = 0 \Leftrightarrow \frac{\partial \gamma_o}{\partial \sigma}\Big|_s = 0 \Leftrightarrow \frac{\partial \Lambda_{12}}{\partial \sigma}\Big|_{\gamma_o} = 0. \tag{80}$$

Equations (77) and (78) show the following relation

$$\frac{\partial \Lambda_{12}}{\partial \sigma}\Big|_{\gamma_o} = \frac{\partial s}{\partial \sigma}\Big|_{\gamma_o} (\sigma - \sigma_{ps}(\sigma))(\Gamma_{II}(\sigma) - \Gamma_I(\sigma)). \tag{81}$$

Similarly since $\Gamma_{II}(\sigma) - \Gamma_I(\sigma) > 0$ and $(63)_1$ gives that $\sigma - \sigma_{ps}(\sigma) < 0$ whenever $\sigma \neq \sigma_c$ or

$\sigma \neq 1$ it follows that $\left.\dfrac{\partial \Lambda_{12}}{\partial \sigma}\right|_{\gamma_o}$ and $\left.\dfrac{\partial s}{\partial \sigma}\right|_{\gamma_o}$ have opposite signs for $\sigma_c < \sigma < 1$. Although equation (79) and equation (81) are similar, they have different meanings. Equation (81) implies that any extremum values of the hard device energy function Λ_{12} along the lines of constant γ_o takes place where s is stationary on the curves of constant γ_o as a function of σ. To determine whether these extrema of energy are a maximum or a minimum we calculate the second partial derivative of Λ_{12} with respect to σ from (78) and then using (80) gives

$$\left.\frac{\partial^2 \Lambda_{12}}{\partial \sigma^2}\right|_{\gamma_o} = \Lambda_{12}^{**''}(\sigma) = \left.\frac{\partial^2}{\partial \sigma^2}\gamma_o\right|_s (\sigma - \sigma_{ps}(\sigma)). \tag{82}$$

Again since $(63)_1$ gives that $\sigma - \sigma_{ps}(\sigma) < 0$ whenever $\sigma \neq \sigma_c$ or $\sigma \neq 1$ it follows that

$\left.\dfrac{\partial^2 \Lambda_{12}}{\partial \sigma^2}\right|_{\gamma_o}$ and $\left.\dfrac{\partial^2}{\partial \sigma^2}\gamma_o\right|_s$ have opposite signs for $\sigma_c < \sigma < 1$. Since, from Section 6.2, γ_o has

a minimum on the lines of constant s at points on $\varnothing_2$, it follows that Λ_{12} has maximum on the lines of constant γ_o at $\varnothing_2$. Thus $\varnothing_2$ is not only the set of ordered pairs (σ, γ_o) which are minimum points to the family of constant s curves, but $\varnothing_2$ also gives the set of ordered pairs (σ, γ_o) which are maximum points to the energy Λ_{12} along the family of constant γ_o lines.

Returning to the question of which state A or B on the line of constant γ_o has more energy we see that if $\gamma_o \geq 1$ then state B has more energy than state A since the hard device energy function Λ_{12} increases monotonically with σ whenever $\gamma_o \geq 1$. But if $\gamma_o < 1$ then since the hard device energy function Λ_{12} will increase monotonically to a maximum point on $\varnothing_2$ and then will decrease monotonically. It follows that state B is not necessarily carrying more energy than state A.

Let's define $\varnothing_3$ to be the set of ordered pairs (σ, γ_o) with $\sigma_c < \sigma \leq 1$ that are not

pure phase-I solutions but which have the same energy Λ_{12} as the pure phase-I solution at the same constant γ_o. Then it is found that

$$\varnothing_3 = \{ (\sigma, \gamma_o) \mid \gamma_o = (2\sigma_{ps}(\sigma) - \sigma), \sigma_c < \sigma \leq 1 \}, \tag{83}$$

where $\sigma_{ps}(\sigma)$ is defined in (58). Therefore, at a given constant γ_o obeying $\sigma_c < \gamma_o < 1$, the hard device energy function Λ_{12} at points on $\varnothing_1$ and $\varnothing_3$ are equal, and this energy is less than the hard device energy function Λ_{12} at points on $\varnothing_2$ (see Figure 15). With the help of (53) it can be concluded, at a given constant γ_o obeying $\sigma_c < \gamma_o < 1$, that

$$\Lambda_{12}\big|_{\text{on } \sigma = \sigma_c} < \Lambda_{12}\big|_{\text{on } \varnothing_1} = \Lambda_{12}\big|_{\text{on } \varnothing_3} < \Lambda_{12}\big|_{\text{on } \varnothing_2}. \tag{84}$$

6.4 The hard device energy function on the curves of constant s

We now look at he behavior of the hard device energy function Λ_{12} on the curves of constant s. Recall from Section 5 that there are two types of behavior to the constant s curves in the (σ, γ_o) -plane: monotonically decreasing ($s \leq s_{trans}$) and decreasing then increasing ($s > s_{trans}$). For the first type it is found that Λ_{12} also decreases on the constant s curves as $\sigma : \sigma_c \rightarrow 1$. In the second type with the help of (a.14) or (b.14) it is found that Λ_{12} also decreases on the constant s curves as $\sigma : \sigma_c \rightarrow \sigma_{\Phi_2}(s)$ but then Λ_{12} increases on the constant s curves as $\sigma : \sigma_{\Phi_2}(s) \rightarrow 1$. To show this we take the partial derivative with respect to σ in (24) with fixed s. It is found that $\Lambda_{12} = \Lambda_{12}^{**}(\sigma)$ and from (24) and (60)

$$\frac{\partial \Lambda_{12}}{\partial \sigma}\bigg|_s = \Lambda_{12}^{**\prime}(\sigma) = (\Gamma_I{}'(\sigma)s + \Gamma_{II}{}'(\sigma)(1-s))\sigma. \tag{85}$$

From (85), (34), (79) and (81) we find the following relations.

$$\frac{\partial \Lambda_{12}}{\partial \sigma}\bigg|_s = \frac{\partial \gamma_o}{\partial \sigma}\bigg|_s \sigma = \frac{\partial \Lambda_{12}}{\partial \sigma}\bigg|_{\gamma_o} \frac{\sigma}{\sigma - \sigma_{ps}(\sigma)} = \frac{\partial s}{\partial \sigma}\bigg|_{\gamma_o} \sigma(\Gamma_{II}(\sigma) - \Gamma_I(\sigma)). \tag{86}$$
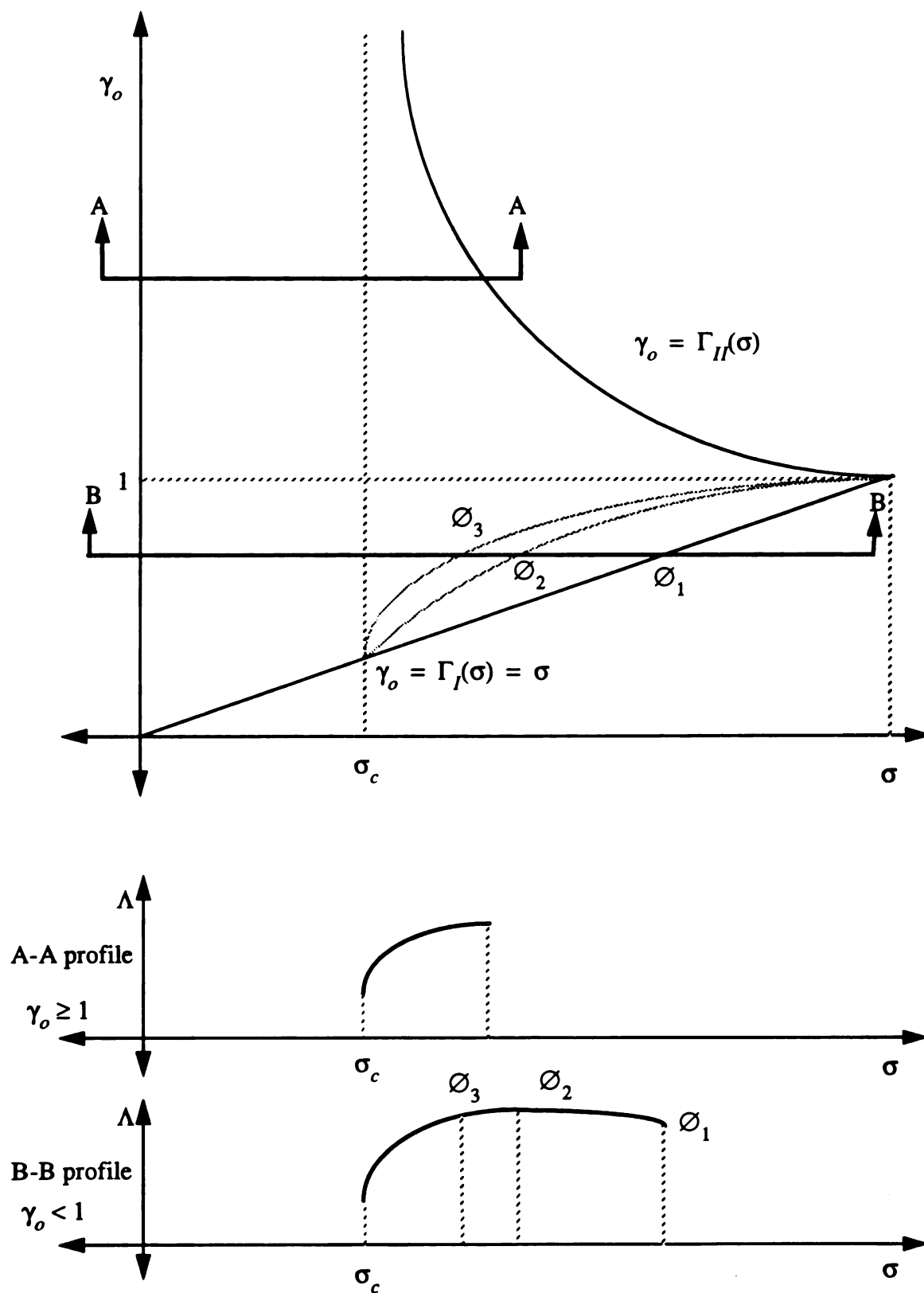
Figure 15. The hard device energy function Λ_{12} in the solution region Ω_{12}.

Since $\sigma > 0$, $\sigma - \sigma_{ps}(\sigma) < 0$ and $\Gamma_{II}(\sigma) - \Gamma_{I}(\sigma) > 0$ in the interval $\sigma_c < \sigma < 1$ it follows

that $\left.\dfrac{\partial \Lambda_{12}}{\partial \sigma}\right|_s$, $\left.\dfrac{\partial \gamma_o}{\partial \sigma}\right|_s$ and $\left.\dfrac{\partial s}{\partial \sigma}\right|_{\gamma_o}$ have the same signs while $\left.\dfrac{\partial \Lambda_{12}}{\partial \sigma}\right|_{\gamma_o}$ has the opposite sign. This

implies from (85) and (86) that

$$\Gamma_I'(\sigma)s + \Gamma_{II}'(\sigma)(1-s) = 0 \Leftrightarrow \left.\frac{\partial \Lambda_{12}}{\partial \sigma}\right|_s = \left.\frac{\partial \gamma_o}{\partial \sigma}\right|_s = \left.\frac{\partial \Lambda_{12}}{\partial \sigma}\right|_{\gamma_o} = \left.\frac{\partial s}{\partial \sigma}\right|_{\gamma_o} = 0. \tag{87}$$

Meanwhile, from (85) we can obtain the second partial derivative of Λ_{12} with respect to σ

and then using (87) gives

$$\left.\frac{\partial^2 \Lambda_{12}}{\partial \sigma^2}\right|_s = \Lambda_{12}^{***}{}''(\sigma) = \left.\frac{\partial^2}{\partial \sigma^2}\gamma_o\right|_s \sigma. \tag{88}$$

From (88), (82), and (77) it is found that

$$\left.\frac{\partial^2 \Lambda_{12}}{\partial \sigma^2}\right|_s = \left.\frac{\partial^2}{\partial \sigma^2}\gamma_o\right|_s \sigma = \left.\frac{\partial^2 \Lambda_{12}}{\partial \sigma^2}\right|_{\gamma_o} \frac{\sigma}{\sigma - \sigma_{ps}(\sigma)} = \left.\frac{\partial^2 s}{\partial \sigma^2}\right|_{\gamma_o} \sigma\,(\Gamma_{II}(\sigma) - \Gamma_I(\sigma)). \tag{89}$$

It is important to note that $\sigma > 0$, $\sigma - \sigma_{ps}(\sigma) < 0$ and $\Gamma_{II}(\sigma) - \Gamma_I(\sigma) > 0$. Recall from Section 6.3 and with the help of (89) that Λ_{12} and γ_o on the lines of constant s are minimum

at $\varnothing_2$, and that s on the lines of constant γ_o is minimum at $\varnothing_2$, and that Λ_{12} on the lines

of constant γ_o is maximum at $\varnothing_2$. Therefore $\varnothing_2$ is an interesting curve. *It not only gives*

the location of the minimum energy and the minimum γ_o value on the curves of constant s,

but it also gives the location of the maximum energy and the minimum s value on the lines

of constant γ_o.

6.5 The minimum energy criterion for the hard device

Recall from Section 6.3 and Figure 15 that if $\gamma_o \geq 1$ then the hard device energy function

Λ_{12} monotonically increases as σ goes from σ_c to $\bar{\sigma}_{II}(\gamma_o)$. However if $\gamma_o < 1$, then the

hard device energy function Λ_{12} will increase monotonically to a maximum point as σ goes from σ_c to $\bar{\sigma}_{\varnothing_2}(\gamma_o)$, but then it will decrease monotonically as σ goes from $\bar{\sigma}_{\varnothing_2}(\gamma_o)$ to γ_o. The minimum energy solution for the hard device will be the $\gamma_o = \Gamma_I(\sigma) = \sigma$ line for $0 < \gamma_o \leq \sigma_c$. However according to the profile's shown in Figure 15, the minimum energy solution would be the $\sigma = \sigma_c$ line for $\gamma_o > \sigma_c$ if this line was attainable (see Figure 16).

In fact for a given γ_o there are 3 situations: $0 < \gamma_o \leq \sigma_c$, $\sigma_c < \gamma_o \leq 1$ and $\gamma_o > 1$. In the first situation, $0 < \gamma_o \leq \sigma_c$, the solution is unique. In the second situation, $\sigma_c < \gamma_o \leq 1$, every point on the line segment $\sigma_c < \sigma < \bar{\sigma}_I(\gamma_0)$ of the constant γ_o line correspond to a two-phase solution, while $\sigma = \gamma_o$ is a pure phase-I solution. In the third situation, $\gamma_o > 1$, every point on the line segment $\sigma_c < \sigma < \bar{\sigma}_{II}(\gamma_0)$ of the constant γ_o lines also corresponds to a two-phase solution while $\sigma = \bar{\sigma}_{II}(\gamma_0)$ is a pure phase-II solution.

For the second and third types there are an infinite number of possible solutions even for the (1,2)-case, however the values of Λ_{12} varies among these candidate solutions. Under a *minimum energy solution criterion* if the bar is elongated at its end with a quasi-
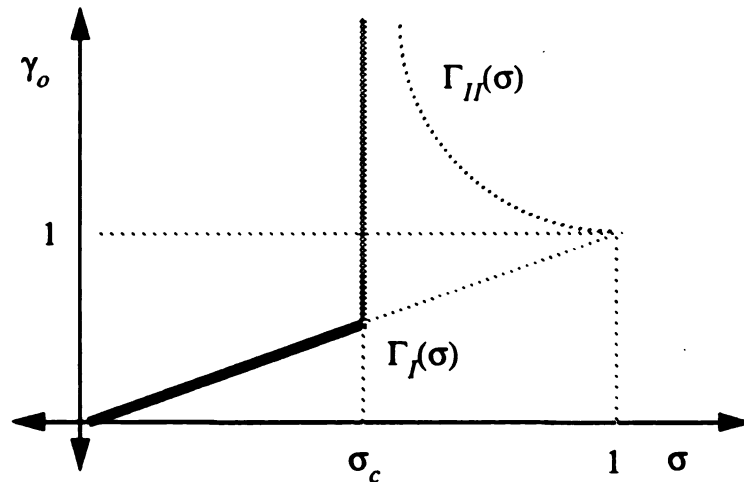
Figure 16. The minimum energy solution for the hard device.

static monotonically increasing displacement $\delta_o = \delta_o(t)$, $\dot{\delta}_o(t) \geq 0$ (a more detailed discussion of quasi-static loading is given in Section 8), then the loading diagram will be as shown in Figure 17. This figure shows that under a minimum energy solution criterion the material first behaves as if it were linearly elastic and then behaves as if it were perfectly plastic for the hard device loading. However, unlike conventional plasticity, unloading after $\gamma_o > \sigma_c$ (corresponding to yielding in plasticity) simply retraces the path in Figure 17.
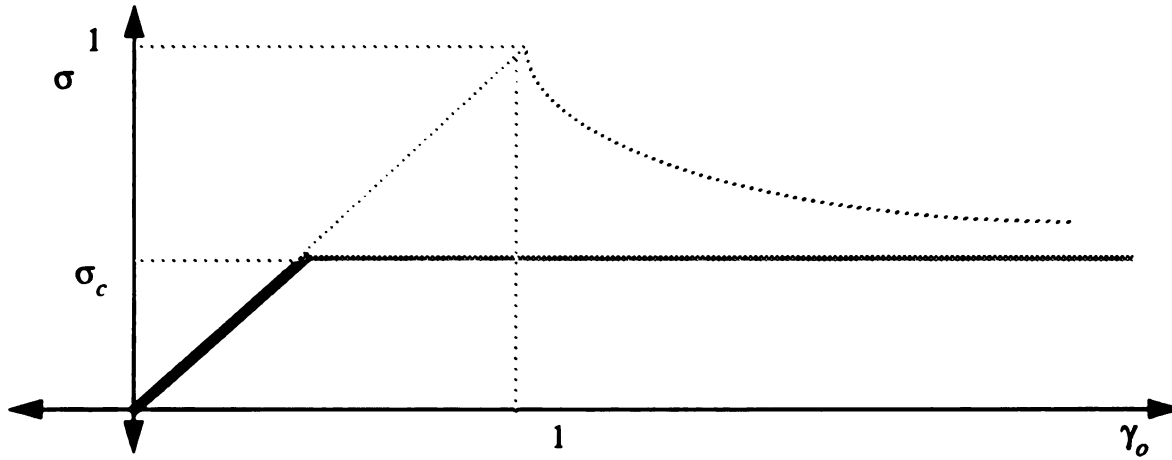
Figure 17. The loading-deformation diagram for the hard device under a minimum energy solution criterion.

7. The soft device energy function on Ω_{12}

Section 6 was concerned with the analysis of the hard device energy function Λ_{12} on the solution region. In this section we conduct a similar analysis for the soft device energy function Ξ_{12}. According to (26), the soft device energy function Ξ_{12} is given by

$\Xi_{12} = \hat{\Xi}_{12}(\sigma, \gamma_o) = W_I(\Gamma_I(\sigma))\hat{s}_{12}(\sigma, \gamma_o) + W_{II}(\Gamma_{II}(\sigma))(1 - \hat{s}_{12}(\sigma, \gamma_o)) - \sigma\gamma_o$. The corresponding level curves of fixed Ξ_{12} in the region Ω_{12} are also functions of γ_o and σ. An example of these level curves is given in Figure 18 for the same particular material used for the constant s curves in Figure 10 and for the level curves of fixed Λ_{12} in Figure 12. For this material and each fixed value of $\Xi_{12} \in (-0.5, \infty)$, the equation $\hat{\Xi}_{12}(\sigma, \gamma_o) = \Xi_{12}$ defines a smooth curve on the (σ, γ_o)-plane. There is a family of such curves in the (σ, γ_o)-plane which correspond to the different values of $\Xi_{12} \in (-0.5, \infty)$. This section is organized similar to that of Section 6, we examine the soft device energy function $\hat{\Xi}_{12}(\sigma, \gamma_o)$ on the boundary of Ω_{12}, on the lines of constant σ, on the lines of constant γ_o and on the lines of constant s.

7.1 The soft device energy function on the boundary of Ω_{12}

The soft device energy function Ξ_{12} on the boundary of Ω_{12} is given by

$$\Xi_{12} = \begin{cases} W_I(\Gamma_I(\sigma)) - \sigma^2 = -\dfrac{\sigma^2}{2} = -\dfrac{\gamma_o^2}{2}, & \text{on } \gamma_o = \Gamma_I(\sigma), \\[2mm] W_{II}(\Gamma_{II}(\sigma)) - \sigma\Gamma_{II}(\sigma), & \text{on } \gamma_o = \Gamma_{II}(\sigma), \\[2mm] W_I(\Gamma_I(\sigma_c)) + W_{II}(\Gamma_{II}(\sigma_c))\dfrac{\gamma_0 - \sigma_c}{\Gamma_{II}(\sigma_c) - \sigma_c} - \sigma_c\gamma_0 = -\dfrac{\sigma_c^2}{2}, & \text{on } \sigma = \sigma_c. \end{cases} \tag{90}$$

The boundary $\gamma_o = \Gamma_I(\sigma)$ of the solution region Ω_{12} gives the pure phase-I solutions. As a result, the soft device energy function is $\Xi_{12} = -\sigma^2/2$. The boundary $\gamma_o = \Gamma_{II}(\sigma)$ of the

51
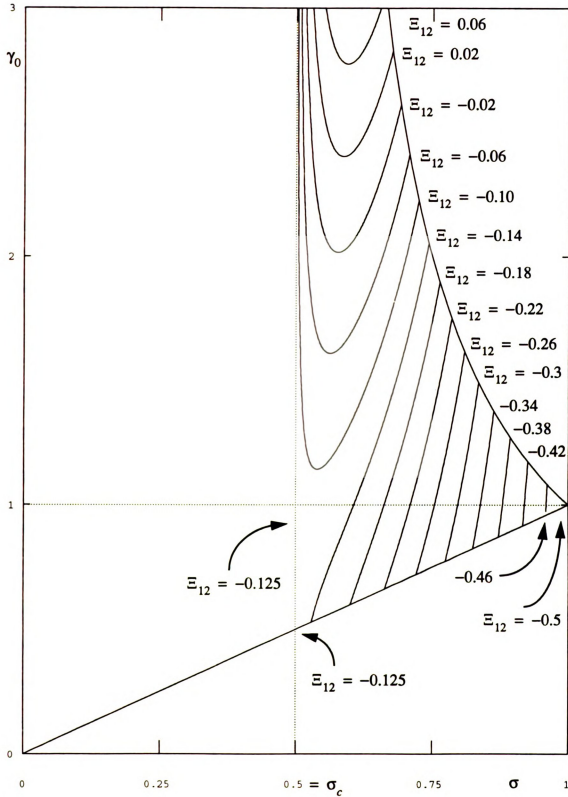
Figure 18. The level curves of constant soft device energy function Ξ_{12} in the solution region Ω_{12} with the choice of the function $\overline{\sigma}_{II}(\gamma)$ by (a.1) of Appendix-A.

solution region Ω_{12} gives pure phase-II solutions. Consequently, the soft device energy function is $\Xi_{12} = W_{II}(\Gamma_{II}(\sigma)) - \sigma\Gamma_{II}(\sigma)$ and it will depend on the choice of the function $\bar{\sigma}_{II}(\gamma)$. We now show that the soft device energy function Ξ_{12} on $\sigma = \sigma_c$, which is the non-attainable limit, is given by $\Xi_{12} = -\sigma_c^2/2$. From (26), (25) and (6) the soft device energy function Ξ_{12} is given by

$$\Xi_{12} = \left. \left(W_I(\Gamma_I(\sigma_c)) \frac{\gamma_R - \gamma_0}{\gamma_R - \gamma_L} + W_{II}(\Gamma_{II}(\sigma_c)) \frac{\gamma_0 - \gamma_L}{\gamma_R - \gamma_L} - \sigma\gamma_0 \right) \right|_{\substack{\gamma_L = \sigma_c \\ \gamma_R \to \infty}} \qquad \text{on } \sigma = \sigma_c. \quad (91)$$

With the help of (51), (52) and (91) it is found that

$$\Xi_{12} = \sigma_c (\gamma_0 - \frac{\sigma_c}{2}) - \sigma\gamma_0 = -\frac{\sigma_c^2}{2}. \qquad (92)$$

It is to be noted that if $\gamma_o = \sigma_c$, then $\Xi_{12} = -\sigma_c^2/2$ which indeed matches the energy for the pure phase-I solution.

7.2 The soft device energy function for Ω_{12} on the lines of constant σ

Having investigated the soft device energy function Ξ_{12} on the boundary of solution region Ω_{12}, naturally we now study the soft device energy function Ξ_{12} inside the solution region Ω_{12}. We first explore the lines of constant σ. Consider two different states with the same stress but different strains: state A corresponds to $(\sigma, \gamma_o) = (\sigma_A, \gamma_A)$; state B corresponds to $(\sigma, \gamma_o) = (\sigma_B, \gamma_B) = (\sigma_A, \gamma_B)$ with $\gamma_B > \gamma_A$. To determine which state has a larger energy value we take partial derivative of Ξ_{12} with respect to γ_o in (26) with constant σ. Since σ is a constant, $\gamma_L = \Gamma_I(\sigma)$ and $\gamma_R = \Gamma_{II}(\sigma)$ are constants too. Therefore, $\Xi_{12} = \Xi_{12}^*(\gamma_o)$ and $s = s^*(\gamma_o)$ are also functions of γ_o only, and it is found that

$$\left.\frac{\partial \Xi_{12}}{\partial \gamma_o}\right|_\sigma = \Xi_{12}^{*\prime}(\gamma_o) = (W_I(\Gamma_I(\sigma)) - W_{II}(\Gamma_{II}(\sigma)))\, s^{*\prime}(\gamma_o) - \sigma. \tag{93}$$

Finally, substitution from (56) into (93) yields

$$\left.\frac{\partial \Xi_{12}}{\partial \gamma_o}\right|_\sigma = \frac{W_{II}(\Gamma_{II}(\sigma)) - W_I(\Gamma_I(\sigma))}{\Gamma_{II}(\sigma) - \Gamma_I(\sigma)} - \sigma = \sigma_{ps}(\sigma) - \sigma > 0. \tag{94}$$

Equation (94) shows that the soft device energy function Ξ_{12} monotonically increases with γ_o along the lines of constant σ for $\sigma_c < \sigma < 1$ so that the value $\gamma_o = \Gamma_I(\sigma)$ always gives the minimum energy solution for a given constant σ. In conclusion, state B has more energy than state A. It is to be noted from (94) and (57) that the energy functions Λ_{12} and Ξ_{12} of both devices monotonically increase with γ_o along the lines of constant σ for $\sigma_c < \sigma < 1$.

7.3 The soft device energy function for Ω_{12} on the lines of constant γ_o

We now explore the lines of constant γ_o and investigate whether the soft device energy function Ξ_{12} on the lines of constant γ_o is increasing or decreasing with σ. Recall from Section 6.3 that we considered two different states with the same strain but different stresses: state A corresponding to $(\sigma, \gamma_o) = (\sigma_A, \gamma_A)$ and state B corresponding to $(\sigma, \gamma_o) = (\sigma_B, \gamma_B) = (\sigma_B, \gamma_A)$ where $\sigma_B > \sigma_A$. Do we find a conclusion similar to (84)? To answer this question we take partial derivative with respect to σ in (26) with fixed γ_o. For a given constant γ_o, $\Xi_{12} = \Xi_{12}^{**}(\sigma)$ and $s = s^{**}(\sigma)$ are functions of σ only. From (26) and (60) it is found that

$$\left.\frac{\partial \Xi_{12}}{\partial \sigma}\right|_{\gamma_o} = \Xi_{12}^{**\prime}(\sigma) = (W_I(\Gamma_I(\sigma)) - W_{II}(\Gamma_{II}(\sigma)))\, s^{**\prime}(\sigma) +$$
$$\sigma \Gamma_I^{\prime}(\sigma) s^{**}(\sigma) + \sigma \Gamma_{II}^{\prime}(\sigma)(1 - s^{**}(\sigma)) - \gamma_o. \tag{95}$$

Equations (58), (95) and (77) show that

$$\left.\frac{\partial \Xi_{12}}{\partial \sigma}\right|_{\gamma_o} = \left(\Gamma_I'(\sigma)s^{**}(\sigma) + \Gamma_{II}'(\sigma)(1 - s^{**}(\sigma))\right)(\sigma - \sigma_{ps}(\sigma)) - \gamma_o. \qquad (96)$$

According to (34) and (86) equation (96) is equivalent to

$$\left.\frac{\partial \Xi_{12}}{\partial \sigma}\right|_{\gamma_o} = -\gamma_o + \left.\frac{\partial \gamma_o}{\partial \sigma}\right|_s (\sigma - \sigma_{ps}(\sigma))$$

$$\left. = -\gamma_o + \frac{\partial s}{\partial \sigma}\right|_{\gamma_o} (\Gamma_{II}(\sigma) - \Gamma_I(\sigma))(\sigma - \sigma_{ps}(\sigma)). \qquad (97)$$

Recall from (79) that in the hard device $\left.\frac{\partial \Lambda_{12}}{\partial \sigma}\right|_{\gamma_o}$ and $\left.\frac{\partial \gamma_o}{\partial \sigma}\right|_s$ have opposite signs provided that

$\sigma < \sigma_{ps}(\sigma)$. However now for the soft device $\left.\frac{\partial \Xi_{12}}{\partial \sigma}\right|_{\gamma_o}$ and $\left.\frac{\partial \gamma_o}{\partial \sigma}\right|_s$ might have opposite signs

or might have same sign. For example, since $\sigma < \sigma_{ps}$ and $\gamma_o > 0$ if we have $\left.\frac{\partial \gamma_o}{\partial \sigma}\right|_s > 0$ then

we find $\left.\frac{\partial \Xi_{12}}{\partial \sigma}\right|_{\gamma_o} < 0$. But we find $\left.\frac{\partial \Xi_{12}}{\partial \sigma}\right|_{\gamma_o} > 0$ only if $\left.\frac{\partial \gamma_o}{\partial \sigma}\right|_s < 0$. Also recall from Section 5

that since the distributions of the lines of constant s are dependent on the material only as shown in Figure 10, the distributions are typical for both devices. Therefore the points on $\emptyset_2$ give the minimum values of s in the solution region Ω_{12} on the lines of constant γ_o which are the same for both the hard device and the soft device. Also recall from Section 5 and Section 6 that the points on $\emptyset_2$ give the maximum values of hard device energy function Ξ_{12} in the solution region Ω_{12} on the lines of constant γ_o. But now the points on $\emptyset_2$ do not give the extremum points of the soft device energy function Ξ_{12} on the lines of constant γ_o. From (97) it is found that

$$\left.\frac{\partial \Xi_{12}}{\partial \sigma}\right|_{\gamma_o} = 0 \Rightarrow \left.\frac{\partial \gamma_o}{\partial \sigma}\right|_s < 0. \qquad (98)$$

This implies that the possible extrema of the soft device energy function Ξ_{12} along constant γ_o lines can only occur where the curves of constant s have negative slope in the (σ, γ_o) - plane. Hence it is to the left of the curve $\varnothing_2$. Similar developments can be found in the relation between $\left. \dfrac{\partial \Xi_{12}}{\partial \sigma} \right|_{\gamma_o}$ and $\left. \dfrac{\partial s}{\partial \sigma} \right|_{\gamma_o}$.

To determine whether any such extremum of the soft device energy function Ξ_{12} is a maximum or a minimum we calculate the second partial derivative of the soft device energy function Ξ_{12} with respect to σ. Thus (97), (98) and (64) give

$$\left. \frac{\partial^2 \Xi_{12}}{\partial \sigma^2} \right|_{\gamma_o} = \Xi_{12}^{**}{}''(\sigma) =$$

$$\left. \frac{\partial^2 s}{\partial \sigma^2} \right|_{\gamma_o} (\Gamma_{II}(\sigma) - \Gamma_I(\sigma)) \; (\sigma - \sigma_{ps}(\sigma)) + \left. \frac{\partial s}{\partial \sigma} \right|_{\gamma_o} (\Gamma_{II}(\sigma) - \Gamma_I(\sigma)) \, . \tag{99}$$

Substitution from (89) and (86) into (99) gives

$$\left. \frac{\partial^2 \Xi_{12}}{\partial \sigma^2} \right|_{\gamma_o} = \Xi_{12}^{**}{}''(\sigma) = \left. \frac{\partial^2}{\partial \sigma^2} \gamma_o \right|_s (\sigma - \sigma_{ps}(\sigma)) + \left. \frac{\partial \gamma_o}{\partial \sigma} \right|_s < 0, \tag{100}$$

where from (46), (63)$_1$ and (98) we find $\left. \dfrac{\partial^2}{\partial \sigma^2} \gamma_o \right|_s > 0$, $\sigma < \sigma_{ps}(\sigma)$ and $\left. \dfrac{\partial \gamma_o}{\partial \sigma} \right|_s < 0$. Therefore if the point (σ, γ_o) satisfies $\left. \dfrac{\partial \Xi_{12}}{\partial \sigma} \right|_{\gamma_o} = 0$ then the point (σ, γ_o) gives a maximum soft device energy function value Ξ_{12}.

It is easy to show from (90), at a given constant γ_o obeying $\sigma_c < \gamma_o \leq 1$, that the energy on $\sigma = \sigma_c$ is greater than the energy on $\sigma = \bar{\sigma}_I(\gamma_o)$. For example the difference between the energy on $\sigma = \sigma_c$ and the energy on $\sigma = \bar{\sigma}_I(\gamma_o)$ is given by

$$\Xi_{12}\big|_{\text{on } \sigma = \sigma_c} - \Xi_{12}\big|_{\text{on } \sigma = \bar{\sigma}_I(\gamma_o)} = \left(-\frac{\sigma_c^2}{2}\right) - \left(-\frac{\gamma_o^2}{2}\right) = \frac{\gamma_0^2}{2} - \frac{\sigma_c^2}{2} > 0. \tag{101}$$

Comparing this result to (53) it is seen that the soft device behaves in a completely different manner. As for a comparison of the energy Ξ_{12} on $\sigma = \sigma_c$ and on $\sigma = \bar{\sigma}_{II}(\gamma_o)$ for $\gamma_o > 1$, examination of Figure 19 shows that neither $\sigma = \sigma_c$ nor $\sigma = \bar{\sigma}_{II}(\gamma_o)$ is ensured to have less energy on the lines of constant $\gamma_o > 1$. Further investigation of this interesting issue (which is a possible topic for future study) might yield rules for constructing profile curves similar to those in Figure 15 but for the soft device.

7.4 The soft device energy function for Ω_{12} on the curves of constant s

Recall from Section 5 that there are two types of behavior to the constant s curves: one has γ_o monotonically decreasing as a function of σ ($s \le s_{trans}$) and the other has γ_o decreasing as a function of σ then increasing as a function of σ ($s > s_{trans}$). It is found for both types that the soft device energy function Ξ_{12} decreases as $\sigma : \sigma_c \to 1$. To show this we take the partial derivative with respect to σ in (26) with fixed s, and it is found that $\Xi_{12} = \Xi_{12}^{**}(\sigma)$ and

$$\left. \frac{\partial \Xi_{12}}{\partial \sigma} \right|_s = \Xi_{12}^{**\prime}(\sigma) = -\gamma_o < 0. \tag{102}$$
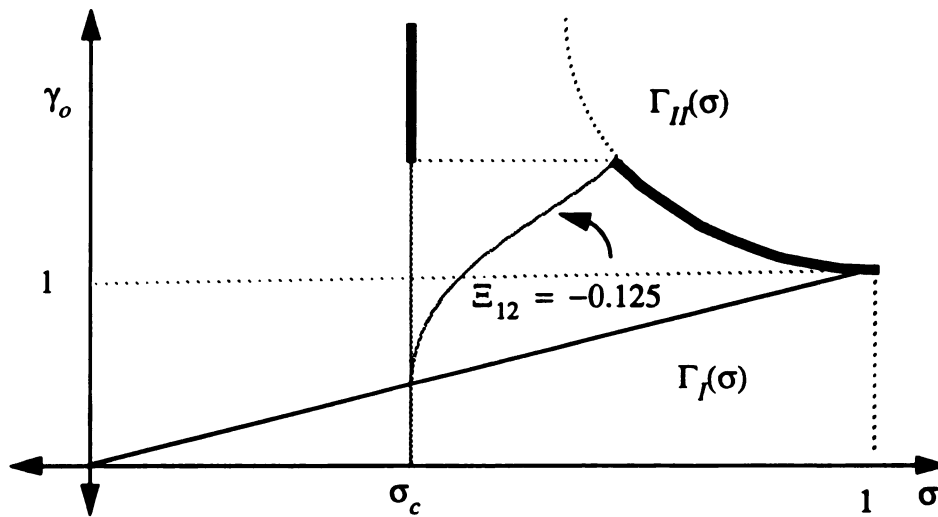
Figure 19. The minimum soft device energy solution on the constant γ_o lines for $\gamma_o > 1$.

7.5 The minimum energy criterion for the soft device

Recall from Section 7.2 that the soft device energy function Ξ_{12} monotonically increases with γ_o on the lines of constant σ. Therefore the minimum energy solution for the soft device will be the line $\gamma_o = \Gamma_I(\sigma)$ which corresponds to a pure phase-I solution (see Figure 20).

Therefore under a minimum energy solution criterion if the bar is elongated at the end with a quasi-static monotonically increasing displacement $\sigma = \sigma(t)$, $\dot{\sigma}(t) \geq 0$, then the loading diagram will be as shown in Figure 21. This figure shows that the material behaves as if it were linearly elastic up to the maximum load value $\sigma = 1$.
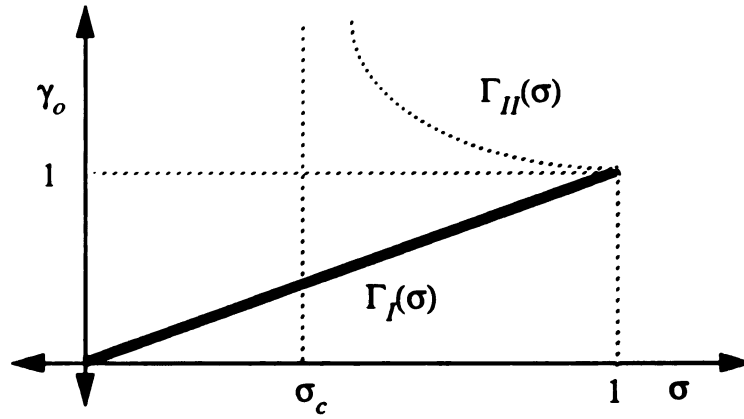
Figure 20. The minimum energy solution path for the soft device.
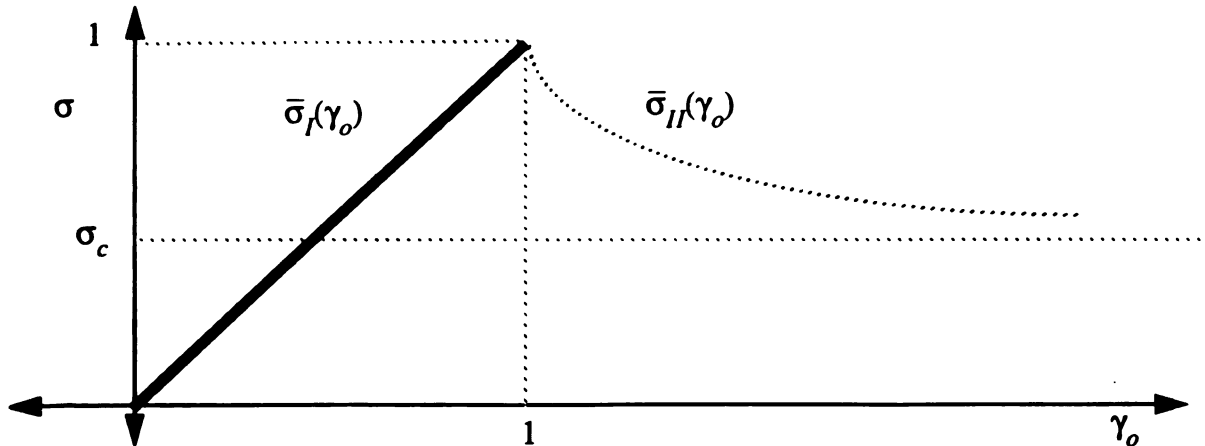
Figure 21. The loading diagram for the soft device under the minimum energy criterion.

8. Quasi-static motions with a single phase boundary

8.1 Definition

We now turn our attention to quasi-static motions of the bar. Following Knowles [1979K] and Pence [1991PP] a quasi-static solution to either the soft device problem or the hard device problem is a sequence of equilibrium states which at each instant t obeys the boundary conditions. Note that no inertia effects are considered here. Now the time t is being introduced and it plays only the role of a history parameter. Thus in the hard device $\gamma_o(t)$ is prescribed and is assumed to be a continuous function. At each instant t if $0 < \gamma_o(t) \leq \sigma_c$ then there is an unique equilibrium solution $\sigma = \gamma_o(t)$. Moreover at each instant t if $\gamma_o(t) > \sigma_c$ then for both the (1,2)-case and also for the (2,1)-case there is a family of equilibrium solutions parametrized by the instantaneous value of spatially constant stress σ (see Section 5). The parameter σ will thus vary with time so that $\sigma = \sigma(t)$ and $\bar{\sigma}(\gamma(X, t)) = \sigma(t)$, where $\gamma(X, t)$ is the associated strain field. If we only consider either the (1,2)-case or the (2,1)-case then once the (unprescribed) $\sigma(t)$ is found, it will determine a particular quasi-static solution at each instant t. According to (23) it is necessary that $\sigma(t)$ be continuous for the location of the phase boundary $s(t) = \hat{s}_{ij}(\sigma(t), \gamma_o(t))$ to vary continuously with respect to time t.

If we imagine a bar is in pure phase-I in the beginning and that later a phase boundary is created at $X = L$ which then moves from the right end to the left end, then we have the following different cases during the motion. At first the bar is in the (1,1)-case; and then the phase boundary is created at the right end and moves to the left meaning that the bar has changed from the (1,1)-case to the (1,2)-case; then if the phase boundary hits the left end then the bar changes from the (1,2)-case to the (2,2)-case. From the above observation we can find (1,1), (1,2), (2,2)-cases during the motion. This set of cas-

es which gives the motion of a single phase boundary is the combination of the (1,1), (1,2), (2,2)-cases. The other set of cases which also gives the motion of a single phase boundary is the combination of the (1,1), (2,1), (2,2)-cases. Here the phase boundary is created at the right end and, at least initially, moves to the left. Note that there can be no direct switching between the (1,2)-case and the (2,1)-case. The switching between those two combinations is only through an intermediate pure phase state, either the (1,1)-case or the (2,2)-case.

Similarly, in the soft device, $\sigma(t)$ is prescribed and is assumed to be a continuous function. At each instant t whenever $0 < \sigma(t) \le \sigma_c$ then there is an unique equilibrium solution $\gamma_o = \sigma(t)$. Moreover at each instant t whenever $\sigma_c < \sigma(t) < 1$ then there is a family of equilibrium solutions parametrized by the instantaneous value of elongation $\delta_o(t) = \gamma_o(t)L$ at the end $X = L$. The parameter γ_o will thus vary with time so that $\gamma_o = \gamma_o(t)$. Once the (unprescribed) $\gamma_o(t)$ is found it will then determine a particular quasi-static solution at each instant t. It is also required that $\gamma_o(t)$ be continuous for the location of the phase boundary to vary continuously with respect to time t.

Consider that the bar is elongated with a quasi-static load $\gamma_o(t)$ starting from $(\sigma, \gamma_o) = (0,0)$. For the combinations of the (1,1), (1,2), (2,2)-cases of solutions, since the solution at each instant is represented by a point in the solution region Ω_{12}, a continuous quasi-static motion is represented by a continuous curve in this region. For a prescribed monotonically increasing $\gamma_o(t)$, any continuous curve with increasing $\gamma_o(t)$ in this region represents a possible quasi-static motion. Therefore we can find many possible curves for the motion. Typical curves for such motion which are given as path (a)-(f) in Figure 22. In what follows we explain the meanings of these paths:

(a) The solution path will be restricted to $\gamma_o = \Gamma_I(\sigma) = \sigma$ of the pure phase-I solutions so long as $\gamma_o(t) < \sigma_c$.

(b) The solution path could stay on $\gamma_o = \Gamma_I(\sigma) = \sigma$ of the pure phase-I solutions after

$\gamma_o(t) > \sigma_c$ until $\gamma_o = 1$.

(c) Alternatively, after $\gamma_o(t) > \sigma_c$ but before $\gamma_o(t) = 1$, the solution paths could move

into the interior of the solution region by creating a phase boundary at the right end.

(d) There is another possible path which will first move along the line $\gamma_o = \Gamma_I(\sigma) = \sigma$

of the pure phase-I solutions up to $\gamma_o = \sigma = 1$ and then could move into the interior

of the solution region. Note that this point, $(\sigma, \gamma_o) = (1,1)$ is the only point in the

solution region Ω_{12} which can be regarded both as a pure phase-I solution and as a

pure phase-II solution. Upon leaving this point the strain field could have smooth

transfer from this pure phase solution to a mixed state of phase-I and phase-II by cre-

ating an *internal* phase boundary. To see this start with the pure phase solution point
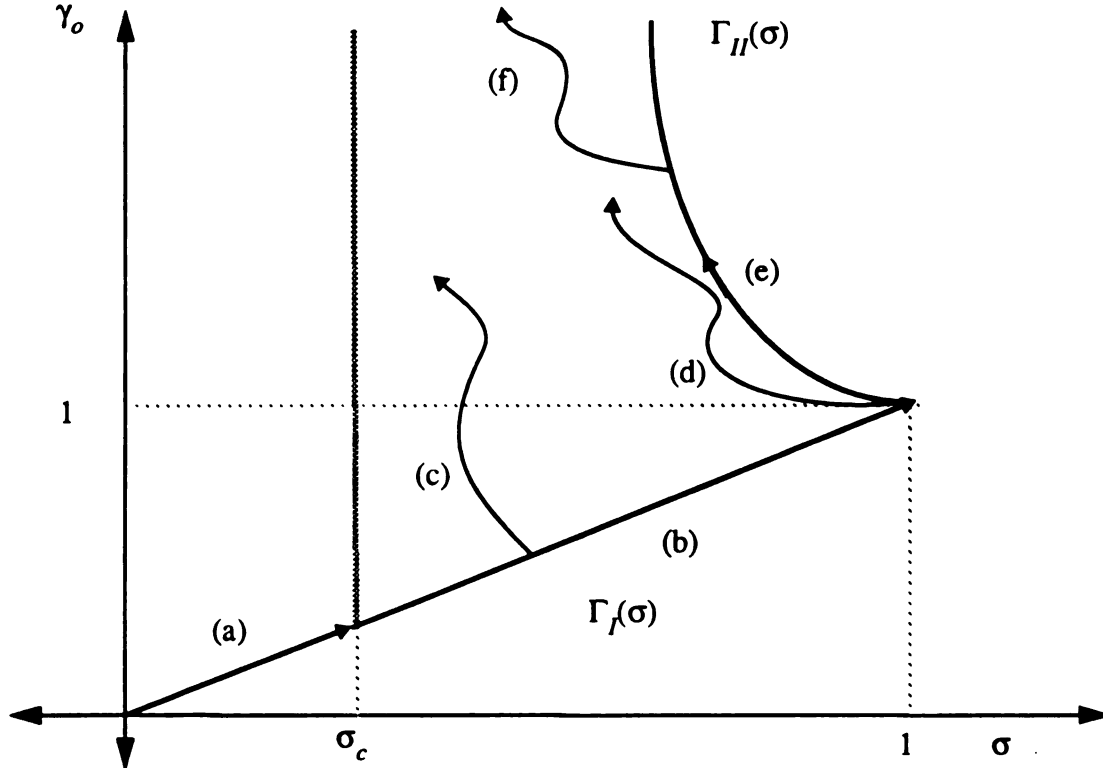
Figure 22. Some possible quasi-static motions in the solution region Ω_{12} as γ_o increases
from $\gamma_o=0$.

$(\sigma, \gamma_o) = (1, 1)$ and imagine some fixed $s = s_o$ between 0 and 1. According to

Section 5 each curve of constant s in the solution region ends at $(\sigma, \gamma_o) = (1, 1)$.

It is to be noted that the strains on both sides of the internal phase boundary s_o are

equal to 1 at the point $(\sigma, \gamma_o) = (1, 1)$ so that at first both sides of the internal phase

boundary s_o have the common strain value of 1. Suppose that the strain γ_R in $x > s_o$

increases and at the same time that the strain γ_L in $x < s_o$ decreases in such a way that

$\bar{\sigma}_{II}(\gamma_R) = \bar{\sigma}_I(\gamma_L)$. This causes the solution path to move into the solution region Ω_{12}

along the $s = s_o$ curve. It was assumed in the above description that the internal

phase boundary remains fixed at $s = s_o$, but it is also possible that the phase bound-

ary could move. This occurs if the solution path (d) enters the solution region Ω_{12} by

a path which does not coincide with the curves of constant s.

(e) Another possible path stays on the curve $\gamma_o = \Gamma_{II}(\sigma)$. The solution will give pure

phase-II solutions as long as the path follows the curve $\gamma_o = \Gamma_{II}(\sigma)$.

(f) The final possible path splits off from the solution path (e) at some $\gamma_o > 1$ and moves

into the interior of the solution region Ω_{12} by creating a phase boundary at the left

end.

8.2 Dissipation and driving traction

Following Knowles [1979K] the rate of dissipation $D(t)$ in a quasi-static motion is the dif-

ference between the rate of the external work $E_e(t)$ and the rate of increase of strain energy

$E_s(t)$, therefore:

$$D(t) = \dot{E}_e(t) - \dot{E}_s(t). \tag{103}$$

As shown by Knowles [1979K], quasi-static problems with non-monotone stress response

do not require that $D(t) = 0$ as it is in conventional linear elasticity. The external work is

$$E_e(t) = \int_0^{\gamma_o(t)} \bar{\sigma}(v)dv \qquad (104)$$

and the rate of external work is

$$\dot{E}_e(t) = \sigma\dot{\gamma}_o(t). \qquad (105)$$

The stored strain energy is

$$E_s(t) = \int_0^1 W(\gamma)d\frac{X}{L} = W(\gamma_L(t))s + W(\gamma_R(t))(1-s). \qquad (106)$$

Note from (6) that $\gamma_L = \Gamma_i(\sigma)$ and $\gamma_R = \Gamma_j(\sigma)$, where $i = I$ or II and $j = I$ or II. Hence the stored strain energy for all four cases could be obtained by equation (106). The rate of increase of the strain energy is then given by

$$\dot{E}_s(t) = (W(\gamma_L(t)) - W(\gamma_R(t)))\dot{s} + (\frac{d}{dt}W(\gamma_L(t)))s + (\frac{d}{dt}W(\gamma_R(t)))(1-s), \qquad (107)$$

where $\dot{s} = \dfrac{ds}{dt}$ is the quasi-static phase boundary velocity. It is to be noted that

$$\frac{d}{dt}W(\gamma_L(t)) = \sigma\dot{\gamma}_L,$$
$$\frac{d}{dt}W(\gamma_R(t)) = \sigma\dot{\gamma}_R. \qquad (108)$$

From (107) and (108) it is found that

$$\dot{E}_s(t) = (W(\gamma_L(t)) - W(\gamma_R(t)))\dot{s} + \sigma\dot{\gamma}_L(t)s + \sigma\dot{\gamma}_R(t)(1-s). \qquad (109)$$

Substitutions from (105) and (109) into (103) yield the rate of dissipation

$$D(t) = \sigma\dot{\gamma}_o(t) - (W(\gamma_L(t)) - W(\gamma_R(t)))\dot{s} - (\sigma\dot{\gamma}_L(t)s + \sigma\dot{\gamma}_R(t)(1-s)). \qquad (110)$$

Taking the derivative with respect to time t in (23) gives

$$\dot{\gamma}_o(t) = (\dot{\gamma}_L(t)s + \dot{\gamma}_R(t)(1-s)) + (\gamma_L(t) - \gamma_R(t))\dot{s}. \qquad (111)$$

Therefore from (110) and (111) it is found that the rate of dissipation is given by

$$D(t) = \dot{s}(W(\gamma_R(t)) - W(\gamma_L(t)) - \sigma(\gamma_R(t) - \gamma_L(t))). \qquad (112)$$

It is to be emphasized that the rate of dissipation for all four cases as given in (21) could be obtained by (112), however $D(t) = 0$ for both the (1,1) and the (2,2) trivial cases since then

$$\gamma_R(t) = \gamma_L(t).$$

Let $f = f_{ij}$ be defined by

$$
\begin{aligned}
f = f_{ij} &= W(\Gamma_j(\sigma)) - W(\Gamma_i(\sigma)) - \sigma\,(\Gamma_j(\sigma) - \Gamma_i(\sigma)) \\
&= (\,(W(\Gamma_j(\sigma)) - \sigma\Gamma_j(\sigma)) - (W(\Gamma_i(\sigma)) - \sigma\Gamma_i(\sigma))\,).
\end{aligned}
\tag{113}
$$

Note that equation (113) can be rewritten as

$$f = f_{ij} = [\,[p]\,] = p_j - p_i \tag{114}$$

where $[[\bullet]]$ indicates the jump across the phase boundary at $x = s(t)$ and $p = W(\gamma) - \sigma\gamma$ which is the one dimensional case of the more general energy-momentum tensor discussed by Eshelby [1975EE]. Substitution from (113) into (112) and with the help of (6) obtains the rate of dissipation

$$D(t) = \dot{s}f. \tag{115}$$

Hence (103) can be rewritten as

$$\dot{E}_e(t) + (-f)\,\dot{s} = \dot{E}_s(t) \tag{116}$$

which may be viewed as a work-energy identity. It means that the sum of rates at which work is being done on the bar by the external forces and done internally at the phase boundary $x = s(t)$, is balanced by the rate at which energy is being stored in the bar. Consequently, $-f$ may be treated as the traction applied by the phase boundary "on" the surrounding material, or similarly, $+f$ can be viewed as a driving traction exerted on the phase boundary by the surrounding material (Abeyaratne and Jiang [1989A]). The driving traction is similar to the notion of the "force on a defect" first derived by Eshelby [1956E]. It is also similar to the force on the interface between two phases derived by Eshelby [1970E] and discussed by Rice [1975R]. It is easily shown that if there are numerous phase boundaries then (116) generalizes to

$$\dot{E}_e(t) + \sum_{\substack{\text{on} \\ \text{discontinuities}}} (-f)\,\dot{s} = \dot{E}_s(t). \tag{117}$$

From (58) it is found that (113) can be written as

$$f_{ij} = (\sigma_{ps}(\sigma) - \sigma)(\Gamma_j(\sigma) - \Gamma_i(\sigma)). \tag{118}$$

Note for the (1,2)-case and the (2,1)-case that this gives

$$f_{12} = (\sigma_{ps}(\sigma) - \sigma)(\Gamma_{II}(\sigma) - \Gamma_I(\sigma)) \equiv \bar{f}_{12}(\sigma),$$

$$f_{21} = (\sigma_{ps}(\sigma) - \sigma)(\Gamma_I(\sigma) - \Gamma_{II}(\sigma)) \equiv \bar{f}_{21}(\sigma) = -\bar{f}_{12}(\sigma). \tag{119}$$

In the (1,2)-case, $(63)_1$ gives $\sigma_{ps} > \sigma$ and $\Gamma_{II}(\sigma) > \Gamma_I(\sigma)$ whenever $\sigma_c < \sigma < 1$. Therefore it follows from $(119)_1$ that the driving traction obeys $f_{12} > 0$. However, in the (2,1)-case, it is found from $(119)_2$ that $f = f_{21} < 0$. In summary

$$f_{12} = -f_{21} > 0, \qquad \text{if } \sigma_c < \sigma < 1. \tag{120}$$

From (113) we also can find that the driving traction for the (1,2)-case is given by

$$\bar{f}_{12}(\sigma) = \int_\sigma^1 (\Gamma_{II}(v) - \Gamma_I(v))\, dv$$

$$= \int_\sigma^1 \Gamma_{II}(v)\, dv - \frac{1 - \sigma^2}{2}. \tag{121}$$

In what follows we examine the function $\bar{f}_{12}(\sigma)$. From (121) the driving traction is always equal to zero whenever $\sigma = 1$ while at $\sigma = \sigma_c$ it is equal to the following

$$\bar{f}_{12}(\sigma_c) = \int_{\sigma_c}^1 \Gamma_{II}(v)\, dv - \frac{1 - \sigma_c^2}{2} \tag{122}$$

so that its value depends on the function $\Gamma_{II}(\sigma)$. For example with the choice of the function $\bar{\sigma}_{II}(\gamma)$ given by (a.1) of Appendix-A it is found for material A that the function $\bar{f}_{12}(\sigma)$ monotonically decreases from $(\sigma, \bar{f}_{12}(\sigma)) = (0.5, \infty)$ at $\sigma = \sigma_c$ to $(\sigma, \bar{f}_{12}(\sigma)) = (1, 0)$. However for Material B with the choice of the function $\bar{\sigma}_{II}(\gamma)$ given by (b.1) of Appendix-B it is found that the function $\bar{f}_{12}(\sigma)$ monotonically decreases from $(\sigma, \bar{f}_{12}(\sigma)) = (0.5, 0.625)$ at $\sigma = \sigma_c$ to $(\sigma, \bar{f}_{12}(\sigma)) = (1, 0)$ (see Figure 23). More generally from (121), the first derivative of $\bar{f}_{12}(\sigma)$ for any choice of $\bar{\sigma}_{II}(\gamma)$ is given by

$$\bar{f}_{12}'(\sigma) = \Gamma_I(\sigma) - \Gamma_{II}(\sigma) \le 0. \tag{123}$$
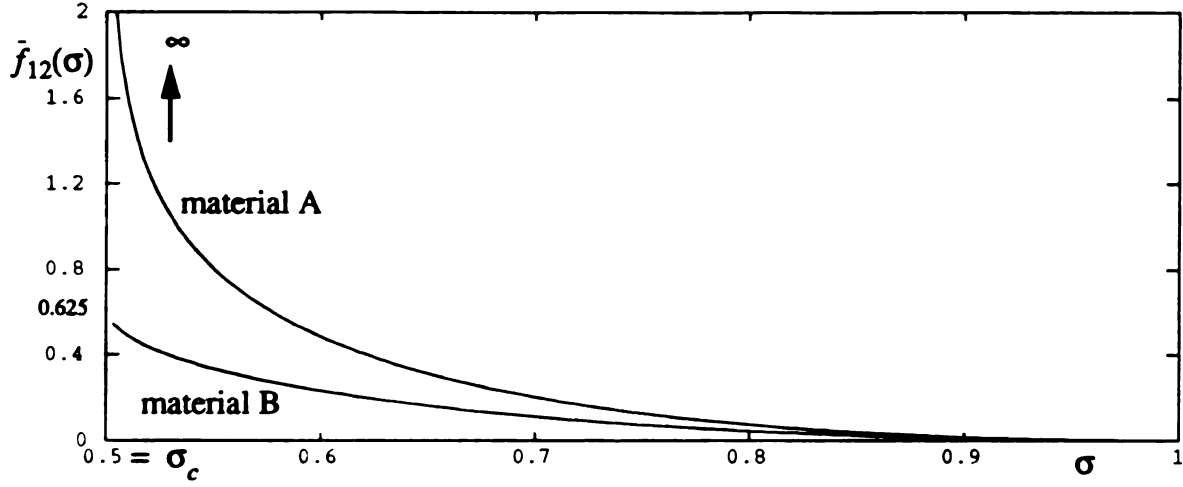
Figure 23. The functions $\bar{f}_{12}(\sigma)$ with the choice of the function $\bar{\sigma}_{II}(\gamma)$ given by (a.1) of Appendix-A for material A and by (b.1) of Appendix-B for material B.

For the example function $\bar{\sigma}_{II}(\gamma)$ given either by (a.1) of Appendix-A or by (b.1) of Appendix-B this derivative monotonically increases from $(\sigma, \bar{f}_{12}{}'(\sigma)) = (0.5, -\infty)$ to

$(\sigma, \bar{f}_{12}{}'(\sigma)) = (1, 0)$ (see Figure 24). The second derivative of $\bar{f}_{12}(\sigma)$ is given by

$$\bar{f}_{12}{}''(\sigma) = \Gamma_I{}'(\sigma) - \Gamma_{II}{}'(\sigma) > 0. \tag{124}$$

Recall form $(39)_2$ and $(43)_2$ that $\Gamma_I{}'(\sigma) = 1$ and $\Gamma_{II}{}'(\sigma) < 0$. Therefore $\bar{f}_{12}{}''(\sigma) > 0$ so that
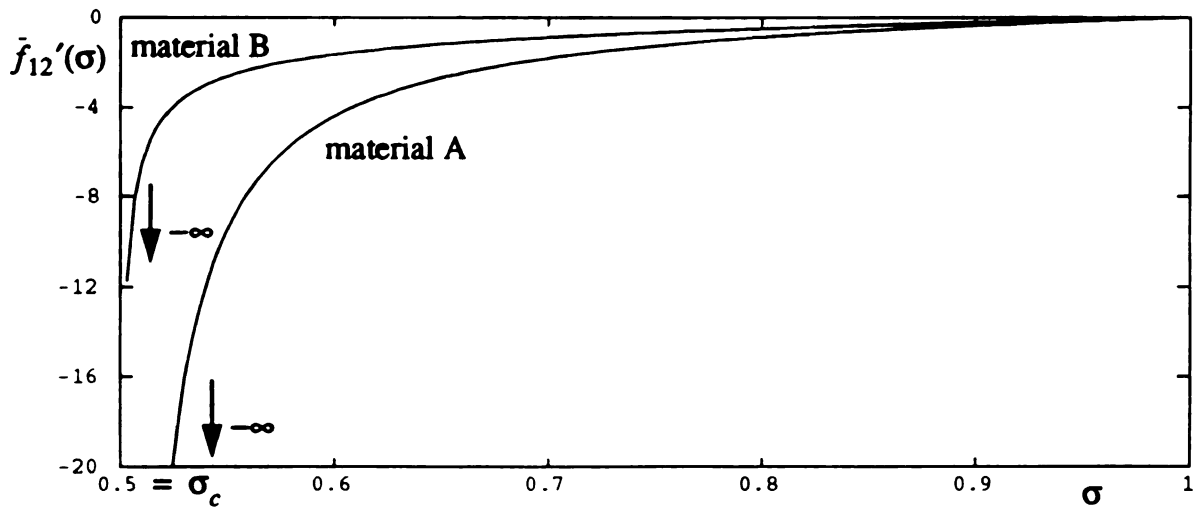
Figure 24. The first derivative of the functions of $\bar{f}_{12}(\sigma)$ for the example function $\bar{\sigma}_{II}(\gamma)$ given by (a.1) of Appendix-A for material A and by (b.1) of Appendix-B for material B.

$\bar{f}_{12}(\sigma)$ is a concave function. Since $\bar{f}_{21}(\sigma) = -\bar{f}_{12}(\sigma)$ it follows that $\bar{f}_{21}(\sigma)$ is a convex function.

For the $(1,1)$-case and the $(2,2)$-case, both the strain γ_L and the strain γ_R are equal which gives $f = f_{11} = f_{22} = 0$ and hence the rate of increase of external work is balanced by the rate of increase of strain energy. This is to be expected, since for these cases an internal phase boundary has no real physical significance.

8.3 Admissible direction of movement of the phase boundary

According to the second law of thermodynamics under isothermal conditions, the rate of increase of strain energy $E_e(t)$ cannot exceed the rate of the external work $E_s(t)$ (Knowles [1979K]). Thus it follows from (115) and (119) that the dissipation rate

$$D(t) = \dot{s}f \geq 0 \tag{125}$$

which restricts the direction of the movement of the phase boundary. A quasi-static motion is *admissible* if the dissipation inequality (125) is obeyed during the motion. Hence it can be concluded that the directions in which the phase boundary can move are not unrestricted, but must obey

$$\dot{s} \begin{cases} \geq 0 & if \quad f > 0, \\ \text{unrestricted} & if \quad f = 0, \\ \leq 0 & if \quad f < 0. \end{cases} \tag{126}$$

Consider the $(1,2)$-case, then from (120) and (126) it is required that $\dot{s} \geq 0$ if $\sigma_c < \sigma < 1$. However if the stress $\sigma = 1$ then the driving traction $f_{12} = 0$ so that inequality (126) does not restrict the sign of $\dot{s}$ at $\sigma = 1$ (see Figure 25). This restricts the possible paths as previously shown in Figure 22. In particular if the bar is elongated with monotonically increasing $\gamma_o(t)$ then the path must follow the line $s = 1$ of pure phase-I solutions when $0 < \gamma_o(t) < 1$. Thus path (c) in Figure 22 cannot occur. Thus the stress eventually reaches its maximum value $\sigma = 1$. After this further elongation allow both pure phase-II
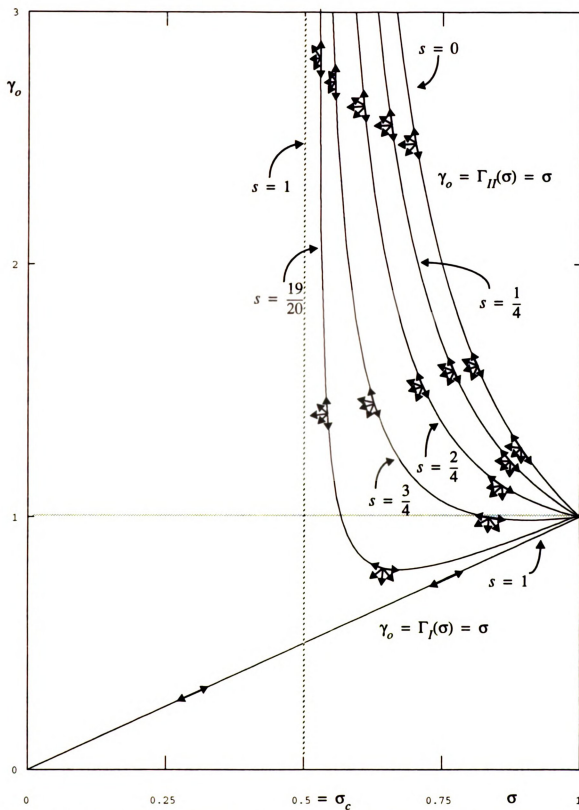
Figure 25. The admissible directions for the quasi-static motions in the solution region Ω_{12}. The constant s curves are for the function $\overline{\sigma}_{II}(\gamma)$ given by (a.1) of Appendix-A, but the diagram is representative for any function obeying (5).

solutions ($s = 0$) and true (1,2)-type solutions. This is because the admissible directions on the curve $s = 0$ of pure phase-II solutions allows the paths to split off and enter the interior of the solution region Ω_{12} (see Figure 25).

The (2,1)-case is similar to the (1,2)-case, but now the phase boundary starts on the other side and moves in the other direction. Hence the admissible path diagram is essentially the same (Figure 26). From the above discussion it is to be noted that the solution paths will start from $(\sigma, \gamma_o) = (0,0)$, follow the $\gamma_o = \sigma$ line, and reach the peak $(\sigma, \gamma_o) = (1, 1)$ for both hard device and soft device loadings in the (σ, γ_o)-plane. Moreover since there is no phase boundary before this peak is reached it follows from (116) that the rate of increase of external work is balanced by the rate of increase of strain energy. Thus, the path $\gamma_o = \sigma$ of pure phase-I solutions is dissipation free. Note that for the same reason the path $\gamma_o = \Gamma_{II}(\sigma)$ of pure phase-II solutions is also dissipation free.

Finally we note for both the (1,2)-case and the (2,1)-case that the phase boundary moves so as to decrease the amount of phase-II and increase the amount of phase-I. This is related to the instability of descending portions of a stress-strain response function as found by other authors for different problems (see Abeyaratne and Knowles [1989A], Kikuchi and Triantafyllidis [1982K]).

8.4 Comments on the admissible paths

In what follows, equation (126) will be required to hold at all times t. We first consider soft device paths in which $\sigma(t)$ is not only specified but is specified to be constant for all future time t. We consider arbitrary initial values of γ_o in the solution region Ω_{12} on the associated line of constant σ. An interesting question is whether paths starting at this initial point are allowed to move to the boundary of the solution region Ω_{12}. For each constant value of σ there are two possible boundary points given by $\gamma_o = \Gamma_I(\sigma)$ or $\gamma_o = \Gamma_{II}(\sigma)$. Every point
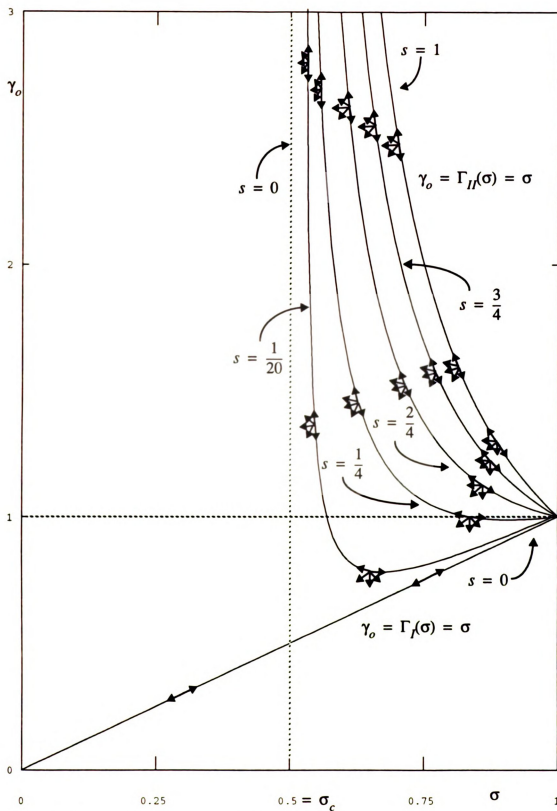
Figure 26. The admissible directions for the quasi-static motions in the solution region Ω_{21}. The constant s curves are for the function $\overline{\sigma}_{II}(\gamma)$ given by (a.1) of Appendix-A, but the diagram is representative for any function obeying (5).
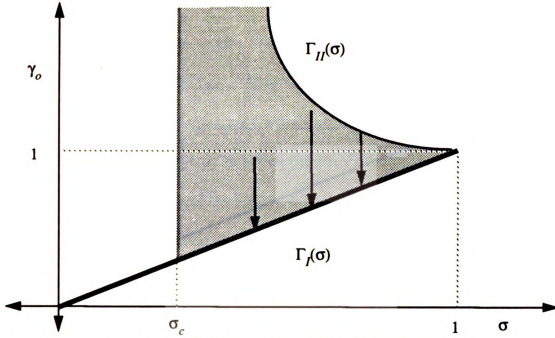
Figure 27. Admissible constant σ paths that reach the boundary $\gamma_o = \Gamma_I(\sigma)$ for the soft device. All points on the constant σ lines can reach points on this boundary.

in the solution region could move to the boundary point $\gamma_o = \Gamma_I(\sigma)$ (see Figure 27) since a downward path is always admissible (see Figure 25). The points inside the solution region could not move to the boundary point $\gamma_o = \Gamma_{II}(\sigma)$ since the upward direction is not admissible (see Figure 25). Therefore the only point that can "move" to $\gamma_o = \Gamma_{II}(\sigma)$ on an admissible constant σ path is the boundary point $\gamma_o = \Gamma_{II}(\sigma)$ itself which is already there (see Figure 28).

Similarly let's consider hard device paths in which $\delta_o(t)$ is not only specified but is specified to be constant at all instants t so that γ_o is fixed. The same interesting question is whether similar paths could move to the boundary of the solution region. For each constant value of γ_o, there are two possible boundary points given either by $\sigma = \sigma_c$ and $\gamma_o = \Gamma_I(\sigma)$, or by $\sigma = \sigma_c$ and $\gamma_o = \Gamma_{II}(\sigma)$ depending on the constant value of γ_o. Those points inside the solution region with $\overline{\sigma}(\gamma_o) > \overline{\sigma}_{\varnothing_2}(\gamma_o)$ and $\gamma_o \leq 1$ could move to the bound-
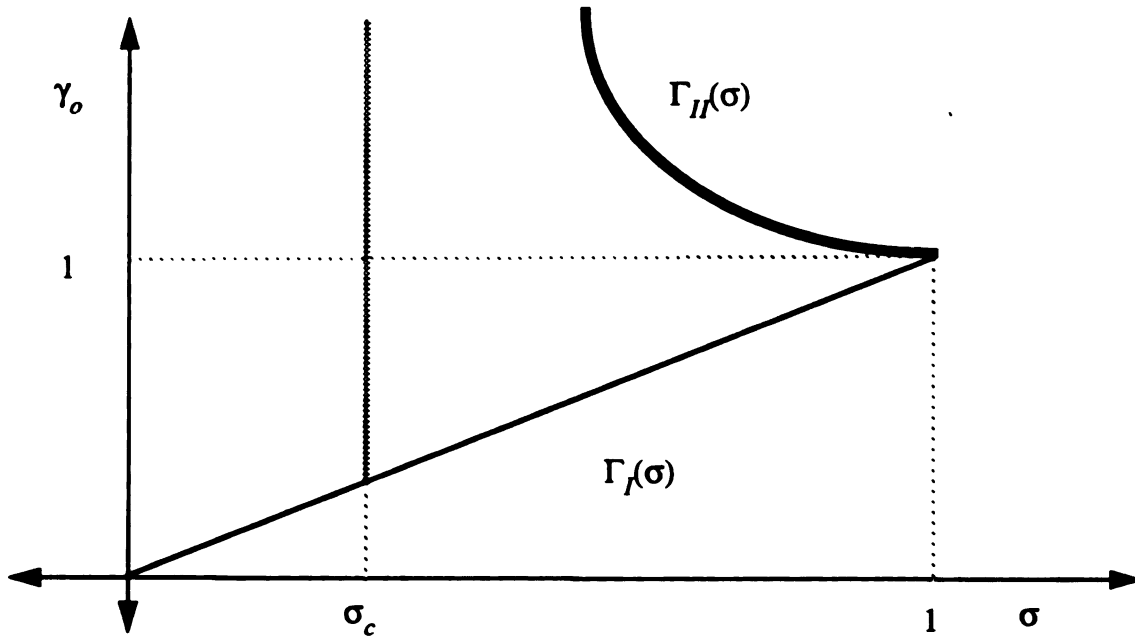
Figure 28. Admissible constant σ paths that reach the boundary $\gamma_o=\Gamma_{II}(\sigma)$ for both the hard and soft device. No points, other than the boundary points themselves, can reach the points on this boundary.
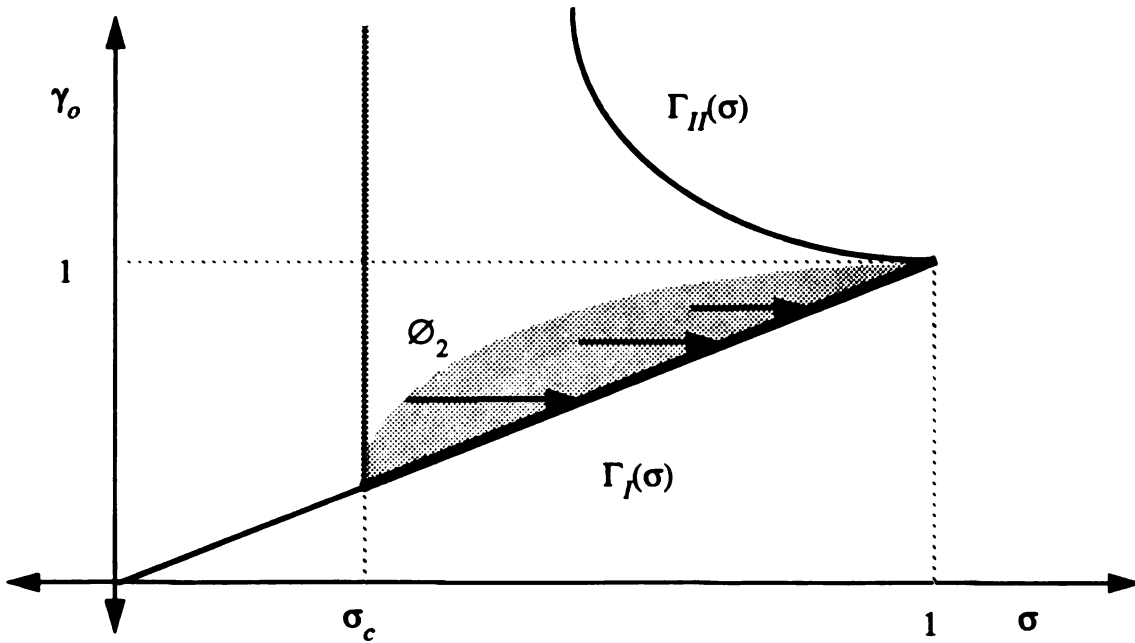
Figure 29. Admissible constant γ_o paths that reach the boundary $\gamma_o=\Gamma_I(\sigma)$ for the hard device. Those points which are on the constant γ_o line with $\bar{\sigma}(\gamma_o)>\bar{\sigma}_{\varnothing_2}(\gamma_o)$ can reach this boundary.

ary point $\gamma_o = \Gamma_I(\sigma)$ (see Figure 29) since the rightward path is also admissible in this area (see Figure 25). Those points inside the solution region with $\bar{\sigma}(\gamma_o) < \bar{\sigma}_{\varnothing_2}(\gamma_o)$ and $\gamma_o \leq 1$, as well as those points inside the solution region with $\gamma_o > 1$ could move toward the boundary point $\sigma = \sigma_c$ (see Figure 30) since the leftward direction is admissible in these areas (see Figure 25). It is to be recalled that the boundary point $\sigma = \sigma_c$ is an unattainable limit associated with minimum energy. Recall from Section 6 that the point $(\bar{\sigma}_{\varnothing_2}(\gamma_o), \gamma_o)$ on the curve $\varnothing_2$ represents an energy maximum on lines of constant γ_o. Thus admissible motions in Figure 29 and Figure 30 must move down the energy hills of Λ (see Figure 15). From the above discussions it is again seen in all cases that the final states on the boundary of Ω_{12} always like to reduce phase-II and extend the amount of phase-I.

Because of the restriction in the direction of solution path we shall now briefly reconsider the six possible solution paths (a)-(f) previously depicted in Figure 22 and discussed in Section 8.1. We again consider motions in which the bar is elongated with monotonically increasing applied displacement $\dot{\gamma}_o(t) > 0$ starting from $(\sigma, \gamma_o) = (0, 0)$ (see Figure 31).

(a) As before, the solution path is restricted to $\gamma_o = \Gamma_I(\sigma) = \sigma$ of the pure phase-I solutions until $\gamma_o(t) > \sigma_c$. The bar behaves as if it were linearly elastic for both devices.

(b) The solution path must now stay on $\gamma_o = \Gamma_I(\sigma) = \sigma$ of the pure phase-I solutions after $\gamma_o(t) > \sigma_c$ until $\gamma_o = 1$.

(c) After $\gamma_o(t) > \sigma_c$ but before $\gamma_o(t) = 1$ the possible solution path(c) of Section 8.1 cannot occur since this violates (125).

(d) Other admissible paths enter the interior of solution region after the initial departure from $(\sigma, \gamma_o) = (1, 1)$. However the solution path cannot move arbitrarily, that is there is less variation since it cannot violate the directional restrictions in Figure 25
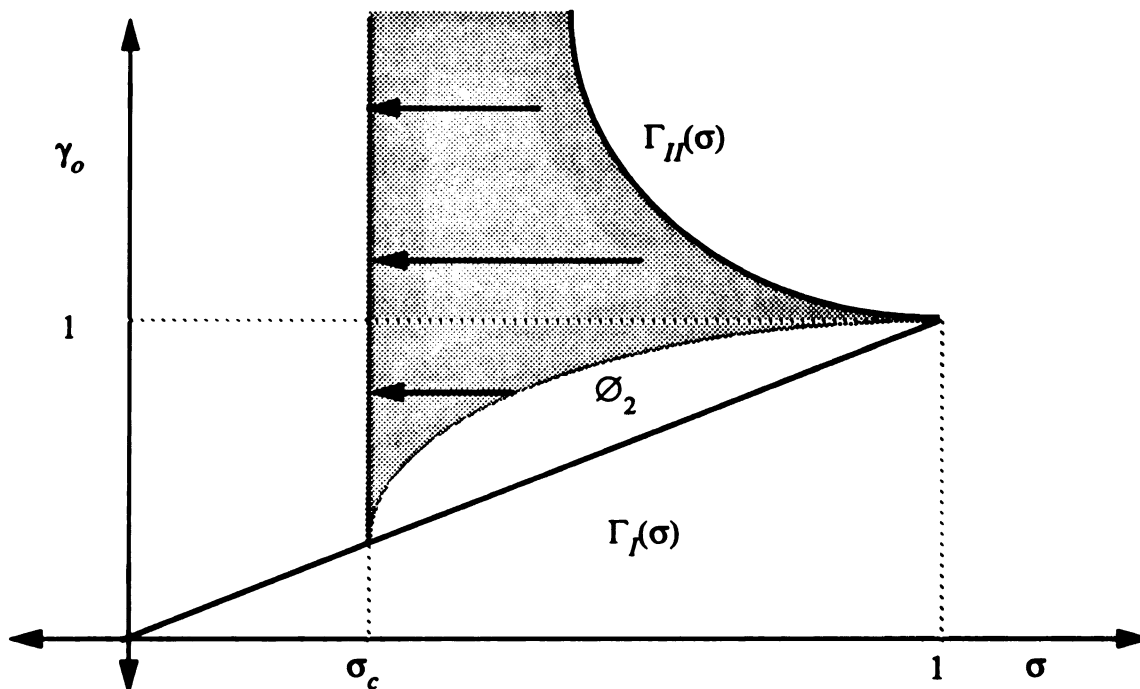
Figure 30. Admissible constant γ_o paths that reach the boundary $\sigma = \sigma_c$ for the hard device. Those points which can reach this boundary are on the constant γ_o line with $\sigma_c < \bar{\sigma}(\gamma_o) < \bar{\sigma}_{\varnothing_2}(\gamma_o)$ whenever $\sigma_c < \gamma_o < 1$, or with $\sigma_c < \bar{\sigma}(\gamma_o) < \bar{\sigma}_{II}(\gamma_o)$ whenever $\gamma_o \geq 1$.
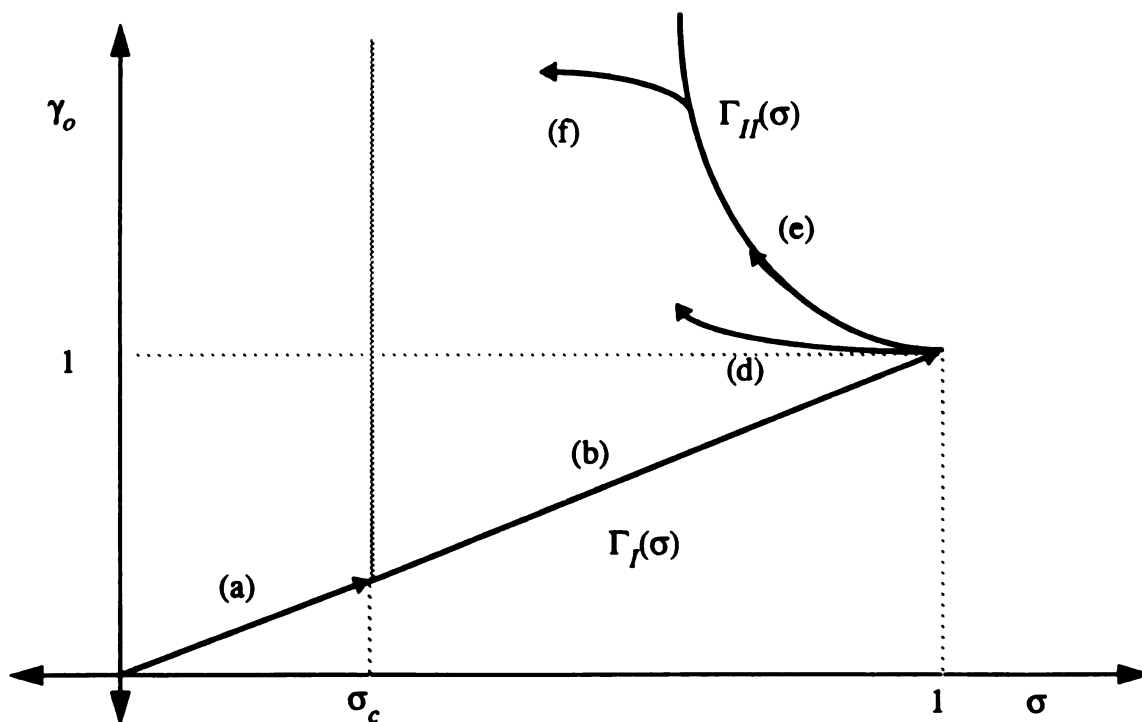
Figure 31. Some admissible possible quasi-static motions in the solution region Ω_{12} as γ_o increases from $\gamma_o = 0$.

after it enters the interior of solution region.

(e) The path stays on the curve $\gamma_o = \Gamma_{II}(\sigma)$ of the pure phase-II solutions.

(f) The solution path enters the interior of the solution region Ω_{12}. However the path must obey the directional restrictions in Figure 25 as do the paths (d).

From the above discussions we find that the paths (a), (b) and (e) in Figure 31 are exactly the same as their corresponding paths in Figure 22 since there is no other choice. However the paths (c), (d) and (f) in Figure 31 are not necessarily equal to their corresponding paths in Figure 22 since those paths in Figure 22 do not need to satisfy (125) while these paths in Figure 31 must obey (125).

Now that we have looked at the admissible paths, we return to the minimum energy solution diagrams in Sections 6 and 7. We find from (120) and (126) that, for a soft device case, the loading curve in Figure 21 is admissible. However, for a hard device case, the loading curve in Figure 17 is *not* admissible whenever $\sigma_c < \gamma_o < 1$. This is because there is an energy hump on the curve $\varnothing_2$ (see Figure 15), so that attaining the absolute minimum on the line $\sigma = \sigma_c$ requires a climb over an energy barrier to leave the local minimum on the line $\varnothing_1$.

9. The kinetic criterion

Due to the non-uniqueness of the quasi-static motions solutions some additional criterion is needed which determines the unprescribed $\sigma(t)$ for the hard device and which gives the unprescribed $\gamma_o(t)$ for the soft device. Requirements of minimum energy provide one such criterion, but as mentioned at the end of the previous section, this can lead to violations of the admissibility condition (125). An example of a different type of criterion involves the use of a "kinetic criterion". Abeyaratne and Knowles [1989A] have shown for problems with similar nonuniqueness that the quasi-static response of a prescribed force problem is then fully determined if one introduces the idea of an additional kinetic criterion.

Here the kinetic criterion will be described by a relation

$$f = \varphi(\dot{s}), \tag{127}$$

where $\varphi(\dot{s})$ is a materially determined function that relates the driving traction f and phase boundary velocity $\dot{s}$. Similar kinetic criteria were considered in [1988A], [1988AA], [1989A], [1990A], [1991A], [1991AA] and [1992A]. A necessary and sufficient condition to ensure that the dissipation rate $D(t)$ obeys (125) is that $\varphi(\dot{s})$ satisfies

$$\dot{s}\varphi(\dot{s}) \geq 0, \tag{128}$$

for all values of its argument $\dot{s}$. If (128) holds, then the admissible directions in Figure 25 are ensured through the motion. Suppose that the materially determined function is given by the linear relation $\varphi(\dot{s}) = \dot{s}/k$, then the kinetic relation is

$$\dot{s}(t) = kf(t). \tag{129}$$

Condition (128) is then ensured provided that k is a positive constant. Equation (129) provides a linearly "viscous" kinetic relation between "force" f and velocity $\dot{s}(t)$, and is similar to the kinetic relation considered by Abeyaratne and Knowles [1988AA].

9.1 The governing differential equation for phase boundary motion

Equation (129) leads to a differential equation whose solution give the quasi-static motion. We shall derive this for (1,2)-case. Let $T(\sigma)$ be the difference between $\Gamma_{II}(\sigma)$ and $\Gamma_I(\sigma)$,

$T(\sigma) \equiv \Gamma_{II}(\sigma) - \Gamma_I(\sigma)$, and

$$\Gamma_{II}(\sigma(t)) - \Gamma_I(\sigma(t)) \equiv T(\sigma(t)). \tag{130}$$

Thus from (129) and (119) the phase boundary velocity is given by

$$\dot{s}(t) = k\bar{f}_{12}(\sigma(t)) = k\,(\sigma_{ps}(\sigma(t)) - \sigma(t))\,T(\sigma(t)) \tag{131}$$

for the (1,2)-case. Now equation (25) can be rewritten as

$$s(t) = 1 + \frac{-\gamma_o(t) + \Gamma_I(\sigma(t))}{T(\sigma(t))} = 1 - \frac{\gamma_o(t) - \sigma(t)}{T(\sigma(t))} \tag{132}$$

for (1,2)-case. Using (131) and taking the derivative with respect to t from (132) with the help of (119) gives

$$\begin{aligned}
k\,(\sigma_{ps}(\sigma(t)) - \sigma(t))\,T^3(\sigma(t)) = \\
\{T(\sigma(t)) + [\gamma_o(t) - \sigma(t)]\,T'(\sigma(t))\}\,\dot{\sigma}(t) - T(\sigma(t))\dot{\gamma}_o(t).
\end{aligned} \tag{133}$$

Equation (133) also holds for the (2,1)-case. To see this note that (120) gives $f_{21} = -f_{12}$ while (25) gives

$$s(t) = \frac{\gamma_o(t) - \sigma(t)}{T(\sigma(t))} \tag{134}$$

so that $\dot{s}_{21}(t) = -\dot{s}_{12}(t)$. Thus the minus signs compensate for each other, and (133) again results.

For each loading device, either $\sigma(t)$ is given or $\gamma_o(t)$ is given, equation (133) is a first order differential equation relating the specified quantity to the unknown quantity. For example if $\sigma(t)$ is given, then (133) can be rearranged to

$$\dot{\gamma}_o(t) - \frac{\dot{\sigma}(t)}{T(\sigma(t))} T'(\sigma(t))\gamma_o(t)$$

$$= (1 - \frac{\sigma(t)T'(\sigma(t))}{T(\sigma(t))}) \dot{\sigma}(t) - k (\sigma_{ps}(\sigma(t)) - \sigma(t)) T^2(\sigma(t)) \tag{135}$$

which is a first order linear ordinary differential equation for $\gamma_o(t)$. Hence its solution is given by

$$\gamma_o(t) =$$

$$e^{\int H(t)dt} \left(\int \left[(\dot{\sigma}(t) - h(t)\sigma(t) - k (\sigma_{ps}(\sigma(t)) - \sigma(t)) T^2(\sigma(t))) e^{-\int H(t)dt} \right] dt + c \right), \tag{136}$$

where $H(t) = \frac{T'(\sigma(t))}{T(\sigma(t))} \dot{\sigma}(t)$ and c is a constant of integration. It is to be noted that

$$e^{\int H(t)dt} = T(\sigma(t)), \text{ so that (136) is further simplified to}$$

$$\gamma_o(t) = T(\sigma(t)) (\int \left[\frac{\dot{\sigma}(t) - h(t)\sigma(t)}{T(\sigma(t))} - k (\sigma_{ps}(\sigma(t)) - \sigma(t)) T(\sigma(t)) \right] dt + c)$$

$$= \sigma(t) - T(\sigma(t)) (\int k (\sigma_{ps}(\sigma(t)) - \sigma(t)) T(\sigma(t))dt + c) \tag{137}$$

and considering the initial condition at $t=0$ gives

$$\gamma_o(t) = \sigma(t) + \frac{T(\sigma(t)) (\gamma_o(0) - \sigma(0))}{T(\sigma(0))} - T(\sigma(t))\int_0^t k (\sigma_{ps}(\sigma(t)) - \sigma(t)) T(\sigma(t))dt. \tag{138}$$

But if $\gamma_o(t)$ is given, then (135) can be rearranged to

$$(1 + \frac{(\gamma_o(t) - \sigma(t)) T'(\sigma(t))}{T(\sigma(t))}) \dot{\sigma}(t) - k (\sigma_{ps}(\sigma(t)) - \sigma(t)) T^2(\sigma(t)) = \dot{\gamma}_o(t) \tag{139}$$

which is a first order nonlinear differential equation and is difficult to solve explicitly.

The above summary also can be seen from the following derivation which applies to the (1,2)-case. Note that the location of the phase boundary obeys

$$s(t) = s(0) + k\int_0^t \bar{f}_{12}(\sigma(t))dt, \tag{140}$$

which determines $s(t)$ for the soft device from any given initial condition. However for the hard device (140) is just a complicated integral equation. Note from (23) that the relation

between $\gamma_o(t)$ and the stress $\sigma(t)$ is given by

$$\gamma_o(t) = \Gamma_I(\sigma(t))s(t) + \Gamma_{II}(\sigma(t))(1 - s(t)) \tag{141}$$

which, using (130), is the same as

$$\gamma_o(t) = \sigma(t) + T(\sigma(t))(1 - s(t)) . \tag{142}$$

Substitution from (140) into (142) gives

$$\gamma_o(t) = \sigma(t) + T(\sigma(t))(1 - (s(0) + \int_0^t k\bar{f}_{12}(\sigma(t))dt)) . \tag{143}$$

Since from (142) it is found that $\gamma_o(0) = \sigma(0) + T(\sigma(0))(1 - s(0))$ at $t=0$, (143) is the

same as (138) once we set $\bar{f}(\sigma(t)) = \bar{f}_{12}(\sigma(t))$ using (119) and (130).

For the soft device case, since $\sigma(t)$ is given, equation (138) is an explicit equation

for $\gamma_o(t)$, so that $\gamma_o(t)$ is easy to obtain. For example, if $\sigma(t) = $ constant, then $\gamma_o(t)$ will be

a linear function of time t. In fact $\gamma_o(t)$ will linearly decrease with respect to time t down

to $\gamma_o(t) = \sigma(t) = $ constant as shown in Figure 27.

But for the hard device, since $\gamma_o(t)$ is given, equation (143) is an implicit equation

for the stress $\sigma(t)$ which is probably difficult to solve. Even when the given $\gamma_o(t)$ is con-

stant, it is not easy to solve for $\sigma(t)$. Moreover, there is no obvious guarantee that solutions

either exist; or if they exist, that they are unique.

9.2 Phase boundary kinematics

In this subsection we further study phase boundary motion governed by the kinetic relation

(129). If we consider a bar which has a single initial internal phase boundary with phase-I

on the left and phase-II on the right, then it represents an internal point (σ_A, γ_A) in the in-

terior of the solution region Ω_{12}. We now discuss the *kinetic solution*, that is the solution

obeying (129), for the following soft device and hard device problems:

(a) soft device: $\sigma(t) = \sigma_A$, with $\sigma_c < \sigma_A < 1$.

(b) hard device: $\gamma_o(t) = \gamma_A$, with $\gamma_A > \sigma_c$.

Our interest will be whether the paths eventually intersect the boundary of solution region Ω_{12} (recall Section 8) and if so, we also wish to know how long it takes and how fast the phase boundary is moving at this final time.

For the soft device since the stress is given by σ_A, $\dot{s} = k\bar{f}_{12}(\sigma_A)$ is constant throughout the motion and is greater than zero. Thus the phase boundary will eventually move all the way to $X = L$ resulting in a pure phase-I solution (see Figure 27). To find how long it will take, the initial location of the phase boundary at point (σ_A, γ_A) is needed. For the (1,2)-case, it is found that

$$s(0) = \frac{\Gamma_{II}(\sigma_A) - \gamma_A}{\Gamma_{II}(\sigma_A) - \Gamma_I(\sigma_A)} = \frac{\Gamma_{II}(\sigma_A) - \gamma_A}{T(\sigma_A)}. \tag{144}$$

(In contrast, if this was the (2,1)-case, then

$$s(0) = \frac{\gamma_A - \Gamma_I(\sigma_A)}{\Gamma_{II}(\sigma_A) - \Gamma_I(\sigma_A)} = \frac{\gamma_A - \Gamma_I(\sigma_A)}{T(\sigma_A)}, \tag{145}$$

note that the sum of the two initial values of $s(0)$ from (144) and (145) is equal to 1). Therefore in the (1,2)-case from (144) the time t is given by

$$t = \frac{1 - s(0)}{\dot{s}} = \frac{\Gamma_I(\sigma_A) - \gamma_A}{k\bar{f}_{12}(\sigma_A)T(\sigma_A)} > 0. \tag{146}$$

(In contrast, if this was the (2,1)-case, then from (145) the time t is given by

$$t = \frac{-s(0)}{\dot{s}} = \frac{\Gamma_I(\sigma_A) - \gamma_A}{-k\bar{f}_{21}(\sigma_A)T(\sigma_A)} > 0. \tag{147}$$

Note that the formula for t is the same for both cases).

Turning to the hard device there are two possibilities. Recall from Section 8.4 for each constant value of γ_A, that there are two possible boundary points to the solution region Ω_{12}. These are given by $\sigma = \sigma_c$ and $\sigma = \gamma_A$ whenever $\sigma_c < \gamma_A \le 1$, and given by $\sigma = \sigma_c$

and $\sigma = \bar{\sigma}_{II}(\gamma_A)$ whenever $\gamma_A > 1$. For the case in which either $\sigma_A < \bar{\sigma}_{\varnothing_2}(\gamma_A)$ with $\gamma_A \leq 1$, or the case with $\gamma_A > 1$ (see the shaded region in Figure 30) it is not easy to solve this problem as the velocity of the phase boundary increases through the motion. As an example for material A the velocity of the phase boundary is $\dot{s} = k\bar{f}_{12}(\sigma_c) = \infty$ when the solution path finally hits the line $\sigma(t) = \sigma_c$ while for material B the velocity of the phase boundary is equal to $5k/8$ when the solution path finally hits the line $\sigma(t) = \sigma_c$. If the stress is obtained from (143) then from (140) the time t when the phase boundary hits the end $X = L$ is given by the following integral equation

$$\begin{aligned}
1 &= s(0) + k\int_0^t \bar{f}_{12}(\sigma(t))dt, &\quad \text{for the } (1,2)\text{-case,} \\
0 &= s(0) + k\int_0^t \bar{f}_{21}(\sigma(t))dt, &\quad \text{for the } (2,1)\text{-case.}
\end{aligned} \tag{148}$$

Similarly for the case in which $\sigma_A > \bar{\sigma}_{\varnothing_2}(\gamma_A)$ with $\gamma_A \leq 1$ (see Figure 29), the velocity of the phase boundary decreases through the motion and is given by $\dot{s} = k\bar{f}_{12}(\gamma_A)$ when the solution path eventually hits the line of phase-I solution at $\sigma = \bar{\sigma}_I(\gamma_A) = \gamma_A$. The time needed is again given by (148).

9.3 Rate dependence of the admissible paths governed by the kinetic criterion

In the previous section we briefly looked at the time needed for a (1,2)-case solution path to "drift" to the boundary of Ω_{12} when the prescribed loading condition (either γ_o or σ) is fixed. Now we turn to investigate the effect of different loading rates. We consider the system starting from the fixed point $(\sigma, \gamma_o) = (0, 0)$ in the solution region Ω_{12}, and we try to find the kinetic solution for both the hard device and the soft device.

For the soft device if $0 < \sigma(t) < 1$, then the solution path will remain in pure phase-I (which is also the minimum energy solution, recall Section 7). While, for the hard device, if $0 < \gamma_o(t) < 1$, then the solution path will also remain in pure phase-I (which does not give

the minimum energy solution for $\sigma_c < \sigma < 1$, recall Section 6).

From the above observations the solution path cannot enter the interior of solution region Ω_{12} so long as either $0 < \sigma(t) < 1$ or $0 < \gamma_o(t) < 1$. Therefore let's consider the system starting from the fixed point $(\sigma, \gamma_o) = (1, 1)$ at $t=0$ which represents a pure phase solution. Under further loading the solution path may now enter the interior of the solution region Ω_{12}. We consider the hard device loading condition

$$
\gamma_o(t) = \begin{cases} 1 + \dfrac{\gamma_F t}{t_o} = 1 + \alpha t & \text{for} \quad 0 < t < t_o, \\ 1 + \gamma_F & \text{for} \quad t > t_o, \end{cases} \tag{149}
$$

where γ_F and t_o are positive constants, and the loading rate $\alpha = \gamma_F/t_o$ (this is shown as (c) in Figure 32). Thus (149) represents a family of loading cases parametrized by t_o and γ_F. We are concerned with the effect of rate, that is the effect of changing t_o with γ_F fixed. If t_o increases, then the loading (c) is changed to some other loading, say (d); if t_o decreases, then the loading (c) is changed to some other loading, say (b). In particular, if $t_o \rightarrow 0$, then the loading (c) switches to the step loading (a). I claim that the solution paths will look like the six corresponding paths as shown in Figure 33. We now show this in the following.
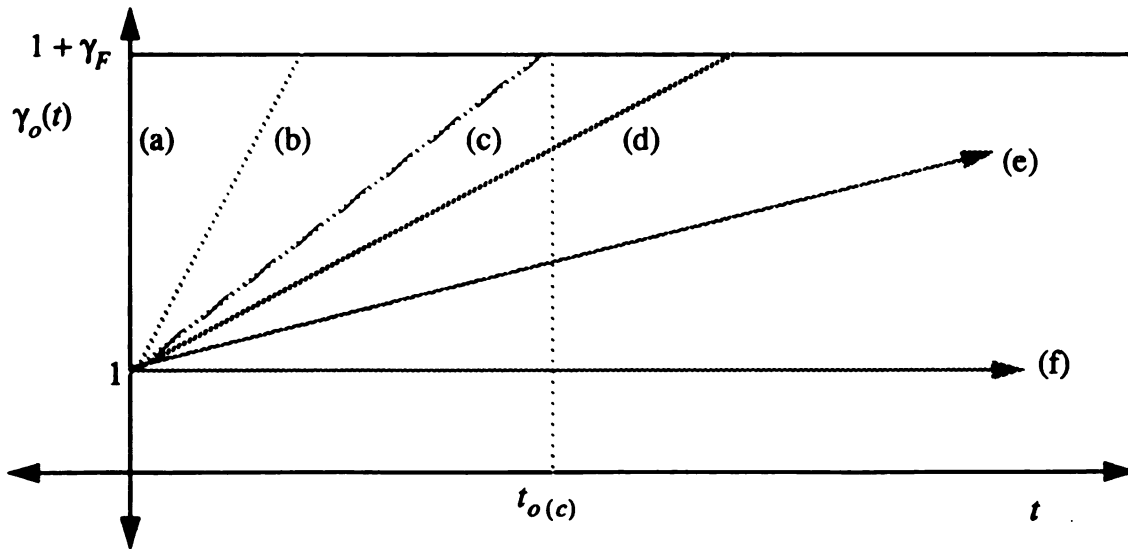
Figure 32. The hard device loading condition (149) for different values t_0. Here $0 = t_{0(a)}$ $< t_{0(b)} < ... < t_{0(e)} < t_{0(f)} = \infty$ so that $\infty = \alpha_{0(a)} > \alpha_{0(b)} > ... > \alpha_{0(e)} > \alpha_{0(f)} = 0$.

From (149) and for a loading with the loading rate $\alpha = 0$, the solution path follows the line

of constant $\gamma_o = 1$ as discussed in Figure 30. But for a loading with the loading rate $\alpha > 0$

we have from (142), for $0 < t < t_o$, that

$$\dot{\gamma}_o(t) = \alpha = \dot{\sigma}(t) (1 + T'(\sigma(t)) (1 - s(t))) - T(\sigma(t))\dot{s}(t) > 0. \qquad (150)$$

From Section 5 if $\gamma_o(t) \geq 1$ and $\sigma_c < \sigma(t) < 1$ we have that the slope of a curve of constant

s in the solution region is negative (see Figure 9):

$$1 + T'(\sigma(t)) (1 - s(t)) = \left.\frac{\partial \gamma_o}{\partial \sigma}\right|_s < 0 \qquad \text{if } \gamma_o(t) \geq 1 \text{ and } \sigma_c < \sigma(t) < 1. \qquad (151)$$

Since $\alpha > 0$ and $\dot{s}(t) > 0$ whenever $\sigma_c < \sigma(t) < 1$, equation (150) now shows that $\dot{\sigma}(t) < 0$.

Hence the slope of the solution path in the solution region Ω_{12} is negative whenever $\alpha > 0$

and $\gamma_o(t) \geq 1$. This means that the stress decreases while the strain increases for a hard de-

vice loading with a constant loading rates $\alpha > 0$.
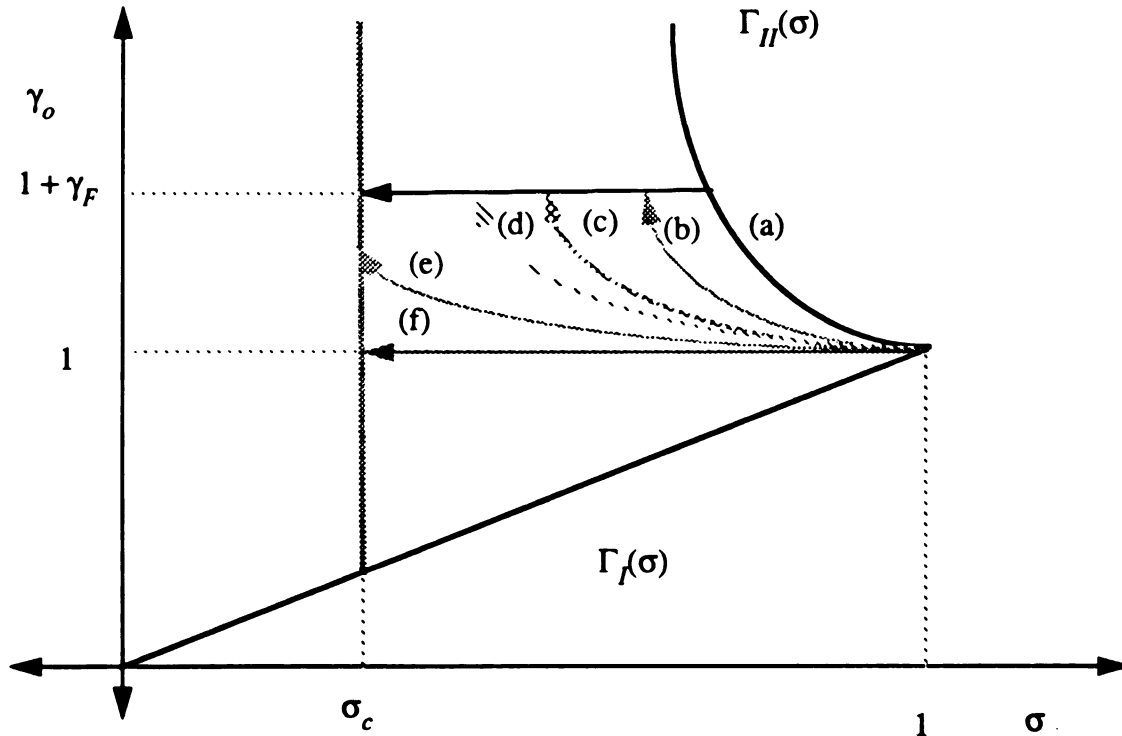
Figure 33. The relation between the solution paths corresponding to the loadings
given in Figure 32 for the hard device.

Each loading ($\therefore$ each α) defines a different solution path $\gamma(\sigma)$ and to show this α dependence we shall put α in the argument $\gamma(\sigma, \alpha)$. To show that a higher α path is above a lower α path (at each σ) it is enough to show that $\alpha^a > \alpha^b \Rightarrow \gamma(\sigma, \alpha^a) > \gamma(\sigma, \alpha^b)$ with σ fixed. A formal argument establishing this ordering is given in Appendix-C, while here we give a shorter (but less formal) explanation. To argue that this is the case, note that we cannot have $\gamma(\sigma, \alpha^a) = \gamma(\sigma, \alpha^b)$ at any fixed $\sigma < 1$ since this would imply that two different γ curves pass through the same point. Thus either $\gamma(\sigma, \alpha^a) > \gamma(\sigma, \alpha^b)$ or $\gamma(\sigma, \alpha^a) < \gamma(\sigma, \alpha^b)$ for all fixed σ which $\alpha^a > \alpha^b$. To find the correct direction to the inequality it is enough to consider a specific example, and so we take $\alpha^b = 0$. However in this case $\gamma(\sigma, 0) = 1$ which is the lowest most possible path, so we conclude that $\gamma(\sigma, \alpha^a) > \gamma(\sigma, \alpha^b)$ when $\alpha^a > \alpha^b$ so that higher α curves are above lower α curves.

We have argued that the rate of loading gives different solution paths. Thus different solutions are generated by different loading rates. Those curves would separate like in Figure 33. Note that some curves like (e) and (f) could hit $\sigma = \sigma_c$ before $t = t_o$.

Physically these results can be concluded by noting that there is a natural tendency for the solution path to drift down to the line $\sigma = \sigma_c$, so that larger values of t_o allow more downward drift before $\gamma_o = 1 + \gamma_F$. For the loading (a), $t_o = 0$ and there is no time response for this drift. Hence the solution path will then follow the path with the smallest possible s which is the curve $\gamma_o = \Gamma_{II}(\sigma)$, $s=0$, with $1 < \gamma_o < 1 + \gamma_F$ and will then follow the line $\gamma_o = 1 + \gamma_F$ toward the line $\sigma = \sigma_c$. For the loading (f), $t_o = \infty$ so that there is enough time for complete drift response. Hence the solution path in this case will be the lowest most path which is the line $\gamma_o(t) = 1$.

Finally the departure of the solution paths in Figure 33 from $(\sigma, \gamma_o) = (1, 1)$ can be analyzed. This is done for Material A in Appendix-D.

10. Finite element analysis

The theoretical analysis in Sections 2-9 shows that the problem under study has nonunique solutions and that this nonuniqueness can be resolved by implementing an extra criterion, either one of minimum energy or else a kinetic relation. Now we study whether numerical analysis based on the finite element method can give the same results. Our problem is finding a state that satisfies the equilibrium equation (11)

$$\frac{d}{dX}\sigma(X) = 0, \qquad 0 < X < L, \tag{152}$$

and the boundary conditions either

$$u(0) = 0, \qquad u(L) = \delta, \tag{153}$$

for the hard loading device or

$$u(0) = 0, \qquad \sigma(X) = \sigma, \tag{154}$$

for the soft loading device. In what follows the finite element method (FEM) analysis of the problem is performed in detail.

10.1 Variational formulation of the equation over a typical element

The FEM is a piecewise application of a variational method. Hence the variational formulation of the equation (152) over a typical element is studied first. Suppose that the domain $R \equiv [0, L]$ is divided into a set of N line elements then we have

$$X_0 = 0 < X_1 < X_2 < ... < X_{N-1} < X_N = L. \tag{155}$$

The i-th element $R^i \equiv [X_{i-1}, X_i]$ is a typical element of the finite element mesh. Since equation (152) is valid over the domain $R \equiv [0, L]$, it is also valid, in particular, over the i-th element. The term "variational formulation" means that the formulation in which the governing differential equation is recast in an equivalent form by trading the differentiation between a test function and the dependent variable. Thus multiplying both sides of (152) with a test function $v(X)$ and integrating over the i-th element gives the variational formu-

85

lation

$$\int_{X_{i-1}}^{X_i} v(X)\frac{d}{dX}\sigma(X)dX = 0. \tag{156}$$

Integrating (156) by parts gives

$$v(X)\sigma(X)\big|_{X_{i-1}}^{X_i} - \int_{X_{i-1}}^{X_i} \sigma(X)\frac{d}{dX}v(X)dX = 0. \tag{157}$$

Recalling (14), since the stress-strain relation can be rewritten by $\sigma(X) = E\frac{d}{dX}u(X)$, equation (157) can be rewritten as

$$v(X)\sigma(X)\big|_{X_{i-1}}^{X_i} - \int_{X_{i-1}}^{X_i} E\frac{d}{dX}u(X)\frac{d}{dX}v(X)dX = 0. \tag{158}$$

Now for the i-th element the finite element method involves seeking approximate solutions of the form

$$u(X) = u^{(i)}(X) = \sum_{j=1}^{m} u_j^{(i)} N_j^{(i)}(X) \tag{159}$$

where the superscript (i) denotes the i-th element and the subscript j denotes the j-th node.

Note also that $u_j^{(i)}$ are the (to be determined) values of displacement u at the node X_j, m is the number of nodes per element, and $N_j^{(i)}(X)$ are the finite element interpolation functions with the property

$$N_j^{(i)}(X_k) = \begin{cases} 1, & j = k, \\ 0, & j \neq k. \end{cases} \tag{160}$$

The corresponding strains are

$$\gamma^{(i)}(X) = \sum_{j=1}^{m} u_j^{(i)} \frac{d}{dX} N_j^{(i)}(X) \tag{161}$$

and the corresponding stresses are

$$\sigma^{(i)}(X) = \bar{\sigma}(\gamma^{(i)}(X)).$$ (162)

Note that $v(X)$ is an arbitrary test function. By the Galerkin method, substitution of equation (159) for $u(X)$ and $v(X) = N_j^{(i)}(X)$ into (158) leads to

$$\sum_{j=1}^{m} K_{kj}^{(i)} u_j^{(i)} = F_k^{(i)},$$ (163)

where the coefficient matrix $K_{kj}^{(i)}$, called the *stiffness matrix for the element*, and the column vector $F_k^{(i)}$, called the *force vector for the element*, are given by

$$K_{kj}^{(i)} = \int_{X_{i-1}}^{X_i} E\frac{d}{dX}N_k^{(i)}(X)\frac{d}{dX}N_j^{(i)}(X)dX,$$ (164)

$$F_k^{(i)} = N_k^{(i)}(X)\sigma^{(i)}(X)\Big|_{X_{i-1}}^{X_i}.$$ (165)

Note that the fact that the cross section has unit area simplifies the above derivation.

10.2 Interpolation functions and element equation

If we consider the simplest element, the two-node element, then the interpolation functions are

$$N_1^{(i)}(X) = 1 - \frac{X - X_{i-1}}{l^{(i)}}, \qquad N_2^{(i)}(X) = \frac{X - X_{i-1}}{l^{(i)}},$$ (166)

where the element length $l^{(i)} = X_i - X_{i-1}$ and the first derivatives of the interpolation functions are

$$\frac{d}{dX}N_1^{(i)}(X) = -\frac{d}{dX}N_2^{(i)}(X) = -\frac{1}{l^{(i)}}.$$ (167)

From (159) the displacement u of the i-th element is expressed as

$$u^{(i)}(X) = \sum_{j=1}^{2} u_j^{(i)} N_j^{(i)}(X) = u_1^{(i)} N_1^{(i)}(X) + u_2^{(i)} N_2^{(i)}(X),$$ (168)

which is a linear function. From (167) and (168) the corresponding *strain* of the i-th element is given by

$$\frac{d}{dX} u^{(i)}(X) = (u_2^{(i)} - u_1^{(i)}) \frac{1}{l^{(i)}} \equiv \gamma^{(i)}(X). \tag{169}$$

Since the interpolation functions are linear, the strain in the i-th element is constant. Similarly by (162) the stress $\sigma^{(i)}(X)$ is constant in the i-th element. The i-th element is said to be in phase-I if $0 < \gamma^{(i)} \leq 1$ but is in phase-II if $\gamma^{(i)} > 1$. Solutions in which all the elements are in phase-I are pure phase-I solutions. Solutions in which all the elements are in phase-II are pure phase-II solutions. All other solutions involve a combination of phase-I and phase-II elements. Nodes separating elements in different phase are phases boundaries.

According to (14), the elastic secant modulus E function in the i-th element is given by

$$E^{(i)} = \frac{\sigma^{(i)} l^{(i)}}{u_2^{(i)} - u_1^{(i)}}. \tag{170}$$

Therefore the elastic secant modulus $E^{(i)}$ function in the i-th element is a constant. Equation (170) can be rewritten as

$$E^{(i)} = E^{(i)}(u_1^{(i)}, u_2^{(i)}) = \begin{cases} E_I = 1, & \dfrac{(u_2^{(i)} - u_1^{(i)})}{l^{(i)}} \leq 1, \\[2mm] E_{II} = \dfrac{\sigma_{II}((u_2^{(i)} - u_1^{(i)})/l^{(i)})}{(u_2^{(i)} - u_1^{(i)})/l^{(i)}}, & \dfrac{(u_2^{(i)} - u_1^{(i)})}{l^{(i)}} \geq 1. \end{cases} \tag{171}$$

From (164) the element stiffness matrix $K_{kj}^{(i)}$ becomes

$$K_{kj}^{(i)} = \frac{E^{(i)}}{l^{(i)}} \begin{bmatrix} 1 & -1 \\ -1 & 1 \end{bmatrix} = k^{(i)} \begin{bmatrix} 1 & -1 \\ -1 & 1 \end{bmatrix} \tag{172}$$

where the element stiffness $k^{(i)} = \dfrac{E^{(i)}}{l^{(i)}} = \dfrac{\sigma^{(i)}}{u_2^{(i)} - u_1^{(i)}}$. The force vector $F_k^{(i)}$ is given by

$$F_k^{(i)} = \begin{bmatrix} -\sigma^{(i)} \\ \sigma^{(i)} \end{bmatrix}. \tag{173}$$

Finally (163) can be rewritten as

$$\frac{E^{(i)}}{l^{(i)}} \begin{bmatrix} 1 & -1 \\ -1 & 1 \end{bmatrix} \begin{bmatrix} u_1^{(i)} \\ u_2^{(i)} \end{bmatrix} = \sigma^{(i)} \begin{bmatrix} -1 \\ 1 \end{bmatrix}. \tag{174}$$

Although the above equation (174), as well as many of the equations to follow, are written in a standard matrix form of a linear system, it is really important to remember that $E^{(i)}$ in (174) is a function of $u_1^{(i)}$ and $u_2^{(i)}$ so that (174) is a nonlinear equation. Therefore, the standard uniqueness and existence results for the linear theory might not hold for this equation. In fact, since this equation of a discrete form comes from a continuous theory which has severe loss of uniqueness (before an additional criterion is considered), we would expect that the discrete approximation provided by FEM would also have this property.

10.3 Assembly of element equations

Since equation (174) is derived for an arbitrary element, it holds for each element from the finite element mesh. For an N-element case, we have the resulting system matrix equation

$$\begin{bmatrix} K \end{bmatrix}_{(N+1) \times (N+1)} \begin{bmatrix} U \end{bmatrix}_{(N+1) \times 1} = \begin{bmatrix} F \end{bmatrix}_{(N+1) \times 1}. \tag{175}$$

Note that $\begin{bmatrix} K \end{bmatrix}$ is the global stiffness matrix and is given by

$$\begin{bmatrix} K \end{bmatrix} = \begin{bmatrix} k_1 & -k_1 & 0 & \cdots & 0 & 0 & 0 \\ -k_1 & k_1+k_2 & -k_2 & \cdots & 0 & 0 & 0 \\ 0 & -k_2 & k_2+k_3 & \cdots & 0 & 0 & 0 \\ \cdots & \cdots & \cdots & \cdots & \cdots & \cdots & \cdots \\ 0 & 0 & 0 & \cdots & k_{N-2}+k_{N-1} & -k_{N-1} & 0 \\ 0 & 0 & 0 & \cdots & -k_{N-1} & k_{N-1}+k_N & -k_N \\ 0 & 0 & 0 & \cdots & 0 & -k_N & k_N \end{bmatrix} \tag{176}$$

where the element stiffnesses k_i are given by $k_i = E^{(i)}/l^{(i)}$. The *nodal displacement vector* $[U]$ is defined as

$$[U] = \left[u_1 \, u_2 \, u_3 \, \cdots \, u_{N-1} \, u_N \, u_{N+1} \right]^T$$

(177)

while the *nodal force vector* is defined as

$$[F] = \left[\sigma_1 \, \sigma_2 \, \sigma_3 \, \cdots \, \sigma_{N-1} \, \sigma_N \, \sigma_{N+1} \right]^T,$$

(178)

where $\sigma_k = \sigma^{(i)} - \sigma^{(i+1)}$ is the force difference across the i-th node. Equation (178) is an assembly result of (165). In fact the forces on the internal nodes are equal to zero because there is no body force and the external forces are applied to the ends only. Therefore it follows that $\sigma^{(i)}$ takes on the same value, say σ, in all elements and (178) is reduced to

$$[F] = \left[-\sigma \, 0 \, 0 \, \cdots \, 0 \, 0 \, \sigma \right]^T.$$

(179)

From (169) and (177) the strain on the i-th element is constant and given by

$$\gamma_i = \frac{u_{i+1} - u_i}{l_i},$$

(180)

where the i-th element length $l_i = l^{(i)}$. Since in this study all of the strains γ_i are positive, it is necessary that

$$u_j < u_k \qquad \text{if } j < k.$$

(181)

10.4 Imposition of boundary conditions

For the hard-device problem, the displacements on the end nodes are given by

$$u_1 = 0, \qquad u_{N+1} = \delta,$$

(182)

while the displacements on the $(N - 1)$ internal nodes are unknown. In this case a new system equation may be obtained by inserting the prescribed boundary conditions (182) into

(175). The first row equation is then given by

$$-k_1 u_2 = -\sigma. \tag{183}$$

This allows us to neglect the first row equation and the $(N+1)$-th row equation. We then move the two known terms, the first and $(N+1)$-th columns, to the right hand side of the equal sign. The first term is the u_1 term which is 0 while the second term is the u_{N+1} term which is equal to δ. Finally the new system equation is given by

$$
\begin{bmatrix}
k_1 + k_2 & -k_2 & \cdots & 0 & 0 \\
-k_2 & k_2 + k_3 & \cdots & 0 & 0 \\
\cdots & \cdots & \cdots & \cdots & \cdots \\
0 & 0 & \cdots k_{N-2} + k_{N-1} & -k_{N-1} \\
0 & 0 & \cdots & -k_{N-1} & k_{N-1} + k_N
\end{bmatrix}
\begin{bmatrix}
u_2 \\
u_3 \\
\cdots \\
u_{N-1} \\
u_N
\end{bmatrix}
=
\begin{bmatrix}
0 \\
0 \\
\cdots \\
0 \\
\delta k_N
\end{bmatrix}. \tag{184}
$$

Note again that the element stiffinesses $k_i = E^{(i)}/l^{(i)}$ are each a function of u_i and u_{i+1} so that from (171) the element stiffinesses are given by

$$
k_i = k_i(u_i, u_{i+1}) =
\begin{cases}
\dfrac{1}{l_i}, & \dfrac{(u_{i+1} - u_i)}{l_i} \leq 1, \\[2ex]
\dfrac{\bar{\sigma}_{Il}((u_{i+1} - u_i)/l_i)}{(u_{i+1} - u_i)}, & \dfrac{(u_{i+1} - u_i)}{l_i} > 1,
\end{cases}
\tag{185}
$$

where $l_i = l^{(i)}$. Hence the stiffness matrix $[K]$ and the nodal force vector $[F]$ are each a function of the nodal displacements: u_i. Thus equation (184) is a nonlinear system of equations for the $N-1$ unknown values $u_2, \ldots, u_N$ which is simply written in the usual linear equation form. Note that the unknown value of stress can be obtained from (183) after solving (184).

For the rest of this thesis we shall limit attention to an FEM model in which all elements have equal lengths. Thus for an N-element model the common length is $l = L/N$.

We now consider the possibility of solutions to (184) in which all the stiffnesses k_i are equal. Then by using Gaussian elimination one finds that the nodal displacement vector

must be given by

$$
\begin{bmatrix} u_2 \\ u_3 \\ \cdots \\ u_{N-1} \\ u_N \end{bmatrix} = \begin{bmatrix} 1 \\ 2 \\ \cdots \\ N-2 \\ N-1 \end{bmatrix} \frac{\delta}{N}.
\tag{186}
$$

We then verify from (185) that (186) indeed allows for equality of all the k_i so that (186)

is a solution to (184). Using (180) the strain γ_i in each element is thus given by $\gamma_i =$

$\delta / (Nl) = \delta / L = \gamma_o$. Here the strain in each element is the same constant so that all ele-

ments are in the same phase. Thus (186) represents a pure phase solution to (184). Hence

FEM always allows the possibility of a pure phase solution (we shall soon see that other

solutions are also possible). This pure phase solution is a pure phase-I solution whenever

$0 \leq \gamma_o < 1$ or equivalently $0 \leq \delta_o < L$ and is a pure phase-II solution whenever $\gamma_o > 1$ or

equivalently $\delta_o > L$.

For the soft-device problem, the displacement at the first node and the stress in the

bar are given by

$$
u_1 = 0, \qquad \sigma = \text{a prescribed constant,}
\tag{187}
$$

while the N nodal displacements: $u_2, \ldots, u_{N+1}$ are unknown. Similarly to obtain a new

system equation we first insert the prescribed boundary conditions (187) into (175). After

that we neglect the first row equation and move the u_1 term which is 0 to the right hand

side of the equal sign. Finally the new system equation is given by

$$
\begin{bmatrix}
k_1 + k_2 & -k_2 & \cdots & 0 & 0 & 0 \\
-k_2 & k_2 + k_3 & \cdots & 0 & 0 & 0 \\
\cdots & \cdots & \cdots & \cdots & \cdots & \cdots \\
0 & 0 & \cdots k_{N-2} + k_{N-1} & -k_{N-1} & 0 \\
0 & 0 & \cdots & -k_{N-1} & k_{N-1} + k_N & -k_N \\
0 & 0 & \cdots & 0 & -k_N & k_N
\end{bmatrix}
\begin{bmatrix} u_2 \\ u_3 \\ \cdots \\ u_{N-1} \\ u_N \\ u_{N+1} \end{bmatrix}
=
\begin{bmatrix} 0 \\ 0 \\ \cdots \\ 0 \\ 0 \\ \sigma \end{bmatrix}.
\tag{188}
$$

Just as (184) was a nonlinear equation, so is (188). Now there are N unknowns $u_2, ..., u_{N+1}$. Once again, a pure phase solution is available for (188), it is given by

$$\begin{bmatrix} u_2 \\ u_3 \\ \cdots \\ u_{N-1} \\ u_N \\ u_{N+1} \end{bmatrix} = \begin{bmatrix} 1 \\ 2 \\ \cdots \\ N-2 \\ N-1 \\ N \end{bmatrix} \frac{\sigma}{k_1}. \tag{189}$$

According to (180), the strain on each element is constant so that each element is wholly in one of two possible strain phases: either the lower strain phase (phase-I) or the high strain phase (phase-II). For a solution that is not pure, these phases however could be ordered in many different ways. For example, for $N=4$, these phases might be ordered as the following specific case

$$\begin{bmatrix} I & II & I & I \end{bmatrix}, \tag{190}$$

on which the first element, the third element and the fourth element are in phase-I, and the second element is in phase-II. The number of phase permutations to (190) is 4 and the total number of phase arrangements is $2^4 = 16$. As another example, for $N=20$, these phases might be ordered as the following specific case

$$\begin{bmatrix} I & II & I & I & I & II & II & I & I & II & II & II & I & I & II & II & II & II & I & II \end{bmatrix}. \tag{191}$$

Here there are nine elements being in phase-I while there are eleven elements being in phase-II. The number of phase permutations to (191) is 21 and the total number of phase arrangements is 2^{20} for a twenty-element model. In general the number of phase arrangements is 2^N for an N-element model. This also can be clarified by Pascal's triangle, which has the terms of polynomials of various degrees in the two variables I and II as shown in Figure 34. For a binary expression $(I + II)^N$, we have

Pascal's triangle	Number of elements (N)	Number of cases (2^N)	Number of terms ($N+1$)
1			
I II	1	2	2
I^2 $2I\Pi$ Π^2	2	4	3
I^3 $3I^2\Pi$ $3I\Pi^2$ Π^3	3	8	4
I^4 $4I^3\Pi$ $6I^2\Pi^2$ $4I\Pi^3$ Π^4 (s=1) (s=.75) (s=.5) (s=.25) (s=0)	4	16	5
... ...	...	...	...

Figure 34. The coefficients in Pascal's triangle gives the number of phase permutations at fixed phase volume fraction for two-phase problems with different number of elements. Here 2^N gives the number of possible phase arrangements, and $N+1$ gives the number of distinct volume fractions of phase-I to phase-II.

$$(I + \Pi)^N = \sum_{m=0}^{N} C(N, m)I^m\Pi^{N-m}, \tag{192}$$

where N is the number of elements, m is the number of elements being in phase-I, N-m is

the number of elements being in phase-II and $C(N, m) = \dfrac{N!}{m!\,(N-m)!}$ is the number of

possible permutations for which m elements are in phase-I and N-m elements are in phase-II. For equal element lengths and fixed m, all the $C(N, m)$ permutations represent the same volume fraction of phase-I to phase-II.

Note that pure phase solutions imply $m = 0$ or $m = N$ in (192). Since $C(N, 0)=$ $C(N, N) = 1$ there is only one member in a pure phase permutation. For $0 < m < N$ the phase permutation corresponds to a multi-phase solution. Exactly one member of the permutation group has phase-I on left and phase-II on right and so corresponds to the (1,2)-case solution of Section 4. Moreover exactly one member of the permutation group has phase-I on right

and phase-II on left and so corresponds to the (2,1)-case solution of Section 4. The above two members are the only multiple-phase solutions with a single phase boundary. This phase boundary location is limited to nodal values and so must be at

$$s = 0, \frac{1}{N}, \frac{2}{N}, ..., 1. \tag{193}$$

For the (1,2)-case solution the phase boundary location in (193) also gives the fraction of phase-I.

Note also that all the remaining $C(N, m)$-2 permutations involve more than one phase boundary. It will be convenient to identify all members of the permutation group by its (1,2)-representative. Thus the specific case of (190) would be represented by the following general case

$$\langle\, I\ I\ I\ II\,\rangle, \tag{194}$$

where

$$\langle\, I\ I\ I\ II\,\rangle = \left[II\ I\ I\ I\right], \left[I\ II\ I\ I\right], \left[I\ I\ II\ I\right], \left[I\ I\ I\ II\right]. \tag{195}$$

There are a total of $N+1$ possible permutation groups, denoted by $<\,>$. Each of these $N+1$ groups corresponds to a different phase boundary location (or equivalently volume fraction of phase-I) as given in the list (193).

10.5 Iterative solutions to the system equation

To solve the nonlinear system equations (184) and (188) an iterative method may be chosen. Both equations can be rewritten as an iterative form in the following way

$$\underline{k}(u_{j_i})u_{j_{i+1}} = \underline{f}(u_{j_i}). \tag{196}$$

Note that the subscript j is the nodal number and the subscript i is the iteration number. The iteration procedure represented by (196) is the following:

(a) Choose an initial guess ($i = 1$) for the nodal displacements u_{j_i}.

(b) Compute the element stiffness $\underline{k}(u_{j_i})$ using (185). Compute the nodal force vector

$f(u_{j_i})$ from the nodal displacements u_{j_i} using (184) and (185) for the hard device problem or using (185) and (188) for the soft device problem.

(c) Solve (196) for new nodal displacements $u_{j_{i+1}}$.

(d) Check the norm between $u_{j_{i+1}}$ and u_{j_i} by

$$\left\| u_{j_{i+1}} - u_{j_i} \right\|_{\infty} = max \left(\left| u_{1_{i+1}} - u_{1_i} \right|, \left| u_{2_{i+1}} - u_{2_i} \right|, ..., \left| u_{N+1_{i+1}} - u_{N+1_i} \right| \right). \tag{197}$$

If the norm $\left\| u_{j_{i+1}} - u_{j_i} \right\|_{\infty} < \varepsilon$, where ε is sufficiently small then the problem is considered solved and the process is stopped. Otherwise replace $u_{j_{i+1}}$ by u_{j_i}, go back to the step (b) and repeat again.

In step (d) there are many possible methods to compute the norm. The best known of these is the Euclidean norm, such as used in the least-square method. But this is not our main concern, and we choose (197) to compute the norm.

The method outlined above is the well known method of direct iteration or successive approximation [1980O]. Other more sophisticated iteration procedures are also possible (such as Newton-Rhapson [1980O]) which may have advantages from the point of view of convergence or convergence rate. This direct iteration procedure, however, will be sufficient for our purposes.

From the above steps we expect to be able to find one solution from each initial guess (provided that the iteration procedure converges). But since the system equation, either (184) or (188), is nonlinear, it is possible that there may be multiple solutions. How can we find all of these solutions? This will be explored next.

To find all of the solutions, the initial guess displacements u_j are chosen from throughout the possible range. There are several restrictions to this range and thus to the initial guess displacements u_j. For example all of the u_j obey (181). Moreover for the hard device the displacement at $N+1$ node is equal to δ: $u_{N+1} = \delta$.

For the hard device, since δ is given the possible range of the u_{j_i} could be from 0

to δ. But for the soft device, the stress σ is given while δ is unknown. However for a given

σ the strain γ_o varies from $\Gamma_I(\sigma)$ to $\Gamma_{II}(\sigma)$. Therefore the possible range of the u_{j_i} could

be from $\Gamma_I(\sigma)L$ to $\Gamma_{II}(\sigma)L$, where L is the total length of the bar.

11. Solutions of the system equation with $N=2$

11.1 Formulation

System equations (184) and (188) for an N-element model were set up in Section 10. To better understand the relation between the solutions to those equations (possibly nonunique) and the initial guess displacements we will explore them for the simple case of 2 elements ($N=2$). For this simple case we also study how the energy functions depends on the nodal displacements. Under a hard device loading with 2 elements there are two prescribed conditions: $u_1 = 0$, $u_3 = \delta$, so that there are one unknown displacement u_2 and one unknown stress σ. Hence equation (184) is reduced to

$$\left[\frac{E_1}{l} + \frac{E_2}{l}\right][u_2] = \left[\frac{E_2}{l}\delta\right], \tag{198}$$

where l is the length of each element and $l = L/2$. But under a soft device loading, the given conditions are $u_1 = 0$, $\sigma =$ a prescribed constant, so that there are two unknown displacement u_2, u_3. Hence equation (188) becomes

$$\begin{bmatrix} \dfrac{E_1}{l} + \dfrac{E_2}{l} & -\dfrac{E_2}{l} \\ -\dfrac{E_2}{l} & \dfrac{E_2}{l} \end{bmatrix} \begin{bmatrix} u_2 \\ u_3 \end{bmatrix} = \begin{bmatrix} 0 \\ \sigma \end{bmatrix}. \tag{199}$$

Both equations (198) and (199) are nonlinear since E_1 and E_2 are also functions of the unknown nodal displacements in the problem. For the hard device loading of equation (198), E_1 and E_2 are given by

98

$$E_1 = E_1(u_2) = \begin{cases} E_I = 1, & u_2/l \le 1, \\ E_{II} = \dfrac{\bar{\sigma}_{II}(u_2/l)}{u_2/l}, & u_2/l \ge 1, \end{cases}$$

$$E_2 = E_2(u_2) = \begin{cases} E_I = 1, & (\delta - u_2)/l \le 1, \\ E_{II} = \dfrac{\bar{\sigma}_{II}((\delta - u_2)/l)}{(\delta - u_2)/l}, & (\delta - u_2)/l \ge 1. \end{cases} \tag{200}$$

For the soft device loading in equation (199), equation (200) continues to hold, provided that the prescribed value δ is regarded as unknown. Thus one can replace δ by u_3 in (200) so that $E_2 = E_2(u_2, u_3)$. For both loading devices it is easy to see that $\sigma = E_1 u_2/l = E_2(u_3 - u_2)/l$. In what follows our main concern is the hard device loading, so that (198) holds. For each E_i equation (200) gives two choices which are determined by the strains:

$\gamma_1 = u_2/l$ and $\gamma_2 = (\delta - u_2)/l$. Therefore there are $2^2 = 4$ possible forms to (198) corresponding to the phase arrangements [I I], [I II], [II I] and [II II]. The pure phase solutions (186) give $u_2 = \delta/2$ for the phase arrangements [I I] and [II II]. In what follows the following notations are the same:

$$(1, 1) = [\text{I, I}], \ (1, 2) = [\text{I, II}], \ (2, 1) = [\text{II, I}], \ (2, 2) = [\text{II, II}]. \tag{201}$$

11.2 Direct search for FEM solutions

In this section we directly analyze each of four cases (201) individually. Such a direct search is feasible in this case ($N=2$) since these are only 4 possible phase arrangements to examine. In order to understand more about (198) it is convenient to define $\hat{\Theta}(u_2)$ to be the following "system function"

$$\hat{\Theta}(u_2) = \left(u_2 - \frac{E_2 \delta}{E_1 + E_2} \right) \frac{1}{L}, \tag{202}$$

so that solutions of (198) are given by roots of $\hat{\Theta}(u_2) = 0$. If the following non-dimensional parameters are introduced:

$$\bar{u}_2 = \frac{u_2}{L}, \qquad \gamma_o = \frac{\delta}{L}, \tag{203}$$

then

$$\Theta(\bar{u}_2) = \bar{u}_2 - \frac{E_2 \gamma_o}{E_1 + E_2}. \tag{204}$$

Applying the inequality conditions on the right hand side of (200) with $u_1 = 0$ and $u_3 = \delta$

gives the following conditions on u_2 and δ for the four cases (201):

$$(1,1)\text{-case} \Leftrightarrow u_2 \leq l \text{ and } \delta - u_2 \leq l \Rightarrow \delta \leq L \Leftrightarrow \gamma_o \leq 1,$$

$$(1,2)\text{-case} \Leftrightarrow u_2 \leq l \text{ and } \delta - u_2 > l \Rightarrow u_2 \leq \frac{\delta}{2} \Leftrightarrow \bar{u}_2 \leq \frac{\gamma_o}{2},$$

$$(2,1)\text{-case} \Leftrightarrow u_2 > l \text{ and } \delta - u_2 \leq l \Rightarrow u_2 > \frac{\delta}{2} \Leftrightarrow \bar{u}_2 > \frac{\gamma_o}{2},$$

$$(2,2)\text{-case} \Leftrightarrow u_2 > l \text{ and } \delta - u_2 > l \Rightarrow \delta > L \Leftrightarrow \gamma_o > 1.$$

$$\tag{205}$$

Note that $\bar{u}_2$ is restricted to $0 = \bar{u}_1 \leq \bar{u}_2 \leq \bar{u}_3 = \gamma_o$ (see Figure 35). There are four different regions: region A for the (1,1)-case, region B for the (1,2)-case, region C for the (2,1)-case and region D for the (2,2)-case. Figure 35 also verifies that both the (1,1)-case and the (2,2)-case cannot exist for the same γ_o.
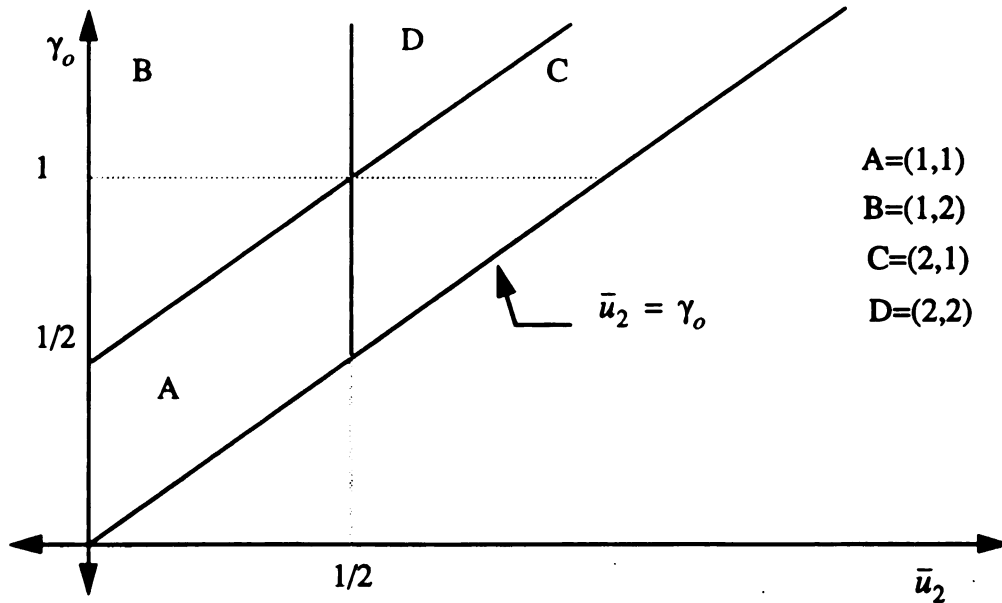
Figure 35. The regions of four cases of possible $\bar{u}_2$ considering a given γ_o for material A.

The roots of $\Theta(\bar{u}_2) = 0$ in (204) are the solutions of (198). Thus the operator $\Theta(\bar{u}_2)$ in (204) for the four cases (201) are now given by the following:

$$\Theta(\bar{u}_2)\big|_{(1,1)\text{-case}} \equiv \Theta_{11}(\bar{u}_2) = \bar{u}_2 - \frac{\gamma_o}{2}, \tag{206}$$

$$\Theta(\bar{u}_2)\big|_{(2,2)\text{-case}} \equiv \Theta_{22}(\bar{u}_2) = \bar{u}_2 - \frac{(\bar{u}_2^2/2 + (\gamma_o - \bar{u}_2)\bar{u}_2^2)\gamma_o}{(1/2 + \bar{u}_2)(\gamma_o - \bar{u}_2)^2 + \bar{u}_2^2/2 + (\gamma_o - \bar{u}_2)\bar{u}_2^2}$$

$$= \frac{\bar{u}_2(\bar{u}_2 - \gamma_o)(\bar{u}_2 - \gamma_o/2)}{(1/2 + \bar{u}_2)(\gamma_o - \bar{u}_2)^2 + \bar{u}_2^2/2 + (\gamma_o - \bar{u}_2)\bar{u}_2^2}, \tag{207}$$

$$\Theta(\bar{u}_2)\big|_{(1,2)\text{-case}} \equiv \Theta_{12}(\bar{u}_2) = \bar{u}_2 - \frac{2(\gamma_o - \bar{u}_2) + 1}{8(\gamma_o - \bar{u}_2)^2 + 2(\gamma_o - \bar{u}_2) + 1}\gamma_o, \tag{208}$$

$$\Theta(\bar{u}_2)\big|_{(2,1)\text{-case}} \equiv \Theta_{21}(\bar{u}_2) = \bar{u}_2 - \frac{2\bar{u}_2^2}{2\bar{u}_2^2 + \bar{u}_2/2 + 1/4}\gamma_o. \tag{209}$$

In (206)-(209) the expression for $\Theta_{11}(\bar{u}_2)$ is independent of $\bar{\sigma}_{II}(\gamma)$ and so holds for all strain-softening materials of the type under consideration here. However the expressions for $\Theta_{12}(\bar{u}_2)$, $\Theta_{21}(\bar{u}_2)$ and $\Theta_{22}(\bar{u}_2)$ depend on $\bar{\sigma}_{II}(\gamma)$ and we have used material A given in Appendix-A for the expressions presented in (207)-(209).

For $\gamma_o = 0.8$ the functions $\Theta(\bar{u}_2)$: $\Theta_{11}(\bar{u}_2)$, $\Theta_{12}(\bar{u}_2)$ and $\Theta_{21}(\bar{u}_2)$ are shown in Figure 36. Since $\gamma_o = 0.8 < 1$, from (205)$_4$ the pure phase-II solution is not allowed and this is why $\Theta_{22}(\bar{u}_2)$ is not shown. The strain γ_1 on first element is less than 1 whenever $0 \le \bar{u}_2 \le \frac{1}{N} = 0.5$, while the strain γ_2 on the second element is less than 1 whenever $\gamma_o - \frac{1}{N} = 0.3 \le \bar{u}_2 \le \gamma_o = 0.8$. Since the value of $\bar{u}_2$ determines the phase for each element according to Figure 35, the function $\Theta(\bar{u}_2)$ that applies is dependent on $\bar{u}_2$. For $\gamma_o = 0.8$ these are:

(1,2)-case: $0 \le \bar{u}_2 \le 0.3$,   (region-B),

(1,1)-case: $0.3 \le \bar{u}_2 \le 0.5$,   (region-A),   (210)

(2,1)-case: $0.5 \le \bar{u}_2 \le 0.8$,   (region-C).

Therefore for different ranges of $\bar{u}_2$ we should follow different curves of $\Theta(\bar{u}_2)$. From (210) the final trace of those different functions $\Theta(\bar{u}_2)$ is shown in Figure 37. Although Figure 36 and Figure 37 show functions $\Theta(\bar{u}_2)$ for $\gamma_o = 0.8$ these figures are representative for all $\gamma_o < 1$.

The functions $\Theta(\bar{u}_2)$: $\Theta_{22}(\bar{u}_2)$, $\Theta_{12}(\bar{u}_2)$ and $\Theta_{21}(\bar{u}_2)$ for $\gamma_o = 2$ are shown in Figure 38. Similarly since $\gamma_o = 2 > 1$ from $(205)_1$ the pure phase-I solution is not allowed and this is why it is not shown. The strain γ_1 on the first element is less than 1 whenever $0 \le \bar{u}_2 \le \frac{1}{N} = 0.5$ while the strain γ_2 on the second element is less than 1 whenever $\gamma_o - \frac{1}{N} = 1.5 \le \bar{u}_2 \le \gamma_o = 2$. For $\gamma_o = 2$ the phase arrangements change with $\bar{u}_2$ as fol-
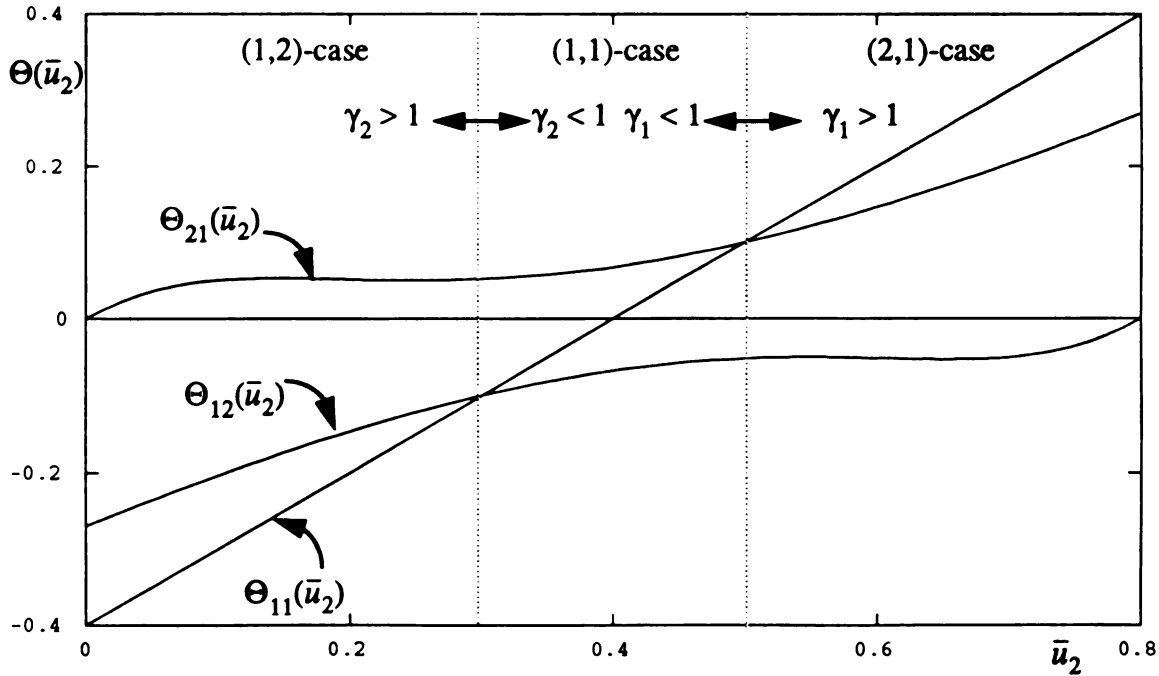
Figure 36. The functions $\Theta(\bar{u}_2)$ with two equal element lengths and γ_o=0.8 for material A.
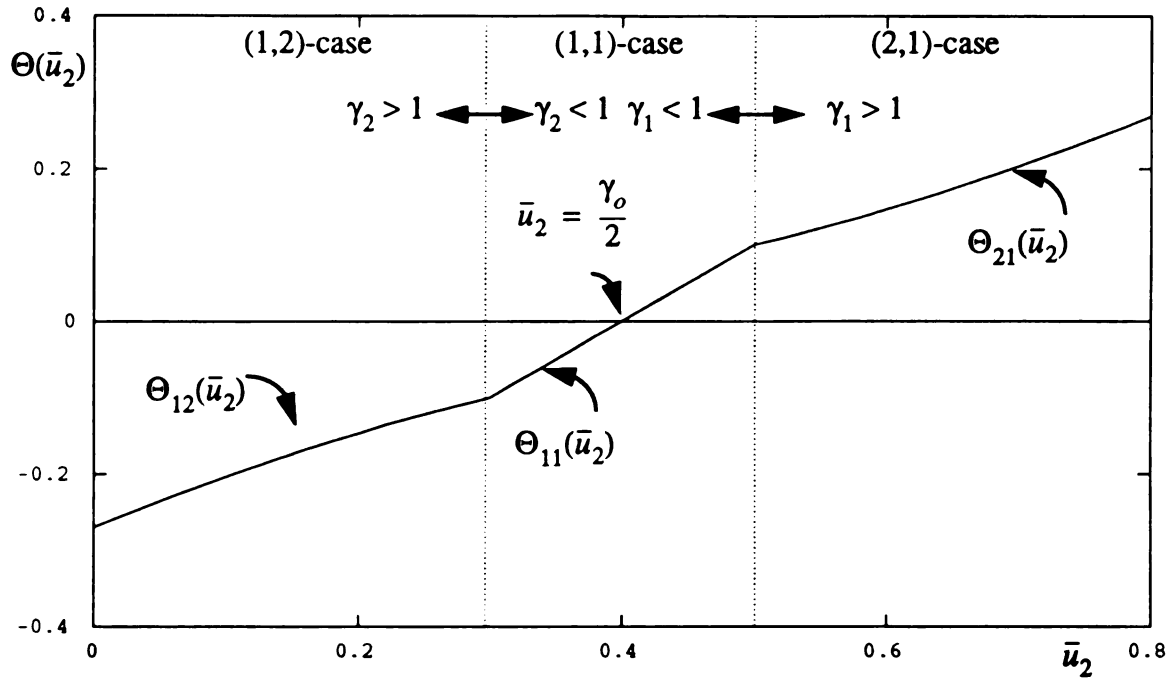
Figure 37. The final trace of the different functions $\Theta(\bar{u}_2)$ for $\gamma_o=0.8$ shown in Figure 36. There is one solution to the composite trace $\Theta(\bar{u}_2)=0$.
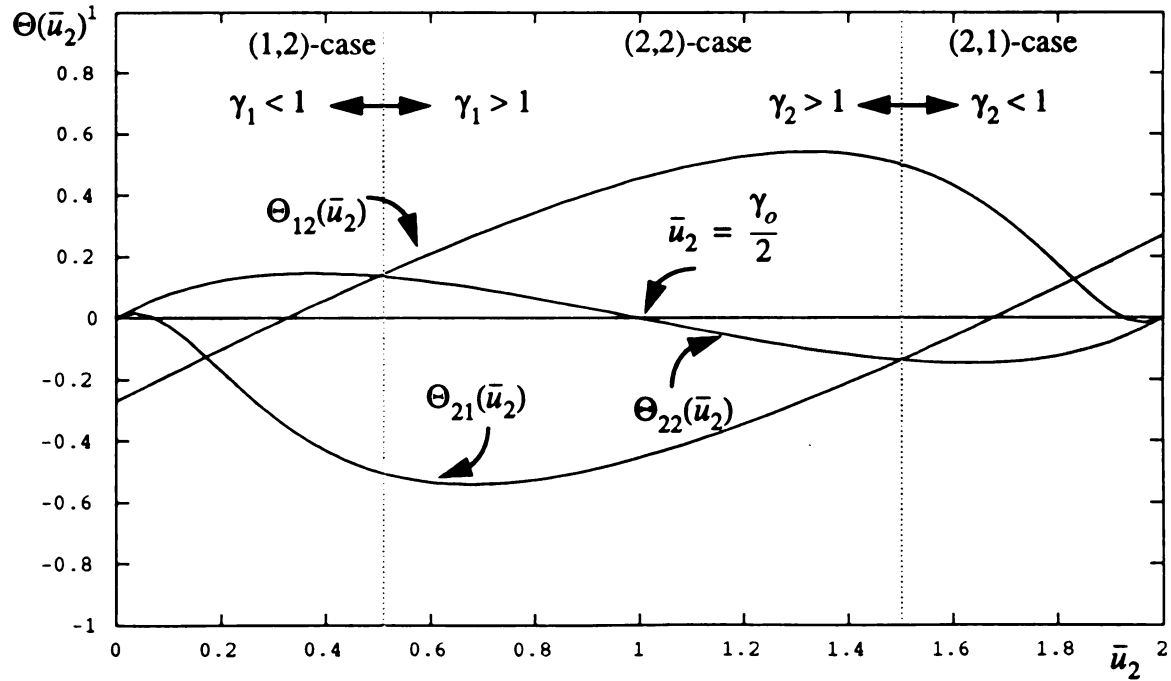
Figure 38. The different functions $\Theta(\bar{u}_2)$ with two equal element lengths and $\gamma_o=2$ for material A.

lows:

$$\text{(1,2)-case:} \quad 0 \le \bar{u}_2 \le 0.5, \quad \text{(region-B)},$$

$$\text{(2,2)-case:} \quad 0.5 \le \bar{u}_2 \le 1.5, \quad \text{(region-D)}, \qquad (211)$$

$$\text{(2,1)-case:} \quad 1.5 \le \bar{u}_2 \le 2, \quad \text{(region-C)}.$$

Therefore from (211) for different ranges of $\bar{u}_2$ we should follow different curves of $\Theta(\bar{u}_2)$.

Figure 39 shows the final composite trace of these different functions $\Theta(\bar{u}_2)$. Although Figure 38 and Figure 39 show functions $\Theta(\bar{u}_2)$ for $\gamma_o = 2$ both figures are representative for all $\gamma_o > 1$.

Note for a given γ_o in the interval $0 \le \gamma_o < 1$ that there is exactly one solution, $\bar{u}_2 = \gamma_o/2$, which is the pure phase solution; alternatively this pure phase-I solution can be thought of as a (1,2)-solution with the phase boundary at the end node $s=1$ or as a (2,1)-solution with the phase boundary at $s=0$. However for a given $\gamma_o > 1$ there are three roots: one pure phase-II solution, $\bar{u}_2 = \gamma_o/2$, and two non-uniform solutions (see Figure 40 and-
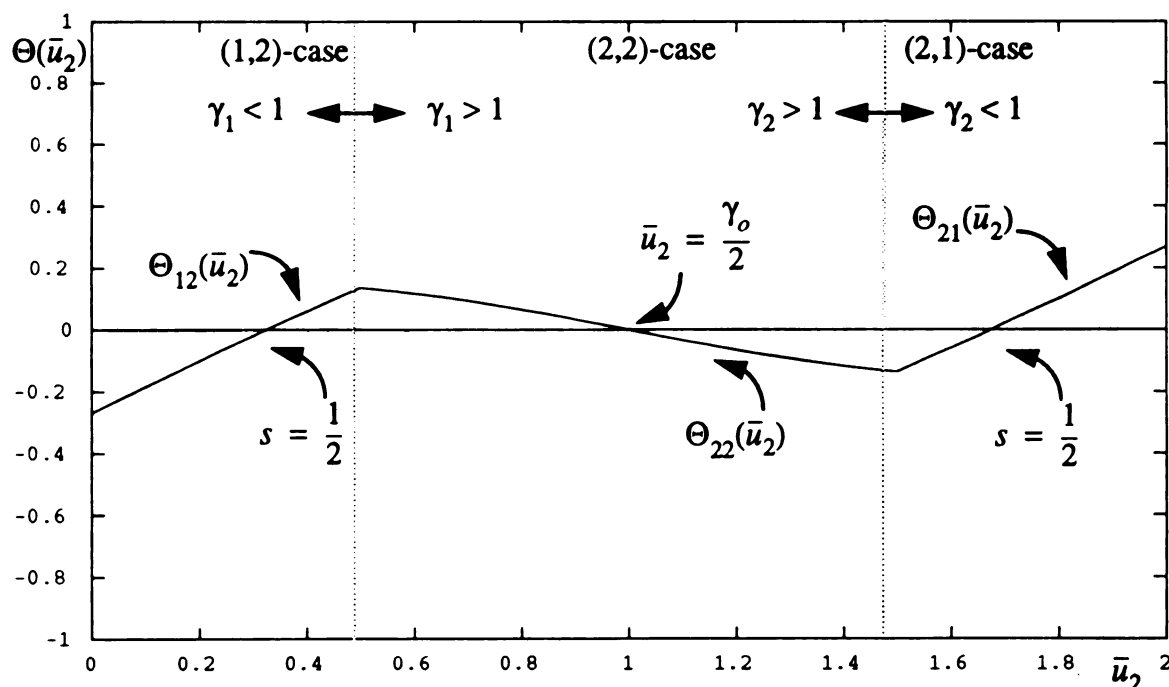
Figure 39. The final trace of the functions $\Theta(\bar{u}_2)$ for $\gamma_o=2$ shown in Figure 38. There are three solutions to the composite trace $\Theta(\bar{u}_2)=0$.
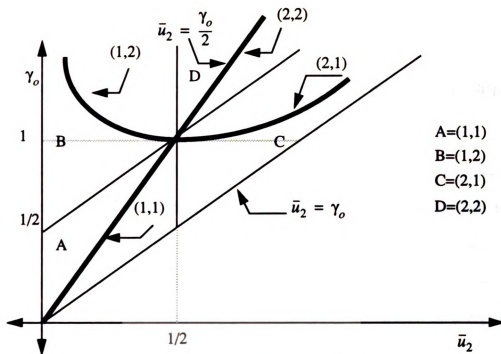
Figure 40. A schematic diagram of the possible solutions $\bar{u}_2$ for a given γ_o.
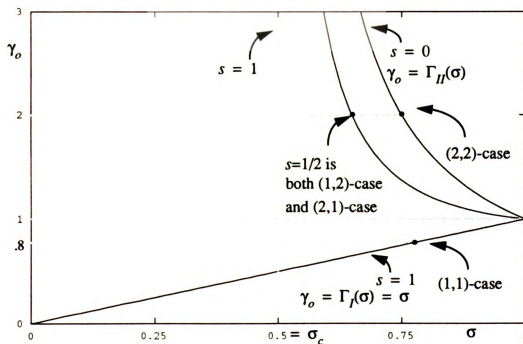
Figure 41. The possible $N=2$ FEM solutions as represented in Ω_{12} for $\gamma_o=2$ and for $\gamma_o=.8$ for material A.

Figure 41). The non-uniform solutions have the graphical interpretation of being the intersection of the $s=1/2$ line in Figure 10 with the associated line of constant γ_o

11.3 The hard device energy function Λ as a function of the possible nodal displacements

In Section 11.2 we gave a careful analysis to find the nodal displacements $\bar{u}_2$ that solve (198) for different displacements δ and hence different γ_o. In this section the hard device energy function Λ is explored. We show directly that values of $\bar{u}_2$ that solve (198) are extremum points of Λ, while values of that do not solve (198) are not extremum points.

From (23) and the non-dimensional parameters (203), the hard device energy function is given by

$$\bar{\Lambda}(u_2) \equiv \bar{\Lambda}(\bar{u}_2) = \frac{1}{2} (W(\frac{\bar{u}_2}{1/2}) + W(\frac{\gamma_o - \bar{u}_2}{1/2})). \tag{212}$$

Graphs of (212) for material A are given in Figure 42 and Figure 43 for the values $\gamma_o = 0.8$ and $\gamma_o = 2$ considered in Section 11.2. Recall from (210) for $\gamma_o = 0.8$ that there are three possible ranges as shown in Figure 36 and these are also indicated on Figure 42. Figure 42 shows that the pure phase solution at $\bar{u}_2 = \gamma_o/2 = 0.4$ (Figure 37) gives the global minimum to the hard device energy function $\bar{\Lambda}$. For $\gamma_o = 2$, Figure 43 shows that the pure phase-II solution at $\bar{u}_2 = \gamma_o/2 = 1$ gives the local maximum to the hard device energy function while there are two global minima to the hard device energy functions located at the other two roots of the composite trace in Figure 39. The value $\gamma_o = 1$ is a turning point to have either one extremum or three extrema. From Figure 37, Figure 39, Figure 42 and Figure 43 it is seen that the solutions of Section 11.2 are associated with either energy minimum or energy maximum. The standard interpretation is that the former are stable and the latter are unstable. Thus here the pure phase-I solutions are stable (no other FEM solutions
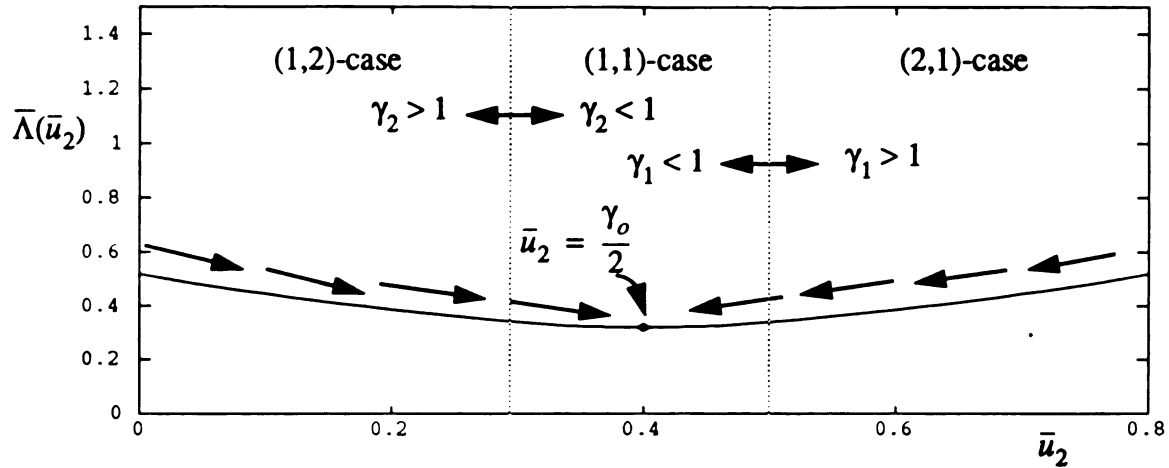
Figure 42. The hard device energy functions $\overline{\Lambda}(\overline{u}_2)$ with two equal element lengths and $\gamma_o = 0.8$ for material A.

Figure 43. The hard device energy functions $\overline{\Lambda}(\overline{u}_2)$ with two equal element lengths and $\gamma_o = 2$ for material A.

are available), while the pure phase-II solutions are unstable. Figure 44 shows how the hard device energy functions varies with both $\overline{u}_2$ and γ_o.

11.4 Iteration solutions and the initial guess displacements

From Section 11.3 the distributions of the hard device energy function were explored for the two special cases: $\gamma_o < 1$ and $\gamma_o > 1$. We now show how this relates to the iteration scheme given in Section 10.5. To find all of the solutions, the initial guess displacements
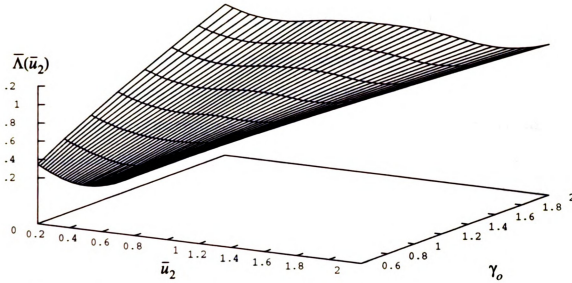
Figure 44. The hard device energy functions $\overline{\Lambda}(\bar{u}_2)$ with two equal element lengths and different γ_o for material A.

are chosen from the possible range $0 < \bar{u}_2 < \gamma_o$. Consider first a displacement such that $\gamma_o < 1$. We then find that if the iteration scheme given in Section 10.5 is implemented, then the associated iterates u_{2_j} will follow the direction of the arrows on the energy curve in Figure 42 and approach the final solution $\bar{u}_2 = \gamma_o/N = \gamma_o/2$. To any initial guess displacement, the final solution is always the same, and is the pure phase-I solution (see Figure 42).

Now consider a displacement with $\gamma_o > 1$. In this case there are three solutions (Figure 39). Thus different initial guesses could converge to a different final $\bar{u}_2$. We find that the associated iterates u_{2_j} will follow the direction of arrows on the energy curve in Figure 43. Hence there are the following conclusions for $\gamma_o > 1$:

    (a) If the initial guess is chosen exactly at $\bar{u}_2 = \gamma_o/N = \gamma_o/2$, which is the pure phase-II solution, then it is the final solution. Otherwise for other initial guess displacements the pure phase solution cannot be found.

    (b) If the initial guess is chosen at $\bar{u}_2 < \gamma_o/N = \gamma_o/2$, then the final solution of the (1,2)-

case will be found by several iteration steps.

(c) Similarly if the initial guess is chosen at $\bar{u}_2 > \gamma_o/N = \gamma_o/2$, then the final solution

of the (2,1)-case will be found by several iteration steps.

In summary the domains of attraction for the initial guess to the FEM solutions are given by the well structure of the energy Λ. The minimum can be converged to, but the maximum requires an exact initial guess. However numerical irregularities and the finite size of ε in (197) might permit an actual FEM code to stay near the maximum long enough to be found as a solution.

In this section there were at most 3 FEM solutions for any γ_o. Thus 3 initial guesses are necessary to locate all solutions, that is all solutions of type [I I], [I II], [II I] and [II II]. However if we only need to find the possible solutions with different volume fraction, then we only have 3 general cases <I I>, <I II> and <II II>. It is found that only 2 of these can exist at the same time since <I I> and <II II> cannot both occur. Thus only 2 initial guesses would be needed to find the different volume fraction solutions.

12. Solutions of the system equation with $N=3$

In Section 11 we have explored the relations between the solutions to (198) and the possible nodal displacements for $N=2$. Can similar relations happen for the $N=3$ case? This will be explored next. Only the hard device loading is considered. Once again the energy as a function of the possible nodal displacement are studied.

12.1 Formulation

Under a hard device loading with three elements ($N=3$) there are two prescribed conditions: $u_1 = 0$, $u_4 = \delta$, and three unknown quantities to be determined: u_2, u_3, σ, where

$$0 < u_2 < u_3 < \delta. \tag{213}$$

Equation (184) becomes

$$\begin{bmatrix} \dfrac{E_1}{l} + \dfrac{E_2}{l} & -\dfrac{E_2}{l} \\[2mm] -\dfrac{E_2}{l} & \dfrac{E_2}{l} + \dfrac{E_3}{l} \end{bmatrix} \begin{bmatrix} u_2 \\ u_3 \end{bmatrix} = \begin{bmatrix} 0 \\ \dfrac{E_3 \delta}{l} \end{bmatrix} \tag{214}$$

where l is the length of each element so that $l = L/3$. Equation (214) is also nonlinear since E_1, E_2 and E_3 are functions of the unknown nodal displacements in the problem. E_1, E_2 and E_3 are given by

$$E_1 = E_1(\gamma_1) = \begin{cases} E_I = 1, & \gamma_1 \le 1, \\[2mm] E_{II} = \dfrac{\bar{\sigma}_{II}(\gamma_1)}{\gamma_1}, & \gamma_1 > 1, \end{cases}$$

$$E_2 = E_2(\gamma_2) = \begin{cases} E_I = 1, & \gamma_2 \le 1, \\[2mm] E_{II} = \dfrac{\bar{\sigma}_{II}(\gamma_2)}{\gamma_2}, & \gamma_2 > 1, \end{cases} \tag{215}$$

$$E_3 = E_3(\gamma_3) = \begin{cases} E_I = 1, & \gamma_3 \le 1, \\[2mm] E_{II} = \dfrac{\bar{\sigma}_{II}(\gamma_3)}{\gamma_3}, & \gamma_3 > 1, \end{cases}$$

110

where

$$\gamma_1 = \frac{u_2}{l}, \qquad \gamma_2 = \frac{u_3 - u_2}{l}, \qquad \gamma_3 = \frac{\delta - u_3}{l}. \tag{216}$$

For each E_i there are two choices which are determined by the strain in the i-th element.

Therefore there are $2^N = 2^3 = 8$ possible phase arrangements: [I, I, I], [II, I, I], [I, II, I], [I, I, II], [II, II, I], [II, I, II], [I, II, II] and [II, II, II]. From the above observation the complexity of the problem is increasing very quickly as the number of elements increases. Equation (214) can be inverted and the result is given by

$$\begin{bmatrix} u_2 \\ u_3 \end{bmatrix} = \frac{E_3 \delta}{E_1 E_2 + E_1 E_3 + E_2 E_3} \begin{bmatrix} E_2 \\ E_1 + E_2 \end{bmatrix}. \tag{217}$$

For the pure phase case, either [I, I, I] or [II, II, II], the solution to (217) is simplified to the

pure phase solution: $\begin{bmatrix} u_2 \\ u_3 \end{bmatrix} = \gamma_o \begin{bmatrix} l \\ 2l \end{bmatrix} = \frac{\delta}{3} \begin{bmatrix} 1 \\ 2 \end{bmatrix}$ given previously in (186).

12.2 The hard device energy function Λ as a function of the possible nodal displacements

In Section 12.1 we found that the formulation for $N=3$ is similar in structure to the formulation in Section 11.1 for $N=2$. However the analysis complicated by the additional degree of freedom. The possible nodal displacements that satisfy (217) will again be given by extrema of the energy function. Therefore we neglect a direct search for FEM solutions (as in Section 11.2 for $N=2$) and instead study the energy function directly. Let's define non-dimensional parameters in the same way as done in (203)

$$\bar{u}_i = u_i / L, \qquad i = 0, 1, 2, 3, \tag{218}$$

so that from (213) that those displacements satisfy the following relation

$$0 < \bar{u}_2 < \bar{u}_3 < \gamma_o. \tag{219}$$

Hence from (24), and the non-dimensional parameters (218) the energy function is given by

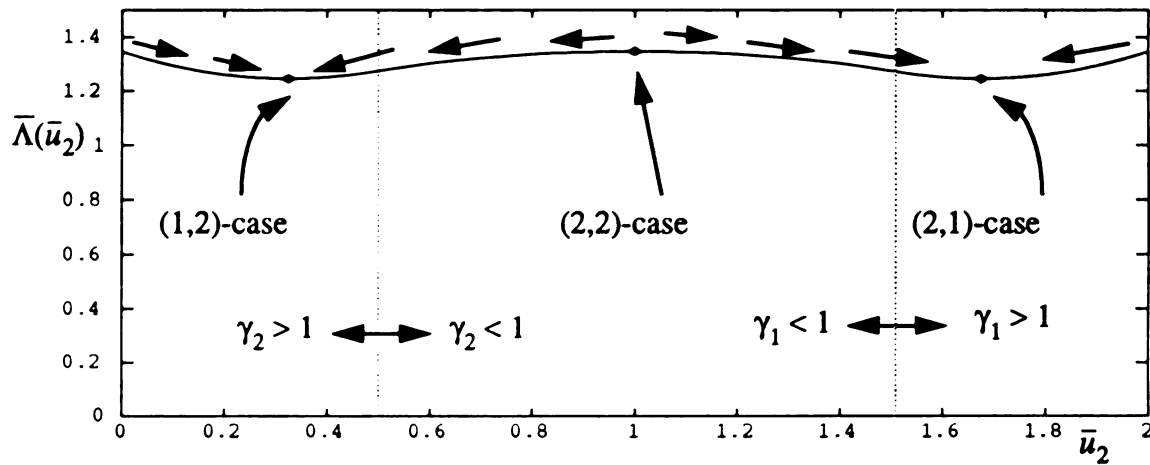Figure 45. The hard device energy functions $\Delta(\bar{u}_2, \bar{u}_3)$ with three equal element lengths and $\gamma_o=0.8$ for material A. A similar picture results for material B at $\gamma_o=0.8$.

$$\Lambda(u_2, u_3) \equiv \Delta(\bar{u}_2, \bar{u}_3) = \frac{1}{3} \, (W(\frac{\bar{u}_2}{1/3}) + W(\frac{\bar{u}_3 - \bar{u}_2}{1/3}) + W(\frac{\gamma_o - \bar{u}_3}{1/3})) \, . \tag{220}$$

Note that (219) is the domain of the energy function in (220). We will again look at $\gamma_o = 0.8$ and $\gamma_o = 2$, as we did in Section 11.

Figure 45 and Figure 46 give the energy surface Δ for material A as a function of the possible nodal displacements for $\gamma_o = 0.8$ and $\gamma_o = 2$ respectively. From the diagrams we can observe the critical points: minimum, maximum and saddle points which are the solutions to (217).

Figure 47 shows the contour diagram of the energy function for $\gamma_o = 0.8$. There is only one critical point, which is the minimum to the energy function at $(\bar{u}_2, \bar{u}_3) = (\gamma_o/N, 2\gamma_o/N) = (0.8/3, 1.6/3)$. This corresponds to a solution of (217) with phase arrangement [I, I, I] (see Figure 45). This solution can also be thought of as a (1,2) type solution with its phase boundary at $s=1$.

For $\gamma_o = 2$, Figure 46 shows the energy surface while Figure 49 shows its contour
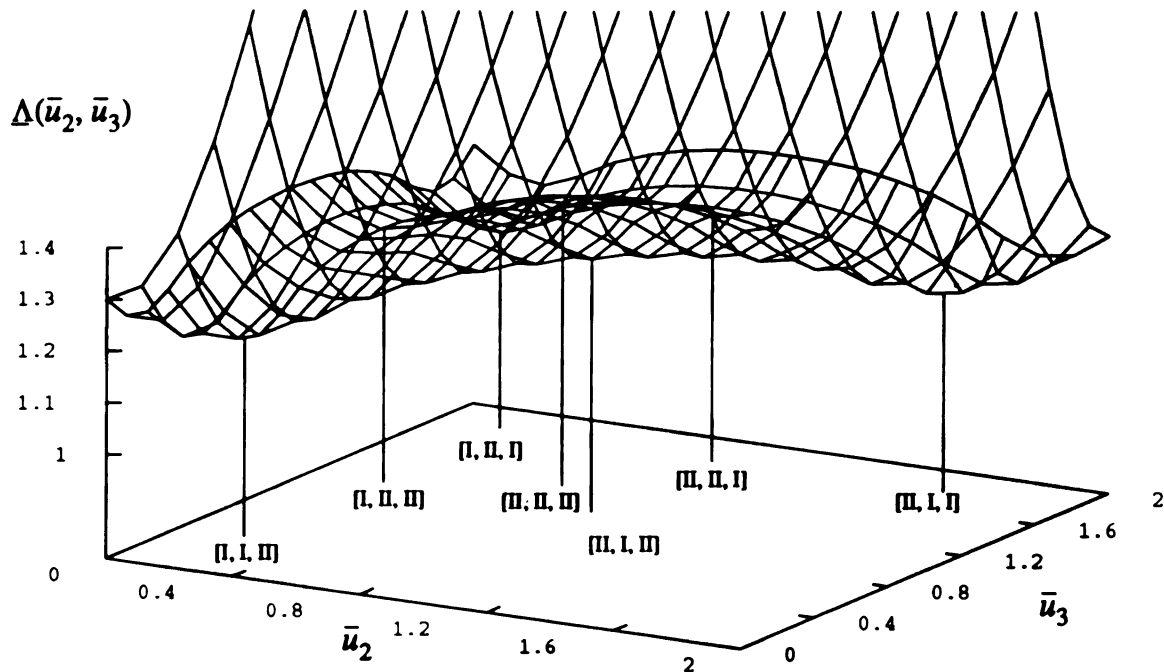
Figure 46. The hard device energy function $\Delta(\bar{u}_2, \bar{u}_3)$ with three equal element lengths and $\gamma_o=2$ for material A. Material B gives a similar picture. This picture is representative for all $\gamma_o>1$, both for material A and for material B.
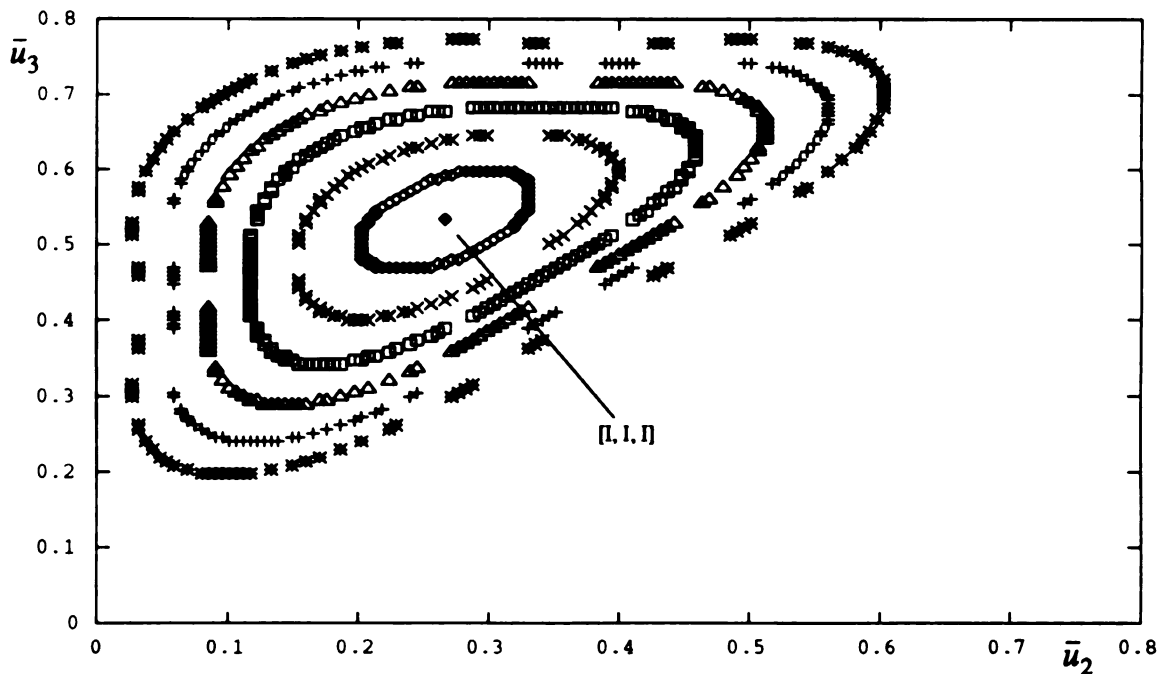
Figure 47. The contour diagram of the hard device energy functions $\Delta(\bar{u}_2, \bar{u}_3)$ on the domain (219) with three equal element lengths and $\gamma_o=0.8$ for material A. A similar picture results for material B at $\gamma_o=0.8$.

diagram. There is a pure phase-II solution to (217) at $(\bar{u}_2, \bar{u}_3) = (\gamma_o/N, 2\gamma_o/N) =$ $(2/3, 4/3)$ which is a hill point to the energy function. Moreover there are three valley points and three saddle points to the energy function. The maximum corresponds to phase arrangement [II, II, II]. This solution can also be thought of as a (1,2) type solution whose phase boundary is at $s=0$. The minima correspond to phase arrangements [I, I, II], [I, II, I] and [II, I, I]. The first of these is a (1, 2)-type solution whose phase boundary is at $s=2/3$. The saddle points correspond to phase arrangements [I, II, II], [II,I, II] and [II, II, I]. The first of these is a (1, 2)-type solution whose phase boundary is at $s=1/3$. For any $\gamma_o > 1$ the energy function and the contour diagram are similar in form to that for $\gamma_o = 2$. It can be shown for material A that $\gamma_o = 1$ is also the turning point to have either one such critical point (minimum, maximum, saddle) or multiple critical points.

In summary, for $\gamma_o = 0.8$ there is one solution and it is of type [I, I, I]. For $\gamma_o = 2$ there are 7 solutions, and they are of type [I, I, II], [I, II, I], [II, I, I], [I, II, II], [II, I, II], [II, II, I] and [II, II, II] (see Figure 49). These solutions correspond to the intersection of the horizontal lines $\gamma_o = 0.8$ and $\gamma_o = 2$ with the curves $s=0$, $s=1/3$, $s=2/3$ and $s=1$ of Figure 10. This is shown here in Figure 48. There is one exception to this, namely only the pure phase solution for $s=1$ is found, the nonattainable limit for $s=1$ at $\sigma = \sigma_c$ is not represented by the FEM.

In all cases discussed so far (for both $N=2$ and $N=3$ cases) there was at most one solution for each phase arrangement. That is if one phase arrangement is chosen (say [I, II, I]), then one could get the individual E_i's in (217) by taking the appropriate formula. The resulting system equation, although still nonlinear, had at most one solution. We now show that this does not always happen. Specifically, as we now show, material B gives two solutions each for phase arrangements [II, I, I], [I, II, I], [I, I, II] when $0.97 < \gamma_o < 1$ (see Figure 50).
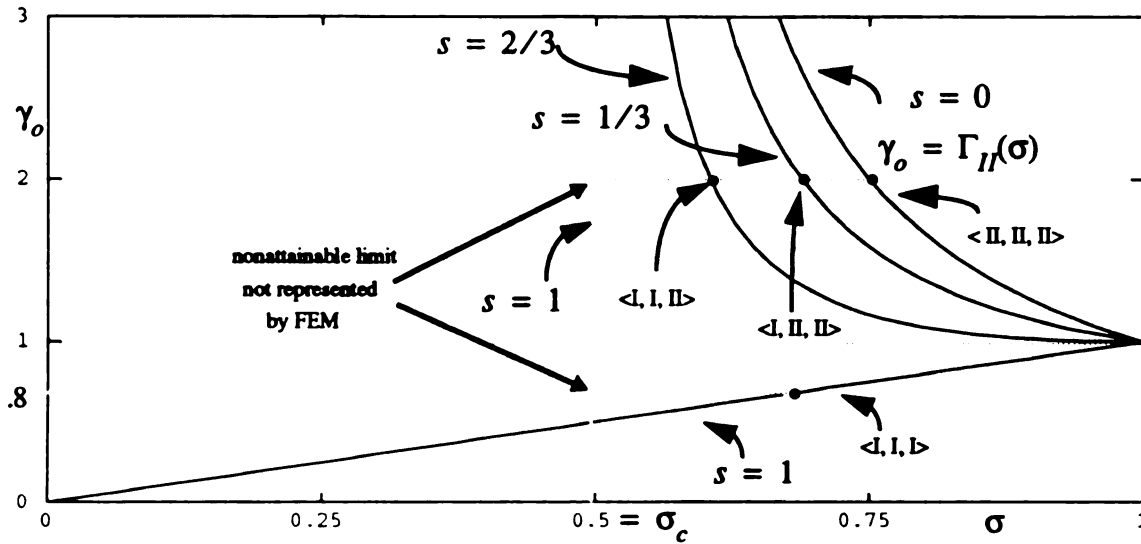
Figure 48. The possible $N=3$ FEM solutions as represented in Ω_{12} for $\gamma_o=2$ and for $\gamma_o=.8$ for material A. Comparing this diagram to Figure 41, it is noted that now two internal constant s curves ($s=1/3$, $s=2/3$) are available for non-pure FEM solutions.
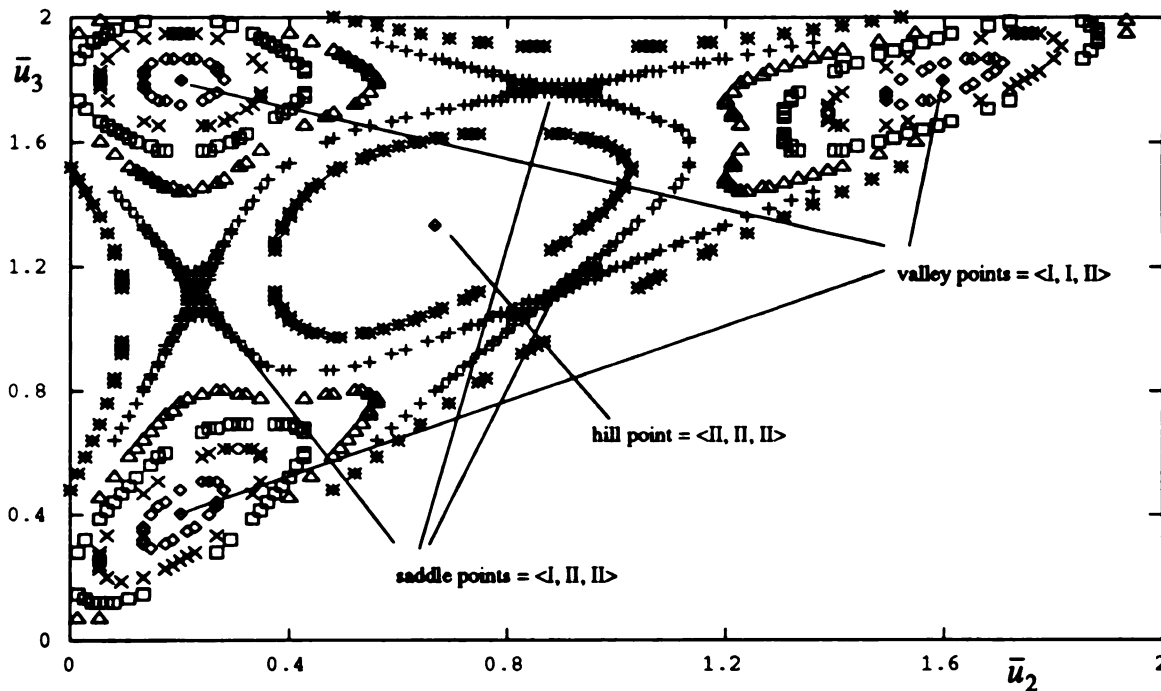
Figure 49. The contour diagram of the hard device energy functions $\Delta(\bar{u}_2, \bar{u}_3)$ with three equal element lengths and $\gamma_o=2$ for material A. This picture is representative for all $\gamma_o>1$, both for material A and for material B.
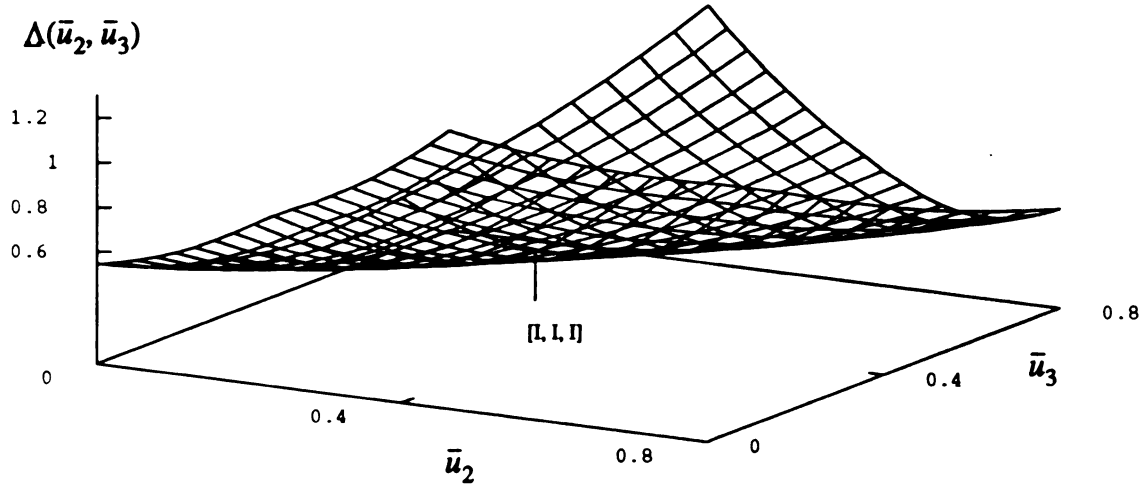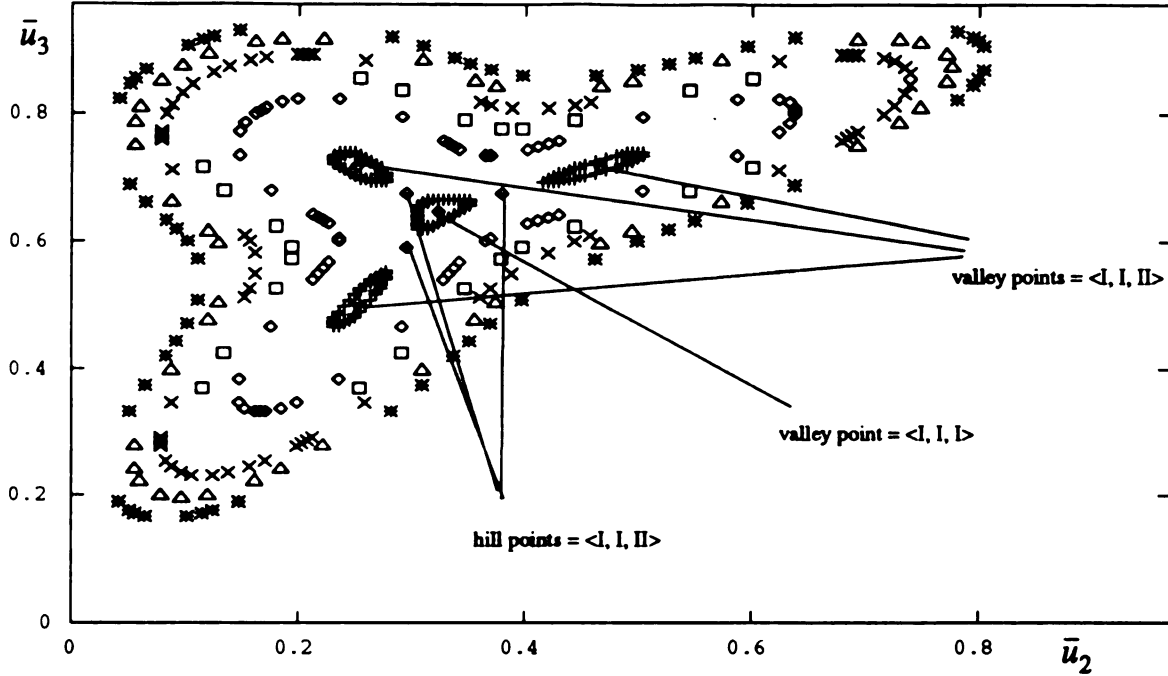
Figure 50. The contour diagram of the hard device energy functions $\Delta(\bar{u}_2, \bar{u}_3)$ with three equal element lengths and $\gamma_o{=}0.97$ for material B. This is different from the contour diagram for material A with $\gamma_o{=}0.97$ (which is similar to the diagram in Figure 47).

Recall from Section 5.4 for a given constant $s > s_{trans}$ that there is a minimum point

on the curve of constant s at the point $(\sigma_{\Phi_2}, \gamma_{\Phi_2})$. For material A we have $s_{trans}{=}2/3$,

while for material B we have $s_{trans} = 1/2$. Therefore for material B the curve $s{=}2/3$ (which

obeys $s > s_{trans}$) is not monotonic in Ω_{12}. There exists a minimum at $\gamma_{\Phi_2}(s{=}2/3){=}$

$$\frac{s}{2} + \frac{3\,(s)^{1/3}\,(1-s)^{2/3}}{2}\Bigg|_{s=2/3} \cong 0.9633. \text{ If } \gamma_{\Phi_2} < \gamma_o < 1, \text{ then there are solutions to } (217)$$

with two different stresses which are not pure phase-I solutions. For example, for

$\gamma_o = 0.97$, there are seven solutions to (217) for material B. This is similar to what happens

when $\gamma_o = 2$. But the main difference is that all six multi-phase solutions to (217) corre-

spond to $s{=}2/3$ in Ω_{12} and no solutions to (217) correspond to $s{=}1/3$ in Ω_{12}.

To show this consider $\gamma_o = 0.97$ for material B. The contour diagram of the energy
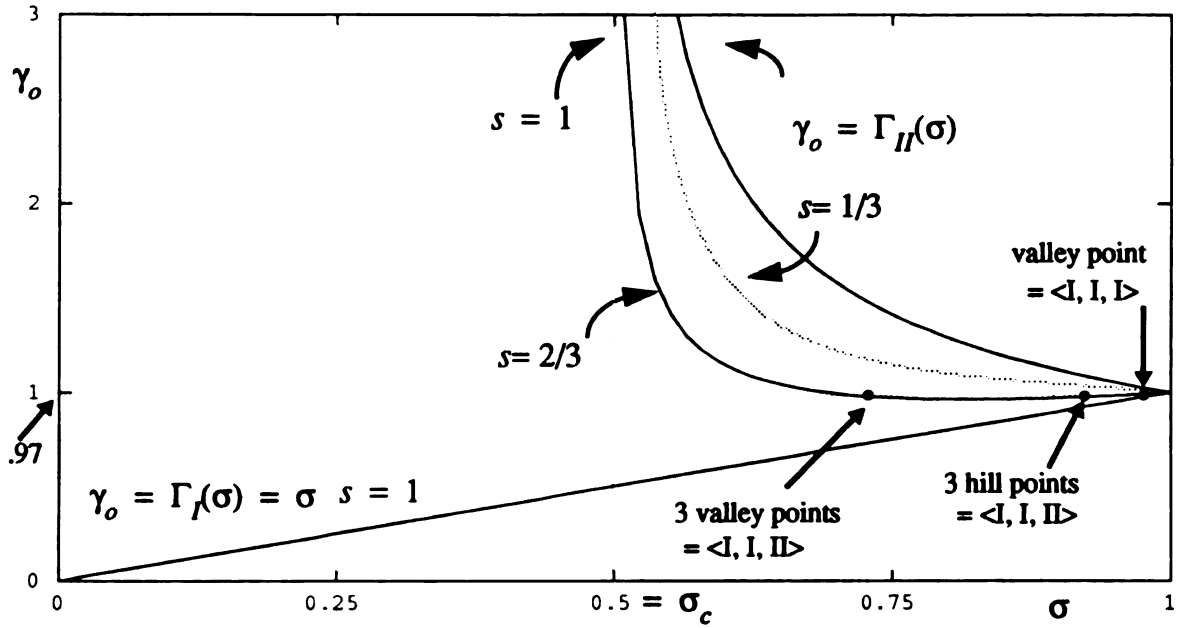
Figure 51. The possible $N=3$ FEM solutions to (217) as represented in Ω_{12} for $\gamma_0=0.97$ for material B. In addition to the pure phase solutions, FEM solutions are associated with the curves $s=1/3$ and $s=2/3$. There is no intersection of $\gamma_0=0.97$ with $s=1/3$ (dotted). There are 2 intersections of $\gamma_0=0.97$ with $s=2/3$, each of which corresponds to 3 phase permutations.
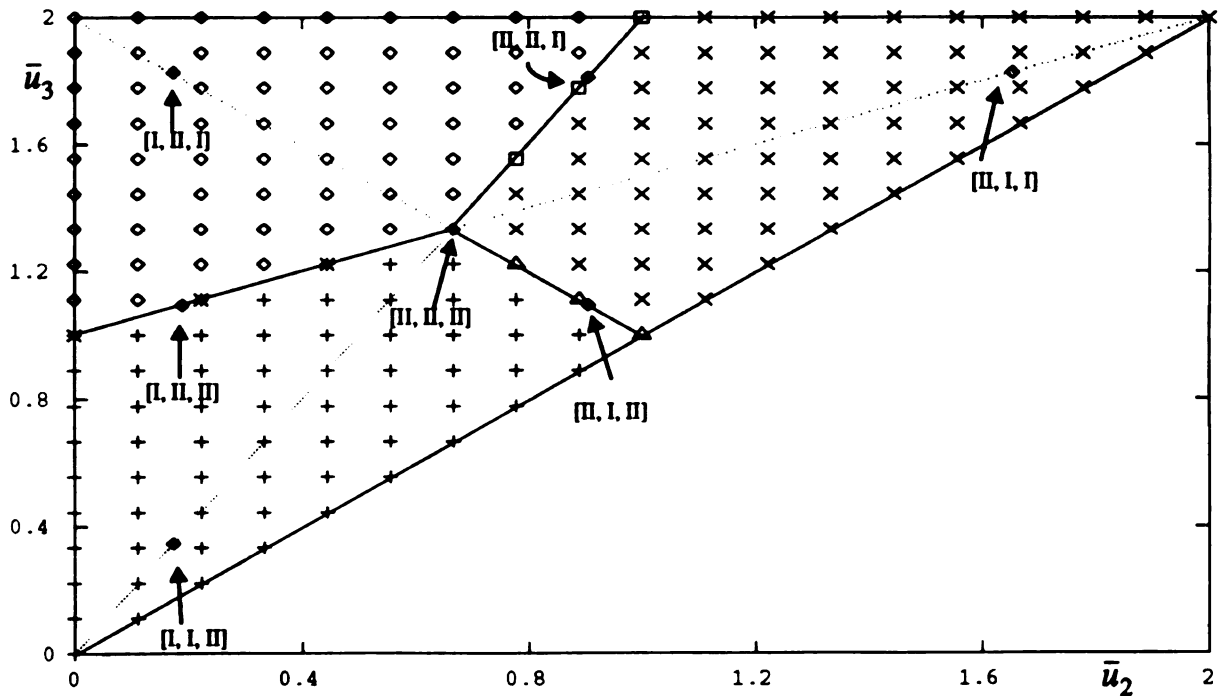
Figure 52. The solutions to (217) and the distributions of initial guesses in the $(\bar{u}_2, \bar{u}_3)$-plane with three equal element lengths and $\gamma_0=2$ for material B.
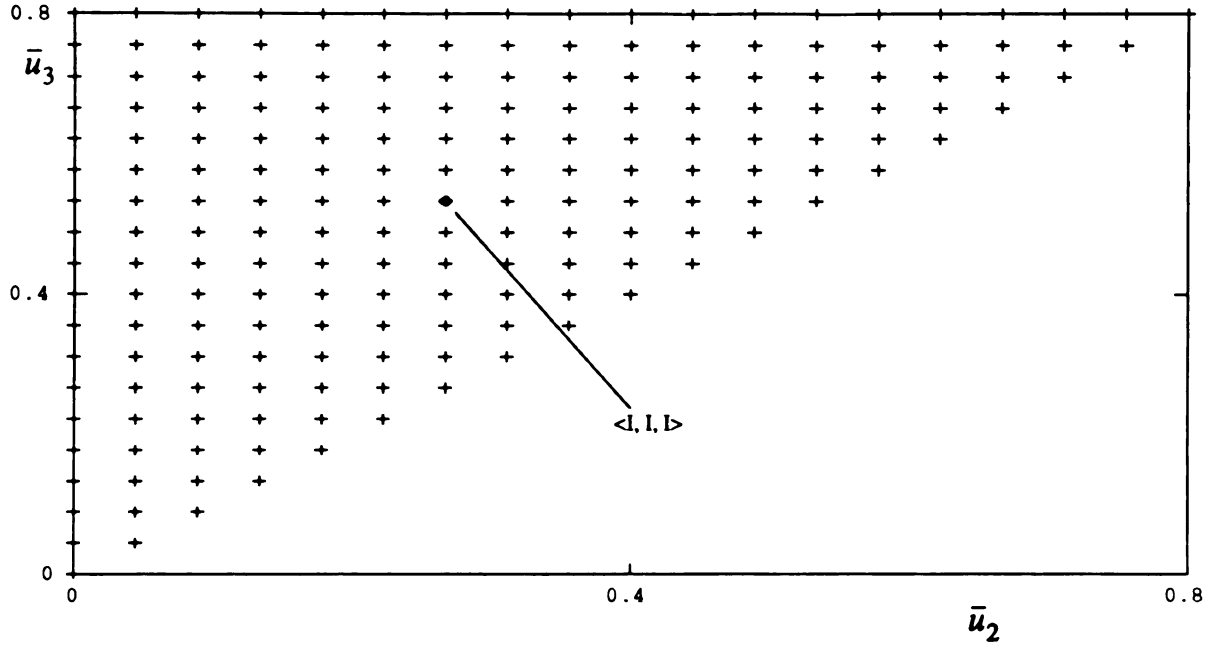
Figure 53. The solution to (217) and the distributions of initial guesses in the $(\bar{u}_2, \bar{u}_3)$-plane with three equal element lengths and γ_o=0.8 for material B.

functions $\Delta(\bar{u}_2, \bar{u}_3)$ is shown in Figure 50. There are also seven solutions to (217) in the diagram. The energy function at the pure phase-I solution to (217) is a valley point of energy surface. There are also three other solutions to (217) that are also valley points of the energy surface. These correspond to solutions of the type <I, I, II>. There are also three different solutions to (217) that are hill points of energy surface. These also correspond to solutions of the type <I, I, II>. Figure 51 shows these solutions as intersection points of

$\gamma_o = 0.97$ with the curve s=2/3 in Ω_{12}.

12.3 Iterative solutions and the initial guess displacements

In Section 11.4 we found that if the iteration scheme given in Section 10.5 is implemented, then the associated iterates u_{2_j} will follow the direction of arrows on the energy curves in Figure 42 and Figure 43. In this section we implement the iteration scheme given in Section 10.5 for finding the solutions to (217) for $N = 3$. We find that the iteration scheme flows
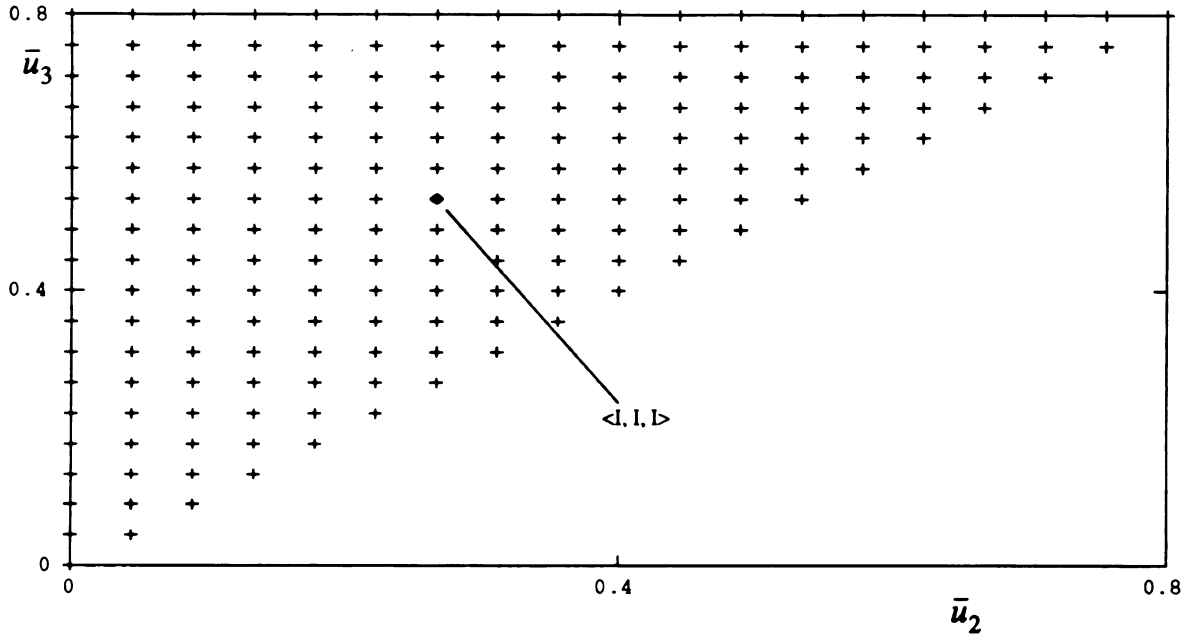
Figure 54. The solution to (217) and the distributions of initial guesses in the $(\bar{u}_2, \bar{u}_3)$-plane with three equal element lengths and γ_o=0.8 for material A. All initial guesses flow downhill to the <I, I, I> solution under the iteration scheme of Section 10.5.

down the energy contours of Figure 47, Figure 49 and Figure 50.

12.3.1 Material A

To find all of the solutions to (217), the initial guess displacements $\bar{u}_2, \bar{u}_3$ are chosen around the possible ranges from (219). Under a hard device loading with $\gamma_o < 1$ there is one solution to (217) only (see Figure 54). To any initial guess, the final solution to (217) is always the same, it is the pure phase solution $(\bar{u}_2, \bar{u}_3) = (\gamma_o/N, 2\gamma_o/N)$. We note that the iteration scheme flows down hill to the minimum, similar to the N=2 case of Figure 42.

Under a hard device loading with $\gamma_o \geq 1$ there are seven phase arrangements. Consider $\gamma_o = 2$, the $(\bar{u}_2, \bar{u}_3)$ -plane of initial guesses is shown in Figure 55. We find that we need at least 28 initial guesses (for material A) in a $(\bar{u}_2, \bar{u}_3)$ -plane to find all of the solutions to (217). This will be explained later.
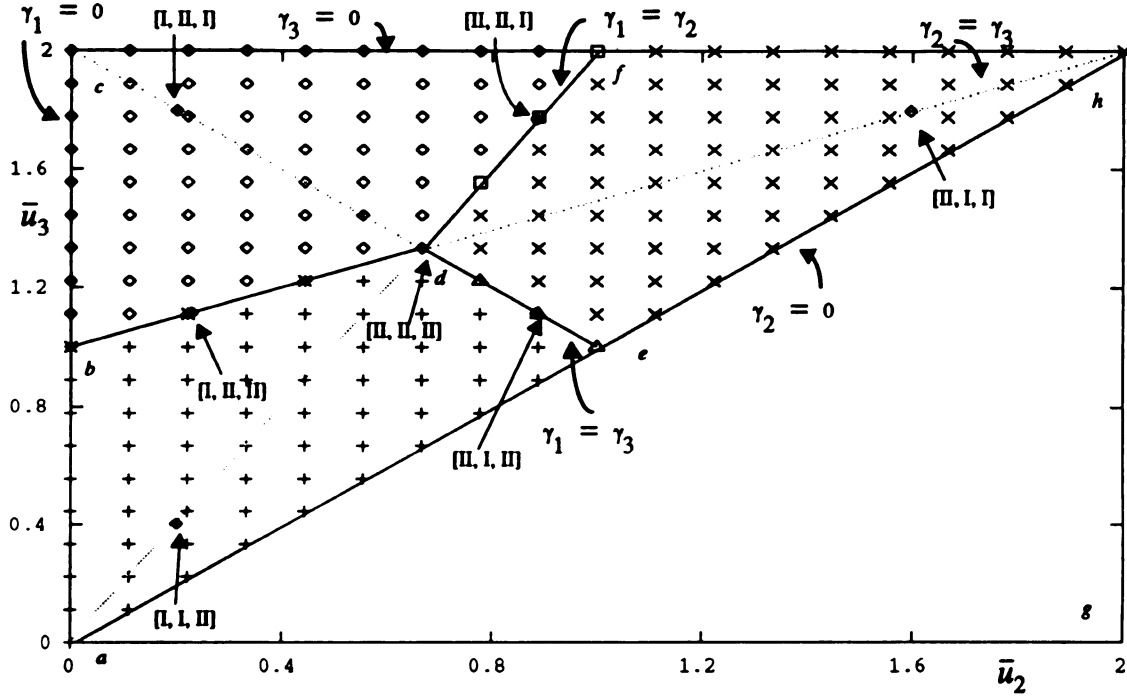
Figure 55. The solutions to (217) and the possible initial guesses in the $(\bar{u}_2, \bar{u}_3)$-plane with three equal element lengths and $\gamma_o=2$ for material A.

The whole region is symmetric with respect to the line $\overline{cg}$, which is the line of $\bar{u}_2 + \bar{u}_3 = \gamma_o$. There is no solution to (217) in the region Δagh, $\bar{u}_2 > \bar{u}_3$ region, since this violates (219). There are three different regions which have their own solutions to (217). The three regions are $\square\, aedb$, $\square\, bdfc$ and $\square\, dehf$. These regions are separated by the three lines $\overline{bd}$, $\overline{de}$ and $\overline{df}$.

In the whole region there are three lines which pass through these regions that have special meanings. They are $\overline{af}$, $\overline{ce}$ and $\overline{bh}$. Since $\gamma_o = 2 > 1$ the pure phase-I solution to (217) is not allowed. For example, on the line $\overline{af}$, the strains on the first and second elements are equal, $\gamma_1 = \gamma_2$. Hence there are three phase arrangements to (217): [I, I, II], [II, II, II] and [II, II, I] on the line $\overline{af}$. The distributions of the solutions to (217) on the line $\overline{af}$ are also similar to the two-element case. Namely there is one initial guess which is the pure

phase solution, while initial guesses which are on the different sides of the pure phase solution will be attracted to the other solutions. Thus 3 initial guesses are needed to find all of the solutions to (217) on the line $\overline{af}$.

On the line $\overline{bh}$, the strains on the second and third elements are equal, $\gamma_2 = \gamma_3$. Hence there are three phase arrangements to (217): [I, II, II], [II, II, II] and [II, I, I] on the line. It is also similar to two-element case, and three initial guesses are needed to find all of the solutions to (217) on the line $\overline{bh}$.

On the line $\overline{ce}$, the strains on the first and third elements are equal, $\gamma_1 = \gamma_3$. Hence there are three phase arrangements to (217): [I, II, I], [II, II, II] and [II, I, II] on the line $\overline{ce}$ which is the line of symmetry. It is also similar to two-element case which needs three initial guesses to find all of the solutions on the line. In conclusion seven initial guesses are needed to find all seven solutions to (217) for a given γ_o if only these three lines are considered. From the above observation a three-element model which gives a two-dimensional case of initial guesses can be reduced to three two-element models which give a one-dimensional case of initial guesses.

Point d is a hill point and is only found from the iteration scheme if it starts from d. With the exception of this point, iterations starting on the lines $\overline{db}$, $\overline{de}$ and $\overline{df}$ stay on these lines and converge to the saddle points associated with phase arrangements <I, II, II> while iteration starting within the open regions □ $aedb$, □ $bdfc$ and □ $dehf$ stay on the regions and converge to the valley points associated with phase arrangements <I, I, II>. But no iteration scheme will converge to a hill point and so the hill point is only found if it is the initial guess itself.

There are two line segments, $\overline{cd}$ and $\overline{de}$, on the line $\overline{ce}$. The line segment $\overline{cd}$ belongs to the region □ $bdfc$ while the line segment $\overline{de}$ separates □ $aedb$ from □ $dehf$. The phase arrangement [I, II, I] is on the region □ $bdfc$, while phase arrangement [II, I, II] is on

the line $\overline{de}$. Therefore it is easy to find the phase arrangement [I, II, I] to (217) since it belongs to the region $\square\,bdfc$. If the initial guess is chosen anywhere in this region then the phase arrangement [I, II, I] to (217) will be found. But it is difficult to find the phase arrangement [II, I, II] to (217) since it belongs to a line. The phase arrangement [II, I, II] to (217) cannot be found unless the initial guess falls on the line $\overline{de}$. There are similar conditions for the other two lines, $\overline{af}$ and $\overline{bh}$. Hence to find all solutions to (217) the initial guesses are required to fall on the lines $\overline{de}$, $\overline{db}$ and $\overline{df}$. If we chose initial guesses in the region $\Delta\,ahc$ by forcing these initial guesses to fall on the lines $\overline{de}$, $\overline{db}$ and $\overline{df}$, then we found that 28 initial guesses were required to find all of the solutions to (217).

It is easier to find a set of solutions which represents all the possible volume fractions of phase-I. This is done by neglecting the ordering the strain phases. Thus if we only consider (1,2)-type solutions, then all such solutions either involve an internal phase boundary either at $s = 1/3$ or $2/3$, or else are pure phase solutions with phase boundaries at the ends $s=0$ and $s=1$ (but the (1,2)-type solutions with $s=0$ and $s=1$ cannot exist for the same γ_o). Hence if the initial guesses are chosen on the lines $\overline{af}$, $\overline{bh}$ or $\overline{ce}$ then, at least, three different initial guesses are needed to find all of the solutions to (217) with different s. For example on the line $\overline{af}$, $\gamma_1 = \gamma_2$ so that the first initial guess could be $(\bar{u}_2, \bar{u}_3) = (\gamma_o/N, 2\gamma_o/N)$, the second one could be $(\gamma_o/N - \varepsilon, 2\gamma_o/N - 2\varepsilon)$ and the third one could be $(\gamma_o/N + \varepsilon, 2\gamma_o/N + 2\varepsilon)$ where ε is a small number. Note that these three initial guesses are always with $\bar{u}_3 = 2\bar{u}_2$ so that the strains of first and second elements are initially equal. There are similar developments either for the first and third element or for the second and third element. Therefore seven initial guesses which lie on the lines $\overline{af}$, $\overline{bh}$ or $\overline{ce}$ are needed to find all solutions to (217).

12.3.2 Material B

For a given $s > s_{tran}$ if $\gamma_o < \gamma_{\Phi_2}(s)$ then the analysis is similar to material A with $\gamma_o < 1$,

while if $\gamma_o > 1$ then analysis similar to material A with $\gamma_o > 1$. For $\gamma_{\Phi_2}(s) < \gamma_o < 1$ the

whole region of $(\bar{u}_2, \bar{u}_3)$ -initial guesses is divided into four subregions: $\square$ aejib, $\square$ ehfkj,

$\square$ fcbik and Δijk. Since these regions: $\square$ aejib, $\square$ ehfkj, $\square$ fcbik and Δijk give the ener-

gy wells, the initial guesses which fall into one of these four regions converge to different

final solutions to (217). The pure phase-I solution to (217) belongs to the triangle region

Δijk. The three regions $\square$ aejib, $\square$ ehfkj and $\square$ fcbik are the energy wells for solutions to

(217) of the type <I, I, II>. The initial guess which lie on one of the internal boundaries (the

lines $\bar{bi}$, $\bar{ij}$, $\bar{je}$, $\bar{jk}$, $\bar{kf}$ and $\bar{ki}$) between these four regions also converge to the pure phase-

I solution at point d, unless the initial guess on these internal boundaries is located exactly

at one of the three hill points. These hill points are also solutions to (217) of the type <I, I,

II> (see Figure 56).
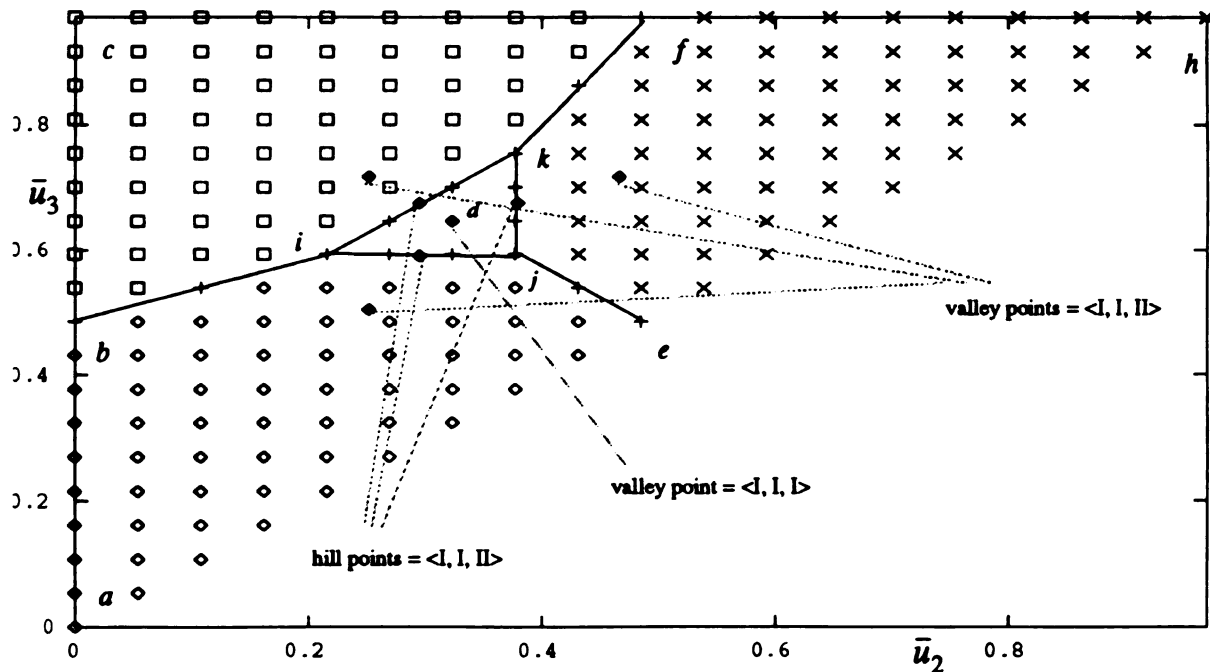
Figure 56. The solutions to (217) and the distributions of initial guesses in the $(\bar{u}_2, \bar{u}_3)$-
plane with three equal element lengths and $\gamma_o=0.97$ for material B. The con-
tour diagram for this case is given in Figure 50.

13. FEM solutions for $N>3$

In this section we consider the number of different phase permutation groups described in Section 10.4. Recall from Section 11 and Section 12 that the number of phase permutation groups is dependent on γ_o and the number of elements N. Section 11 was devoted to the $N=2$ case while Section 12 was devoted to the $N=3$ case. In all cases, there is always exactly one pure phase solution. In the completely trivial one-element case, all solutions are pure phase solutions. For the two-element case, all solutions belong to one permutation group, the pure phase solution <I,I> for $\gamma_o \leq 1$, while all solutions belong to one of two phase permutation groups for $\gamma_o > 1$ either <I,II> or <II,II>. For material A with a three-element case, all solutions belong to the pure phase permutation group <I,I,I> for $\gamma_o \leq 1$ while all solutions belong to one of three phase permutation groups for $\gamma_o > 1$, either <I,I,II>, <I,II,II> or <II,II,II>. We also recall that the solution for $N=3$ with material B was more complicated. In this section we will explore the $N>3$ cases to see whether there are similar results.

The number of elements determines the number of nodes and hence the possible phase boundary locations. Thus the number of elements gives the available constant s curves in Ω_{12} according to (193). There are $N+1$ phase permutation groups (see Figure 34). Each of which has $C(N, m)$ members. The intersections of constant γ_o lines with constant s curves in Ω_{12} determine the FEM solutions. Each such intersection with a constant s curve corresponds to exactly one solution of type (1, 2). However it also corresponds to the other $C(N, m)-1$ members of the permutation group which are not type (1,2) solutions (where $s = m/N \Leftrightarrow m = sN$).

If N is large enough, then some of the curves of constant s curves will obey $s > s_{trans}$ and certain lines of constant γ_o will intersect the same curve of constant s twice.

124

For example this will occur for $s = 1-1/N$ if $1-1/N > s_{trans} > 1-2/N$. Thus the condition for such a double intersection to occur is that N obeys

$$N > \frac{1}{1 - s_{trans}}.$$

(221)

For $N=3$, this occurred for material B ($s_{trans} = 1/2$), but did not occur for material A ($s_{trans} = 2/3$). This also shows that the inequality in (221) is strict.

For material A ($s_{trans}=2/3$), condition (221) is first obeyed when $N=4$. Then the curve of constant $s = 3/4$ satisfies the condition $s > s_{trans}$, and some range of γ_o will intersect this curve twice. Note that each such intersection represents C (4, 3) $=6$ solutions, and both intersections give solutions from the same permutation group: $<I\ I\ I\ II>$. We shall say that these two intersections give two solutions that are distinct to within a permutation (permutationally distinct). From Appendix-A we have $\gamma_{\Phi_2}(3/4) < 1$. Hence we conclude that the number of solutions that are distinct to within a permutation is: exactly one for $\gamma_o < \gamma_{\Phi_2}(3/4)$; two for $\gamma_o = \gamma_{\Phi_2}(3/4)$; three for $\gamma_{\Phi_2}(3/4) < \gamma_o < 1$; two for $\gamma_o=1$; four for $\gamma_o > 1$. It is easy to show the similar development for a higher number of elements. The permutationally distinct solutions for N from $N=1$ to $N=8$ with either material A and with material B under a hard device loading are shown in Figure 57. The number inside the [.] indicates the number of the permutationally distinct solutions. Note that the positions of γ_{Φ_2} are not in scale.

The number of permutationally distinct solutions in Figure 57 is found by counting the number of intersections that a constant γ_o line in Ω_{12} has with the internal constant s-curves: $1/N, 2/N,..., (N-1)/N$ that are interior to Ω_{12}. This number is then increased by one to account for the single pure phase solution. Consider, for example, the eight-element case with material A. There are two values of s, $7/8$ and $6/8$, which are greater than the value of $s_{trans} = 2/3$. Hence these two constant s-curves have one intersection point, which is
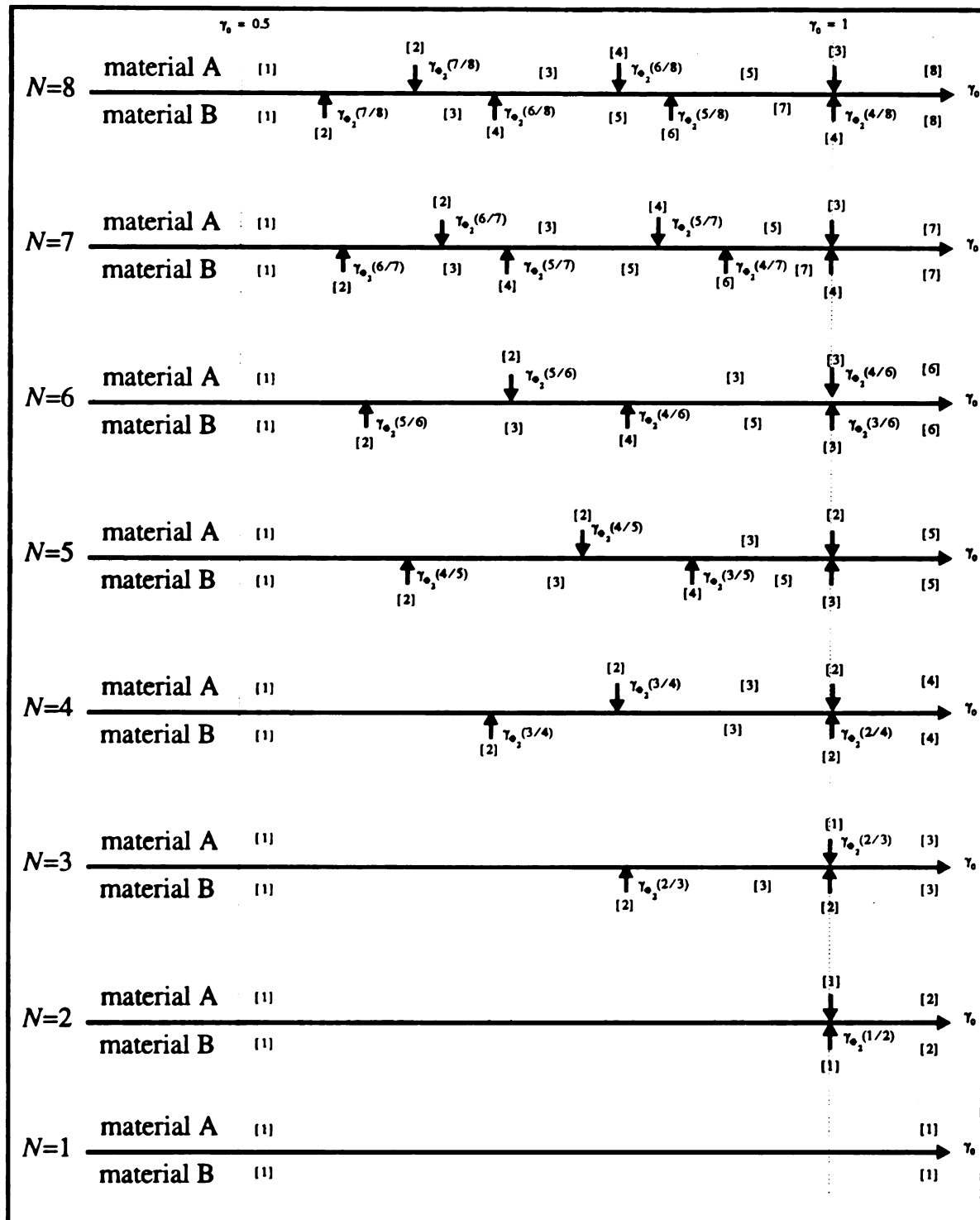
Figure 57. The permutationally distinct solutions for N from $N=1$ to $N=8$ with material A and material B under the hard device loading. The number inside the [.] indicates the number of permutationally distinct solutions. Note that the positions of $\gamma_{\Phi 2}$ are not in scale. The ↑ give values of γ_0 at which the number of permutationally distinct solutions suddenly changes. Often the number of permutationally distinct solutions exactly at the ↑ values is different from the number of permutationally distinct solutions that is available on either side of the ↑ values.

not the end point, with the horizontal line $\gamma_o = 1$. The number of the permutationally distinct solutions increases from 1 to 8 as γ_o increases from 0 to values greater than 1. For $\gamma_o < \gamma_{\Phi_2}(7/8)$ there is no intersection point with internal constant s curves and there is only the pure phase-I solution. When $\gamma_o = \gamma_{\Phi_2}(7/8)$, the curve of constant $s = 7/8$ is just tangent to the horizontal line of constant γ_o and there are two permutationally distinct solutions, the intersection point and the pure phase-I solution. Since $\gamma_{\Phi_2}(7/8) < \gamma_{\Phi_2}(6/8)$, if γ_o is in the range of $\gamma_{\Phi_2}(7/8) < \gamma_o < \gamma_{\Phi_2}(6/8)$, then the curve of constant $s = 7/8$ intersects the horizontal line of constant γ_o twice and there are three permutationally distinct solutions, two intersection points with $s = 7/8$ and one pure phase-I solution. When the value of γ_o reaches to $\gamma_o = \gamma_{\Phi_2}(6/8)$, the curve of constant $s = 6/8$ is just tangent to the horizontal line of constant γ_o and there are four permutationally distinct solutions which are given by the two previous intersection points ($s = 7/8$), one tangent point ($s = 6/8$) and one pure phase-I solution. Similarly when $\gamma_{\Phi_2}(6/8) < \gamma_o < 1$ there are five permutationally distinct solutions which are given by the four internal intersection points (two for $s = 7/8$ and two for $s = 6/8$) and the one pure phase-I solution. The load value $\gamma_o = 1$ is more interesting, since then half of the internal intersection points now coincide with the pure phase solution. Thus it is difficult to distinguish whether the solution to (217) is a pure phase-I solution, a pure phase-II solution or a mixed state solution. Hence there are three permutationally distinct solutions which are given by the two remaining internal intersection points ($s = 7/8$ and $s = 6/8$) and the one "pure phase-I" solution. When $\gamma_o > 1$ it is similar to a general number of elements case and there are eight permutationally distinct solutions. These eight permutationally distinct solutions are given by the seven internal intersection points of the seven different curves of constant s with the horizontal line of constant γ_o, along with the one pure

phase-II solution. The discussion above shows the maximum possible number of permutationally distinct solutions. From the FEM point of view, the possible permutation groups that are presented for each N depend crucially on γ_o (see Figure 57).

14. Numerical results using the finite element method for material A

In this section several numerical examples using the finite element method are studied. The goal is to use the two separate criteria, the minimum energy solution criterion and the kinetic relation, to pick out an unique solution as done in Sections 6, 7, 8 and 9 for the continuous problem. For both criteria and for a given loading all of the permutationally distinct solutions which are explained in Section 13 are considered as found and so are available as candidates for satisfying the criteria under consideration. The selected solution is chosen from all of these permutationally distinct solutions so as to best satisfy the two separate criteria under consideration. The main issue in this section is how to implement these two criteria numerically.

Recall from Section 13 that we only consider the permutationally distinct solution as given in Section 10.4 and so neglect the ordering of the phases. Thus we only consider pure solutions and (1,2) type solutions so that at most only a single phase boundary is present. In this section a quasi-static motion is considered and so we introduce discrete time steps: t_1, t_2,... For such quasi-static motions the phase boundary is allowed to change its location.

Let a discrete time step begins at $t = t_i$ and ends at t_{i+1}. At both t_i and t_{i+1} the values of s are restricted to the set of nodal values

$$\varpi = \{0, \frac{1}{N}, \frac{2}{N}, ..., \frac{N}{N}\}, \tag{222}$$

for a N-element model with equal element lengths. From the given conditions, either initial conditions or a calculation from the previous time step, the FEM solution at time t_i is regarded as known. Thus $s(t_i) \in \varpi$ is also known. It is desired to determine the FEM solution at $t = t_{i+1}$. By using FEM we seek to find $s(t_{i+1}) \in \varpi$ which satisfies the criterion under consideration in the best possible way.

14.1 Minimum energy criterion

For the minimum energy criterion the solution path is independent of the past history of the system. The associated values of the energy Λ are computed for all of the possible phase arrangements

$$\Lambda(u_1, u_2, \ldots, u_{N+1}) = \frac{1}{N} \sum_{n=1}^{N} W(\frac{u_{n+1} - u_n}{L/N}).$$

(223)

The minimum energy criterion gives the solution which has the least energy from among all of the available solutions at each instant time t. For example let's consider a hard device loading with a monotonically increasing end elongation. For the two-element case the minimum energy path first follows the pure phase-I solution, the line of $s=1$ in Ω_{12}, from the origin O, $(\sigma, \gamma_o) = (0, 0)$, to the point P, $(\sigma, \gamma_o) = (1,1)$, secondly it traces the curve $s = 1/2$ in the (σ, γ_o) -plane (Figure 58). In particular there is no jump in the solution path. This is
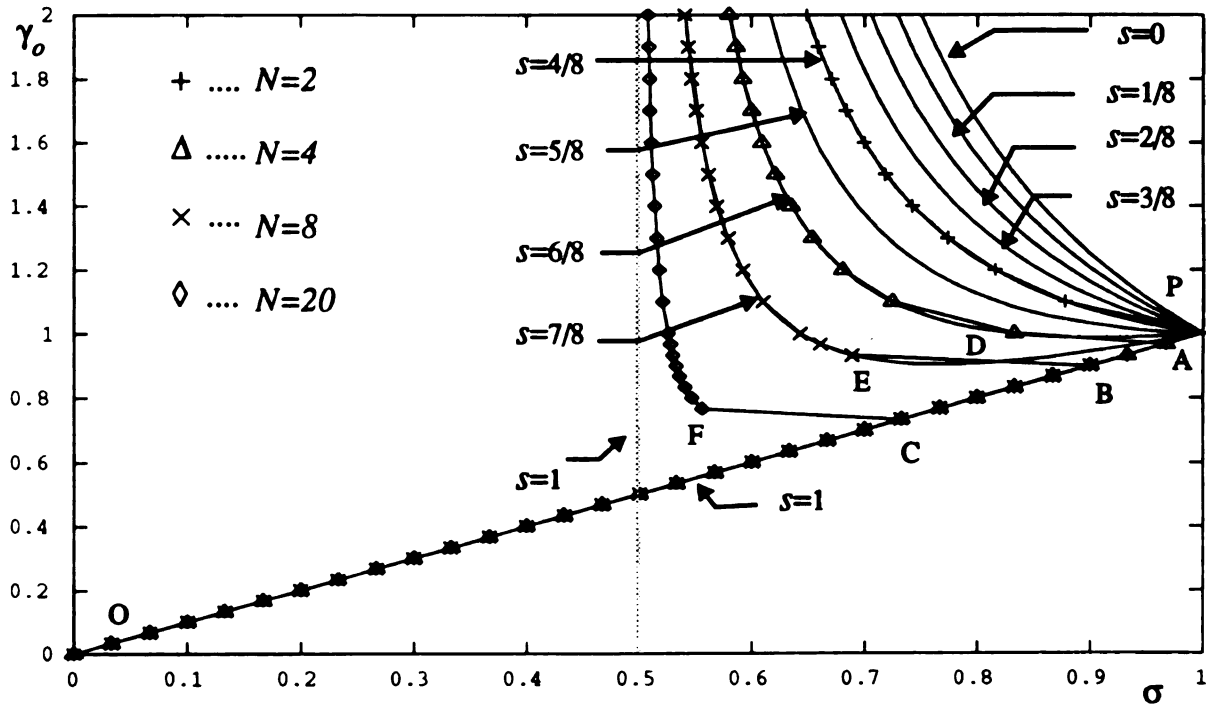
Figure 58. The solution paths in Ω_{12} obeying the minimum energy solution criterion for the two-element, the four-element, the eight-element and the twenty-element cases under a monotonically increasing hard device loading with material A.

because the available FEM solutions are only the pure phase solution and multi-phase solution on the curve $s=1/2$.

For the four-element case the available FEM solutions are the pure phase solution as well as the curves $s=1/4$, $s=1/2$, $s=3/4$. Recall from Section 6 that for $\gamma_o > 1$ the energy Λ decreases as σ decreases on the lines of constant γ_o. Thus for $\gamma_o > 1$ the lowest energy path will be on the leftmost available s-curve (the path closest to $\sigma = \sigma_c$). However for $\sigma_c < \gamma_o < 1$ the energy is minimum as $\sigma \to \sigma_c$ (the unattainable limit), with the energy decreasing toward this limit only for $\sigma_c < \sigma < \bar{\sigma}_{\varnothing_2}(\gamma_o)$ as shown in Figure 15. Thus for $\sigma_c < \gamma_o < 1$ the minimum energy path will either be on the rightmost available path (the pure phase solution) or else will be on the leftmost available path (that closest to $\sigma = \sigma_c$). Unlike the situation when $\gamma_o > 1$, it is not always the latter (namely $s = 1 - 1/N$). Instead a transition will take place at $\gamma_o = \gamma_{\varnothing_3}(1 - 1/N)$. Before this transition the minimum energy is given by the pure phase solution, while after this transition the minimum energy path will be the leftmost available path (the path $s=1-1/N$). For $N=4$ the path first follows the curve $s=1$ from the origin as in the two-element case. However at the point A the value of Λ is the same as the value of Λ at the point D (which is the intersection point of the curve $\varnothing_3$ and the curve $s=1 - 1/N = 3/4$). Thus the path will jump from the point A to the point D and from then on will follow the curve $s=3/4$ as γ_o continues to increase.

For the eight-element case the minimum energy path first follows the curve $s=1$ from the origin as in the two-element case and the four-element case. At the point B the value of Λ is the same as the value of Λ at the point E (which is the intersection point of the curve $\varnothing_3$ and the curve given by $s= 7/8$). At this value of γ_o the path will jump from point B to point E and finally follow the curve $s=7/8$ as γ_o continues to increase.

Accordingly if the number of elements is increased, then the path will approach the

unattainable limit $\sigma_c = 1/2$ which matches the conclusion of section 6.5 as we expect. For example for a twenty-element case, the minimum energy path will be even further to the left. The path first follows the curve $s=1$ from the origin as in the previous cases. At the point C the value of Λ is the same the value of Λ at the point F (which is the intersection point of curve $\varnothing_3$ and the curve given by $s=19/20$). At this value γ_o the path will jump from the point C to the point F and finally will follow the curve given by $s=19/20$ as γ_o continues to increase.

14.2 Kinetic criterion

For the kinetic criterion the solution path is dependent on the rate of loading and so the FEM implementation requires more work. Recall from Section 12 that the kinetic criterion gives (129). Thus if the kinetic criterion is used as the extra condition to find the unique solution from the available FEM solutions, then this solution should be chosen so as to best satisfy (129) from the available FEM solutions.

Recall from Figure 25 for the (1,1)-case, (1,2)-case and (2,2)-case combination that the value of s always increases and this increase is continuous, except for possible sudden changes at $\sigma = 1$. For example if the initial value $s = s(t_i) = 1$ and $\sigma \neq 1$ from t_i to t_{i+1}, then the only possible solution at the next time step is the solution with the final $s = s(t_{i+1}) = 1$. But if the initial value $s = s(t_i) < 1$ and $\sigma \neq 1$ from t_i to t_{i+1}, then from (140) the solution at the next time step should have the phase boundary $s = s(t_{i+1})$ at the location

$$s(t_{i+1}) = s(t_i) + k\int_{t_i}^{t_{i+1}} \bar{f}_{12}(\sigma(t))dt. \tag{224}$$

Since the FEM is a discrete representation of a continuous physical system, the FEM provides the several discrete values of s which are given by (222). Equation (224) can be approximated by many possible ways in a discrete fashion. Given an FEM solution at $t = t_i$,

so that $\gamma_o(t_i)$, $\sigma(t_i)$ and $s(t_i)$ are known, and given $\gamma_o(t_{i+1})$, the problem is to determine the

FEM solution at $t = t_{i+1}$ whose values $\sigma(t_{i+1})$ and $s(t_{i+1})$ best satisfy (224).

14.2.1 Several algorithms to find s (t_{i+1})

One way to implement (224) is by the following algorithm:

Algorithm 1a:

(a) Compute s_{est} by

$$s_{est} = s(t_i) + k\bar{f}_{12}(\sigma(t_i))\,(t_{i+1} - t_i).$$

(b) For each available FEM solution at $t=t_{i+1}$ extract $s(t_{i+1})$.

(c) For each result in (b) compute

$$\Psi = \left| s(t_{i+1}) - s_{est} \right|.$$

(d) After cycling through (b) and (c), select the FEM solution that minimizes

$$\Psi.$$

Physically, this algorithm estimates the integral (224) by assuming that the stress is constant from t_i to t_{i+1}. Hence the phase boundary moves with constant velocity which is the

initial velocity at $t= t_i$. Note that *Algorithm 1a* is equivalent to the following: choose the

FEM solution at $t= t_{i+1}$ that minimizes Ψ_{1a}, where Ψ_{1a} is

$$\Psi_{1a}(s(t_{i+1}), s(t_i), \sigma(t_i), t_{i+1} - t_i) = \left| s(t_{i+1}) - s(t_i) - k\,(\bar{f}_{12}(\sigma(t_i))\,(t_{i+1} - t_i)) \right|. \quad (225)$$

In *Algorithm 1a* the stress is assumed to be the constant which is the stress at $t= t_i$. How-

ever the stresses of the available FEM candidates at time $t=t_{i+1}$ may be different. There-

fore *Algorithm 1a* can be modified by assuming that the stress is equal to $\sigma(t_{i+1})$ in the

integral (224). This gives the following algorithm.

Algorithm 1b:

(a) For each available FEM solution at $t=t_{i+1}$ extract $s(t_{i+1})$ and $\sigma(t_{i+1})$.

(b) For each choice in (a) compute s_{est} by

$$s_{est} = s(t_i) + k \, (\bar{f}_{12}(\sigma(t_{i+1}))) \, (t_{i+1} - t_i)) \, .$$

(c) For each result in (b) compute

$$\Psi = |s(t_{i+1}) - s_{est}| \, .$$

(d) After cycling through (a), (b) and (c), select the FEM solution that minimizes Ψ.

Here the phase boundary moves with a constant velocity which is the velocity at $t = t_{i+1}$

Note that **Algorithm 1b** is equivalent to the following: choose the FEM solution at $t = t_{i+1}$

that minimizes Ψ_{1b}, where Ψ_{1b} is

$$\Psi_{1b}(s(t_{i+1}), s(t_i), \sigma(t_{i+1}), t_{i+1} - t_i) = |s(t_{i+1}) - s(t_i) - k\bar{f}_{12}(\sigma(t_{i+1})) \, (t_{i+1} - t_i)| \, . \quad (226)$$

In both **Algorithm 1a** and **Algorithm 1b** the phase boundary is assumed to move with constant velocity. However the velocity of phase boundary is probably not the same from t_i to t_{i+1}. Other algorithms involve more sophisticated functions for approximating the integral in (224).

Algorithm 2:

(a) For each available FEM solution at $t = t_{i+1}$ extract $s(t_{i+1})$ and $\sigma(t_{i+1})$.

(b) For each choice in (a) compute s_{est} by

$$s_{est} = s(t_i) + k \, (\bar{f}_{12}(\sigma(t_i)) + \bar{f}_{12}(\sigma(t_{i+1}))) \, \frac{(t_{i+1} - t_i)}{2} \, .$$

(c) For each result in (b) compute

$$\Psi = |s(t_{i+1}) - s_{est}| \, .$$

(d) After cycling through (a), (b) and (c), select the FEM solution that minimizes Ψ.

Note that **Algorithm 2** is equivalent to the following: choose the FEM solution at $t = t_{i+1}$

that minimizes Ψ_2, where Ψ_2 is

$$\Psi_2(s(t_{i+1}), s(t_i), \sigma(t_i), \sigma(t_{i+1}), t_{i+1} - t_i)$$

$$= \left| s(t_{i+1}) - s(t_i) - k \left(\bar{f}_{12}(\sigma(t_i)) + \bar{f}_{12}(\sigma(t_{i+1})) \right) \frac{(t_{i+1} - t_i)}{2} \right|. \tag{227}$$

Note that **Algorithm 2** is a numerical method using a trapezoid rule to compute the integral. Thus the velocity of phase boundary is assumed to be the average of the velocities at the two time endpoints: t_i and t_{i+1}.

There are many other possible ways to estimate the integral in (224). Simpson's rule is more accurate than the trapezoid rule but it needs at least three function values to compute the integral. However in the FEM process examined here the problem is solved step by step. Therefore if the FEM solutions at t_i and t_{i-1} are known then the following algorithm is possible:

Algorithm 3:

(a) For each available FEM solution at $t = t_{i+1}$ *extract* $s(t_{i+1})$ *and* $\sigma(t_{i+1})$.

(b) For each choice in (a) compute s_{est} *by*

$$s_{est} = s(t_{i-1}) + k \left(\bar{f}_{12}(\sigma(t_{i-1})) + 4\bar{f}_{12}(\sigma(t_i)) + \bar{f}_{12}(\sigma(t_{i+1})) \right) \frac{(t_{i+1} - t_{i-1})}{6}.$$

(c) For each result in (b) compute

$$\Psi = \left| s(t_{i+1}) - s_{est} \right|.$$

(d) After cycling through (a), (b) and (c), select the FEM solution that minimizes Ψ.

Note that **Algorithm 3** is equivalent to the following: choose the FEM solution at $t = t_{i+1}$ that minimizes Ψ_3, where Ψ_3 is

$$\Psi_3(s(t_{i+1}), s(t_{i-1}), \sigma(t_{i-1}), \sigma(t_i), \sigma(t_{i+1}), t_{i+1} - t_{i-1}) =$$

$$= \left| s(t_{i+1}) - s(t_{i-1}) - k \left(\bar{f}_{12}(\sigma(t_{i-1})) + 4\bar{f}_{12}(\sigma(t_i)) + \bar{f}_{12}(\sigma(t_{i+1})) \right) \frac{(t_{i+1} - t_{i-1})}{6} \right|. \tag{228}$$

It is to be emphasized that there could be different $s = s(t_{i+1})$ for different solutions which have different stresses. In the above algorithms the solution is chosen to best satisfy (224).

Hence the selected solution is always the solution which is closest to one of the possible candidates $s \in \overline{\omega}$.

14.2.2 Computation of an "exact" solution path $(\sigma(t), \gamma_0(t))$ which satisfies the kinetic criterion

Recall from Section 12 that solution paths which satisfy the kinetic criterion (129) are given by pairs $(\sigma(t), \gamma_0(t))$ that satisfy the O.D.E. (135). This section is devoted to a quick construction of such an "exact" solution path which will then be used in the next section to compare FEM solutions given by **Algorithms 1a, 1b, 2, 3** of Section 14.2.1. We desire a path in Ω_{12} which begins from

$$\sigma(0) = 1 \qquad \gamma_0(0) = 1 \tag{229}$$

and moves with increasing γ_0 and decreasing σ as in Figure 33. For a given material (such as material A or material B) it is not easy to construct such path. I find that the choice of

$$\text{material A,} \quad k = 4.05 \tag{230}$$

in (143) and

$$\sigma(t) = \frac{1}{2}\left(1 + \frac{1}{1 + \dfrac{0.9t}{1.1 - t}}\right) \tag{231}$$

gives an integral (143) whose solution $\gamma_0(t)$ is monotonically increasing, and is given by

$$\gamma_0(t) = \sigma(t) + T(\sigma(t))\left(1 - 4.05\int_0^1 \left(\frac{(\sigma(t)^2 - 1)}{2} - \frac{\ln(2\sigma(t) - 1)}{2}\right)dt\right). \tag{232}$$

Therefore we use (231) in the following. The time history for $\sigma(t)$ and $\gamma_0(t)$ are given in Figure 59. Note that $\sigma(t)$ is close to being linearly decreasing. Although the $\gamma_0(t)$ can be found explicitly by (232). I compute it by Simpson's rule using either 10, 20 or 30 time steps as t increases from 0 to 1. Those three results, which are very close, are shown in Figure 59(b). I find that slightly changing k or the form of $\sigma(t)$ can cause $\gamma_0(t)$ to change its
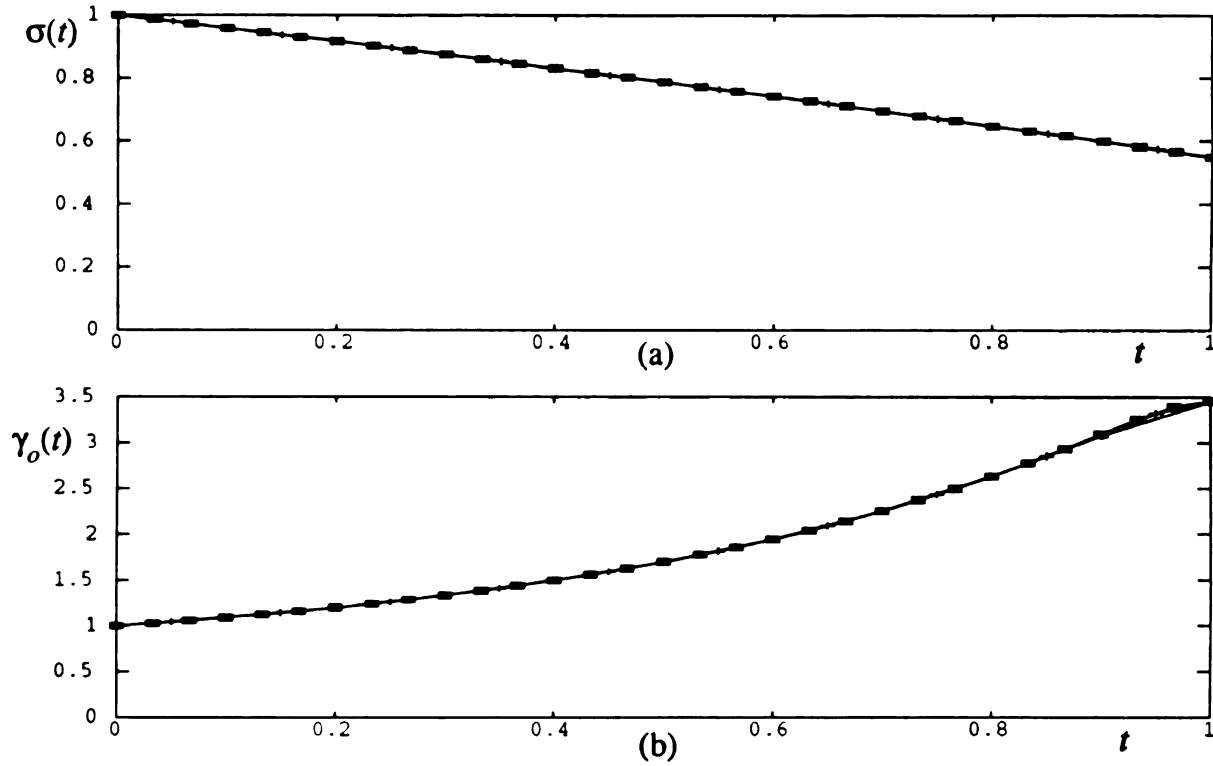
Figure 59. (a) The loading σ(t) given by (231). (b) The corresponding response function γ₀(t) which is given by (232) using (231) for material A with k=4.05. Three different total number of time steps, 10, 20 and 30, are considered in the numerical computation of this "exact" solution.

monotone behavior. This accounts for the somewhat specialized value of k and special function of $\sigma(t)$ used here.

Recall from (a.1), (a.4) and (a.24) for material A that the driving traction force is given by

$$\bar{f}(\sigma(t)) = \frac{(\sigma(t)^2 - 1)}{2} - \frac{\ln(2\sigma(t) - 1)}{2}.$$

(233)

From (140) and (233) the location of phase boundary is given by

$$s(t) = s(0) + k\int_0^t \bar{f}(\sigma(t))dt = 4.05\int_0^1 \bar{f}(\sigma(t))dt$$

$$= 4.05\int_0^1 \left(\frac{(\sigma(t)^2 - 1)}{2} - \frac{\ln(2\sigma(t) - 1)}{2} \right) dt.$$

(234)

14.2.3 Solutions obeying the kinetic relation obtained by using the finite element method

In Section 14.2.2, a pair $(\sigma(t), \gamma_o(t))$ that satisfies the kinetic criterion was found to be given by (232). Thus for a hard device problem if the $\gamma_o(t)$ of this pair is given, then the solution which satisfies the kinetic criteria will be the $\sigma(t)$ from this pair. Alternatively for the soft device if the $\sigma(t)$ of the pair is given by (231) then the kinetic criterion will predict the $\gamma_o(t)$ of the pair as given by (232) in Figure 59(b). In this section we consider the hard device loading. Thus we take $\gamma_o(t)$ as given in (232) and implement the FEM solutions using the different algorithms of Section 14.2.1. Our object is to compare the FEM solutions generated by these algorithms to the "exact" solution.

To obtain the solutions using FEM any algorithm in the Section 14.2.1 is possible. But since the use of *Algorithm 3* requires the solutions from the previous two time steps, the first step of *Algorithm 3* will use *Algorithm 2*.

Figure 60 shows the comparison of those algorithms for the same load, same $N=8$, and same time steps. Recall that FEM solutions must lie on the available s-curves. The "exact" solution is computed numerically from (231) and (234) using Simpson's rule, it is *not* restricted to lie on the available s-curves. Note that all the different algorithms give fairly close agreement to the "exact" solution and give jumps between the available s-curves at different time steps. The solution paths considered by *Algorithm 1a* is slow while the solution paths considered by *Algorithm 1b* is fast. For $N=8$, the *Algorithm 2* and the *Algorithm 3* give the same results which are better than the results of either *Algorithm 1a* or *Algorithm 1b*.

Recall from Figure 23 and equation (129) that $\dot{s} = 0$ when $\sigma = 1$ for both materials, while $\dot{s} \to \infty$ for material A and $\dot{s} \to 5k/8$ for material B when $\sigma \to 1/2$. Therefore the phase boundary will start to move slowly but will finally move very fast.
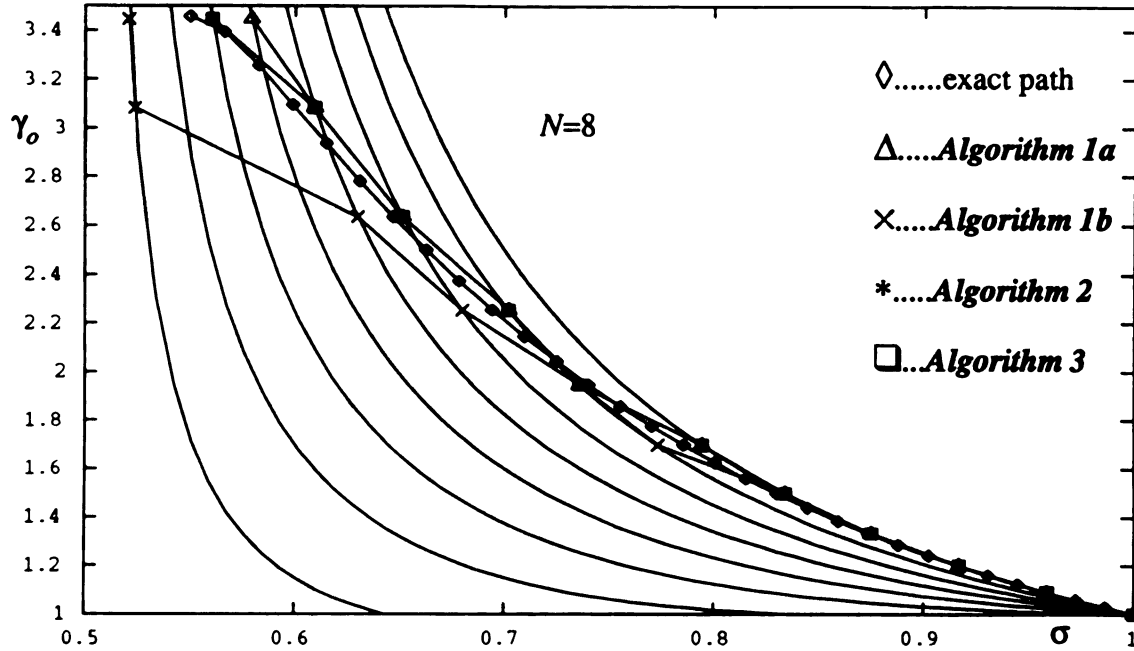
Figure 60. The solution paths obeying the kinetic criterion for different algorithms under a hard device loading with 10 loading time steps. Here the conditions are given by (229) and (231) with material A and k=4.05.

To see the effect of the number of elements on the FEM process, three different number of elements: $N = 2, 4$ and 8 are considered. Then for each different N, the influence of changing the number of time steps is examined by considering 10, 20 and 30 time steps (see Figure 61).

In Figure 61 we have used a *Combination Algorithm* which is a combination of *Algorithm 2* and *Algorithm 3*. In the *Combination Algorithm* at the odd numbered time steps the integral in (224) is computed using *Algorithm 2* while at the even numbered time steps the integral in (224) is computed using *Algorithm 3*.

For $N=2$, the phase boundary location only has three choices, 0, 1/2 and 1. Figure 61(a) shows that s increases monotonically. At the beginning the solution path will follow the curve $s=0$, jump to the curve $s=1/2$, and then follow the curve $s=1/2$. Due to the availability of only one internal s curve for a two-element discretization there are big errors between the FEM solution paths and the exact solution path. Therefore increasing the number

of time steps gives little improvement for $N=2$.

But for $N=4$, there are five choices for the phase boundary location s: 0, 1/4, 2/4, 3/4, and 1. Moreover s also increases monotonically. The solution path will first follow the curve $s=0$, jump to the curve $s=1/4$, and then follow the curve $s=1/4$. After that the solution path will jump to the curve $s=2/4$ and so on. The errors between the FEM solution paths and the exact solution path have been reduced. Obviously increasing the number of time steps gives more improvement for $N=4$ than it does for $N=2$ (Figure 61(b)).

For $N=8$, there are nine choices for s: 0, 1/8, 2/8,...., 7/8, and 1. Again s increases monotonically. The solution path will first follow the curve $s=0$, jump to the curve $s=1/8$, and then follow the curve $s=1/8$. After that the solution path will follow the curve $s=2/8$ and so on. The solution paths for $N=8$ are similar to those for $N=4$ (Figure 61(c)).

Figure 61 shows that improvements take place with an increasing number of time steps when the number of elements is held fixed. Three time step discretizations for $N=2$ are shown in (a); those for $N=4$ are shown in (b); those for $N=8$ are shown in (c). Correspondingly if the nine FEM solution paths in Figure 61 are rearranged, then the improvements obtained by increasing the number of elements N when the number of time steps is held fixed are shown in Figure 62.

14.2.4 Three ramp loadings with different loading rates

In the previous subsection, the finite element program is checked against an example which has an "exact" solution. The results are very close. The influences of the loading rates on the solution paths as computed by FEM are explored in this section. Let's consider three different ramp loadings with different loading rates α which are similar to those loading as given in Section 9.3 and shown in Figure 63. Our goal is to show that FEM gives the rate dependence predicted in Section 9.3.

Again the *Combination Algorithm* which alternates between *Algorithm 2* and *Al-*

Figure 61. The effect of refining the spatial discretization. The solution paths obeying the kinetic criterion for the two-element (a), the four-element (b) and the eight-element cases(c). This is done by a hard device loading with three different loading time steps. Here the conditions are given by (229) and (231) with material A and k=4.05. The curves indicated by ↓ are available for the value of N being considered. The combination algorithm was used for implementing the kinetic criterion.
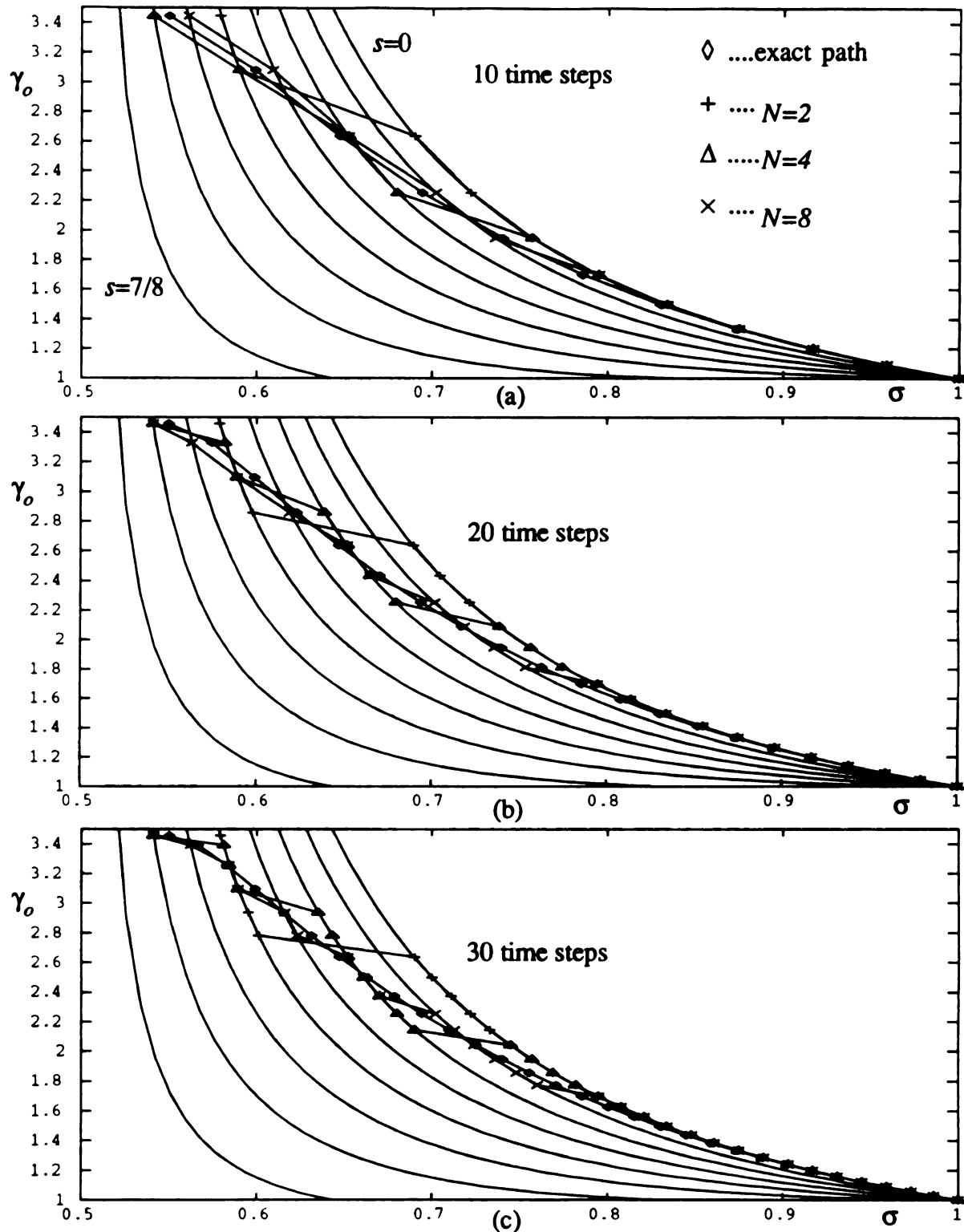
Figure 62. The effect of refining the time discretization. The solution paths obeying kinetic criterion for the two-element, the four-element and the eight-element cases. This is done by a hard device loading with three different loading time steps, 10 time steps (a), 20 time steps (b) and 30 time steps (c) for initial conditions given by (229) with material A and k=4.05. The combination algorithm was used for implementing the kinetic criterion.
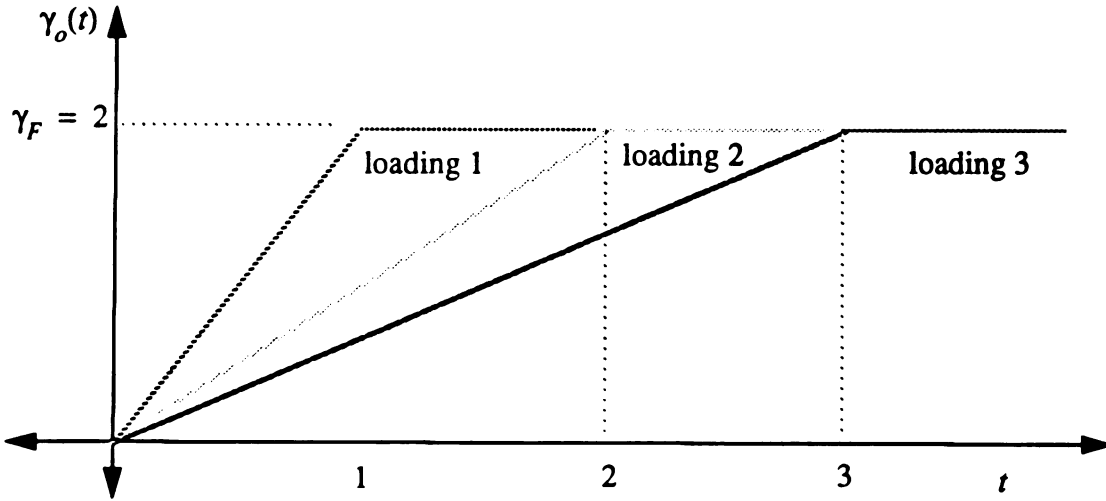
Figure 63. Three loadings with different loading rates.

gorithm 3 is used in the finite element program. The following conditions are assumed:

$$\gamma_o(0) = 0,\ \sigma(0) = 0,\ s=0 \text{ when } \sigma=1. \tag{235}$$

We consider material A and k=10. The values of α are given by 2,1 and 2/3 in loading 1, 2 and 3 respectively. Figure 64 shows the FEM solution paths obeying the kinetic criterion (129) for a two-element discretization (a), a four-element discretization (b) and an eight-element discretization (c) under these loadings. This figure shows that the solution path of the fast loading rate, loading 1, will follow the curve of pure phase solution s=0 longer than those of the lower rates and always remains to the right of the solution paths associated with lower loading rates. Similarly the solution path of the slowest loading rate, loading 3, will follow the curve of pure phase solution s=0 shorter than those of the high rates and always remains to the left of the solution paths associated with high loading rates. Note also that the loading 2 (which is located between loading 1 and loading 3 in Figure 63) has a solution path in Figure 64 that is also located between those of loading 1 and loading 3.

Figure 65 shows the effect of the number of elements under the same loading. The solution path associated with a larger number of elements always leaves the pure phase solution curve s=0 earlier and has more variation. This is because these solution paths have
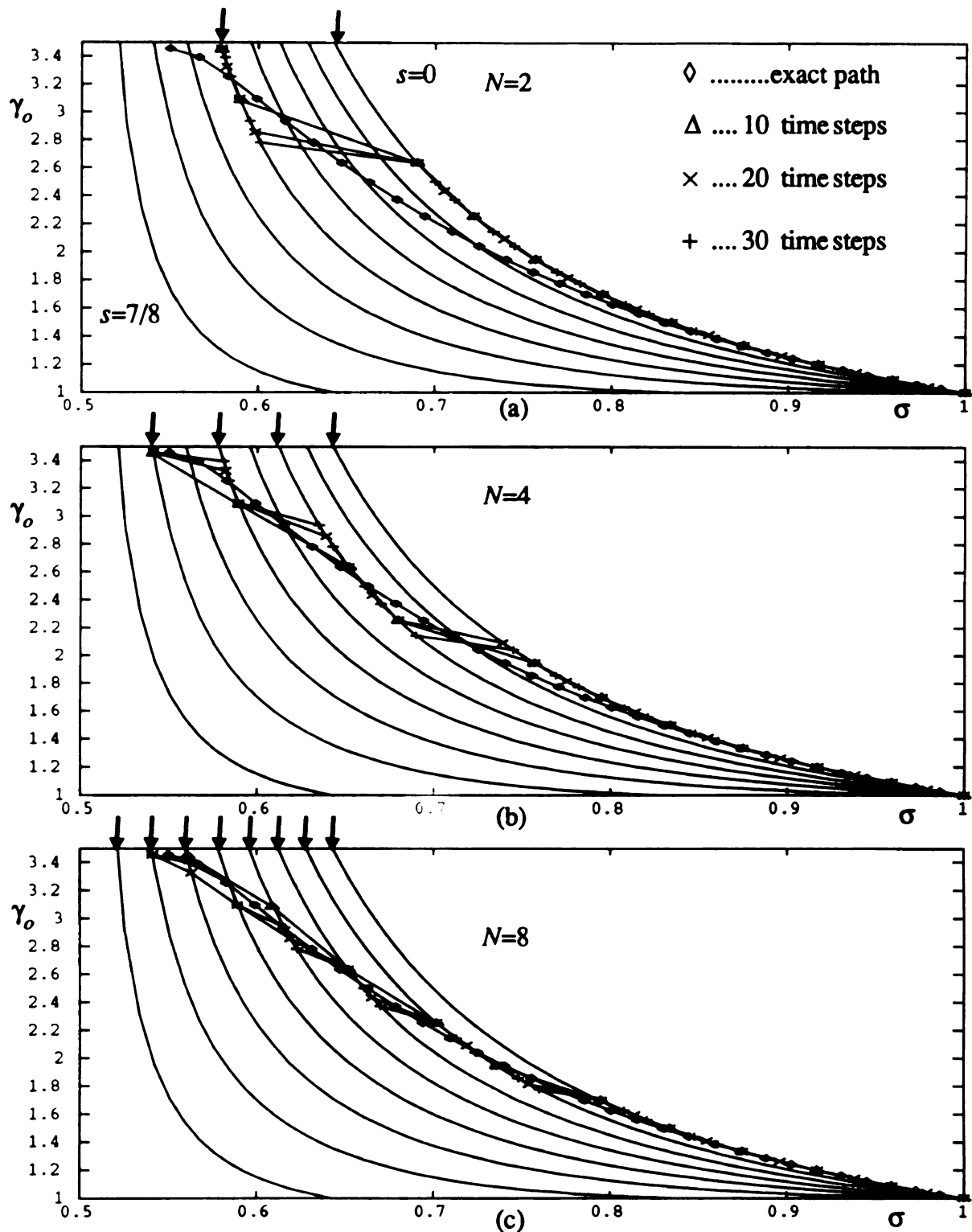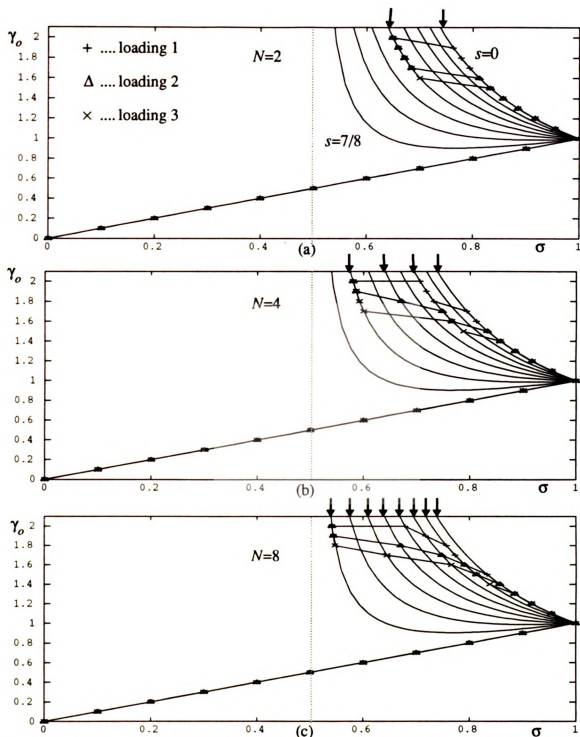
Figure 64. The effect of refining the spatial discretization. The solution paths obeying the kinetic criterion for the two-element (a), the four-element (b) and the eight-element cases (c) under the three hard device ramp loadings. Each loading has a different loading rate for conditions given by (235) with material A and $k=10$. The curves indicated by $\downarrow$ are available for the different element discretizations. The combination algorithm was used for implementing the kinetic criterion.
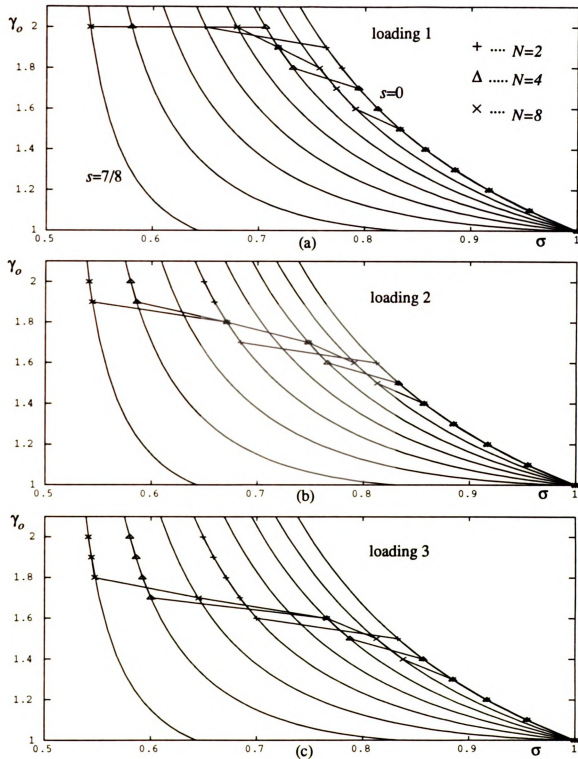
Figure 65. The solution paths previously displayed in Figure 64 are here displayed (for $\gamma > 1$ and material A). Here we group the FEM paths associated with the same loading rate on the same frame. Within each frame we see the effect of increasing the number of elements.

more choices to adjust themselves to match the requirement of approximating (224). As a consequence it will give a better result. The exact solution would be expected to leave the curve $s=0$ immediately.

The solution path for the lowest rate will be closer to the curve $s=1$, which is the unattainable limit. This means that the solution paths will also approach the minimum energy solution while the loading rate is very low. But there is a difference, namely the solution path obeying the kinetic criterion cannot jump away from a pure phase solution until it passes the yield point $(\sigma, \gamma_o) = (1, 1)$ while the solution path obeying the minimum energy could jump earlier.

15. Numerical results using the finite element method for material B

In the previous section several numerical examples for material A were studied. Several similar numerical examples for material B are presented next. We find that the results are similar.

15.1 Minimum energy criterion

Let's consider the loading as given in Section 14.1 under the minimum energy criterion. We find that the solution paths for material B, although similar to those of material A, will involve an earlier jump (see Figure 66).

15.2 Kinetic criterion

For the kinetic criterion, the main difference between material A and material B is that functions for the driving tractions are different. For material B we have $\dot{s} = 0$ when $\sigma = 1$
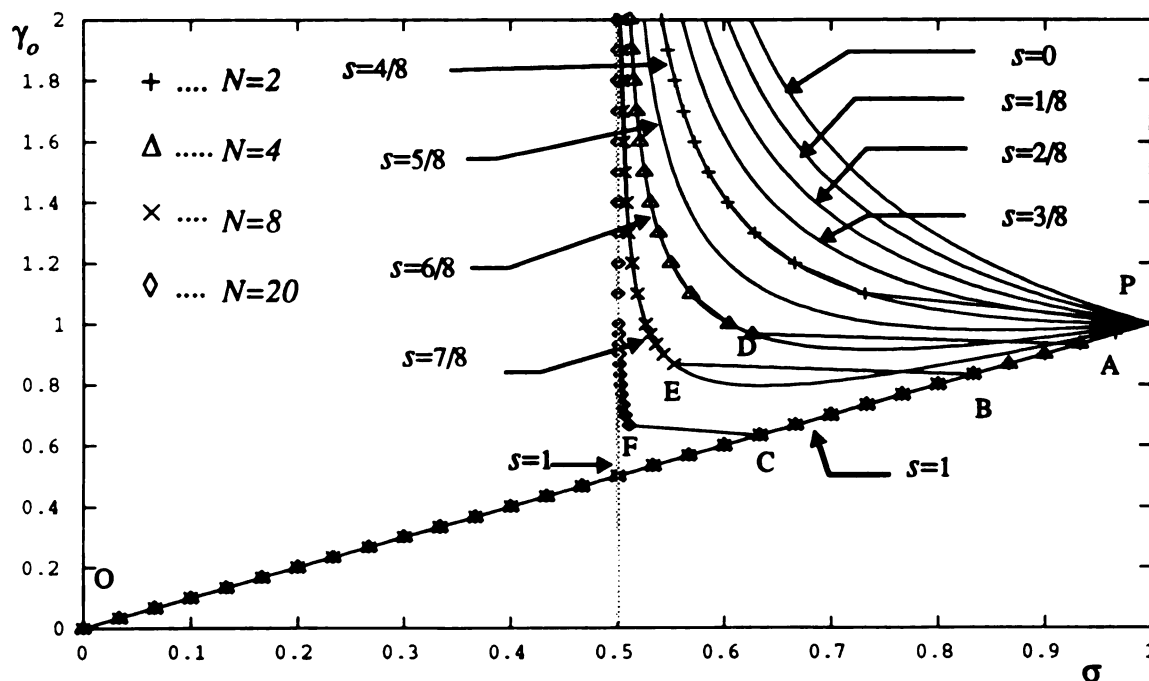
Figure 66. The solution paths in Ω_{12} obeying the minimum energy solution criterion for the two-element, the four-element, the eight-element and the twenty-element cases under a monotonically increasing hard device loading with material B.

and we have $\dot{s} \to 5k/8$ when $\sigma \to 1/2$. Note that, therefore, the velocity of phase boundary for material B is always finite while the velocity of phase boundary for material A could approach infinity. Hence FEM solution paths for material B will typically stay longer on the curve $s{=}0$ of pure phase-II solutions.

15.2.1 Computation of an "exact" solution path $(\sigma(t), \gamma_o(t))$ which satisfies the kinetic criterion

Since material B is different from material A, the same applied stress $\sigma(t)$ will give a different kinetic response $\gamma_o(t)$. Thus if $\sigma(t)$ is again given by (231) and Figure 59(a), the function $\gamma_o(t)$ will no longer be given by Figure 59(b). Recall from (143) that we find that $\gamma_o(t)$ is given by

$$\gamma_o(t) =$$
$$\Gamma_{II}(\sigma(t)) + (\Gamma_I(\sigma(t)) - \Gamma_{II}(\sigma(t))) \left(4.05 \int_0^1 \left(\frac{(\sigma(t)^2 + 1)}{2} - \sqrt{(2\sigma(t) - 1)} \right) dt \right). \tag{236}$$

Recall from (b.1), (b.4) and (b.24) for material B that the driving traction $\bar{f}(\sigma)$ is given by

$$\bar{f}(\sigma(t)) = \frac{(\sigma(t)^2 + 1)}{2} - \sqrt{(2\sigma(t) - 1)}. \tag{237}$$

Therefore from (140) and (237) the location of phase boundary is given by

$$s(t) = s(0) + k \int_0^t \bar{f}(\sigma(t)) dt = 4.05 \int_0^1 \bar{f}(\sigma(t)) dt$$
$$= 4.05 \int_0^1 \left(\frac{(\sigma(t)^2 + 1)}{2} - \sqrt{(2\sigma(t) - 1)} \right) dt. \tag{238}$$

To find the integral in (236) Simpson's rule is again chosen with three different number of time steps,10, 20 and 30, as t increases from 0 to 1. As in Section 14.2.2, $\sigma(t)$ is given by (231) and $k{=}4.05$. Figure 67 shows these three results for $\gamma_o(t)$, they are all very close. But the corresponding response $\gamma_o(t)$ of material B is smaller than that for material A (Figure 59(b)).
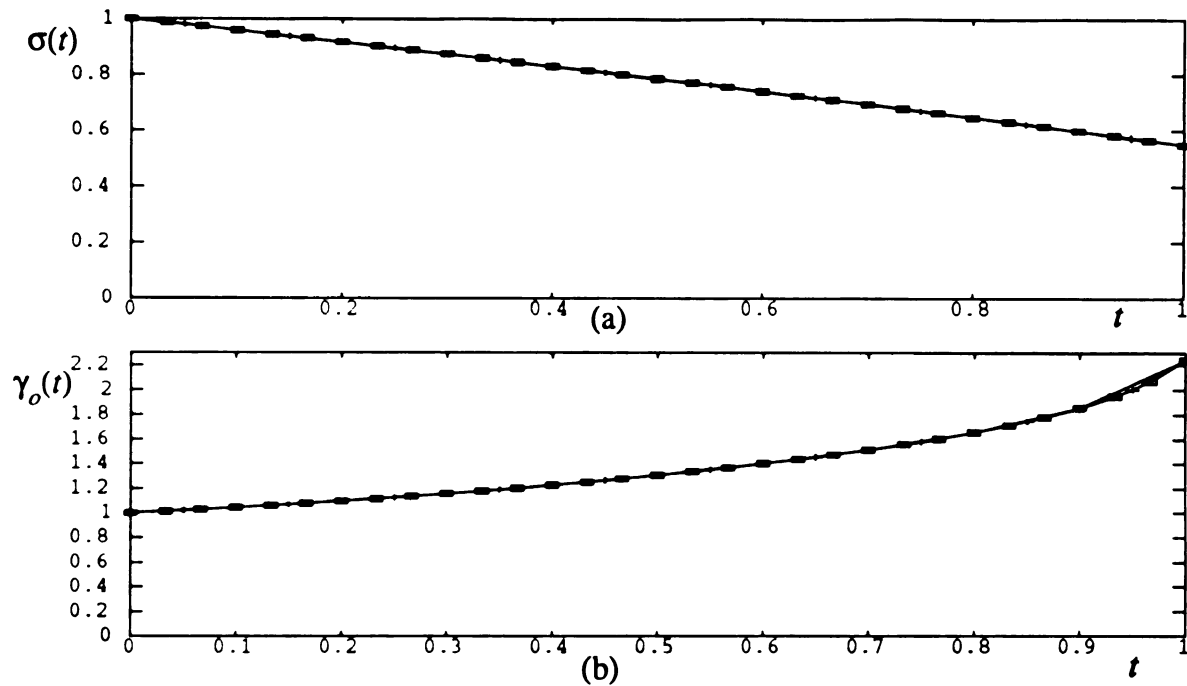
Figure 67. (a) The loading σ(t) given by (231) which is also considered for material A. (b) The corresponding response function $\gamma_o(t)$ which is given by (236) using (231) for material B with k=4.05. Three different total number of time steps, 10, 20 and 30, are considered in the numerical computation of this "exact" solution.

15.2.2 Solutions obeying the kinetic relation obtained by using the finite element method

Let's consider three different number of elements, N=2, 4, 8, and three different number of time steps, 10, 20 and 30, as given in Section 14 for material A. In what follows the *Combination Algorithm* is also considered. The FEM solution paths of these cases for material B are similar to the corresponding FEM solution paths for material A as shown in Figure 68. Figure 68 shows the effect of refining the spatial discretization. The phase boundary location of the exact path for material B is distributed form s=0 to s=3/8 (while those for material A ranged from s=0 to s=7/8 (Figure 60)). Correspondingly Figure 69 shows the effect of refining the time discretization.
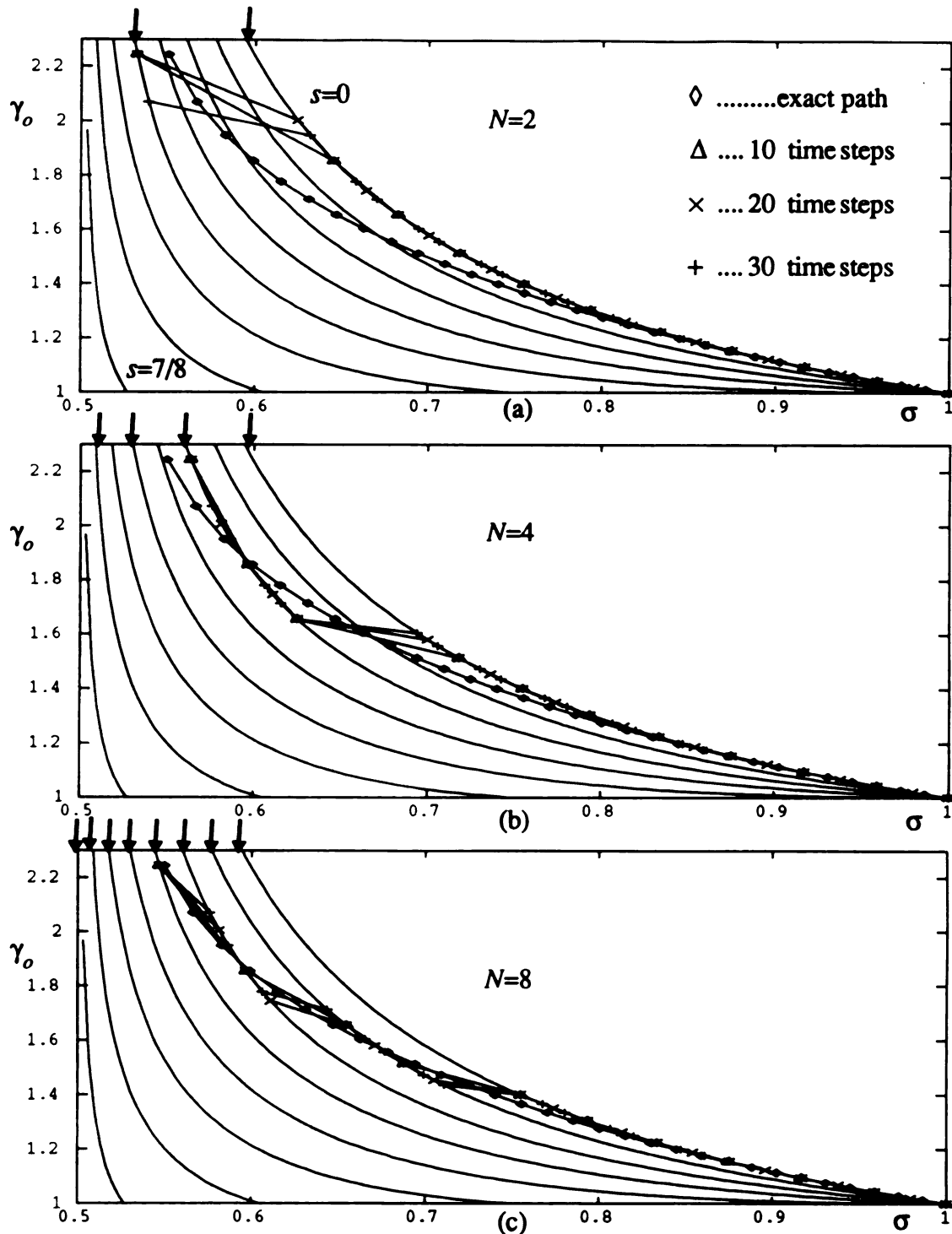
Figure 68. The effect of refining the spatial discretization. The solution paths obeying the kinetic criterion for the two-element (a), the four-element (b) and the eight-element cases(c). This is done by a hard device loading with three different loading time steps. Here the conditions are given by (229) and (231) with material B and $k=4.05$. The curves indicated by $\downarrow$ are available for the value of N being considered. The combination algorithm was used for implementing the kinetic criterion.
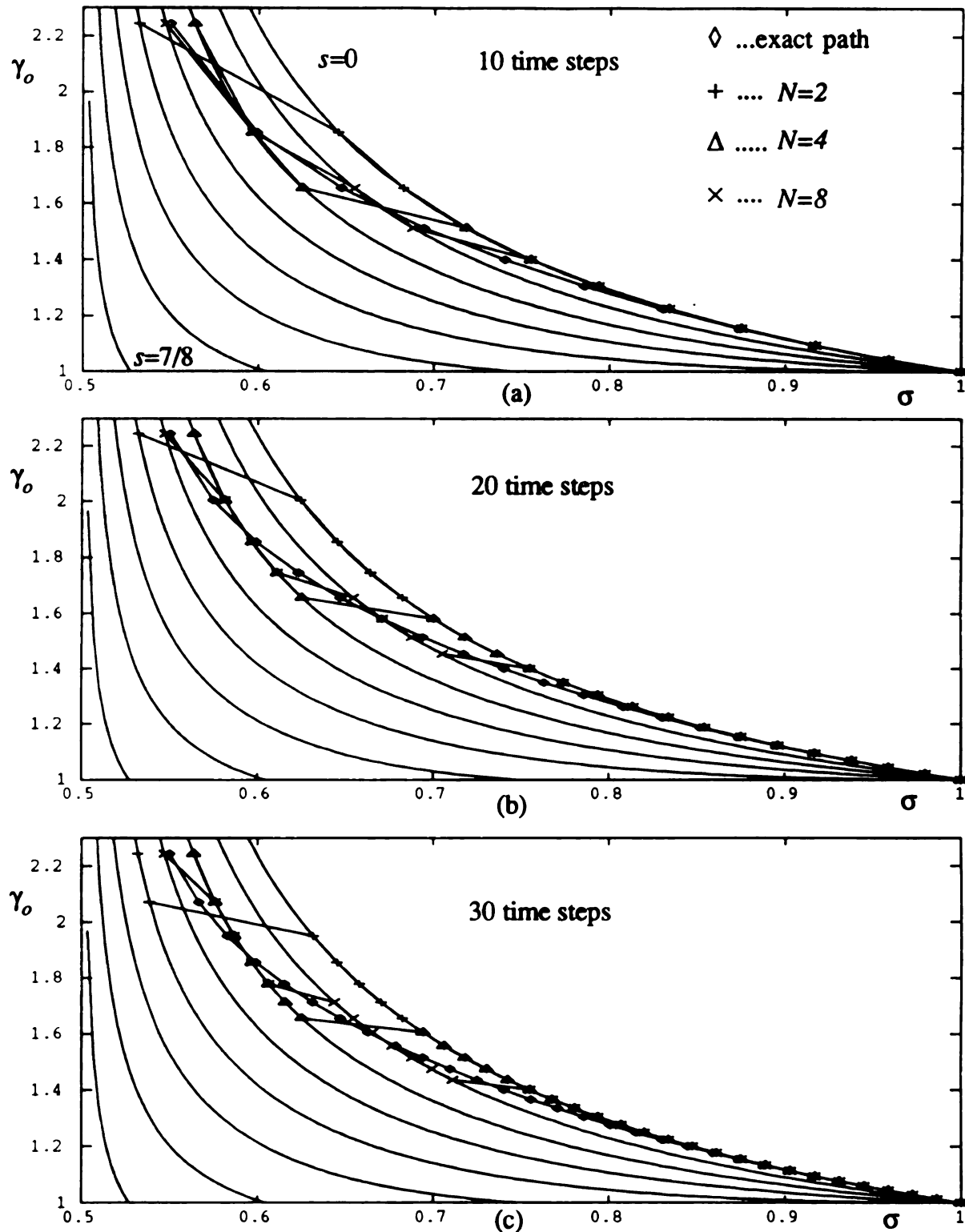
Figure 69. The effect of refining the time discretization. The solution paths obeying the kinetic criterion for the two-element, the four-element and the eight-element cases. This is done by a hard device loading with three different loading time steps, 10 time steps (a), 20 time steps (b) and 30 time steps (c) for initial conditions given by (229) with material B and k=4.05. The combination algorithm was used for implementing the kinetic criterion.

15.2.3 Three ramp loadings with different loading rates

We saw in Section 14.2.4 that the loading rates do have different effects on the solution paths of material A. Naturally it is desired to see whether the loading rates have a similar effect on material B. Let's again consider the three different loadings with different loading rates as given in Figure 63.

Figure 70 shows the effect of refining the spatial discretization. Figure 70 shows the solution paths obeying the kinetic criterion for the two-element (a), the four-element (b) and the eight-element cases (c) under the three hard device ramp loadings. Each loading has a different loading rate for conditions given by (235) with material B and k=10. Figure 71 groups the FEM paths associated with the same loading rate on the same figure. Within each frame we see the effect of increasing the number of elements. The solution paths for material B are also similar to those for material A.
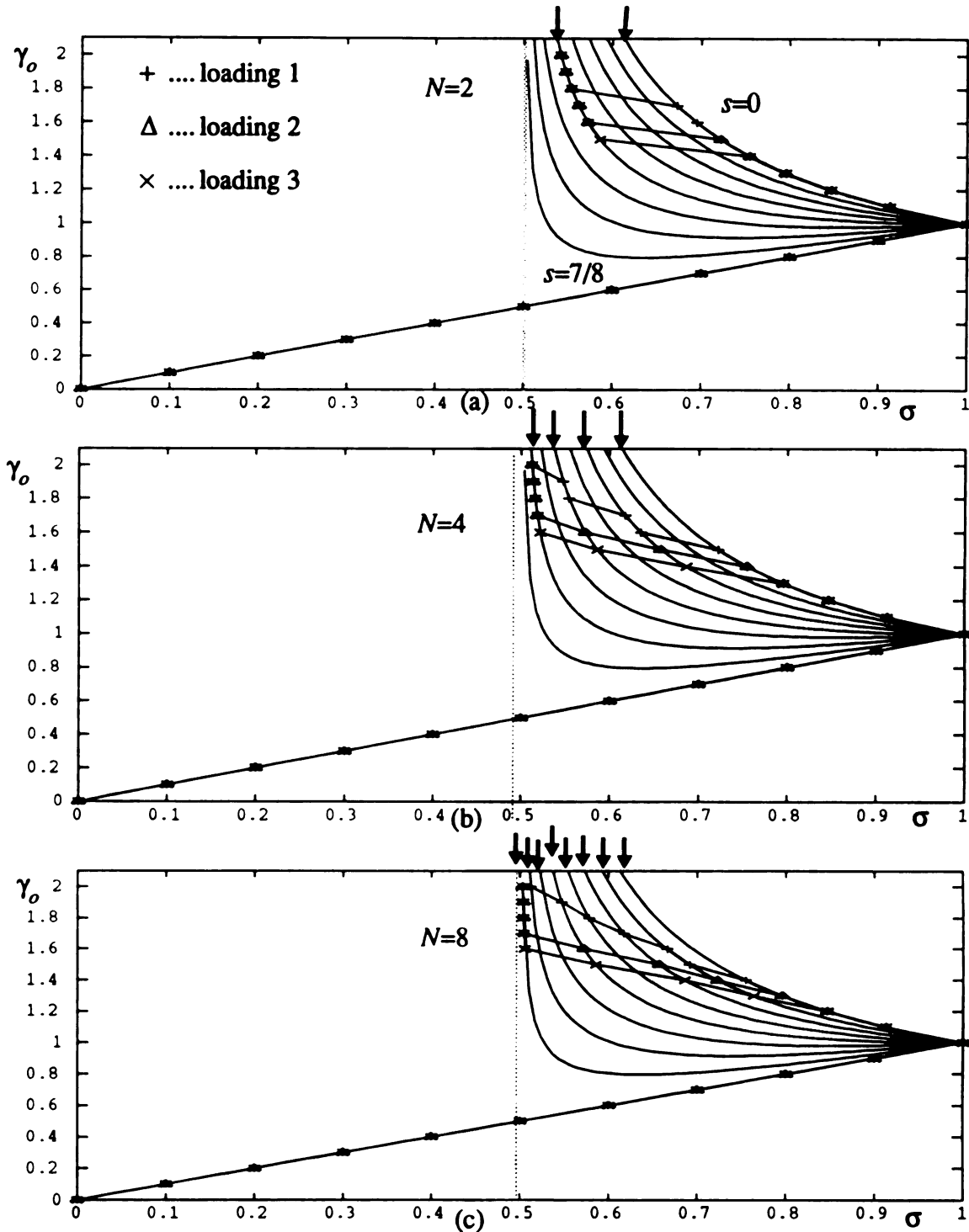
Figure 70. The effect of refining the spatial discretization. The solution paths obeying the kinetic criterion for the two-element (a), the four-element (b) and the eight-element cases (c) under the three hard device ramp loadings. Each loading has a different loading rate for conditions given by (235) with material B and $k=10$. The curves indicated by $\downarrow$ are available for the different element discretization. The combination algorithm was used for implementing the kinetic criterion.
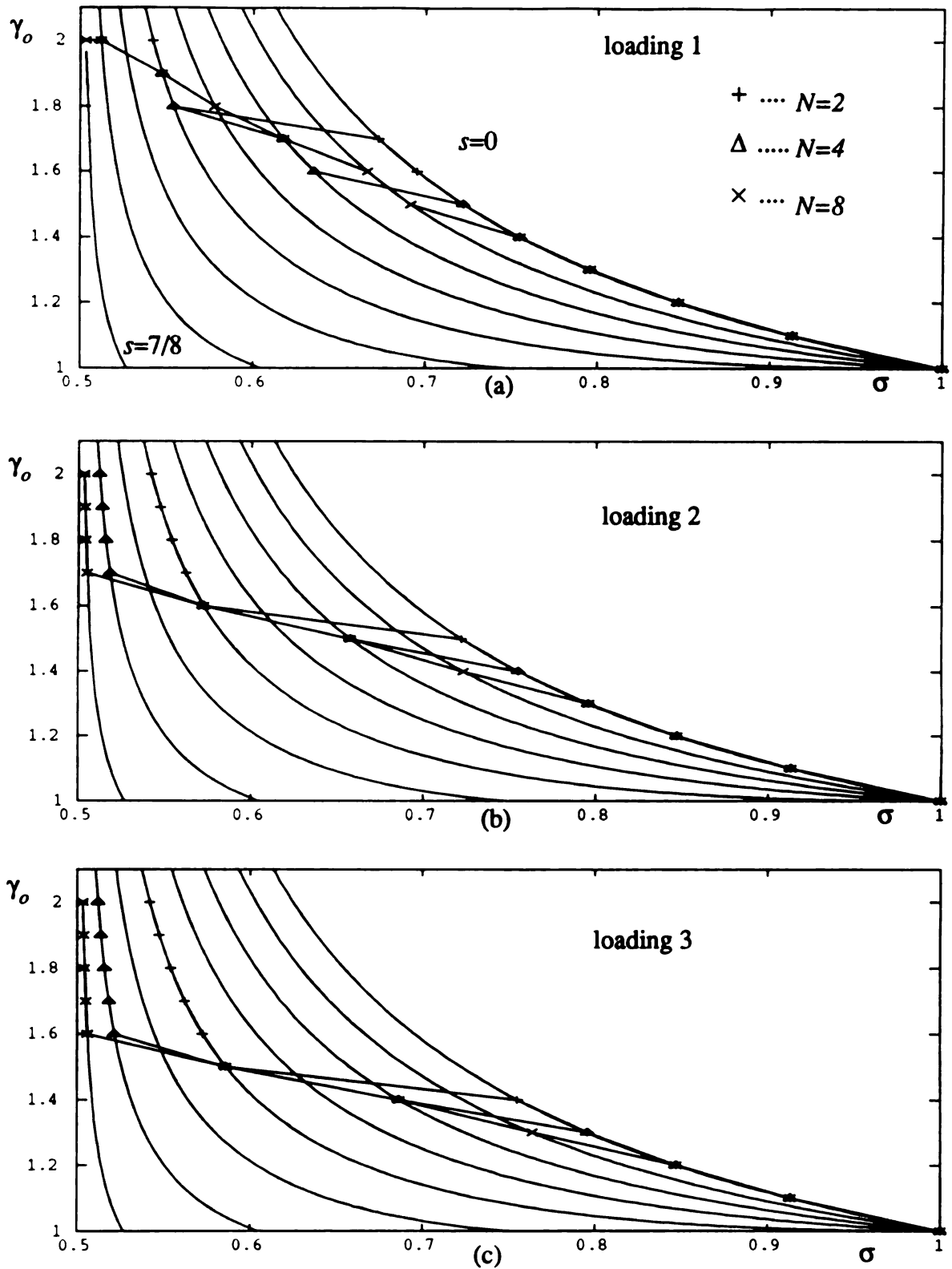
Figure 71. The solution paths previously displayed in Figure 70 are here displayed (for γ>1 and material B). Here we group the FEM paths associated with the same loading rate on the same frame. Within each frame we see the effect of increasing the number of elements.

16. Conclusions and recommendations for future work

16.1 Conclusions

From this study we may draw several conclusions:

1. The nonuniqueness of the analytical solutions to the boundary value problem translates into nonuniqueness of the numerical FEM solutions to the boundary value problem in the simplest model (a bar).

2. It is possible to successfully implement two separate selection criteria, either the kinetic relation criterion or the minimum energy solution criterion, to the phase transition problem by using FEM.

3. If the number of elements is increased, then the number of internal s curves in Ω_{12} also increased. Therefore the FEM solution paths are more smooth. Finally the solution path will approach to the exact path as N gets larger. But at the same time the number of initial guess solutions needed to obtain the available FEM solutions increases dramatically as N gets larger.

4. Even though in this study two separate criteria are implemented on the FEM process to a one-dimensional problem, it is reasonable to apply these two separate criteria to other phase transformation problems using FEM.

5. In this study we only considered quasi-static motions which neglect the effect of inertia. As shown in Lin and Pence [1993LL] these should give the large time solution of the dynamical problem. Thus quasi-static FEM might give good predictions for the ultimate fate of fully dynamical solutions.

16.2 Recommendations for future work

A lot of issues can be explored after this study. For example these could include the following:

1. In this study the hard device problem is the main concern. However it would be inter-

155

esting to explore further the soft device problem.

2. In this study a bar which has unit cross-section area is explored. Therefore the stresses on each element of the bar are equal in the FEM analysis. But if a *tapered* bar is considered by the similar process described in this study then one should have N different stresses in the N-element case. Therefore there could be N different solution paths which are obtained from each elements.

3. In this study a linear relation between the phase boundary velocity and the driving traction is considered. There are other kinetic relations to explore the strain-softening behavior of the bar. Moreover one can try other criteria.

4. The boundary value problem given in Figure 3 are solved by quasi-static motions. However it might be possible to solve this kind of problem by considering fully dynamical motions.

5. It might also be possible to find a spring-dashpot model to represent the strain-softening behavior for both the hard device and the soft device.

6. In this study two example materials which can resist an infinite strain are concerned. But it is possible to consider hypothetical example materials with the specific material behavior which model different processes. For example choosing a material which only can resist a finite strain could model damage accumulation within a material.

Appendices

Appendix-A: Material A

In this Appendix and the next appendix, two example materials which have the behavior of strain-softening are introduced. This simply means that particular functions for the function $\bar{\sigma}_{II}(\gamma)$ of (5) are considered. Material A is taken to be the following:

$$\bar{\sigma}(\gamma) = \begin{cases} \bar{\sigma}_I(\gamma) = \gamma, & \gamma \leq 1, \\ \bar{\sigma}_{II}(\gamma) = \dfrac{1}{2} + \dfrac{1}{2\gamma}, & \gamma > 1. \end{cases} \tag{a.1}$$

Note that the constant $\sigma_c = 1/2$ so that the behavior of strain-softening $\bar{\sigma}_{II}(\gamma) \rightarrow 1/2$ when $\gamma \rightarrow \infty$. The first derivative of $\bar{\sigma}_{II}(\gamma)$ is given by

$$\bar{\sigma}_{II}'(\gamma) = \frac{-1}{2\gamma^2} < 0, \tag{a.2}$$

which shows the strain-softening. The second derivative of $\bar{\sigma}_{II}(\gamma)$ is given by

$$\bar{\sigma}_{II}''(\gamma) = \frac{1}{\gamma^3} > 0, \tag{a.3}$$

which shows the curvature restriction. From $(a.1)_2$ the inverse function of $\bar{\sigma}_{II}(\gamma)$ is given by

$$\Gamma_{II}(\sigma) = \frac{1}{2\sigma - 1}. \tag{a.4}$$

From (7) and $(a.1)_2$ the energy density function $W(\gamma)$ for $\gamma > 1$ is given by

$$W(\gamma) = \frac{\gamma}{2} + \frac{ln(\gamma)}{2}, \quad \text{if } \gamma > 1. \tag{a.5}$$

Thus from (a.4) and (a.5) the energy density function $W(\Gamma_{II}(\sigma))$ can be rewritten as

$$W(\Gamma_{II}(\sigma)) = \frac{1}{2}\left(\frac{1}{(2\sigma - 1)} + ln(\frac{1}{2\sigma - 1})\right), \quad \text{while } \Gamma_{II}(\sigma) > 1. \tag{a.6}$$

Note from (10), (a.4) and (a.5) that the limit W_c is

$$W_c \equiv \lim_{\gamma \rightarrow \infty} (W(\gamma) - \gamma\sigma_c) = \lim_{\gamma \rightarrow \infty} \frac{1}{2} ln(\gamma) = \infty. \tag{a.7}$$

157

This means that the area under the strain-stress curve that is also above the horizontal line $\sigma = \sigma_c$ is infinite. According to (a.4), the equation (23) which involves the boundary conditions $u(0) = 0$ and $u(L) = \delta_o$ can be rewritten as

$$\sigma s + \sigma(1-s) = \sigma = \gamma_o, \qquad \text{(1,1)-case,}$$

$$\sigma s + \frac{1}{2\sigma-1}(1-s) = \gamma_o, \qquad \text{(1,2)-case,}$$

$$\frac{1}{2\sigma-1}s + \sigma(1-s) = \gamma_o, \qquad \text{(2,1)-case,} \qquad \text{(a.8)}$$

$$\frac{1}{2\sigma-1}s + \frac{1}{2\sigma-1}(1-s) = \frac{1}{2\sigma-1} = \gamma_o, \qquad \text{(2,2)-case.}$$

From (a.8) it is found that

$$\hat{s}_{12}(\sigma, \gamma_o) = \frac{(2\sigma-1)\gamma_o - 1}{(2\sigma+1)(\sigma-1)},$$

$$\hat{s}_{21}(\sigma, \gamma_o) = \frac{(2\sigma-1)\sigma - \gamma_o(2\sigma-1)}{(2\sigma+1)(\sigma-1)}, \qquad \text{(a.9)}$$

while $\hat{s}_{11}(\sigma, \gamma_o)$ and $\hat{s}_{22}(\sigma, \gamma_o)$ do not have meaning. Alternatively (a.9) can be found directly from (25) and (a.4) using $\Gamma_f(\sigma) = \sigma$.

From (24), (a.4) and (a.6) the hard device energy function Λ for material A is given by

$$\Lambda_{11} = \frac{\sigma^2}{2} = \hat{\Lambda}_{11}(\sigma, \gamma_o), \qquad \text{(1,1)-case,}$$

$$\Lambda_{12} = \frac{\sigma^2}{2}s + \left(\frac{\frac{1}{2\sigma-1} + \ln(\frac{1}{2\sigma-1})}{2}\right)(1-s) = \hat{\Lambda}_{12}(\sigma, \gamma_o), \qquad \text{(1,2)-case,}$$

$$\text{(a.10)}$$

$$\Lambda_{21} = \left(\frac{\frac{1}{2\sigma-1} + \ln(\frac{1}{2\sigma-1})}{2}\right)s + \frac{\sigma^2}{2}(1-s) = \hat{\Lambda}_{21}(\sigma, \gamma_o), \qquad \text{(2,1)-case,}$$

$$\Lambda_{22} = \frac{\frac{1}{2\sigma-1} + \ln(\frac{1}{2\sigma-1})}{2} = \hat{\Lambda}_{22}(\sigma, \gamma_o), \qquad \text{(2,2)-case,}$$

where s is given by (a.9). The soft device energy function Ξ for material A can be obtained

from (26) and (a.10)

$$\Xi_{11} = \hat{\Lambda}_{11}(\sigma, \gamma_o) - \sigma\gamma_o, \qquad \text{(1,1)-case,}$$

$$\Xi_{12} = \hat{\Lambda}_{12}(\sigma, \gamma_o) - \sigma\gamma_o, \qquad \text{(1,2)-case,}$$

$$\Xi_{21} = \hat{\Lambda}_{21}(\sigma, \gamma_o) - \sigma\gamma_o, \qquad \text{(2,1)-case,} \qquad \text{(a.11)}$$

$$\Xi_{22} = \hat{\Lambda}_{22}(\sigma, \gamma_o) - \sigma\gamma_o, \qquad \text{(2,2)-case.}$$

Note that the difference between the hard device energy function Λ and the soft device energy function Ξ is $\sigma\gamma_o$.

A.1 The solution region Ω_{12} for material A

After material properties and the energy functions being introduced, from (29) and (a.1) the solution region Ω_{12} is given by

$$\Omega_{12} = \{ \, (\sigma, \gamma_o) \mid \frac{1}{2} < \sigma < \gamma_o, \text{ if } \sigma_c < \gamma_o < 1; \frac{1}{2} < \sigma < \frac{1}{2} + \frac{1}{2\gamma_o}, \text{ if } \gamma_o \geq 1 \, \}. \qquad \text{(a.12)}$$

From (36), (37) and (a.4) it is found that $s_{trans} = 2/3$. Moreover from (36) for $s > s_{trans}$ the location of the minimum point on the curve of constant s can be found by

$$s - \frac{2(1-s)}{(2\sigma - 1)^2} = 0, \qquad \text{(a.13)}$$

where the root of (a.13) is given by

$$\sigma = \sigma_{\Phi_2}(s) = \frac{1}{2} (1 + \sqrt{\frac{2(1-s)}{s}}). \qquad \text{(a.14)}$$

Hence from (47), (a.4) and (a.14) the minimum γ_o on the constant s curve is given by

$$\gamma_o|_s = \frac{s}{2} + \sqrt{2s(1-s)} \equiv \gamma_{\Phi_2}(s). \qquad \text{(a.15)}$$

Therefore from (a.14) and (a.15) the minimum point on the curve of constant $s > s_{trans}$ is given by

$$(\sigma, \gamma_o) = (\sigma_{\Phi_2}(s), \gamma_{\Phi_2}(s)) = (\frac{1}{2} + \frac{1}{2}\sqrt{\frac{2(1-s)}{s}}, \frac{s}{2} + \sqrt{2s(1-s)}). \qquad (a.16)$$

Note from (a.14) that $\sigma = \sigma_{\Phi_2} = 1$ when $s = s_{trans} = 2/3$. Note also that the stress in Ω_{12} must obey $1/2 < \sigma_{\Phi_2} \leq 1$. This gives the following conditions:

$$\frac{1}{2} < \sigma_{\Phi_2} \Leftrightarrow s < 1,$$

$$\sigma_{\Phi_2} \leq 1 \Leftrightarrow s \geq \frac{2}{3}. \qquad (a.17)$$

For example it is found that $s = 2/3$ and $\gamma_o = 1$ whenever $\sigma = \sigma_{\Phi_2} = 1$; therefore $(\sigma, \gamma_o) = (1, 1)$ is the minimum point. It is found that $2/3 < s < 1$ and $\gamma_o < 1$ whenever $1/2 < \sigma_{\Phi_2} < 1$; therefore (a.16) gives a minimum point which is not the end point $(\sigma, \gamma_o) = (1, 1)$ (see Figure 10). Thus, if $0 \leq s \leq 2/3$, then there doesn't exist an internal minimum point in the (σ, γ_o)-plane on the curves of constant s; if, however, $2/3 < s < 1$, then there exists an internal minimum point.

A.2 The hard device energy function Λ_{12} for material A

From (25) and (a.10)$_2$ the hard device energy function Λ_{12} is given by

$$\Lambda_{12} = \hat{\Lambda}_{12}(\sigma, \gamma_o) = \frac{\sigma^2}{2} \frac{\Gamma_{II}(\sigma) - \gamma_o}{\Gamma_{II}(\sigma) - \Gamma_I(\sigma)} + \frac{(\frac{1}{2\sigma - 1} + \ln(\frac{1}{2\sigma - 1}))}{2} \frac{\gamma_o - \Gamma_I(\sigma)}{\Gamma_{II}(\sigma) - \Gamma_I(\sigma)}. \qquad (a.18)$$

Taking derivatives with respect to γ_o along the curves of constant σ gives

$$\left. \frac{\partial \Lambda_{12}}{\partial \gamma_o} \right|_\sigma > 0. \qquad (a.19)$$

This indicates that the hard device energy function Λ_{12} monotonically increases along the curves of constant σ as γ_o increasing from σ to $1/(2\sigma - 1)$.

It is also found that

$$\frac{\partial \Lambda_{12}}{\partial \sigma}\bigg|_{\gamma_o} > 0 \qquad \text{when} \qquad \gamma_o \geq 1. \tag{a.20}$$

This implies that hard device energy function Λ_{12} monotonically increases on the line of constant γ_o, $\gamma_o \geq 1$, as stress increases from $1/2$ to $1/2 + 1/(2\gamma_o)$. Moreover the hard device energy function Λ_{12} increases from $1/2$ to $\bar{\sigma}_{\varnothing_2}(\gamma_o)$ and decreases from $\bar{\sigma}_{\varnothing_2}(\gamma_o)$ to σ on the line of constant γ_o, with $\gamma_o < 1$.

Note from (48) and (a.4) that the curve $\varnothing_2$ is given by

$$\varnothing_2 = \{ (\sigma, \gamma_o) | \gamma_o = \frac{4\sigma - 1}{(2\sigma - 1)^2 + 2}, \frac{1}{2} < \sigma \leq 1 \}. \tag{a.21}$$

Recall from Section 5 and Section 6 that the points on $\varnothing_2$ not only give the minimum of the hard device energy function and the minimum γ_o value on the curves of constant s, but also give the maximum of the hard device energy function and the minimum s value on the line of constant γ_o. From (58), (a.4) and (a.6) the pseudo-stress function $\sigma_{ps}(\sigma)$ is

$$\sigma_{ps}(\sigma) = \frac{(1 - \sigma^2(2\sigma - 1)) - (2\sigma - 1)\ln(2\sigma - 1)}{2(1 - \sigma(2\sigma - 1))}. \tag{a.22}$$

Therefore from (83) and (a.22) it also can be found at a given constant γ_o, with $1/2 < \gamma_o \leq 1$, that the points on the curve $\varnothing_3$ are

$$\varnothing_3 = \{ (\sigma, \gamma_o) | \gamma_o = \frac{(1 - \sigma) - (2\sigma - 1)\ln(2\sigma - 1)}{1 - \sigma(2\sigma - 1)}, \frac{1}{2} < \sigma \leq 1 \}. \tag{a.23}$$

For a given constant γ_o, with $1/2 < \gamma_o \leq 1$, the hard device energy function Λ_{12} at points on $\varnothing_1$ and $\varnothing_3$ are equal.

According to (119), (a.22) and (a.4) the driving traction $\bar{f}_{12}(\sigma)$ is a function of σ and is given by

$$\bar{f}_{12}(\sigma) = (\sigma_{ps}(\sigma) - \sigma)(\Gamma_{II}(\sigma) - \Gamma_I(\sigma)) = \frac{-(1 - \sigma^2)}{2} - \frac{\ln(2\sigma - 1)}{2}. \tag{a.24}$$

Note that $\bar{f}_{12}(\sigma) > 0$ whenever $1/2 < \sigma < 1$. From (123) and (a.24) the first derivative of $\bar{f}_{12}(\sigma)$ is given by

$$\bar{f}_{12}{}'(\sigma) = \sigma - \frac{1}{2\sigma - 1} < 0, \qquad \text{if } 1/2 < \sigma < 1 \qquad (a.25)$$

which means that the driving traction $\bar{f}_{12}(\sigma)$ decreases as a function of σ whenever $1/2 < \sigma < 1$.

Appendix-B: Material B

The previous Appendix was devoted to the material A. In this Appendix the material B is explored. Both materials have the strain-softening behavior but they have different limits W_c defined in (10). Material A has $W_c = \infty$ while material B has a finite value of W_c.

The stress response for material B is taken to be the following

$$\bar{\sigma}(\gamma) = \begin{cases} \bar{\sigma}_I(\gamma) = \gamma, & \gamma \leq 1, \\ \bar{\sigma}_{II}(\gamma) = \dfrac{1}{2} + \dfrac{1}{2\gamma^2}, & \gamma > 1. \end{cases} \tag{b.1}$$

Note also that the constant $\sigma_c = 1/2$ and the behavior of strain-softening $\bar{\sigma}_{II}(\gamma) \to 1/2$ when $\gamma \to \infty$ which are similar to that of material A. The first derivative of $\bar{\sigma}_{II}(\gamma)$ is given by

$$\bar{\sigma}_{II}{}'(\gamma) = \frac{-1}{\gamma^3} > 0, \tag{b.2}$$

which shows the different strain-softening from that of material A. The second derivative of $\bar{\sigma}_{II}(\gamma)$ is given by

$$\bar{\sigma}_{II}{}''(\gamma) = \frac{3}{\gamma^4} > 0, \tag{b.3}$$

which shows the different curvature restriction. From (b.1)$_2$ the inverse function of $\bar{\sigma}_{II}(\gamma)$ is given by

$$\Gamma_{II}(\sigma) = \frac{1}{(2\sigma - 1)^{1/2}}. \tag{b.4}$$

From (7) and (b.1)$_2$ the energy density function $W(\gamma)$ for $\gamma > 1$ is given by

$$W(\gamma) = \frac{1}{2} + \frac{\gamma}{2} - \frac{1}{2\gamma}, \qquad \text{if } \gamma > 1. \tag{b.5}$$

Thus from (b.4) and (b.5) the energy density function $W(\Gamma_{II}(\sigma))$ can be rewritten as

163

$$W_{II}(\Gamma_{II}(\sigma)) = \frac{1}{2}(1 + \frac{1}{\sqrt{2\sigma - 1}} - \sqrt{2\sigma - 1}), \qquad \text{if } \Gamma_{II}(\sigma) > 1. \tag{b.6}$$

One of the main differences between this material and material A involves the limit defined in (10). Note from (10), (b.4) and (b.5) that the limit of W_c for material B is given by

$$W_c \equiv \lim_{\gamma \to \infty} (W(\gamma) - \gamma\sigma_c) = \lim_{\gamma \to \infty} \frac{1}{2} - \frac{1}{2\gamma} = \frac{1}{2} \tag{b.7}$$

while recall from (a.7) that the limit for material A is given by $W_c = \infty$. Hence the area under the strain-stress curve that is also above the horizontal line $\sigma = \sigma_c$ is finite. According to (b.4), the equation (23) which involves the boundary conditions $u(0) = 0$ and $u(L) = \delta_o$ can be rewritten as

$$\sigma s + \sigma(1 - s) = \sigma = \gamma_o, \qquad \text{(1,1)-case,}$$

$$\sigma s + \frac{1}{\sqrt{2\sigma - 1}}(1 - s) = \gamma_o, \qquad \text{(1,2)-case,}$$

$$\frac{1}{\sqrt{2\sigma - 1}}s + \sigma(1 - s) = \gamma_o, \qquad \text{(2,1)-case,} \tag{b.8}$$

$$\frac{1}{\sqrt{2\sigma - 1}}s + \frac{1}{\sqrt{2\sigma - 1}}(1 - s) = \frac{1}{\sqrt{2\sigma - 1}} = \gamma_o, \qquad \text{(2,2)-case.}$$

From (b.8) it is found that

$$\hat{s}_{12}(\sigma, \gamma_o) = \frac{\gamma_o - \sigma}{\frac{1}{\sqrt{2\sigma - 1}} - \sigma},$$

$$\hat{s}_{21}(\sigma, \gamma_o) = \frac{\gamma_o - \frac{1}{\sqrt{2\sigma - 1}}}{\sigma - \frac{1}{\sqrt{2\sigma - 1}}}, \tag{b.9}$$

while $\hat{s}_{11}(\sigma, \gamma_o)$ and $\hat{s}_{22}(\sigma, \gamma_o)$ do not have meaning too. Alternatively (b.9) can be found directly from (25) and (b.4) using $\Gamma_I(\sigma) = \sigma$.

From (24), (b.4) and (b.6) the hard device energy function Λ for material B is given by

$$\Lambda_{11} = \frac{\sigma^2}{2} = \hat{\Lambda}_{11}(\sigma, \gamma_o) \qquad \text{(1,1)-case,}$$

$$\Lambda_{12} = \frac{\sigma^2}{2}s + \frac{1 + \frac{1}{\sqrt{2\sigma - 1}} - \sqrt{2\sigma - 1}}{2}(1 - s) = \hat{\Lambda}_{12}(\sigma, \gamma_o) \qquad \text{(1,2)-case,}$$

$$\Lambda_{21} = \frac{1 + \frac{1}{\sqrt{2\sigma - 1}} - \sqrt{2\sigma - 1}}{2}s + \frac{\sigma^2}{2}(1 - s) = \hat{\Lambda}_{21}(\sigma, \gamma_o) \qquad \text{(2,1)-case,}$$

$$\Lambda_{22} = \frac{1 + \frac{1}{\sqrt{2\sigma - 1}} - \sqrt{2\sigma - 1}}{2} = \hat{\Lambda}_{22}(\sigma, \gamma_o) \qquad \text{(2,2)-case,}$$

(b.10)

where s is given by (b.9). The soft device energy function Ξ for material B can be obtained from (26), and (b.10)

$$\Xi_{11} = \hat{\Lambda}_{11}(\sigma, \gamma_o) - \sigma\gamma_o, \qquad \text{(1,1)-case,}$$

$$\Xi_{12} = \hat{\Lambda}_{12}(\sigma, \gamma_o) - \sigma\gamma_o, \qquad \text{(1,2)-case,}$$

$$\Xi_{21} = \hat{\Lambda}_{21}(\sigma, \gamma_o) - \sigma\gamma_o, \qquad \text{(2,1)-case,}$$

$$\Xi_{22} = \hat{\Lambda}_{22}(\sigma, \gamma_o) - \sigma\gamma_o, \qquad \text{(2,2)-case.}$$

(b.11)

B.1 The solution region Ω_{12} for material B

The material properties and the energy functions are different between material A and material B. How about the solution regions? From (29) and (b.1) the solution region for material B is given by

$$\Omega_{12} = \{ (\sigma, \gamma_o) | \frac{1}{2} < \sigma < \gamma_o, \text{ if } \sigma_c < \gamma_o < 1; \frac{1}{2} < \sigma < \frac{1}{2} + \frac{1}{2\gamma_o^2}, \text{ if } \gamma_o \geq 1. \qquad \text{(b.12)}$$

From (36), (37) and (b.4) it is found that $s_{trans} = 1/2$ while from (36) for $s > s_{trans}$ the location of the minimum point on the curve of constant s can be found by

$$s - \frac{(1 - s)}{(2\sigma - 1)^{1.5}} = 0. \qquad \text{(b.13)}$$

Thus the root of (b.13) is given by

$$\sigma = \sigma_{\Phi_2}(s) \equiv \frac{1}{2}\left(1 + (\frac{(1-s)}{s})^{2/3}\right). \tag{b.14}$$

Hence from (47), (b.4) and (b.14) the minimum γ_o on the constant s curve is found to be

$$\gamma_o|_s = \frac{s}{2} + \frac{3\,(s)^{1/3}\,(1-s)^{2/3}}{2} \equiv \gamma_{\Phi_2}(s). \tag{b.15}$$

Therefore, from (b.14) and (b.15) for a curve of constant $s > s_{trans}$, the minimum point is given by

$$(\sigma, \gamma_o) = (\sigma_{\Phi_2}(s), \gamma_{\Phi_2}(s)) =$$
$$\left(\frac{1}{2} + \frac{1}{2}(\frac{(1-s)}{s})^{2/3}, \frac{s}{2} + \frac{3\,(s)^{1/3}\,(1-s)^{2/3}}{2}\right). \tag{b.16}$$

Note that the stress in Ω_{12} must obey $\frac{1}{2} < \sigma_{\Phi_2} \leq 1$. This gives correspondingly

$$\frac{1}{2} < \sigma_{\Phi_2} \Leftrightarrow s < 1,$$
$$\sigma_{\Phi_2} \leq 1 \Leftrightarrow s \geq \frac{1}{2}. \tag{b.17}$$

As an example it is found that $s = 1/2$ and $\gamma_o = 1$ whenever $\sigma = \sigma_{\Phi_2} = 1$; therefore $(\sigma, \gamma_o) = (1, 1)$ is the minimum point. It is found that $1/2 < s < 1$ and $\gamma_o < 1$ whenever $1/2 < \sigma_{\Phi_2} < 1$; therefore equation (b.16) gives a minimum point which is not the end point $(\sigma, \gamma_o) = (1, 1)$ (see Figure 10). Thus, if $0 \leq s \leq 1/2$, then there doesn't exist an internal minimum point in the (σ, γ_o)-plane on the curves of constant s; if, however, $1/2 < s < 1$, then there exists an internal minimum point. The above behavior is similar to the behavior of material A.

B.2 The hard device energy function Λ_{12} for material B

From (25) and $(b.10)_2$, the hard device energy function Λ_{12} is obtained by

$$\Lambda_{12} = \hat{\Lambda}_{12}(\sigma, \gamma_o) = \frac{\sigma^2 (\Gamma_{II}(\sigma) - \gamma_o)}{2 (\Gamma_{II}(\sigma) - \Gamma_I(\sigma))} + \frac{(1 + \frac{1}{\sqrt{2\sigma - 1}} - \sqrt{2\sigma - 1}) (\gamma_o - \Gamma_I(\sigma))}{2 (\Gamma_{II}(\sigma) - \Gamma_I(\sigma))}. \tag{b.18}$$

Taking derivatives with respect to γ_o along the curves of constant σ obtains

$$\left. \frac{\partial \Lambda_{12}}{\partial \gamma_o} \right|_\sigma > 0. \tag{b.19}$$

This means that the hard device energy function Λ_{12} monotonically increases along the curves of constant σ as γ_o increases from σ to $1/\sqrt{2\sigma - 1}$.

It is also found that

$$\left. \frac{\partial \Lambda_{12}}{\partial \sigma} \right|_{\gamma_o} > 0 \qquad \text{when} \qquad \gamma_o \geq 1. \tag{b.20}$$

This implies that the hard device energy function Λ_{12} monotonically increases form σ_c to $1/2 + 1/(2\gamma_o^2)$ on the line of constant $\gamma_o \geq 1$. However the hard device energy function Λ_{12} increases from $1/2$ to $\bar{\sigma}_{\varnothing_2}(\gamma_o)$ and decreases from $\bar{\sigma}_{\varnothing_2}(\gamma_o)$ to σ on the line of constant $\gamma_o < 1$.

Note that from (48) and (b.4) it is found that

$$\varnothing_2 = \{ (\sigma, \gamma_o) | \gamma_o = \frac{3\sigma - 1}{(2\sigma - 1)^{1.5} + 1}, \frac{1}{2} < \sigma < 1 \}. \tag{b.21}$$

Recall from Section 5 and Section 6 that the points on the curve $\varnothing_2$ not only give the minimum of the hard device energy and the minimum γ_o value on the curve of constant s but also give the maximum for the hard device energy and the minimum s value on the lines of constant γ_o. From (58), (b.4) and (b.6) the pseudo stress function $\sigma_{ps}(\sigma)$ is

$$\sigma_{ps}(\sigma) = \frac{2 - 2\sigma + (1 - \sigma^2)\sqrt{2\sigma - 1}}{2(1 - \sigma\sqrt{2\sigma - 1})}.$$ (b.22)

Therefore from (83) and (b.22) it also can be found for a given constant γ_o that the point on the curve $\varnothing_3$ are

$$\varnothing_3 = \{ (\sigma, \gamma_o) | \gamma_o = \frac{2 - 3\sigma + \sqrt{2\sigma - 1}}{1 - \sigma\sqrt{2\sigma - 1}}, \frac{1}{2} < \sigma < 1 \}.$$ (b.23)

For a given constant $\gamma_o < 1$ the hard device energy function Λ_{12} at the points on both $\varnothing_1$ and $\varnothing_3$ are equal.

According to (119), (b.4) and (b.22) the driving traction $\bar{f}_{12}(\sigma)$ is a function of σ and is given by

$$\bar{f}_{12}(\sigma) = \frac{(1 + \sigma^2)}{2} - \sqrt{(2\sigma - 1)}.$$ (b.24)

Note that $\bar{f}_{12}(\sigma) > 0$ whenever $1/2 < \sigma < 1$. From (123) and (b.24) the first derivative of $\bar{f}_{12}(\sigma)$ is given by

$$\bar{f}_{12}'(\sigma) = \sigma - \frac{1}{\sqrt{2\sigma - 1}} < 0, \qquad 1/2 < \sigma < 1,$$ (b.25)

which means that the driving traction $\bar{f}_{12}(\sigma)$ decreases as a function of σ whenever $1/2 < \sigma < 1$. Note that the rate of change of the driving traction $\bar{f}_{12}(\sigma)$ for material B is lower than that for material A.

Appendix-C: Ordering of the solution paths in Figure 33

In this Appendix we show that $\alpha^a > \alpha^b \Rightarrow \gamma(\sigma, \alpha^a) > \gamma(\sigma, \alpha^b)$ at each fixed σ in $\sigma_c < \sigma < 1$ under the loading given in (149):

$$\gamma_o = 1 + \alpha t. \tag{c.1}$$

From (142) the loading $\gamma_o(t)$ is related to $\sigma(t)$ and $s(t)$ by

$$\gamma_o(t) = \sigma(t) + T(\sigma(t))(1 - s(t)). \tag{c.2}$$

Taking the partial derivative of $\gamma(\sigma, \alpha)$ with respect to the loading rate α from (c.2) with fixed σ gives

$$\left.\frac{\partial \gamma_o}{\partial \alpha}\right|_\sigma = -T(\sigma(t)) \left.\frac{\partial s}{\partial \alpha}\right|_\sigma. \tag{c.3}$$

Similarly taking partial derivative with respect to the loading rate α from (c.1) with fixed σ gives

$$\left.\frac{\partial \gamma_o}{\partial \alpha}\right|_\sigma = t + \alpha \left.\frac{\partial t}{\partial \alpha}\right|_\sigma. \tag{c.4}$$

Recall from (148) that s is given by $s = s(0) + k\int_0^t \bar{f}_{12}(\sigma(t))dt$, thus

$$\left.\frac{\partial s}{\partial \alpha}\right|_\sigma = k\bar{f}_{12}(\sigma(t)) \left.\frac{\partial t}{\partial \alpha}\right|_\sigma. \tag{c.5}$$

Now (c.4) can be rewritten, with the help of (c.5), as

$$\left.\frac{\partial \gamma_o}{\partial \alpha}\right|_\sigma = t + \frac{\alpha \left.\frac{\partial s}{\partial \alpha}\right|_\sigma}{k\bar{f}_{12}(\sigma(t))}. \tag{c.6}$$

From (c.3) and (c.6) it is found that

$$\left.\frac{\partial \gamma_o}{\partial \alpha}\right|_\sigma = t + \frac{(-\alpha) \left.\frac{\partial \gamma_o}{\partial \alpha}\right|_\sigma}{k\bar{f}_{12}(\sigma(t))T(\sigma(t))}. \tag{c.7}$$

Solving (c.7) for $\left.\dfrac{\partial \gamma_o}{\partial \alpha}\right|_\sigma$ gives

$$\left.\frac{\partial \gamma_o}{\partial \alpha}\right|_\sigma = \frac{t}{1 + \dfrac{\alpha}{k \bar{f}_{12}(\sigma(t)) T(\sigma(t))}}. \qquad (c.8)$$

If we consider $t > 0$ then

$$\left.\frac{\partial \gamma_o}{\partial \alpha}\right|_\sigma > 0. \qquad (c.9)$$

We note also that (c.3) and (c.5) now also give that

$$\left.\frac{\partial s}{\partial \alpha}\right|_\sigma < 0, \qquad \left.\frac{\partial t}{\partial \alpha}\right|_\sigma < 0, \qquad \text{(for } t > 0). \qquad (c.10)$$

From (c.9) we can conclude that

$$\left.\gamma_o\right|_{\substack{\alpha^a \\ \sigma}} > \left.\gamma_o\right|_{\substack{\alpha^b \\ \sigma}} \qquad \text{if } \alpha^a > \alpha^b. \qquad (c.11)$$

Hence the solution path with loading rate α^a is always above the solution path with loading rate α^b if $\alpha^a > \alpha^b$, except at the starting point $(\sigma, \gamma_o) = (1,1)$ where $t = 0$.

Appendix-D: Local analysis of the solution paths in Figure 33 near $t=0$ for material A.

In this Appendix we show the local analysis of the solution paths of Appendix-C near $t=0$ for Material A. From (139) we can obtain

$$(T(\sigma(t)) + (\gamma_o(t) - \sigma(t)) \, T'(\sigma(t))) \, \dot\sigma(t) - k \, (\sigma_{ps}(\sigma(t)) - \sigma(t)) \, T^3(\sigma(t)) = \dot\gamma_o(t) T(\sigma(t)). \quad \text{(d.1)}$$

Consider the loading given in (149):

$$\gamma_o = 1 + \alpha t. \quad \text{(d.2)}$$

From (a.4) we have that $T(\sigma(t))$, for Material A, is given by

$$T(\sigma(t)) = \Gamma_{ll}(\sigma(t)) - \sigma(t) = \frac{1}{2\sigma(t) - 1} - \sigma(t). \quad \text{(d.3)}$$

Since $\sigma(t) \approx 1$ when t is near zero, we let

$$p = \sigma(t) - 1 \quad \text{(d.4)}$$

so that

$$\dot p = \dot\sigma(t). \quad \text{(d.5)}$$

Then $T(\sigma(t))$ in (d.3) can be expanded to give

$$T(\sigma(t)) = \bar T(p) = -3p + O(p^2). \quad \text{(d.6)}$$

and

$$T^2(\sigma(t)) = \bar T^2(p) = 9p^2 + O(p^3). \quad \text{(d.7)}$$

The first derivative of $T(\sigma(t))$ is given by

$$T'(\sigma(t)) = \bar T'(p) = -3 + O(p). \quad \text{(d.8)}$$

From (119), (121) and (130) we have

$$\bar f_{12}(\sigma(t)) = (\sigma_{ps}(\sigma(t)) - \sigma(t)) \, T(\sigma(t)) = \int_{\sigma(t)}^1 T(v)dv. \quad \text{(d.9)}$$

Therefore with the help of (d.4) and (d.6) we have

$$(\sigma_{ps}(\sigma(t)) - \sigma(t)) \, T(\sigma(t)) = \int_p^0 \bar T(v)dv = -\frac{3}{2}p^2 + O(p^3). \quad \text{(d.10)}$$

Now (d.1), with the help of (d.2), (d.4), (d.5), (d.6), (d.7), (d.8) and (d.10), can be rewritten

171

as

$$[-3p + O(p^2) + (\alpha t - p)(-3 + O(p))]\dot{p}$$
$$= k(-\frac{3}{2}p^2 + O(p^3))[9p^2 + O(p^3)] + \alpha(-3p + O(p^2)). \tag{d.11}$$

Since $|p| \ll 1$, if $\alpha \neq 0$ then (d.11) is dominated by

$$-3\alpha t\dot{p} = -3\alpha p. \tag{d.12}$$

Differential equation (d.12) for $p(t)$ is to be solved subject to $p(0) = \sigma(0) - 1 = 1 - 1 = 0$. Therefore the leading order solution for $p(t)$ is

$$p(t) = c \cdot t, \tag{d.13}$$

where c is an *undetermined* constant. Hence from (d.5) we obtain

$$\dot{\sigma}(t) = c + o(1), \qquad \sigma(t) = 1 + ct + o(t). \tag{d.14}$$

Therefore the initial slope of the solution path at $t = 0$ is

$$\frac{d\gamma}{d\sigma} = \frac{\alpha}{c}. \tag{d.15}$$

The value of which is not provided by the present analysis.

This slope is, however, related to the constant s curves in Ω_{12} which the solution path follows as it leaves $(\sigma_o, \gamma_o) = (1,1)$, since (25) now gives

$$s(t) = \frac{1}{3}(2 + \frac{\alpha}{c}) + o(1). \tag{d.16}$$

Thus c is given in terms of the loading rate α and the initial nucleation site s_o, by

$$c = \frac{\alpha}{3s_o - 2}, \tag{d.17}$$

and we note with $\alpha > 0$ that $c > 0$ if $2/3 < s_o \leq 1$ while $c < 0$ if $0 \leq s_o < 2/3$ with $c \to \infty$

and $s_o \to \frac{2}{3} = s_{trans}$.

If we consider an extended expansion

$$p(t) = ct + dt^2 + et^3 + gt^4 + o(t^4), \tag{d.18}$$

then (d.1) can also be expanded to yield

$$(-4c^3 + 4\alpha c^2 - 3d\alpha)\, t^2 + (16c^4 - 16c^3\alpha - 16c^2 d + 16cd\alpha - 6e\alpha)\, t^3 +$$

$$(-48c^5 + 48\alpha c^4 + 13.5kc^4 + 80dc^3 - 72d\alpha c^2 - 20ec^2 + 24e\alpha c - 20d^2 c \qquad \text{(d.19)}$$

$$- 9\alpha f + 12d^2\alpha)\, t^4 + o(t^4) = 0.$$

According to the coefficient of t^2 in (d.19) we have

$$d = \frac{4c^2}{3}\left(1 - \frac{c}{\alpha}\right) = \frac{4\alpha^2(s_o - 1)}{(3s_o - 2)^3}. \qquad \text{(d.20)}$$

Thus the coefficient d is dependent on the value α and s_o, but is independent of k. According-

ing to the coefficient of t^3 in (d.19) it is found that

$$e = \frac{8}{9}\frac{c^3(4c^2 - 5\alpha c + \alpha^2)}{\alpha^2} = \frac{8\alpha^3(s_o - 1)(s_o - 2)}{(3s_o - 2)^5}. \qquad \text{(d.21)}$$

Hence the coefficient e is also dependent on the value α and s_o, but is independent of k.

According to the coefficient of t^4 in (d.19) we have

$$g = \frac{-1}{54}\frac{c^4(640c^3 - 960\alpha c^2 + 288\alpha^2 c - 81k\alpha^2 + 32\alpha^3)}{\alpha^3} =$$

$$\qquad \text{(d.22)}$$

$$\frac{-\alpha^3}{2(3s_o - 2)^7}(32\alpha(s_o - 1)(s_o^2 + 2s_o - 4) + 3k(-27s_o^3 + 54s_o^2 - 36s_o + 8)).$$

Therefore the coefficient g is dependent on the value α, s_o and k. Hence from (d.5) we

obtain

$$\dot{\sigma}(t) = c + 2dt + 3et^2 + 4gt^3 + o(t^3), \qquad \sigma(t) = 1 + ct + dt^2 + et^3 + gt^4 + o(t^4), \qquad \text{(d.23)}$$

where d, e, and g are given in (d.20), (d.21), and (d.22), respectively. Hence from (25),

(d.2), (d.23), (d.6) we can find

$$s(t) = \frac{1}{3}\left(2 + \frac{\alpha}{c}\right) - \frac{1}{2}kc^2 t^3 + o(t^3) = s_o - \frac{1}{2}\frac{k\alpha^2}{(3s_o - 2)^2}t^3 + o(t^3). \qquad \text{(d.24)}$$

Note with the help of (d.9) and (d.10) that (d.24) also can be found by integrating $\dot{s} = kf$.

List of References

List of References

[1956E] J.D. Eshelby, The continuum theory of lattice defects, *Solid State Physics (Edited by F. Seitz and D. Turnbull) vol 3, Academic Press, New York*, 79-144.

[1970E] J.D. Eshelby, Energy relations and the energy-momentum tensor in continuum mechanics, *Inelastic Behavior of Solids (Edited by M.F. Kanninen et al.), MacGraw-Hill, New York*, 77-115.

[1973D] C.M. Dafermos, The entropy rate admissibility criterion for solutions of hyperbolic conservation laws, *J. Differ. Equations 14*, 202-212.

[1973L] P.D. Lax, Hyperbolic systems of conservation laws and the mathematical theory of shock waves, *CBMS Regional Conference Series in Applied Mathematics, 11, SIAM Publications: Philadelphia.*

[1975E] J.L. Ericksen, Equilibrium of bars, *J. Elasticity 5*, 191-201.

[1975EE] J.D. Eshelby, The elastic energy-momentum tensor, *J. Elasticity 5*, 321-335.

[1975R] J.R. Rice, Continuum mechanics and thermodynamics of plasticity in relations to microscale deformation mechanisms, *Constitutive Equations in Plasticity (Edited by A.S. Argon), MIT press, Cambridge, MA.* 23-79.

[1977K] J.K. Knowles, The finite anti-plane shear field near the tip of a crack for a class of incompressible elastic solids, *International J. of Fracture 13*, 611-639.

[1978K] J.K. Knowles and E. Sternberg, On the failure of ellipticity and the emergence of discontinuous deformation gradients in plane finite elastostatics, *J. Elasticity 8*, 329-379.

[1979B] Z.P. Bazant and S.S. Kim, Plastic-fracturing theory for concrete, *J. Eng. Mech. Div., ASCE III*, 407-428.

[1979K] J.K. Knowles, On the dissipation associated with equilibrium shocks in finite elasticity, *J. Elasticity 9*, 131-158.

[1980J] R.D. James, The propagation of phase boundaries in elastic bars, *Arch. Ration. Mech. & Anal. 73*, 125-158.

[1980O] D.R.J. Owen and E. Hinton, Finite elements in plasticity: theory and practice, *Pin-*

174

eridge Press Limited, 13-31.

[1982K] N. Kikuchi and N. Triantafyllidis, On a certain class of elastic materials with non-elliptic energy densities, *Quarterly of Applied Mathematics 40*, 241-248.

[1983A] R. Abeyaratne. An admissibility condition for equilibrium shocks in finite elasticity, *J. Elasticity 13*, 175-184.

[1983H] R. Hagan and M. Slemrod, The viscosity-capillarity criterion for shocks and phase transitions, *Arch. Ration. Mech. & Anal. 83*, 333-361.

[1984R] H.E. Read and G.A. Hegemier, Strain softening of rock, soil and concrete - a review article, *Mech. of Material 3*, 271-294.

[1985B] Z.P. Bazant and T.B. Belytschko, Wave propagation in a strain-softening bar: exact solution, *J. Eng. Mech. Div. ASCE III*, 381-389.

[1985O] M. Ortiz, A constitutive theory for the inelastic behavior of concrete, *Mech. of Material 4*, 67-93.

[1986H] H. Hattori, The Riemann problem for a van der Waals fluid with entropy rate admissibility criterion - isothermal case, *Arch. Ration. Mech. & Anal. 92*, 247-263.

[1986P] T.J. Pence, On the emergence and propagation of a phase boundary in an elastic bar with a suddenly applied end load, *J. Elasticity 16*, 3-42.

[1987A] R. Abeyaratne and J.K. Knowles, Non-elliptic elastic materials and the modeling of dissipative mechanical behavior: an example, *J. Elasticity 18*, 227-278.

[1987AA] R. Abeyaratne and J.K. Knowles, Non-elliptic elastic materials and the modeling of elastic-plastic behavior for finite deformation, *J. Mechanics and Physics of Solids 35*, 343-365.

[1987B] T. Belytschko, X.J. Wang, Z.P. Bazant and Y. Hyun, Transient solitons for one-dimensional problems with strain softening, *J. Applied Mechanics 54(3)*, 513-518.

[1987P] R.L. Pego, Phase transitions in one-dimensional nonlinear viscoelasticity: admissibility and stability, *Arch. Ration. Mech. & Anal. 97*, 353-394.

[1988A] R. Abeyaratne and J. K. Knowles, On the dissipative response due to discontinuous strains in bars of unstable elastic material, *International J. of Solids and Structures 24*, 1021-1044.

[1988AA] R. Abeyaratne and J. K. Knowles, Unstable elastic materials and the viscoelastic

response of bars in tension, *J. Applied Mechanics 55*, 491-492.

[1988S] S.A. Silling, Numerical studies of loss of ellipticity near singularities in an elastic materials, *J. Elasticity 19*, 213-239.

[1988SS] S.A. Silling, Finite-difference modeling of phase changes and localization in elasticity, *Comput. Methods Appl. Mech. Eng. 70*, 251-273.

[1989A] R. Abeyaratne and G.H. Jiang, Dilatationally nonlinear elastic materials-I, some theory, *International J. of Solids and Structures 25*, 1201-1219.

[1990A] R. Abeyaratne and J.K. Knowles, On the driving traction acting on a surface of strain discontinuity in a continuum, *J. Mechanics and Physics of Solids 38*, 345-360.

[1991A] R. Abeyaratne and J.K. Knowles, Kinetic relations and the propagation of phase boundaries in solids, *Arch. Ration. Mech. & Anal. 114*, 119-154.

[1991AA] R. Abeyaratne and J.K. Knowles, Implications of viscosity and strain gradient effects for the kinetics of propagating phase boundaries in solids, *SIAM J. Applied Math. 51*, 1205-1221.

[1991AAA] M. Affouf and R.E. Caflisch, A Numerical study of Riemann problem solutions and stability for a system of viscous conservation laws of mixed type, *SIAM J. Applied Math. 51*, 605-634.

[1991B] J.M. Ball, P.J. Holmes, R.D. James, R.L. Pego, and P.J. Swart, On the dynamics of fine structure, *J. Nonlinear Sci. 1*, 17-70.

[1991G] M.E. Gurtin, On thermomechanical laws for the motion of a phase interface, *J. Applied Math. and Physics 42*, 369-388.

[1991P] T.J. Pence, On the encounter of an acoustic shear pulse with a phase boundary in an elastic material: reflection and transmission behavior, *J. Elasticity 25*, 31-74.

[1991PP] T.J. Pence, On the encounter of an acoustic shear pulse with a phase boundary in an elastic material: energy and dissipation, *J. Elasticity 26*, 95-146.

[1992A] R. Abeyaratne and J.K. Knowles, On the propagation of maximally dissipative phase boundaries in solids, *Quarterly of Applied Mathematics 50*, 149-172.

[1992L] J. Lin and T.J. Pence, Energy dissipation in an elastic materials containing a mobile phase boundary subjected to concurrent dynamic pulses, *Transaction of the Ninth Army Conference on Applied Math. and Comput., (Edited by F. Dressel)*, 437-450.

[1993L] J. Lin and T.J. Pence, Kinetically driven elastic phase boundary motion activated by concurrent dynamic pulses, *Transaction of the Tenth Army Conference on Applied Math. and Comput., (Edited by F. Dressel)*, 69-86.

[1993LL] J. Lin and T.J. Pence, On the dissipation due to wave ringing in non-elliptic elastic materials, To appear in *J. Nonlinear Science*.

[1993S] S.P. Shah, C. Ouyang, and D.A. Lange, Fracture behavior of cement-based materials. *Materials Research Society Bulletin*, 55-59.